

THÈSE

Pour obtenir le grade de

DOCTEUR DE L'UNIVERSITÉ GRENOBLE ALPES

École doctorale : PHYS - Physique

Spécialité : Physique appliquée

Unité de recherche : Institut LAUE LANGEVIN

Analyse des facteurs régulant l'activité de l'isoforme PLA1-1 : une étude de réflectivité neutronique et de spectrométrie de masse

Analysis of the Factors Regulating the Activity of the PLA1-1 isoform: A Neutron Reflectivity and Mass-Spectrometric study

Présentée par :

Giacomo CORUCCI

Direction de thèse :

Giovanna FRAGNETO
Chercheur HDR, Institut Laue-Langevin
Krishna BATCHU
Chercheur Institut Laue-Langevin

Directrice de thèse

Co-encadrant de thèse

Rapporteurs :

FREDERIC CARRIERE
Directeur de recherche, CNRS DELEGATION PROVENCE ET CORSE
YURI GERELLI
Chercheur HDR, CNR de Rome

Thèse soutenue publiquement le **13 mars 2023**, devant le jury composé de :

FREDERIC CARRIERE Directeur de recherche, CNRS DELEGATION PROVENCE ET CORSE	Rapporteur
YURI GERELLI Chercheur HDR, CNR de Rome	Rapporteur
JUDITH PETERS Professeur des Universités, UNIVERSITE GRENOBLE ALPES	Présidente
ELISABETTA BOERI ERBA Ingénieur HDR, CEA CENTRE DE GRENOBLE	Examinatrice
CYRILLE BOTTE Directeur de recherche, CNRS DELEGATION ALPES	Examineur
ROBERT JACOBS Docteur en sciences, University of Oxford	Examineur



Contents

Abstract	ix
Acknowledgements	xi
1 Introduction	1
1.1 Introduction to phospholipids and phospholipases	1
1.1.1 Phospholipids: importance, synthesis and biophysical properties	1
1.1.2 Phospholipases: classification and state of art of the reaction mechanism	13
1.1.3 Similarities between lipases and PLA1s	19
1.2 Aims of the project	21
2 Materials and Methods	23
2.1 Phospholipase: expression, purification and characterization	23
2.1.1 Vector description	23
2.1.2 Rare codons and <i>E. coli</i> strains used	25
2.1.3 Expression procedures	26
2.1.4 Protein purification	28
2.1.5 Sequence analysis	30
2.1.6 Structural and functional analysis	31
2.2 Lipid production	32
2.2.1 Partially deuterated PC molecules	32
2.2.2 Natural GPL mixtures	33
2.3 Sample preparation	35
2.3.1 Crystals for NR and QCM-D, description and cleaning procedures	35
2.3.2 Solid supported model membranes preparation	36
2.3.3 LUV preparation for activity assays and MS kinetics analysis	38
2.4 Pre-characterisation studies by physico-chemical techniques	38
2.4.1 Ellipsometry	38
2.4.2 Quartz Crystal Microbalance with Dissipation monitoring	39
2.5 Experimental setup	40
2.5.1 Scattering techniques	40
2.5.2 High-throughput lipidomic analysis (MS analysis)	45
3 Results: Protein and lipids production	51
3.1 PLA1-1 production	51
3.1.1 Expression and purification	51
3.1.2 MBP tag removal, cleavage mediated by Factor Xa	56
3.1.3 cDNA sequencing	57
3.1.4 Mass spectrometry analysis of the uncleaved and cleaved PLA1-1	57
3.1.5 PLA1-1 structure prediction	61
3.1.6 Summary of the results on protein production	64
3.2 Lipid production	67
3.2.1 Natural lipids production and characterisation	67

3.2.2	Partially deuterated lipids production	76
3.2.3	Summary of the results for the protein and lipid production	82
4	Results: Protein-lipid interaction studies	83
4.1	NR analysis	83
4.1.1	PLA1-1 kinetics with partially deuterated PC molecules	84
4.1.2	Natural lipids	100
4.1.3	Appearance of a Bragg peak	103
4.1.4	Summary of the NR results	104
4.2	MS analysis	106
4.2.1	Kinetics assays - synthetic PC molecule mixtures	106
4.2.2	Kinetics assays - natural mixtures	113
4.2.3	Summary of the MS results	117
4.3	Additional biophysical characterisation studies	118
4.3.1	QCM-D	118
4.3.2	Ellipsometry	120
4.3.3	SANS	122
4.3.4	Summary of the additional biophysical characterisations	125
5	Discussion	127
5.1	Conclusions and Perspectives	142
6	CoruxFit	145
6.1	Introduction on the program	145
6.2	Model	146
6.2.1	Lipid bilayer modeling in CoruxFit	146
6.2.2	Membrane proteins and protein/organic molecule-membrane interaction	149
6.2.3	Kinetic plug-in for phospholipase system	153
6.3	SLD profile calculation	155
6.3.1	Contrast variation method in neutron scattering	156
6.4	Theory behind reflectivity and Parratt algorithm	158
6.4.1	Brief introduction to the reflectivity theory	158
6.4.2	The Parratt algorithm	158
6.4.3	Q resolution algorithm	161
6.5	Minimisation routine	164
6.5.1	Simulated Annealing algorithm	164
6.5.2	Error calculation of the fitted parameters	166
6.6	Software description	168
6.6.1	Installation of CoruxFit	168
6.6.2	Data analysis with CoruxFit	169
6.6.3	The new CoruxFit environment	172
6.7	Summary of the program	173
6.7.1	Future developments of CoruxFit	174
7	Other open access programs	175
7.1	Mass spectrometry program - for MS hydrolysis kinetics	175
7.2	GCMS and MS peak integration program	177
7.3	BAM image recognition	177

A Appendix	179
A.1 Stock solution concentration	179
A.2 Nucleotide and amino acid sequences for MBP - PLA1-1	179
A.2.1 Nucleotide sequences	179
A.2.2 Amino acid sequences	181
A.2.3 Deconvolution of the gel filtration chromatogram	181
A.3 GC-MS peaks identification table	182
A.4 Pictures of used equipment	182
A.4.1 NR cells - Pictures and description	182
A.4.2 Langmuir troughs	184
A.4.3 Ellipsometry cell	185
A.5 NR fitted parameters	186
A.5.1 Natural lipids	186
A.6 CoruxFit raspberry server	187
Bibliography	189

“If you can’t explain it simply, you don’t understand it well enough.”

Albert Einstein

Abstract

Glycero-phospholipids are amphipathic molecules constituted by a polar head and hydrophobic chains. These molecules are involved in several pathways (such as signal transduction) and are also fundamental in the structural containment of cells and their organelles. In fact, lipid membranes are mainly made up of phospholipids and contain other critical elements such as triglycerides, sterols, proteins, etc. For the membrane to be structurally and chemically functional, its fluidity must be retained when changes occur in its surroundings. Therefore, several remodelling and degradation pathways for the phospholipid are constantly active. Within those pathways, phospholipases (PLs) play a key role; whether they are activated or expressed in response to stimuli from the external environment or directly from the lipid membrane (such as fluidity or elasticity).

As described in this thesis, phospholipase group A (PLAs) is taken into consideration and analysed in its complex kinetics and interaction with model lipid membranes. PLAs are lipolytic enzymes that hydrolyse phospholipid substrates at specific ester bonds. They are widespread in nature and play very diverse roles, from signal transduction and lipid mediator production to membrane phospholipid homeostasis. Phospholipases are very diverse in their structure, function, regulation and mode of action. Therefore, a deeper understanding of their dynamics and kinetics is crucial. The present study involves employing neutron reflectivity, mass spectrometry and other physico-chemical techniques as to better understand the principles underlying the phospholipases substrate specificity. PLA reactions occur in multiple steps, some involving the specificity of the PLA under examination. More specifically, efflux propensity and active site accommodation are the two restricting reaction steps and within these two steps the preferred substrate is selected to be cleaved. The efflux propensity is the ability of a phospholipid molecule to move out of its membrane. This property is related directly to the physical properties of the phospholipid molecule and the membrane, such as hydrophobic interactions, which play a key role in this process. The second crucial step is the active site accommodation: describing how well a phospholipid molecule adapts in the PLA active pocket site. This thesis evaluated the effects of acyl chain length and unsaturation of phospholipids on the hydrolysis activity of PLA1-1 (sourced from *Aspergillus oryzae*). This was done in order to assess how the preferred phospholipid was selected, to better understand which step is important in the process. The PLA1-1 was expressed in *E. coli* and purified to its purest form. Structural changes of the model lipid membrane were also analysed, including how these changes affect the activity and the kinetics course mediated by the PLA1-1.

The results obtained show a clear preference of PLA1-1 for high efflux propensity phospholipid molecules, where shorter acyl chains containing a higher number of double bonds in phospholipids appear to be the ones cleaved at high rates. Additionally, an inhibition mediated by the free fatty acids released from the hydrolysis reaction seems to occur. Structural changes on the membrane upon hydrolysis reaction are found to be critical for the reaction rate in some cases. Products of the hydrolysis of phospholipids form a diluted layer on the top of the model membrane under examination, showing a plateauing the degradation profile. This layer appears only when the reaction rate is below a certain level. A lyso-PLA activity was found for PLA1-1, where after a certain reaction period the second acyl chain is also degraded.

Résumé

Les glycéro-phospholipides sont des molécules amphipathiques constituées d'une tête polaire et de chaînes hydrophobes. Ces molécules sont impliquées dans plusieurs types de réactions (telles que la transduction du signal) et sont également fondamentales dans le confinement structurel des cellules et de leurs organites. En effet, les membranes lipidiques sont principalement constituées de phospholipides et contiennent d'autres éléments critiques tels que les triglycérides, les stérols, les protéines, etc. Pour que la membrane soit structurellement et chimiquement fonctionnelle, sa fluidité doit être conservée lors des changements environnementaux. Par conséquent, plusieurs voies de remodelage et de dégradation du phospholipide sont en constante activités. Au sein de ces voies, les phospholipases (PL) jouent un rôle clé ; qu'ils soient activés ou exprimés en réponse à des stimuli provenant du milieu extérieur ou directement de la membrane lipidique (comme la fluidité ou l'élasticité).

Comme décrit dans cette thèse, la phospholipase groupe A (PLA) est prise en considération et analysée dans sa cinétique complexe et son interaction avec les membranes lipidiques modèles. Les PLA sont des enzymes lipolytiques qui hydrolysent les substrats phospholipidiques au niveau de liaisons ester spécifiques. Ils sont répandus dans la nature et jouent divers rôles, de la transduction du signal et de la production de médiateurs lipidiques à l'homéostasie des phospholipides membranaires. Les phospholipases sont très diverses dans leur structure, leur fonction, leur régulation et leur mode d'action. Par conséquent, une compréhension plus approfondie de leur dynamique et de leur cinétique est cruciale. La présente étude utilise la réflectivité neutronique, la spectrométrie de masse et d'autres techniques physico-chimiques afin de mieux comprendre les principes sous-jacents à la spécificité du substrat des phospholipases. Les réactions PLA se produisent en plusieurs étapes, certaines impliquant la spécificité du PLA examiné. Spécifiquement, la propension à l'efflux et l'accommodation du site actif sont les deux étapes de réaction restrictives. Dans ces deux étapes, le substrat désiré est sélectionné pour être clivé. La propension à l'efflux est la capacité d'une molécule de phospholipide à sortir de sa membrane. Cette propriété est directement liée aux propriétés physiques de la molécule phospholipide et de sa membrane, telles que les interactions hydrophobes, qui jouent un rôle clé dans ce processus. La deuxième étape cruciale est l'adaptation du site actif : décrivant la mesure dans laquelle une molécule de phospholipide s'adapte au site actif PLA. Cette thèse a évalué les effets de la longueur de la chaîne acyle et de l'insaturation des phospholipides sur l'activité d'hydrolyse du PLA1-1 (provenant d'*Aspergillus oryzae*). Cela a été fait afin d'évaluer comment le phospholipide préféré a été sélectionné, de mieux comprendre quelle étape est importante dans le processus. La PLA1-1 a été exprimée dans l'*E. coli* et purifiée au maximum. Les changements structurels de la membrane lipidique modèle ont également été analysés, y compris la façon dont ces changements affectent l'activité et l'évolution cinétique médiée par la PLA1-1.

Les résultats obtenus montrent une nette préférence du PLA1-1 pour les molécules phospholipidiques à forte propension à l'efflux, où les chaînes acyle plus courtes contenant un nombre plus élevé de doubles liaisons dans les phospholipides semblent être celles qui sont clivées à des taux élevés. De plus, une inhibition médiée par les acides gras libres libérés de la réaction d'hydrolyse semble se produire. Les changements structurels sur la membrane lors de la réaction d'hydrolyse se révèlent critiques pour la vitesse de réaction dans certains cas. Les produits de l'hydrolyse des phospholipides forment une couche diluée sur le dessus de la membrane modèle à l'examen, montrant un plafonnement du profil de dégradation. Cette couche n'apparaît que lorsque la vitesse de réaction est inférieure à un certain niveau. Une activité lyso-PLA a été trouvée pour PLA1-1, où après une certaine période de réaction, la deuxième chaîne acyle est également dégradée.

Acknowledgements

It has been a really amazing period of my life, very rich in experiences, new things and new people. I learnt really a lot, not only scientifically speaking, but also in my personal side, learning additionally new languages, which is already a great conquest for me. I have really enjoyed every part of the PhD, even when things got really dense. Science is not an easy field, discovery how nature works at the molecular scale, where the only way to see what is happening is through the use of complex instruments, with some times very strong physics behind them. But this is where reside the fun part, where physics, chemistry and biology work together in this amazing multidisciplinary field, which is called biophysics. I have to thank all the people that helped, guided and believed in me, reaching this final point of the PhD, very important step of my life. I have always dreamt working in a laboratory one day, as a researcher/scientist, consequently I must thank all the people that pushed me through the right direction, guiding me step by step, taking me always forward. Thanks to Giovanna Fragneto, who helped me and taught me all the basics of neutron scattering, giving great ideas for projects and always ready to listen and discuss. Thanks to Krishna Batchu, who helped me in different aspects during the PhD, scientifically and personally speaking, pushing me to give always my best, helping with new ideas and suggesting always the best option. Thanks to Robert Jacobs for the help in the understanding the basics of neutrons and for the useful discussions, always ready to help me. Many thanks to the D-Lab, that hosted me during this time, helping me, and exchanging very good discussions and high level scientific topics; thanks especially to Valerie Laux, who helped me a lot during the expression and purification steps, suggesting always the best way to take. Thanks to Yoshiki who helped me during all the MS kinetics experiments with her very high expertise in using mass spectrometry technique and lipids. And thanks to Cyrille as well, who allows us to perform all the MS analysis that are showed in this thesis. I must thank all the PhD students that I have met during this period, especially Moritz, Andreas, Javier, Larissa, Peter, Xaver, Alice, Wenke, Loic, Dominique and many many others, which helped me in assessing the codes, ideas for new experiments for the project and also, last but not the least, moral support. Thanks to all the scientists/staff, such as Lionel, Anne, Philippe, Thomas, Yuri, Alessandra, Ernesto, Martina, Andrea, Sandrine, Samantha, Leonardo, Juliette, Mizar, Martinne, Jennifer, and many many others, for the useful discussions, technical and moral support. Thanks to Alice Aubert, that introduced me to the insect cell culturing and protein expression, it was really nice to work with such difficult lines. Thanks also to Elisabetta and Agneta for performing the TOF-MS of the protein, allowing us to assess the identity of the protein expressed. Thanks to Caterina Ricci, for helping me in some aspects of the project, especially in the structure prediction of the PLA1-1 structure, and for all the very useful discussions. Finally, thanks to all the institutions that help me with the project, such as ILL and PSCM, D-LAB, our L-LAB, IBS, ESRF, EMBL, IBS and UGA.

I have to thank also few more persons, the ones that introduced me to science, the ones who supported me and believed in me from the beginning of my path. My professor Francesco Spinozzi, who introduced me to the biophysics, a much more quantitative thinking, where math is a critical tool to be used for biological studies. He is the one who introduced me to lipids/proteins interactions, that from that period to now is my personal expertise. A big thank also goes to Enrico Baldassarri, who introduced me to the protein expression and purification, that is one of the most important part of my work in the labs. He taught me how the precision and the careful planification of an experiment is a fundamental step to achieve good results. Thanks to Benedetta Come for the support during the SAXS experiments, LUVs preparation and moral support as well. Thanks to Paolo Moretti for the big support during all the period from my master thesis to now. Thanks to Paolo Mariani to giving me the possibility to work with his group. Thanks to Chiara Ardiccioni and Luca Lambertucci for the useful scientific and also non-scientific discussions, that helped me during that period of time. Thanks to all

the master students and internships for the useful discussions, it was really amazing working with them. A huge thanks goes also to all my professors, where along Bachelor and Master degree, transferred to me their passion, meticulousness and the desire of doing very good science, so thank you all!

Very last but not at all least, I want to thank Sara D'Angelo, who was always ready and present to support me in every situation faced during this amazing but at the same time tricky period. And of course, my family, who have always strongly believed in me, pushing me always further, giving huge support and suggestions on what should come next. Thanks to all my friends as well, for the huge moral support given.

Thank you.

List of Figures

1.1	Various classes of phospholipid molecules. The acyl chain displayed are 16:0 and 18:1 for the sn1 and sn2 respectively.	7
1.2	Sketch representing different shape that a lipid can assume, and their preferential structure when they are added into an aqueous solution.	9
1.3	Steps of the hydrolysis reaction mediated by PLAs	19
1.4	The structure of two different lipases, where 3NGM is from the organism <i>Gibberella zeae</i> , whereas 6UNV from <i>Rasamsonia emersonii</i> . It can be noticed as the structure is conserved between the two, while their sequence is not.	20
2.1	Map of the vector (panel A) and zoom of the expression cassette (panel B) . .	25
2.2	Scheme of the steps for cells handling	26
2.3	Scheme of affinity purification steps using MBP-Trap column coupled to the AKTA purifier	29
2.4	Gel filtration sketch, where it is possible to notice how this technique is able to separate the molecules depending on its molecular weight (MW).	30
2.5	Scheme of the geometry during reflection of a beam from a surface	41
2.6	Scheme of the choppers used on FIGARO instrument for the TOF beam . . .	42
2.7	FIGARO instrument setup scheme	43
2.8	Single quadrupole scheme.	46
3.1	Time dependent expression test, performed for Codon Plus and Rosetta strains. The lane "N.I." is the non-induced cells; 1h, 3h at 37 ° and O/N at 25 ° are from induced cells. The two strain expressions resulted in similar protein expression (as indicated by the red arrow).	52
3.2	MBP Trap chromatogram. The black straight lines represent the fraction collected, from the N°7 to the N°11. The "%B" displayed in the second y-axis corresponds to the ratio between the PLA-Buffer (used as running buffer) and the Elution Buffer.	52
3.3	SDS-PAGE gel of the affinity purification step. Where STD is the standard; Pre-Inj is the sample before its injection into the column; F.T. is the flow through (non-bounded proteins); Wash is the washing step of the column; and the last 4 lanes are the 4 eluted fractions. The blue circle represent the protein lost during this purification, as mentioned in the text.	53
3.4	Gel filtration chromatogram. The black straight line represent the fraction taken for the SDS-PAGE gel shown in figure 3.5	54
3.5	SDS-PAGE gel of the gel filtration purification. The fraction loaded are displayed in figure 3.4	54
3.6	Entire purification process SDS PAGE gel. Where N.I. is the non-induced cells and Ind represent the induced cells; STD is the standard; Pre-Inj is the protein sample before its injection into the MBP-Trap; F.T. is the flow through of the non-bounded proteins; A.C. is the affinity chromatography purified sample; and finally the last lanes represent the gel filtration fractions.	55

3.7	TLC representing an activity assay performed on the fractions displayed in the gel filtration chromatogram in figure 3.4. In this experiment, the FFAs released from the reaction are not visible, since the TRITON used covers their signal, migrating in the same spot.	56
3.8	Time dependent Factor Xa cleavage assay. Where STD is the standard; FP is the fusion protein; following the different timings where O/N is the over night digestion; and finally C.MBP is the MBP protein used as control.	57
3.9	Affinity chromatography separation between MBP-tag and cleaved PLA1-1.	58
3.10	Entire process of purification. Where STD is the standard, T.L. is the total lysate, F.T. is the flow through, M.T.P. is the MBP-Trap purified protein, G.F. is the gel filtrated protein, A.D. is after the dialysis, [C] is A.D. concentrated, Cl. cleavage, Xarr is after the Xarrest, PLA is the PLA1-1 purified from the second MBP-Trap step and its concentrated version [PLA] and finally El. that is the eluate from the MBP-Trap	58
3.11	Alignment of the theoretical sequence of the vector (query) and the sequence obtained from the Sanger sequencing (forward). The selected sequence is the query coding for PLA1-1, and there is a clearly perfect match between the two.	59
3.12	MS-TOF analysis of the MBP - PLA1-1. From the deconvoluted spectra it can be noticed a single peak corresponding to 72556.9 Da, which lead to a high purity sample eluted.	60
3.13	MS-TOF analysis of the cleaved PLA1-1. Also in this case mainly one peak was found. Its mass was found to be between the oxidised and reduced protein.	60
3.14	MS-TOF analysis of the cleaved PLA1-1 in the presence of TCEP. In this case the mass corresponds to the totally reduced protein. Therefore, 2 disulfide bridges exist in its active form.	61
3.15	BLAST Protein alignment PLA1-1 vs the Lipase 6UNV chain A	62
3.16	Homology modeled structure for PLA1-1 with 6UNV	62
3.17	AlphaFold prediction of the MBP - PLA1-1	63
3.18	AlphaFold prediction of the cleaved PLA1-1	64
3.19	Superimposition between Predicted and Homology modelled structure	65
3.20	In panel (A) the fit of the experimental curve with the model #15 of Genfit and a cylinder (for aggregates); in panel (B) the p(r) from the fit displayed in (A)	65
3.21	HPLC chromatograms H <i>versus</i> D.	68
3.22	TLC analysis of the three purified classes of phospholipids purified. This step is fundamental for the assessment of the identity and purity of the purified fractions.	68
3.23	H <i>versus</i> D lipid extracts GC-MS chromatograms. It can be noticed a consistent shift of the peaks in low time ranges for the D lipids. The chromatograms are normalised to the highest peak for a better view.	69
3.24	MS spectra of the peak corresponding to 25:0, taken as example because of its symmetric shape. The first peak on the right corresponds to the m/z of the 25:0 FAME, whereas the other signals are fragmentation products. The shift seen in the spectra is caused by the deuterium content.	70
3.25	Effect of deuteration on the GC column retention time. Figure shows the EIC of the same molecule with different deuterium atom content. More deuteriums causes an early elution, whereas lower content gives later elution.	71
3.26	Acyl chain profiling of each purified GPL class. Can be noticed a large difference in the acyl chain profile between H and D lipids.	71

3.27	QCM-D measurements of the dPC mixture. As noticed, the frequency of ≈ -26 and the dissipation of ≈ 0 , shows the good formation and coverage of the lipid bilayer.	72
3.28	Panel (A) displays SANS experimental data for the dPC vesicles suspended in mixtures of D ₂ O and H ₂ O with different D ₂ O content as reported in the legend. In panel (B) is plotted the $\sqrt{\Delta I}$ as function of the D ₂ O content. The plot was used to extrapolate the match point for the dPC lipids analysing the data with a straight line.	73
3.29	Sketch explaining the contrast variation of the vesicles solubilised in solutions containing different amount of D ₂ O	74
3.30	NR measurements and analysis of the PC SLBs. Panel A and C show the NR datasets and its analysis, panel B and D shows the related model. The formation and the good coverage of the lipid membrane can be noticed already by observing the model, since very low amount of solvent was found in the acyl chain region.	75
3.31	NR measurements and analysis for the mixture PC/PS in its hydrogenous and deuterated form. Also in this case the formation of the lipid bilayers and the coverage were found to be quite good.	76
3.32	NR measurements and analysis of the mixture PC/PG. As well as the other two mixtures, the coverage found was very high.	77
3.33	GC chromatograms of the partially deuterated PC molecules synthesised. The standard (shown in black color) used to compare the peaks was constituted by a mixture of FAMES such as 14:0 (R.T. ≈ 4.3), 16:0 (R.T. ≈ 6.8) and 18:0 (R.T. ≈ 10.2) [where R.T. corresponds to the retention time].	78
3.34	NR data and analysis of the synthesised partially deuterated 18:2 PC molecule. In panel A the data and the fit is shown in the 4 contrasts used and in panel B the related model is displayed.	79
3.35	SLD profile calculated from the model shown in figure 3.34.	79
3.36	Isotherm and deposition of the lipids d18:0 h18:0 PC and d16:0 h16:0 PC	80
3.37	Efficiency of the deposition for the lipid d16:0 h16:0 PC, that it was found to be in this case to 100%	81
3.38	Deposition of the second leaflet via Langmuir-Schaefer, in order to obtain the complete bilayer.	81
4.1	DSPC SLB structure profile in 3 different contrasts (A) and parameters used to fit the data in panel (B)	85
4.2	Kinetics recorded using DSPC SLB in incubation with PLA1-1. In panel (A) the NR data and analysis and in panel (B) the correlated SLD profiles are displayed. A slight decrease of the SLD of the outer leaflet only can be noticed, since that leaflet is the only one available for the attachment of the enzyme.	86
4.3	DPPC SLB structure analysis in 3 different contrasts (A) and its fitted parameters in panel (B)	86
4.4	Kinetics recorded on DPPC SLB in incubation with PLA1-1. In panel (A) the NR data and their analysis, in panel (B) the SLD profiles. The degradation is clearly visible from the decrease of the SLD values, where an increase of the SLD occurs around 50 Å from the center of the bilayer (micelle layer).	87
4.5	Integrated R(q) intensity over the hydrolysis reaction time. The integration was carried out between $0.1 < q < 0.14 \text{ \AA}^{-1}$	88
4.6	Degradation level from the d16:0 h16:0 PC SLB kinetics analysis, using the kinetics plug-in for CoruxFit	88

4.7	Extent of flip-flop determined from d16:0 h16:0 PC SLB calculated from the kinetics plug-in analysis.	89
4.8	Topological area per lipid variation upon degradation for the d16:0 h16:0 PC kinetics	90
4.9	Sketch representing a palmitic acid micelle	90
4.10	Plot of the fraction volume distribution of the ERF representing the micellar layer upon degradation.	92
4.11	Model for the time point 12h of the kinetics recorded for d16:0 h16:0 PC SLB.	92
4.12	Sketch representing the course of the kinetics recorded with NR for the d16:0 h16:0 PC SLB	92
4.13	d16:0 h18:2 PC SLB reflectivity data in 4 different contrasts (A) and fitted parameters in panel (B)	93
4.14	Kinetics recorded on d16:0 h18:2 PC SLB. In panel (A) the NR data and their fitted curves, in panel (B) the related SLD profiles. The degradation of the lipid bilayer is clear from the shift to lower values of the SLD profiles.	94
4.15	Graphs from the analysis of the kinetics of d16:0 h18:2 PC SLB. In panel (A) the sn1 degradation is displayed, in panel (B) the sn2 degradation, in panel (C) the flip-flop profile and finally in panel (D) the topological area per lipid profile. With sn2 degradation we mean the sn2 acyl chain that is hydrolysed when the shift from sn2 to sn1 position occurs.	95
4.16	d16:0 h20:4 PC SLB structure analysis in 3 different contrasts (A) and its fitted parameters in panel (B)	96
4.17	Graphs resulting from the analysis of the kinetics performed on the h16:0 h20:4 PC SLB. In panel (A) the NR data and the fitted curves, (B) the correlated SLD profiles, (C) the sn1 degradation, (D) the sn2 degradation, (E) the flip-flop profile and finally (F) the topological area per lipid profile.	97
4.18	Panel A: Degradation parameter as determined from NR data fitting; panel B: zoom of the graph displayed in panel A. The errors of the points are omitted for clarity.	98
4.19	Graphs obtained from the analysis of the kinetics measurements performed on the dPC SLB. In panel (A) the NR data and the fitted curves, (B) the correlated SLD profiles, (C) the sn1 degradation, (D) the sn2 degradation, (E) the flip-flop profile and finally in panel (F) the topological area per lipid profile. Data collected at 5h30 and 8h20 in (A) are offset for clarity.	101
4.20	Graphs obtained from the analysis of the kinetics measurements performed on the hPChPS SLB in H-buffer. In panel (A) the NR data and the fitted curves, (B) the correlated SLD profiles.	102
4.21	sn1 degradation obtained from the analysis of the kinetics measurements performed on the hPChPS SLB in H-buffer.	102
4.22	Bragg peak of a dataset after the wash	103
4.23	Two-dimensional image NR from the detector, where in y-axis is represented the pixel position of the image in the detector, the x-axis represent the TOF channel (energy of the neutrons detected, from which the scattering vector q is calculated)	103
4.24	Example of normalized spectra, where the spectra of the time point "0" is superimposed to the time point "75"	107
4.25	MS degradation graphs of the Mix A in panel (A) and Mix B in panel (B)	107
4.26	Plot of the velocity rates of the hydrolysis reaction vs number of double bonds	109
4.27	Lyso products profile over reaction time: Mix A in panel (A) and Mix B in panel (B)	110

4.28	TIC chromatograms (panel (A)) and its integration plotted as function of time (panel (B)).	111
4.29	Degradation plots using different sized vesicles, where panel (A) displays the degradation graph for the non-extruded vesicles, panel (B) vesicles extruded at 1000 nm and finally panel (C) vesicles extruded at 400 nm	112
4.30	MS spectra of the parent 184 m/z to scan PC molecules from the TLE utilised. The question marks indicates unknown lipids found in the sample.	114
4.31	Degradation graphs achieved from the kinetics analysis of the TLE.	114
4.32	Analysis of the degradation of 36:1 species from various PL classes recorded through DMRM	115
4.33	Lyso profiling MS intensity vs. retention time (RT)	117
4.34	PS 36:2 profiling MS intensities vs. retention time (RT)	118
4.35	Cycled flow QCM-D kinetics measurement	119
4.36	Normal QCM-D measurement	119
4.37	Ellipsometry measurements	121
4.38	Ellipsometry measurement	122
4.39	Picture representing the kinetics using DMPC	123
4.40	Blank (right) and end reaction (left) of DMPC + PLA1-1	123
4.41	Kinetics SANS data, where the two black arrows indicate the differences between	124
5.1	White/blue scan, carried out in order to select the <i>E. coli</i> cells with the recombinant bacmide of interest	143
5.2	Fluorescent microscopy of the hi5 expressing the protein of interest	143
5.3	Expression test with an SDS-PAGE gel, where "WCE" is the whole cell extract and "SN" is the supernatant. The different numbers meant the days after the cells infection. Already a good expression level is achieved after 3 days. The expressed protein appears in the WCE, since the protocol for the extraction is not optimised for this kind of protein, since it is a general one.	144
6.1	CoruxFit official logo	145
6.2	Sketch of the sample measured with NR. The numbers displayed corresponds to each part (layer) described in the main text, which constitutes the sample under analysis.	146
6.3	Cylinder describing the two phospholipid molecules placed along the vertical axis (z-axis) with respect to the bilayer surface.	147
6.4	Example of component group volume fraction distribution model	149
6.5	Top view representation of the hexagonal model configuration used in Corux-Fit to model the dispersion of the interacting objects in/on the SLBs	150
6.6	Sketch of an interacting object in interaction with a portion of an SLB. The blue part of the sketch is the bulk water, whereas the green part is the lipid membrane.	150
6.7	Sketch representing a membrane protein, where the cylindrical part corresponds to the hydrophobic part inserted into the membrane and the spherical portion the hydrophilic part, facing the bulk solution.	151
6.8	Volume fraction distribution of the trans-membrane protein sketched in figure 6.7	152
6.9	Sketch representing the 4 principal parameters for the kinetic model developed for the membrane - PLA1-1 interaction studies	154
6.10	SLD profile of the 16:0 18:2 lipid bilayer taken as example.	156

6.11	Contrast variation of a picture. The figure represent how the contrast plays a key role in the understanding of the structure and details of a photo/sample, where utilising different contrasts, different part of the photo can be seen. . . .	157
6.12	Sketch representing the reflection and refraction phenomenons in a stacked layer sample	160
6.13	Different q resolution reflectivity curve calculation of a POPC lipid bilayer . . .	163
6.14	Profiles of the probability of finding the same system at ΔE energy vs temperature of the system	165
6.15	χ^2 function of a two parameters simulated annealing analysis, where the best values of the two parameters are place on the minima of this function. Simulated annealing	166
6.16	Example of a Hessian matrix from a CoruxFit analysis	168
6.17	Raw plot from CoruxFit	170
6.18	CoruxFit terminal at the end of the simulation	171
6.19	Terminal windows on Ubuntu where CoruxFit environment is running. In this case, the terminal is connected with the raspberry server	172
7.1	Output image from the program, where it is possible to compare the raw image with the treated one.	178
7.2	Examples of graphs from the parameters found by the program on BAM pictures. In figure A is plotted the number of spots and the ratio total area of the spots/ area of the BAM picture vs pressure; in figure B the averaged area per spot vs pressure	178
A.1	Gaussian deconvolution of the gel filtration chromatogram displayed in figure 3.4 in Chapter Results.	182
A.2	Picture representing the PEEK cells and the silicon crystals used in NR experiments	183
A.3	NR cell	183
A.4	Trough Nima, used for the fist leaflet deposition	184
A.5	Trough Nima, used for the second leaflet deposition	184
A.6	Ellipsometry cell, used to assess the amount of protein needed for NR experiments	185
A.7	Raspberry server	187
A.8	"The end" graph	188

List of Tables

2.1	List of the buffers used for the purification of the PLA1-1 and for its activity assays. Pr. inhibitors stands for Proteases inhibitors	28
2.2	List of lipids used for the NR kinetics analysis	33
2.3	Lipid mixture (A) [PC kinetic mix (A)] used for the MS kinetic analysis. . . .	49
2.4	Lipid mixture (B) [PC kinetic mix (B)] used for the MS kinetic analysis. . . .	49
3.1	Parameters from the SAXS data analysis using the model #15 and the cylinder model of Genfit software. $[C]_{th}$ corresponds to the theoretical concentration calculated from the intensity of the SAXS profile, the MW the molecular weight inserted as fixed parameter for the scale factor calculation, Vol is the volume of the protein, r is the radius of the cylinder and d its length.	64
3.2	Scattered intensity corresponding to different q-ranges for the investigated vesicle suspension. The square root ($\sqrt{\Delta I}$) of the difference between the calculated values (ΔI) was used to extrapolate the match point for the dPC lipids (see also Figure 3.28)	74
4.1	Absolute amount expressed in μg of PLA1-1 injected into the NR cell after the complete SLB characterisation. The * values were not experimentally calculated, since for technical reasons linked to the sample cell available, it was not possible to use the ellipsometry technique with layers deposited via the LB-LS method. Consequently those values were estimated from the ellipsometry results from the other PC molecules.	84
4.2	Table of the rates calculated from the Mix A experiment	108
4.3	Table of the rates calculated from the Mix B experiment	108
4.4	Rates of the analysed lipids at different vesicle sizes.	113
4.5	Table representing all the lipids tracked during the kinetics with the TLE of <i>Pichia pastoris</i> . "D.U." is the "degradation unit", since for this experiment was not possible to obtain the precise amount for each lipid specie present into the mix utilised. The sn1 and sn2 position acyl chain displayed in the column 'Possible lipids', can be assumed to be also specular.	115
4.6	Reaction velocities vs. different lipid classes	116
A.1	Storage and usage concentrations of the chemicals for the protein expression .	179
A.2	GC-MS retention time of the found FAMES	182
A.3	Fitted parameters of the SLBs containing different mixtures of natural lipids. .	186

List of Abbreviations

cDNA	copy DeoxyriboNucleic Acid
MBP	Maltose BindingProtein
SOC or SOB	Super Optimal Broth
LB	Lysogen Broth
AMP	Ampicillin
CLO	Chloramphenicol
O/N	Over Night (\approx 16 hours)
SDS-PAGE	Sodium Dodecyl Sulphate - PolyAcrylamide Gel Electrophoresis
OD₆₀₀	Optical Density at 600 nm
CV	Column Volume
SAS	Small Angle Scattering
SAXS	Small Angle X ray Scattering
SANS	Small Angle Neutron Scattering
NR	Neutron Reflectivity
MS	Mass Spectrometer
TOF-MS	Time Of Flight Mass Spectrometer
QQQ-MS	Triple Quad Mass Spectrometer
PDB	Protein Data Bank
GPL	Glycerol Phospho Lilid
MeOH	Methanol
EtOH	Ethanol
IPA	Iso Propilic Acid
FPLC	Fast Protein Liquid Chromatography
HPLC	High Performance Liquid Chromatography
PC	Phosphatidyl Choline
PE	Phosphatidyl Ethanolamine
PS	Phosphatidyl Serine
PG	Phosphatidyl Glycerol
PI	Phosphatidyl Inositol
PA	Phosphatidic Acid
LPC	Lyso Phosphatidyl Choline
FFA	Free Fatty Acid
FA	Fatty Acid
N₂	Nitrogen gas
Ar	Argon gas

... Dedicated to all those who have believed and believe in me ...

Chapter 1

Introduction

1.1 Introduction to phospholipids and phospholipases

1.1.1 Phospholipids: importance, synthesis and biophysical properties

Glycerophospholipid (GPL) existence and its diversity

Cellular membranes are highly complex structures consisting of hundreds of different lipid molecules as well as numerous different proteins. Lipids provide the most efficient form to store energy and they act as messengers in diverse metabolic pathways [1, 2, 3, 4]. They play critical functions in both cellular physiology and pathology. Also from in vivo functional analysis, there is a growing appreciation of the roles of lipids in signal transduction, transcription regulation and protein post-translational modification. Since these molecules are amphipathic in nature, they have the ability to form biological membranes that separate the internal constituents of cells from the external environment and surround diverse organelles. The lipids of natural membranes are structurally diverse and are divided into eight main groups based on their core structures, *i.e.* fatty acids, glycerolipids (GLs), glycerophospholipids (GPLs), sphingolipids (SLs), sterol lipids, prenol lipids, saccharolipids, and polyketides. Of these, GPLs are the most abundant ones in virtually all natural membranes and constitute > 10 different GPL classes, which are mainly defined by the structure of the head group. The major GPL classes are phosphatidylcholines (PC), phosphatidylethanolamines (PE), phosphatidylinositols (PI) phosphatidylserines (PS) phosphatidylglycerols (PG), phosphatidylamines (PA) and cardiolipins (CL). Each GPL class in turn consists of several structurally different molecular species that contain the same headgroup but differ from one another with respect to the acyl chain composition [5, 6]. The hydrocarbon chains at the sn1 and sn2 positions are usually esterified to the glycerol moiety. The number of carbons in the alkyl chain typically varies between 12 and 24 while the number of double bonds ranges between 0 to 6. The alkyl chain in the sn1 position is typically saturated or monounsaturated, while that in the sn2 position is often polyunsaturated. Thus, all these various alkyl chain combinations within each class of GPL can lead to the existence of numerous molecular species within a cellular membrane [7]. The meaning of such diversity is not fully understood, but presumably relates to the multiple functions of GPLs.

Processes maintaining GPL metabolism in cellular systems

As mentioned earlier, cellular systems consist of tens of thousands of lipid molecular species that have been categorised into several classes and these are known to be synthesised by a wide range of enzymes. Enzymes are proteins considered as molecular machines, critical for the normal life of living organisms. Enzymes are biological catalysts, helping to speed up a specific chemical or biochemical reaction in organisms. Enzymes are in fact involved in many metabolic pathways, such as the GPL homeostasis. GPL homeostasis is very crucial for cellular survival as indicated by the fact that GPL-class compositions in the membranes are maintained within very narrow limits, implying that deviation from the optimum composition is deleterious [8, 9]. In fact, a few genetic diseases presenting an altered phospholipid composition are known as well as in vivo model systems, in which knocking out key enzymes responsible for GPL biosynthesis were found to be embryonically-lethal [10, 11]. In particular, not much is known about the coordination of the key GPL metabolic processes, that is biosynthesis, remodeling, *i.e.* exchange of fatty acid residues, degradation and inter-organelle transport. Such coordination is crucial for preventing a futile competition between synthesis and degradation. In order to get a broad overview, each of these processes will now be discussed in detail.

GPL biosynthetic pathways

Of the three hydroxyls of the glycerol in a lipid molecule, the sn1 and sn2 are esterified with fatty acids that lead to the formation of diacylglycerol (DAG), and this is followed by the formation of phosphatidic acid (PA) through the addition of a phosphate to the third hydroxyl of glycerol (sn3), a reaction that is catalysed by the enzyme diacylglycerol kinase (DAGK) [12]. PA has also been shown to be synthesised *de novo* from glycerol-3-phosphate (G-3-P) through the sequential acylation of the sn1 and sn2 hydroxyl groups of the glycerol via the action of enzymes like Acyl-CoA: glycerol-3-phosphate acyl transferase (GPAT) and lysophosphatidic acid acyl transferase (LPAAT) respectively [13, 14]. An alternative mode of synthesis, through the acylation of dihydroxyacetone-P followed by the subsequent reduction of acyl-dihydroxyacetone-P to lyso-PA also contributes to the PA pool [15, 16]. PA can be considered as the simplest GPL molecule that serves as the precursor for the generation of all the other diverse GPL classes of molecules through two pathways. In one of them, PA is converted to CDP-diacylglycerol (CDP-DG) by the action of CDP-diacylglycerol synthase (CDS), thus causing the formation of PI, PG and CL as the key GPL classes [17]. Through the other pathway, PA-dephosphorylation by the enzyme phosphatidate phosphatase (PAP) leads to the formation of DAG that serves as an intermediate precursor for PC and PE synthesis via the CDP-choline or the CDP-ethanolamine pathway, respectively [18, 19, 20]. It is worth mentioning that an alternate biosynthetic route for PE exists, where it can be derived from PS as the substrate that is mediated by decarboxylation [21, 22]. Finally, PS is produced through a calcium-dependent base-exchange reaction catalysed by the enzyme system PSS1

or PSS2, a process that requires replacement of the existing head group of PC or PE by serine [23, 24, 25].

Regulation of PC biosynthesis

PC is present in mammalian cells at $\approx 45\text{--}55\%$ of all GPLs and is the most abundant class. It has been shown to be synthesised via two pathways: the CDP-choline pathway (Kennedy pathway) in all the tissues or the PEMT (phosphatidylethanolamine N-methyl transferase) pathway in the liver [26, 27, 28].

(1) Kennedy pathway - The CDP-choline pathway consists of three steps. First, choline is phosphorylated to phosphocholine in an ATP -dependent manner by choline kinase (CK- α or CK- β) [29, 30]. Studies have shown that under certain conditions, this might be a rate-limiting step in PC synthesis [31, 32, 33]. Next, the enzyme CTP: phosphocholine cytidylyl-transferase (CT) facilitates the condensation of phosphocholine and CTP thus leading to the production of CDP-choline [34, 35]. There exist two mammalian isoforms of CT (CT- α /CT- β), encoded by Pcyt1a or Pcyt1b respectively [36, 37]. CT- α is a soluble protein present both in the cytoplasm as well as in the nucleus; with the latter containing a nuclear localisation sequence (NLS) [38, 39, 40, 41] while the CT- β variant lacking the NLS [42, 41, 43]. Global deletion of CT- α in mice have shown to result in embryonic lethality [11], while its specific inactivation especially in various organs [44, 45, 46, 47] did not seem to be lethal. In contrast, CT- β knockout mice grew normally, but displayed gonadal deformation thus resulting in sterility [48, 37] and its disruption caused axonal branching impairment [49]. Finally, CDP-choline: 1, 2-diacylglycerol choline phosphotransferase (CPT) catalyses the formation of PC by adding the CDP-choline to a diacylglycerol moiety [50]. In humans, two genes coding for enzymes with CPT activity have been identified *i.e.* CPT1 and CEPT1. CPT1 encodes for a CDP choline specific enzyme while CEPT has been shown to have specificity for both CDP-choline as well as CDP-ethanolamine [51, 52].

(2) PEMT pathway - The PEMT pathway primarily exists in hepatocytes [53]. The enzyme that regulates this pathway is PEMT, an intrinsic membrane protein that catalyses three sequential methylation reactions thus allowing for the conversion of PE into PC [27]. The methyl donor within these reactions is S-adenosylmethionine (SAM). Studies have shown that this liver-restricted pathway contributes to $\approx 30\%$ of the PC synthesised within the liver, under circumstances when there is a limited supply of choline [54, 27]. Studies have suggested that this could be a vital pathway in the process of lipoprotein synthesis since it provides the PC substrate for VLDL formation [55, 56, 57]. PEMT-KO mice survived and grew normally upon knocking out PEMT, however upon being fed a choline-deficient diet, the liver failed causing their death within a span of three days [58].

Phospholipid synthesis

PE biosynthesis - Two alternative pathways exist through which PE could be synthesised in mammalian cells. Of these, the CDP-ethanolamine pathway, one that is analogous to the CDP-choline pathway, consists of three enzymatic steps. Initially, ethanolamine is phosphorylated by ethanolamine kinase (EK1/EK2) in an ATP-dependent fashion, thus allowing for the production of phosphoethanolamine [29, 59, 44]. Next, phosphoethanolamine combines with cytidine triphosphate (CTP) to form CDP-phosphoethanolamine (CDP-EA) catalysed by cytosolic protein CTP: phosphoethanolamine cytidylyl transferase (ET) [60], which is considered to be a rate-limiting step. Studies have shown that the gene coding ET (pcyt2) results in embryonic lethality in mice [61]. Another study has demonstrated that mice heterozygous for pcyt2 lead to an accumulation of fat both in the liver and in the adipose tissue triggered by an increase in lipogenesis along with a reduction in the utilisation of fat as a source of energy [61]. In addition, a study by the Jackowski group, showed that ET KO in mice liver resulted in normal growth, although defects in hepatic lipid metabolism were observed [62]. In the final step, CDP-EA reacts with DAG catalysed by CDP-ethanolamine diacylglycerol ethanolamine phosphotransferase (CEPT1) to yield PE [51, 52]. An alternative pathway occurs in the inner mitochondria membrane (IMM) that produces PE upon carboxylation of PS catalysed by phosphatidylserine decarboxylase (PSD). Such a route of synthesis has been recognised as crucial for the production of PE species containing a polyunsaturated acyl chain at the sn2 position [63, 64]. For the reaction to take place, PS has to be first transported from its site of synthesis to the IMM and this process is known to be the rate-limiting step [65, 66]. Studies have shown that deletion of the gene coding for PSD (pisd) was embryonically lethal while PSD-deficient cells showed fragmented and aberrantly shaped mitochondria thus causing impairment in the mitochondria [10].

PS biosynthesis - PS synthesis takes place in the ER by a base-exchange reaction upon headgroup exchange from PC or PE that is catalysed by the phosphatidylserine synthases, PSS1 and PSS2 [64]. PSS1 has the ability to replace the PC headgroup with serine and in a similar fashion, PSS2 catalyses an analogous reaction with PE as the substrate. Both the enzymes are localised within the ER domains in close association with the mitochondrial membrane (MAM) [67]. Previous studies have shown that over-expression of PSS2 caused PS inhibition while PSS1 over-expression did not have any effect [68]. Disruption of genes encoding PSS1 and PSS2 in mice were shown to cause death in-utero, in contrast mice lacking either one of them did not have any obvious defects [68, 69].

PI biosynthesis - PI synthesis occurs in two steps, primarily by converting PA and CTP into an intermediate molecule, CDP-diacylglycerol (CDP-DAG) through the action of CDP-diacylglycerol synthase (CDS1 or CDS2) [70, 71]. Next, CDP-DAG is condensed with myo-inositol, a reaction catalysed by an ER-associated enzyme, PI synthase (PIS) [72]. Imai and Gershengorn had previously shown that ER and PM isolated from rat pituitary cells

when incubated with exogenous PI caused endogenous PI synthesis by up to 91% and a similar kind of PI synthesis was inhibited in intact cells as well in an increasing order [73]. Other studies indicated that when in COS-7 cells, CDS1 and PIS were over-expressed, their activities increased by 25- and 8- fold respectively, although no significant enhancement in PI synthesis was observed thus not leading to any change in the cellular content of both PI and CDP-diacylglycerol [59]. In terms of the acyl chain composition, PI is quite unique compared to the other GPL classes, with 80% of the pool containing stearic acid at the sn1 position and arachidonic acid at the sn2 position. Usually remodeling of these acyl chains in PI happens after its synthesis. Another unique feature of PI, is that its inositol headgroup contains three hydroxyls at the 3rd, 4th and 5th positions, those that can undergo phosphorylation individually or in combination thus generating seven different phosphorylated derivatives [PI4P, PI3P, PI5P, (PI (4,5) P2), PI (3,5) P2, PI (3,4) P2 (PI (3,4,5) P3)].

PG and CL biosynthesis - PG and CL are synthesised through the same pathway with CL requiring PG as its intermediate molecule. The enzymes required for the synthesis of PG and CL are peripheral membrane proteins localised on the mitochondrial matrix. The first committed step during PG synthesis, is catalysed by PGP synthase (PGPS) through combining G-3-P and CDP-DAG thereby resulting in the synthesis of phosphatidylglycerol phosphate (PGP). PGP next undergoes dephosphorylation through the action of PGP phosphatase (PGPS) leading to the generation of PG [42, 40]. Studies by Ohtsuka et al showed that impairment in the activity of PGPS in CHO cells caused a decrease in the PG content by 90% thus affecting the overall morphology of the mitochondria including its function [74, 75]. An over-expression of PGPS in CHO cells led to an increase in the PG content by a fold change of 2.5, this indicating that it can be a rate-limiting enzyme [76]. Condensation of the fully synthesised PG molecule with that of CDP-DAG catalysed through the action of cardiolipin synthase (CLS) lead to the formation of CL. CL is the signature lipid of mitochondria and is synthesised exclusively in that cellular compartment. Following its biosynthesis, the acyl chains are remodeled in such a manner that it mainly contains linolenic acid amongst other species that are harbored in limited amounts.

Acyl chain remodeling of GPLs

The acyl chains of the various newly synthesised GPL molecules are remodeled mainly through two kinds of de novo pathways. Once synthesised, molecular species typically contain a saturated fatty acid at the sn1 position and a mono- or a di-enoic fatty acid at the sn2 position [77], once they entering a remodeling pathway, either one of the acyl chains or both of them will undergo an exchange reaction for structurally different acyl chains. Typically, a remodeling reaction is catalysed through a number of enzymatic steps those that are mediated by PLAs, lysophospholipid acyl transferases (LPLATs) and transacylases [78, 79, 80]. As mentioned earlier, remodeling takes place through either a combination of PLAs

and acyl transferases while on the other hand it can be also be catalysed through the action of transacylases.

Remodeling through the action of PLAs and acyl transferases - This modeling route encompasses fatty acid incorporation into GPL molecules and is mainly dependent on the availability of a lyso-GPL acceptor pool that is maintained by the continuing action of several PLAs, although many of the key enzymes have not been yet identified. A number of studies in the past decade have implicated a major homeostatic enzyme; iPLA β and in addition also a Ca²⁺ - independent PLA2-gamma (iPLA2 γ) in GPL remodeling [81, 82, 83, 84, 85]. A recent study has also indicated that another key player in this process could be cPLA2 γ [86, 87, 88]. Extensive studies have shown that de novo synthesis constitutes incorporation of fatty acids to the glycerol backbone of GPL molecules at both the positions catalysed by the acyl-CoA: glycerol-3-phosphate (GP) acyl transferase and the acyl-CoA:1-acyl-GP acyl transferase systems [89, 79, 90]. It has been observed that both these enzymatic systems have shown strict fatty acid specificity [91, 92, 93, 94]. Several acyl transferases (LPCATs) contribute to the process of PUFA incorporation at the sn2 position of various acceptor lyso-GPL molecules. A number of LPCATs exist each one with a certain specificity: for example; the LPCAT1 isoform catalyses the incorporation of saturated fatty acids (16:0) into a lyso-PC thus allowing for the formation of a disaturated PC [95, 96]. On the other hand, other isoforms such as LPCAT2 and LPCAT4 have been shown to incorporate fatty acids such as arachidonic acid and linoleic acid respectively [97, 98]. Acyl transferases such as LPCAT3 shows broader substrate specificity towards fatty acids such as 18:2 and 20:4 [97, 99, 100, 101]. During the past year another addition has been made into the LPLAT family although these members do not contain the LPAAT motif. Key enzymes belonging to this category have been shown to be mLPCAT3, mLPCAT4 and mLPEAT1 all of which have the ability to remodel lyso-phospholipids into full blown GPLs through the acylation of 18:1, 18:2 and 20:4 into the vacant position [102].

Remodeling of the acyl chains through the transacylases systems - Such a process is catalysed by either the CoA-dependent or the CoA-independent transacylation reactions. Within these reactions a GPL molecule serves as a donor of an acyl chain while another lyso-GPL acts an acceptor [103, 104]. During the course of such a CoA-dependent transacylation process, specific fatty acyl chains that include 18:0, 18:2 and 20:4 harbored in GPLs, once cleaved are transferred to an lyso-acceptor in the presence of CoA [104]. In contrast, a CoA-independent transacylation reaction causes the transfer of polyunsaturated fatty acids belonging to the C20 and C22 class from a donor GPL to an ether bond containing lyso-GPL thus triggering the formation of alkyl and alkenyl GPLs. Such a reaction takes place in the absence of any cofactors such as CoA [105, 106, 107].

The GPL degradation pathway - Several pieces of evidence point out to the fact that PLAs are the key players in regulating the GPL degradation pathway. Several enzymes, that include

PLA1, PLA2, PLB, PLC and PLD, have been shown to actively hydrolyse GPL substrate molecules [108, 109, 110]. Classification of these enzymes have been mainly based on their site of attack on the GPL, for example: PLA1 cleaves the 1-acyl ester while the 2-acyl ester is removed by a PLA2 [111]. A PLB has the ability to simultaneously cleave both the acyl chains [112]. A PLC has the ability to cleave the glycerophosphate bond and a PLD is selective for the base group [113], therefore both these variants are known as phosphodiesterases. Finally, there is a family of enzymes known as lyso-PLAs, that have the ability to remove an existing mono-acyl chain from a lyso-GPL molecule [114, 115].

Molecular structure and biophysics of phospholipid molecules

Phospholipid molecules are fundamental for the described pathways, and they have the ability to form several structures, such as lamellar ones like in the lipid bilayer. This latter has a critical importance in nature, since it is the scaffold of the "cell wall", enclosing the cytoplasm and organelles, and at the same time it mediates the exchanges of information and molecules (for instance nutrients) with the external environment. Phospholipids are amphiphilic molecule, constituted of a polar moiety also called polar head, and hydrophobic chains as shown in figure 1.1. Polar head regions have the tendency to interact with polar molecules such as

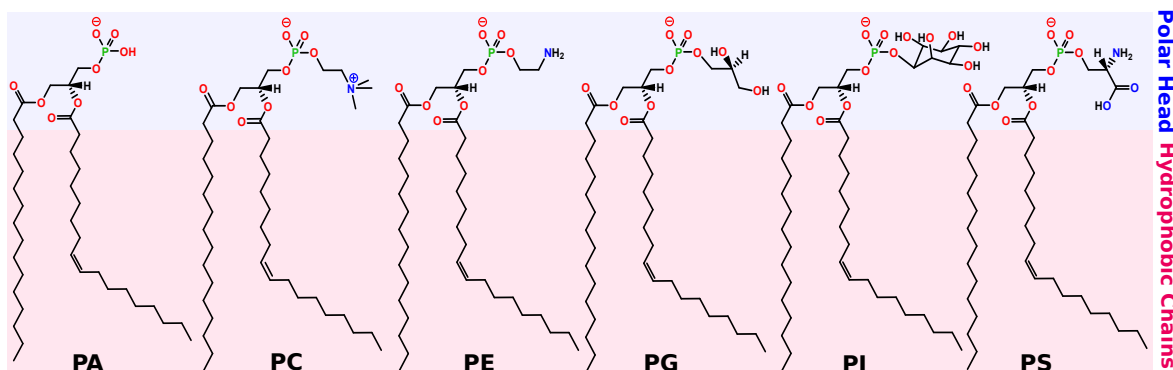


FIGURE 1.1: Various classes of phospholipid molecules. The acyl chain displayed are 16:0 and 18:1 for the sn1 and sn2 respectively.

water molecules, whereas acyl chains interact with apolar molecules, where "like dissolves like". These physical properties lead to the rearrangement of phospholipid molecules when are placed in an aqueous environment. In fact, lipids, depending on their structural properties, can aggregate adopting different conformations, from simple to very complex organisations [116]. Generally, taking into consideration a lipid molecule, if its acyl chain is long enough, above a certain concentration in an aqueous solution, it starts forming structures. This concentration depends on the solubility of the lipid taken into consideration in water, and is known as "critical micellar concentration", CMC. When the lipid concentration keeps increasing in an aqueous solution, above the CMC the number of free lipid molecules in the solution start to plateau (at a maximum concentration represented by the CMC), because of the formation of micelles (which concentration starts to increase at the CMC). This is an equilibrium process,

with some molecules leaving and others forming the micellar structure. As mentioned earlier, similar molecules have the tendency to interact among themselves. Additionally, since lipids are amphiphilic molecules, they can interact with both polar and apolar molecules. For instance, in an emulsion, lipids move preferentially to the interface, where their polar moiety interacts with water whereas the apolar moiety with the hydrophobic molecules, leading to the stabilisation of the emulsion. Lipids can interact also between them, and as mentioned before, they can rearrange themselves into different complex structures. Interactions between polar heads and water molecules is driven by different forces, such as electrostatic repulsion and attraction, dipole dipole interactions, etc. Acyl chains on the other hand, are subjected to hydrophobic interactions, driven by van der Waals forces. Specifically, the driving force of the process is related to the entropy of the system, where higher entropy is generated when acyl chains are in interaction between them compared to their interaction with water molecules. In fact, when a hydrophobe (general hydrophobic molecule) is placed in water, hydrogen bonds that exist between water molecules are partially broken, in order to generate space for the hydrophobe added [117]. This is per-se an endoergonic reaction, since energy is required to break the bonds. Those water molecules whose hydrogen bonds were disrupted by the hydrophobe create new hydrogen bonds, forming an ice-like cage around the hydrophobe (clathrate). This is caused by the inability of the hydrophobe to form hydrogen bonds. This configuration makes the system highly ordered, with a decrease of the total entropy, which is unfavorable. Therefore, there is the tendency of hydrophobes to interact between each other, in order to reduce as much as possible the contact with water. Consequently, acyl chains in phospholipid molecules interact with each other, driving the formation of structures, where polar head regions segregate the hydrophobic part from water.

The form and the dimensions of the structures formed by lipids, are directly connected with their structural properties. Lipid polymorphism in biophysics is defined as the ability of lipids to aggregate in different ways, leading to different structures known as "lipid phases". The basic structures forming the phases can be divided mainly in 3 groups: (1) spheres or micelles, (2) cylinders and finally (3) bilayers. The preference of a certain lipid to form one of these structures depends on its own molecular structure. For instance, lipids with a large polar head region and one acyl chain, are characterised by a conical shape, where they have the tendency to form spherical or micellar structures in aqueous solution. Differently, the majority of phospholipid molecules have a cylindrical shape, especially PC which is the most abundant class within mammalian plasma membranes. This shape confers the preference to form a lamellar structure, such as the lipid bilayer.

An interesting way to evaluate the propensity of a molecule to form one of the 3 structures mentioned earlier, is through the calculation of η . Considering the value N as the number of molecules constituting the structure, L the length of the lipid, S the surface of the structure and v the volume of the lipid, the following relations can be obtained:

$$V = v \cdot N \quad (1.1)$$

$$A_{lipid} = \frac{S}{N} \quad (1.2)$$

Next, the parameter η can be calculated as shown in equation 1.3.

$$\eta = \frac{v}{a \cdot L} \quad (1.3)$$

The parameter η reflects the propensity of the lipid under consideration to form a specific structure, as displayed in the sketch in figure 1.2. From those basic structures, different lipid

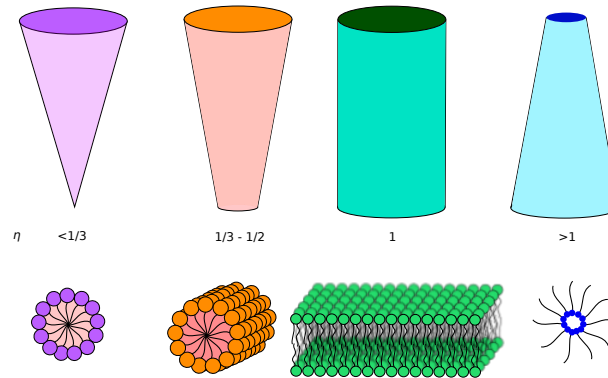


FIGURE 1.2: Sketch representing different shape that a lipid can assume, and their preferential structure when they are added into an aqueous solution.

phases can be distinguished, such as: (1) micelles, (2) lamellar structures (single bilayer, stacked bilayers, vesicles), (3) hexagonal phases (stack of cylinders) and finally, the most complex and variegate phase class is the (4) cubic phase.

The majority of the phospholipid molecules have usually an η equal ≈ 1 , leading to their preferential formation of lamellar structures, such as bilayers. In fact, they are fundamental for the formation and maintenance of the correct structure of the plasma membrane. Micellar structures can be formed for instance by the fatty acids and lysophospholipids, due to their conical shape. Unsaturated PE, CL and PA, can form the hexagonal phases, since (especially CL) they have an inverse conical shape, leading to an inverse micellar structure ($\eta > 1$), and eventually to the hexagonal phase. These characteristics were discussed in detail by [118].

Lipid membranes are constituted by a multitude of lipids, as already discussed. The different surface charge on the membrane is critical as well as its composition. The existence of different lipid molecules forming a lipid membrane, is explained by the fact that different lipids provide different structural and chemical properties to the membrane. In fact, it is known from previous studies [119, 120, 121, 122] that the addition of PC phospholipid molecules in a system composed by PE molecules transforms the lipid phase from hexagonal to lamellar, due to the more cylindrical shape of PC [123]. Also cholesterol plays a key role on the membrane stability. In lipid membranes composed of PC molecules, it causes higher membrane packing and less permeability [124]. In the case of a model membrane composed of PE stabilised with saturated acyl chains containing PC molecules, cholesterol acts as stabiliser of the bilayer [123]. If the PC molecules are unsaturated in the same system,

the presence of cholesterol has a positively disrupting action (with the formation of hexagonal phases) where the presence of SM brings back the system to a bilayer structure [123]. In fact, it seems that SM is a critical lipid for the membrane stability when it contains high amounts of cholesterol. PA and CL, also have a non-bilayer configuration, especially in response to the presence of cations such as Ca^{2+} . In fact it was found that CL forms a lamellar phase in absence of Ca^{2+} . Upon addition of Ca^{2+} , it forms an hexagonal phase, similarly to what happens to PA lipids [124].

Different lipid ratios into a membrane lead to different structural and physical properties. For instance, CL is mainly present in the inner mitochondrial membrane, where the negative curvatures of the mitochondrial cristae are formed [125]. Usually CL in mitochondria has a higher number of unsaturations, causing its conical shape. Some structures, such as lipid rafts, are critical for the function and the stability of some membrane proteins and for the flip-flop process. Some of the non-bilayer structures are fundamental for membrane - membrane fusion mechanisms, including vesicles exo and endocytosis [118]. The bilayer phase is the most abundant phase within living cells, but the hexagonal phase is also important, especially for the fusion of membranes. Inverse micelles can be also formed during the flip-flop process [118]. In summary, the several lipids that form the cell membranes have different structural and chemical functions. Particularly, their self assembly (in addition to other components such as proteins) leads to structures that are critical for fusion, signaling and other fundamentals cell functions. These functions are directly correlated to the molecular structure as well as the chemical properties of those lipids, that could explain why the membrane is composed of such a high variability of lipid molecules.

Functions of the various GPL classes

GPL molecules, apart from serving as structural components of membranes, also do carry out other specialised functions. Each molecular species within a GPL class has the ability to regulate various biological processes, have a role to play in signal transduction and can also help mediate association with certain proteins within the membrane. For example, lysophosphatidic acid can act as a potent mitogen and several molecular species that harbor polyunsaturated fatty acids such as arachidonic acid (the precursor of prostaglandins and other leukotrienes), are said to be involved in cellular signaling processes. Listed below are the functions of the various classes of GPLs.

Functions of PC and PE - PC and PE classes of GPLs are the most abundant ones in all biological membranes. PC and PE majorly contribute to the structure of membranes and also act as substrates for PLAs [126]. Both these classes of GPLs harbor a wide range of polyunsaturated acyl chains (for example: arachidonyl residues) in their sn2 positions which can be cleaved upon the action of PLAs [127, 128] which lends to the idea that such lipids have other roles to play apart from being physical components of the membrane. It has been observed that within the membranes of some of the cellular organelles such as the ER, the

balance of PC and PE is crucial, since a reduction in a ratio between these two lipid classes leads to a loss in the membrane integrity caused by bilayer stress. Also, it has been noticed that such deviations in the cellular PC/PE ratios can influence energy metabolism within the various tissues. In addition, the relative abundance of PC/PE can have an effect on the size and dynamics of lipid droplets. Evidence also shows that PC plays a key role in gene regulation and the homeostatic control of serum glucose concentration [129, 130]. All these experiments provide evidence that PCs and PEs are not only involved in directing the physical properties within mammalian membranes but also has a key role in a number of fundamental metabolic activities in a living organism.

Function of PS - PS represents 10% of the total GPL content in cells and is negatively charged. It contributes to the charge of the inner leaflet of the plasma membrane [131, 132]. Such a property allows quite a number of signaling proteins that possess positively charged motifs to be attached to the plasma membrane. Usually, PS is enriched in the cytosolic leaflet of the plasma membrane that gets exposed to the outer leaflet which is a critical signal leading to the removal of damaged or apoptotic cells by macrophages. Translocation of the PS from the inner to the outer leaflet is catalysed through the action of scramblases. A cell upon entering the apoptotic cycle, triggers activation of caspases that are proteases. These caspases inactivate the ATP-dependent flippases that normally keep the PS restricted to the inner leaflet and simultaneously activate scramblases thereby irreversibly exposing PS to the outer leaflet. Further, PS has also been found in the inner leaflets of intracellular organelles of late endosomes where its function has not been completely elucidated [133]. Finally, PS participates in a wide range of physiological processes that include the coagulation cascade, cell signaling, endocytosis, plate activation and clearance of apoptotic cells [131].

Function of PI - PIs are distributed universally across the cellular membranes, they make up only a small percentage (10 -20%) of the total cellular GPL content (depending on the cell type and tissue) and they are mainly abundant within the inner leaflet of the plasma membrane [134]. ER is considered to be the site of synthesis of PI and the enzymes responsible for its production are PI synthase and CDP-DG synthase, both of which are ER-localised. Once synthesised, PI is transferred from the ER to the various other cellular organelles including the Golgi complex and the PM through a process that is mediated by PI-transfer proteins (PITP) [135, 136] or through vesicular trafficking [137]. Another critical function of PI is that it provides a substrate for causing the synthesis of its phosphorylated derivatives, (PI3Ps) in early endosomes and (PI4Ps) in the Golgi complex, PM, late and early endosomes. Phosphoinositides result upon the phosphorylation of any of the five hydroxyl groups one at a time or in a combination leading to the formation of seven variants in total. PIPs are considered as second messengers and have been shown to play a key role in cellular signaling thus having a strong physical impact on cellular membranes [138, 139]. Also, studies have shown that PIPs have the ability to recruit and activate cytosolic proteins to membranes.

Functions of PG - Both PG and CL are synthesised in the mitochondria by using CDP-DAG through a concerted pathway in the IMM. PG, is an anionic GPL present in mammalian membranes in low amounts and comprises about 1-2% of the total GPL content. Therefore, PG is not considered to be a major structural GPL molecule. Since, PG has a net negative charge, therefore it introduces negative charge onto the surface of the membrane and also to the lipid-protein interface. It's the second most abundant lipid in lung surfactant (about 5-17% of the total lipid content) apart from PC (which constitutes 80%) which helps stabilise type II alveolar structures during the breathing process thereby contributing to the innate immune response.

Functions of CL - CL (also known as diphosphatidylglycerol) is localised to the inner mitochondrial membrane (IMM) and is essential for maintaining the mitochondrial membrane architecture. It constitutes for 20% of the total lipid composition in the IMM. It is crucial for regulating several cellular processes those that involve production of ATP, signaling and dynamics and maintaining the morphology of the mitochondria. It is a well-known that CL has a distinctive shape defined through its four acyl chains. The unique lipid can help organise highly-curved regions within mitochondrial membrane bilayers which is highly convoluted thereby causing an increase in the total surface area leading to the formation of its characteristic cristae. The oxidative phosphorylation process is central for ATP production. Within this respiratory chain system, there are four major protein complexes to which CL is bound thereby allowing for their stability within the IMM. Although CL is recognised as a GPL that has no ability to form bilayer systems but it could be possible that it plays a major role in stabilizing and accommodating a number of transmembrane proteins within the membrane bilayers. Another well feature of CL, is that some of its molecular species contain unsaturated acyl chains (C18:2 n-6) thus making them susceptible to oxidative damage by ROS due to the presence of the unsaturated acyl chains. ROS susceptibility leads to the formation of oxidised CL that favors for the release of cytochrome c into the cytosolic region triggering apoptosis. Mitochondrial damage has been shown to be signaled through externalisation of CL into the outer mitochondrial membrane (OMM). Another key role that CL plays in It has also been deduced that CL plays a vital role in the process of regulating mitochondrial fragmentation and fusion that takes places in response to cellular demand.

GPL homeostasis maintained through coordination of synthesis and degradation processes

Maintenance of the process of GPL homeostasis in a mammalian cell is a task rather difficult to understand given the complexities of the metabolic processes involved, and also given the involvement of several thousands of molecular species. Indeed, very little is known on the precise coordination of GPL biosynthesis and degradation in maintaining GPL homeostasis. It has become quite obvious that selective degradation plays a key role, albeit not much is known on the enzymes involved in these processes. A coordination between the biosynthetic

and degradation pathways is known to be essential as to avoid a futile competition between them. Such coordination is key for maintaining homeostasis as it has been shown from studies demonstrating that triggering an increase in the synthesis of a GPL molecule leads to a proportional increase in its degradation. For example, in one of the studies, an over-expression of the enzyme, cytidylyl-transferase (CT) in HeLa cells caused an increase in the synthesis of PC by 4-5 fold while no significant increase in the PC content was observed since the deacylation of the synthesised PC took place at a similar rate [140, 141]. Analogous results were observed for PS and PE [142, 143]. On the other hand, inhibiting the synthesis of a GPL class leads to an immediate inhibition of its degradation process which again proves that these processes are key to maintain GPL homeostasis. This is proven by the fact that upon mutating the rate-limiting enzyme ethanolamine phosphotransferase (EPT), the synthesis of PE was inhibited, and therefore a compensation effect in the cell was seen through a reduced degradation of the PE content thus again helping maintain homeostasis [144]. All such experimental data point to the fact that GPL synthesis and degradation are coordinated, and provide us with strong evidence that mammalian cells do harbor specific PLAs that have a key role to play in GPL homeostasis processes. Albeit, having proved this point, there is not much knowledge existing on the major players in these processes. There is some data emerging that there is a possibility that some of the members of the Ca^{2+} -independent PLA (iPLA) subfamily, particularly iPLA β and iPLA δ could be involved in this process. [145, 146, 147, 148].

1.1.2 Phospholipases: classification and state of art of the reaction mechanism

Classification of phospholipases

PLAs are acyl hydrolases that cleave the various ester bonds in GPLs. They are ubiquitous in nature, with them playing very diverse roles from aggression in snake venom to signal transduction, production of lipid mediators and membrane lipid homeostasis. There are a number of PLAs and each one of them varies from one another in their site of action, their physiological function and in terms of their regulation. PLAs are in general classified into various subfamilies mainly based on their site of attack on the GPL molecule. Qualifying letters (A, B, C and D) are employed to differentiate each of these enzymes from one another thus helping indicate the target of the specific bond on the GPL molecule. A phospholipase A1 (PLA1) cleaves the acyl chain at the sn1 position of the glycerol moiety in a GPL molecule, while a phospholipase A2 (PLA2) removes the sn2 positioned acyl chain. The action of PLA1 and PLA2 results in the accumulation of free fatty acids along with 2-acyl lysophospholipid (LPL) or 1-acyl LPL, respectively. The resulting LPL pool acts as a substrate reservoir that can be cleaved by enzymes termed lysophospholipases (lyso-PLA). Some PLAs have the ability to hydrolyse both the acyl chains simultaneously and these are termed as phospholipase B (PLA-B). Over the past decade, studies have shown that LPLs generated through PLA-mediated catalysis, harbor a wide range of biological activities, that are mediated through the G-protein coupled receptor (GPCR) family of receptors [149].

Phospholipase A1 - The PLA1 group of enzymes are acyl hydrolases that have the ability to cleave an acyl chain from the sn1 position of an intact GPL molecule mediating the formation of a free fatty acid and a sn2 lyso-GPL molecule [150]. Over the past few decades, several studies have been carried out to help understand the role of various members of the PLA2 superfamily (specifically the cytoplasmic ones) in specific biological functions such as signaling cascades and membrane lipid homeostasis. In contrast, the limited studies carried out on the members of PLA1, tell us that they might not have any key role to play in membrane remodeling or membrane GPL homeostasis. On the contrary, members of the PLA1 family have been implicated in the production of bioactive lyso-PL molecules and also that some of these members play out as virulence factors [151, 152]. Further, PLA1 activities have been detected both intra- and extracellularly depicting that they are well conserved in higher eukaryotes. Several PLA1 members of the mammalian extracellular kind have been observed to exhibit lipase activity thus allowing for the hydrolysis of triacylglycerol thereby contributing to the absorption of the released free fatty acids into the intestinal tract and tissues. Of the extracellular PLA1 enzymes identified, a number of them have been found to be specific towards a certain GPL headgroup. For example; the (PS)-specific PLA1, which is one of the first extra-cellular PLA1 to have been characterised, preferentially cleaves PS thus serving to produce the lysophospholipid mediator: lysophosphatidylserine (Lyso-PS). Similarly, the membrane associated phosphatidic acid selective-PLA1 cleaves the sn1 chain from a PA, thus producing a Lyso-PA. On the other hand, enzymes that include mPA-PLA1a and mPA-PLA1b have also shown selectivity towards sn1 positioned acyl chained-PA, thus making them authentic members of the PLA1 family of enzymes. Because of such an sn1 regio-specificity that is displayed by PLA1s causing for the formation of 2-acyl-lyso-GPL molecules, they are thought to be involved in signaling functions. Such a phenomenon has been evidenced in the case of PS-PLA1 that has the ability to stimulate histamine release from rat peritoneal mast cells in the presence of apoptotic cells [153] which has been attributed to the generation of 2-acyl-1lyso-PS (LPS) that acts through its receptor – GPR34 [154, 155]. Studies involving knockout mice and through human genetic diseases have helped reveal the pathophysiological roles of PLA1s but there is still a lot that needs to be understood regarding their biochemical properties, including their in vivo substrate preferences and the factors that regulate their activities.

Phospholipase A2 - The mammalian phospholipase A2 (PLA2) family is comprised of six types of diverse enzymes: GIV PLA2 [cytosolic PLA2 (cPLA2)], GVI PLA2 [calcium-independent PLA2 (iPLA2)], GVII and GVIII PLA2 [platelet-activating factor-acetyl hydrolases (PAF-AHs)], GXV PLA2 (lysosomal PLA2), GXVI PLA2 (adipose PLA2), and several groups of secreted PLA2 (sPLA2). Each one of them are structurally different from one another and in addition have varying catalytic mechanisms and modes of action. Taking into account these factors PLA2s are broadly classified into (a) Secretory PLA2s, (b) Ca²⁺-dependent PLA2s and (c) Ca²⁺-independent PLA2s.

Secretory PLA2s - sPLA2s are members of a group of low molecular weight enzymes that require Ca^{2+} at mM concentrations in order to regulate their activity. In total, around 11 various mammalian isoforms have been identified [156, 157, 158], in addition to a few other sPLA2s that have been observed in venoms [159, 160, 161, 162]. But of all the various sPLA2s found, the ones belonging to the I, II, V and X groups have been considered as the conventional ones since they are very closely related and share a highly conserved (a) catalytic domain (His-Asp dyad), (b) a Ca^{2+} -binding loop (XCGXGG), and (c) 6-8 disulfide bridges that confer a high degree of stability to the PLA [163]. On the other hand, the sPLA2s belonging to groups III and XII are structurally different from the conventional ones and with their structures having been deduced from their protein sequences [164, 165, 166]. Usually such sPLA2s have a molecular weight ranging between ≈ 13 to 19 kDa within which they all contain a ≈ 15 Å deep active site that allows for the accommodation of a GPL molecule that is inserted in an orientation with the ester adjacent to the catalytic residues [157, 167, 168, 169, 170]. In the presence of high concentrations of Ca^{2+} , sPLA2s show the ability of hydrolysing membrane-bound GPL molecules, a phenomenon called "interfacial activation" [171, 172]. Studies have shown that interfacial activation is caused by the substrate undergoing a specific conformation [171], leading to its aggregated form that could be a micellar or a bilayer one [171, 173] which appear to be the best macrosubstrate for the enzymes to work [174, 175]. As shown earlier by Qin et al through modeling studies, sPLA2s favor the hopping mechanism in the presence of zwitterionic membrane bilayers [176]. For members of the Groups IB, IIA and X, crystal structures both in the presence of an analogue or an inhibitor have been solved [163, 177, 178]. Through all such studies, it is assumed that the His-Asp dyad is crucial for the sPLA2-catalysed acyl chain degradation to be initiated. Catalysis takes place first through the removal of a proton coming from a H_2O molecule, that is followed by a nucleophilic attack on the carbonyl-carbon at the ester bond of the sn2 positioned acyl chain, leading to the rate-limiting formation of a putative tetrahedral intermediate. In the next step, the sn2 oxygen undergoes protonation that is mediated through His48 in concert with the productive collapse of the tetrahedral intermediate, thus leading to the formation of a free fatty acid and a lyso-GPL [161]. sPLA2 have been shown to carry out a wide range of biological functions including dietary GPL digestion [IB] [179, 180], host defense against parasitic, bacterial and viral infections [IIA, V, X, XII] [157] and eicosanoid mediated inflammation [X] [181]. There is no evidence from any of the earlier studies that sPLA2s are involved in GPL homeostasis.

Ca^{2+} dependent PLA2s - The cPLA family is constituted by six paralogs (PLA2GIVA, B, C, D, E and F) referred to as cPLA2 α , β , γ , δ , ϵ and ζ respectively and they all share the lipase consensus sequence GXSGS [86, 182, 183, 184]. Each of these shares only about 30% homology and they also have differences from one another in terms of their enzymatic properties, tissue expression and subcellular localisations. The C2 domain that facilitates membrane binding is also conserved in all the members except in cPLA2 γ which is unique in that it exhibits Ca^{2+} -independent PLA2 activity [86]. cPLA2s utilise the Ser-Asp active site for catalysis, unlike the sPLA2s that involves a His residue [185]. Several studies have

shown that amongst all the cytosolic group of enzymes, it is the cPLA2 α isoform that exhibits preference for hydrolysis of the arachidonic acid containing GPL substrates in response to cellular stimulation [186, 187, 188]. Further, other studies have shown that members of this group also possess relative PLA1, lyso-PLA as well as transacylase activities [189]. Although PLA2s have been under focus over the past few decades, there is not much known on the in vivo function of the various cPLA2 isoforms except for the cPLA2 α isoform. Since, cPLA2 α is the most well studied enzyme of this family, that is discuss much about it. The cPLA2 α enzyme which is ubiquitous in nature, is a 749 amino acid containing enzyme with a molecular weight of 85.2 kDa [190, 191]. It has an established role in initiating the production of lipid mediators. Also, emerging studies that employed cultured cells have shown that cPLA2 α is required for regulating junction proteins [192]. It contains two major domains (*i*) an N-terminal Ca²⁺-dependent C2 domain (CaLB), essential for the initial association of the enzyme with a lipid bilayer [193, 194, 195] in response to increasing intracellular Ca²⁺ and (*ii*) a catalytic domain that contains a hydrolase core and a novel cap region within which a lid exists, that has to move aside for a GPL molecule to enter the active site cavity of cPLA2 α [196, 197]. Apart from Ca²⁺, cPLA2 α activity has also been shown to be regulated through phosphorylation on its multiple serine residues [198] by MAPKs and Ca²⁺/calmodulin-dependent protein kinase II [199, 200, 201, 202]. cPLA2 deficiency has been shown to have led to a wide range of physiological diseases such as arthritis, inflammatory bone resorption, pulmonary fibrosis acute respiratory distress syndrome, autoimmune encephalomyelitis and diabetes [203, 204, 205, 206, 207].

On the other hand, molecular characterisations of two other major Ca²⁺ independent PLA2s that include cPLA2 β and cPLA2 γ have been carried out extensively. cPLA2 β is about 100 kDa and is a 1012-amino acid polypeptide which has a homology similar to cPLA2 α . It has a markedly lesser affinity for the sn2 position in a GPL molecule [208, 209] (Song C et al, Ghosh M et al, 2006). Usually, cPLA2 β is found to be constitutively bound to a membrane under unstimulated conditions localizing to the mitochondria or early endosomes. It has been shown to exhibit activity against 16:0/20:4-PE as well as a low level of lyso activity but then did not show any kind of preference for PC molecules. In contrast, although cPLA2 γ a 541 amino acid - membrane-associated protein shares identity with cPLA2 α in terms of potential critical amino acids within the catalytic acids, it still misses a few key elements that are necessary for the regulation of its activity. It is to be highlighted that this enzyme contains two consensus motifs for lipid modification, one a prenylation motif (-CCLA) at its C-terminus and also a myristoylation site at its N-terminus. cPLA2 γ has been shown to have preference for arachidonic acid that is positioned at the sn2 position indicating that it has a strong PLA2 activity. Interestingly, studies have demonstrated that it also can behave as a PLA1, since the fatty acid at the sn1 position was also cleaved at the same time.

Ca²⁺ independent PLAs (iPLAs) - This subfamily of PLAs belongs to the Group VI PLAs and they are also known as patatin-like PLAs. Seven members have been identified in this group and they include iPLA β [VIA-1 and -2] (PLA2GVIA, PLA2G6, PNPLA9), iPLA2 γ (PLA2GVIB, PNPLA8), iPLA2 δ (PLA2GVIC, NTE, PNPLA6), iPLA2 ϵ (PLA2GVID, Adiponutrin, PNPLA3), iPLA2 ζ (PLA2GVIE, Desnutrin, ATGL, PNPLA2), iPLA2 η (PLA2GVIF, GS2). Other recent additions have been the isoforms of (iPLA2 φ , iPLA2 ι , and iPLA2 κ), however not much is known regarding their activities or mode of action [84, 87, 210, 211, 212, 213]. Substrate hydrolysis by these group of enzymes is catalysed through a catalytic dyad (Ser-Asp) that resides within the active site, further Ca²⁺ is not required for activity to be regulated [197, 214, 145]. For almost of these iPLAs, no crystal structure exists therefore very little information is available. During the recent years, there has been a lot of progress in understanding isoforms specifically those of, iPLA β and iPLA2 γ both of which possess a long N-terminal domain that is thought to be involved in protein-protein interaction. It is to be highlighted that both these variants: iPLA β and iPLA2 γ are considered to be true PLAs, while the remaining isoforms harbor lipase and transacylase activities [215, 216, 213, 217], which is the reason why a great amount of investigations have been carried out in order to understand these two PLAs. Specially, the Group VIA PLA (iPLA β) has been under focus since a few years now. Its gene codes for at least 5 different splice variants (VIA-1, VIA-2, VIA-3, VIA-Ankyrin1 and VIAAnkyrin2) of which the first two are the active variants and manifest both PLA1 and PLA2 as well as lyso-PLA and transacylase activities [216, 215, 213, 217]. The active variant iPLA β is about 85 kDa and is of 752 amino acids length. Its sequence harbors various stretches corresponding to 7 ankyrin repeats, a 10-40 amino acids residue spacer linkage and a catalytic domain that contains the GTSTG stretch [218, 36]. In addition, iPLA β has also been found to contain an ATP binding consensus motif (GGGVKG) which is important for ATP to regulate the activity of the protein. Apart from that, other stretches exist in the form of an N-terminal caspase-3 cleavage site (DVTD), a putative bipartite nuclear localisation sequence (KREFGEHTKMTDVKKPK) and a calmodulin-binding domain (AWSEMVGIQYFR) which allow it to form a signaling complex with CaMKII β [216, 219, 220, 221, 222, 223, 224, 225]. It is known that iPLAs mediate interfacial catalysis through a scooting mode [197] and it carries out hydrolysis of the GPL molecule through the formation of an acyl-enzyme intermediate complex just as in the case of sPLA2, but the difference here is that serine acts as a nucleophile after aspartic acid abstracts a proton [197]. Few recent studies have strongly implicated iPLAs in maintaining GPL homeostasis as well as membrane remodeling [226]. Other studies have shown the involvement of the members of this subfamily of PLAs in major cellular events that include apoptosis, cellular proliferation, insulin secretion and bone formation amongst several others [227, 227, 228, 229, 230]. Also these enzymes have been shown to play a major role in neurological disorders such as infantile neuroaxonal dystrophy (INAD), multiple sclerosis, Alzheimer's and also hypertensive heart failure [231, 232].

Factors that regulate the activity of PLAs

PLA mediated hydrolysis has been the subject of several studies over half a century now. Through these studies it has been well emphasised that a PLA first associates peripherally with a macrosubstrate surface, following which the GPL molecule starts moving upwards and starts embedding within the active site cavity. Upon such an interaction, one of the acyl chains are cleaved through the hydrolysis of the ester bond that causes the release of a free fatty acid and a lyso-GPL molecule from the enzyme [233, 111, 234]. Based on this model, it can be considered that the key determinants of substrate specificity of PLAs are (a) the ability of the GPL molecule to efflux from a macrosubstrate within the periphery of the enzyme and (b) active site accommodation of the GPL acyl chain within the active site of an enzyme. All these steps are represented in the sketch displayed in figure 1.3. All the assumptions were based on studies that were focused on understanding the key principles that regulated the activity of PLA2s.

Substrate efflux from lipid bilayers - For a GPL molecule to be hydrolysed, it will need to be extracted from the membrane before it can reach the active site in the enzyme. This is based on the assumption that since a soluble PLA2 does not have the ability to penetrate a membrane and usually acts only at the interface, the need arises for the molecule to efflux. Such a process involves an upward movement of the substrate molecule from the membrane towards the active site. Investigation through employing cross-linkable and polymerised GPLs as well as MD simulations have revealed the importance of efflux propensity in influencing the substrate specificity of a PLA2 [235]. A number of studies have evidenced that increasing acyl chain length has an inhibitory effect on PLA2-mediated hydrolysis. Although there is little understanding about the underlying mechanism behind this phenomenon, it has been speculated that the hydrolysis rate is inversely proportional to the acyl chain length. This could lead to the fact that higher saturated chain lengths possess higher hydrophobic interactions between other lipid molecules, leading to the need of higher energy to be pulled away from the membrane. All this suggests that efflux propensity could be rate-limiting step in PLA-mediated hydrolysis of GPL molecules.

Active site accommodation of a GPL molecule - Crystallographic data obtained from studies on cobra PLA2 complexed with the non-hydrolysable analogue 1-octyl, 2-heptyl suggested that the sn2 chain had a tighter interaction over the sn1 chain. Similarly, NMR studies on the same enzyme complexed with a truncated non-hydrolyzable PC analogue showed a tighter interaction of the sn2 with the enzyme. These results highlight the importance of acyl chain accommodation of the GPL molecule within the active site of PLA2s. Also, recent studies on factors affecting the substrate specificity of various PLA2s showed that active site accommodation of substrate molecules is a key factor. Upon employing a complex mixture containing PC molecules, each varying from another in terms of the acyl chain length or degree of unsaturation, it was observed that only a selected few species were

hydrolysed, highlighting their ability to fit well into the substrate binding cavities in order to accommodate the acyl chain double bonds. For example, an arachidonic acid containing PC species at the sn2 position seems to fit well within the active site of a PLA2 from bee venom in comparison to other species, thus indicating that the lipid binding cavity in this enzyme can well accommodate a molecule that harbors $\Delta 5$ and/or $\Delta 8$ double bonds.

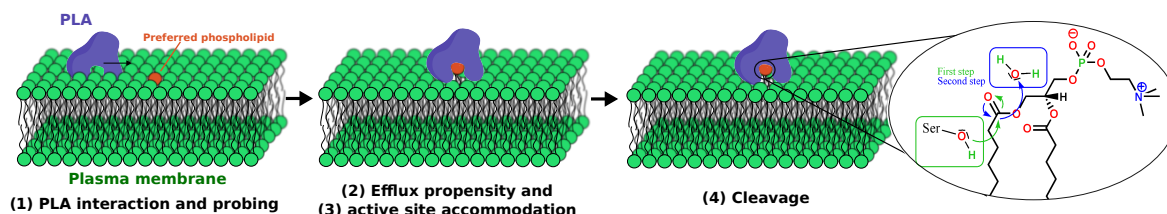


FIGURE 1.3: Steps of the hydrolysis reaction mediated by PLAs

1.1.3 Similarities between lipases and PLA1s

A conspicuous amount of research in the past has demonstrated that PLA1s are evolutionary correlated to the group of lipases [236]. Lipases have been shown to preferentially cleave fatty acyl chains from neutral lipids such as tri-glycerides, di-glycerides and mono-glycerides (TAG, DAG and MAG respectively). In addition, some works demonstrated that some of these lipases exhibit affinity for the sn-1 acyl chain, for example the enzyme, pancreatic lipase [237, 238]. Additionally, within the lipase family of enzymes, the three-dimensional structure is conserved, although the amino acid sequence can differ from one another [236] (see figure 1.4, where the sequence between the two lipases displayed is not conserved). In a functional enzyme, few crucial structures exist, where the most important ones consist of the beta 9 and 5 loops, and the lid [239].

Based on the tertiary structures and sequence analysis of these extracellular lipases, it has been proposed that they contain certain crucial structures those that determine their substrate specificity, thereby causing for proper deacylation of the fatty acid. Such structures include surface loops known as lids and the loops, $\beta 5$ and $\beta 9$ [239]. Studies have shown that enzymes with a short lid and a short β loop (PS-PLA1, mPA-PLA1 α and mPA-PLA1 β) harbour PLA1 activity while enzymes with a short lid and a long β loop (endothelial lipase and PLRP2) exhibit both PLA1 and TAG lipase activities [237]. On the other hand, enzymes containing a long lid and a long β loop only display affinity for TAGs (pancreatic lipase and lipoprotein lipase) [237].

The $\beta 9$ loop shows a certain importance to probe the water/lipids interface, in order to activate the enzyme, interacting with the polar head region of the lipids laying on the lipid membrane. $\beta 5$ loop contains the chemical groups constituting the oxyanion hole, fundamental for the stabilization of the *transition state* during the cleavage [239]. Finally, the lid, which is a structure covering the active site pocket when the interface is not found, in order to maintain the enzyme in solution, through hiding the most hydrophobic part of the protein. In fact, when the enzyme finds a proper interface, usually a structural variation occurs, mediated by

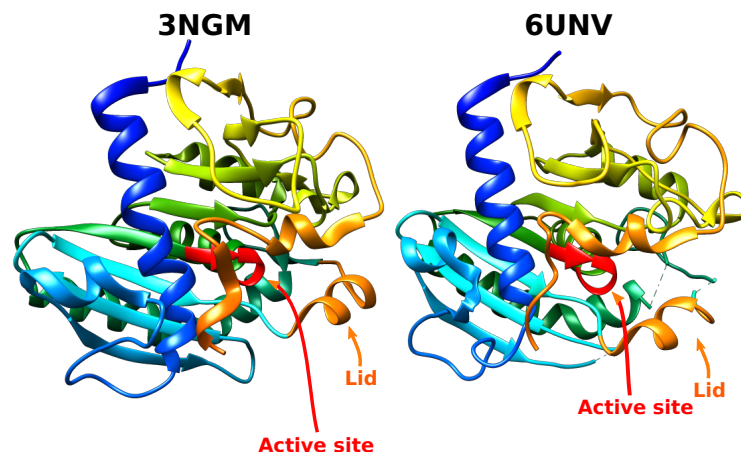


FIGURE 1.4: The structure of two different lipases, where 3NGM is from the organism *Gibberella zeae*, whereas 6UNV from *Rasamsonia emersonii*. It can be noticed as the structure is conserved between the two, while their sequence is not.

the β_9 loop and some other amino acid residues within to the lid structure. This structural variation allows the lid to open, thereafter causing the enzyme to bind onto the interface (such as a lipid membrane), in order to start the process of hydrolysis. This process is also called interfacial activation [236, 237, 240]. There are 3 different lid structures that can affect lipases: (1) closed position, where the lid covers totally the active site pocket, giving a non-active enzyme; (2) open position, where the lid is totally open and the enzyme is catalytically active; (3) position of the lid disordered, where the enzyme is probably active, but not bound to any lipid membrane (*transition state*) [236, 237, 240, 241]. Similar structures were found also in PLA1, where usually the lid is reduced or often absent (since it is usually correlated to neutral lipid interactions as well). The sequence constituting the active site is conserved within lipases and PLAs (G-X-S-X-G, where X could be any amino acid), where the central amino acid serine, plays a role in the hydrolysis reaction [242]. In fact, point mutations of this residue lead to a non-functional enzyme [243]. There are two theories related to the interaction enzyme/lipid membrane: scooting mode and hopping mode [239, 244]. In the scooting mode theory, the enzyme is confined at the interface for many degradation reaction cycles; whereas in the hopping mode, the enzyme leaves the membrane after a certain number of cycles. It has been proved that for the majority of the lipases and PLAs tested, the scooting theory is the preferred mode, as shown by Balashev and colleagues [244] through using AFM.

In summary, PLAs of the type A1, are evolutionary closer to the lipase group, while with some of the other members, it is difficult to discriminate between their PLA and lipase activities. In fact, it is known that, for instance the Guinea pig pancreatic lipase (PLRP2), exhibits lipase activity in the presence of bile salts, whereas when they do not exist, it can hydrolyse GPL molecules as well [238]. Since they have crucial roles in living organisms, and since not much is known about PLA1, it is fundamental to get a deeper understanding of this enzyme type as well. In this thesis work, the kinetics mediated by PLA1-1 enzyme from the organism *Aspergillus oryzae*, was deeply analysed.

1.2 Aims of the project

PLAs play a crucial role in several fundamental pathways in a living cell, where a malfunctioning of one of these pathways could lead to serious problems. No much studies are available in the literature about PLAs interactions with membranes or bilayers and the factors regulating their activity and specificity. Although very few studies are available on the A1 group [243, 150, 245] compared to the A2 one, A1 group plays crucial roles as well on the different pathways mentioned above. Traditionally, evaluation of the specificity of PLAs was done by measuring the rate of hydrolysis of a few radiolabeled substrates individually [246, 168]. Such an approach is tedious if multiple species are to be studied. In addition, variations in enzyme activity could arise from physical properties of the substrate determined by the lipid under study, such as membrane surface charge and fluidity. To improve this, specificity could be studied by comparing the hydrolysis of two GPLs that have different isotope labels, but even this approach is tedious when studying multiple GPL species [233, 111, 234]. In this case a mass-spectrometric approach is much more convenient as it allows one to study a multitude of GPLs simultaneously. Here a high-throughput mass-spectrometric assay was developed to determine the effect of acyl chain length and unsaturation of GPLs on the rate of hydrolysis of PLAs. With NR, structural changes of the system PLA/lipid model membrane, can be achieved, analysing its interaction and kinetics. We started analysing the kinetics mediated by PLA1-1, a A1 phospholipase from *Aspergillus oryzae*, in order to understand its specificity and what factors regulate its activity and specificity. Inspired by seminal works from Wacklin and coworkers [247, 248], structural and analytical techniques were chosen involving mainly Neutron Reflectometry (NR), capable of providing structural information on planar model membranes at a fraction of nanometer resolution, and Mass Spectrometry (MS), allowing to determine the exact compositional variation caused by interactions with membranes. Additional biophysical techniques were utilised, for complementary information or sample preparation optimisation. Model membrane systems were used and lipids were specially synthesised for the neutron studies. PLA1-1 was used as model enzyme, in order to assess and develop all the protocols and tools needed to analyse the phospholipase membrane interactions and kinetics. In fact, all the protocols and tools explained within this thesis, can be used for other phospholipases, such as mammalian PLAs that are key for instance in physiological processes such as membrane homeostasis and remodelling apart from signal cascades. Such studies, carried out through using these techniques, can generate a wealth of information on these PLAs. The final aim would be the application in medicine, where through the use of these studies, inhibitory molecules can be developed and analysed, in order to be used as treatment of a disease correlated to an over-activity of a PLA.

Chapter 2

Materials and Methods

2.1 Phospholipase: expression, purification and characterization

Heterologous protein expression was carried out by transformation (via the expression vector described in paragraph 2.1.1) of *E. coli* cells, followed by sequential purification steps, including affinity chromatography and gel filtration, to purify the desired protein, PLA1-1, in its active state. The term heterologous protein expression derives from the fact that *E. coli* cells normally do not express that protein, since it comes from a different organism, while the strain created after the transformation process can. The advantage of the method lies in the easy cultivation of the cells. The expression performed is also called recombinant protein expression, since the sequence was modified in order to add a tag to facilitate the purification of the protein of interest from the endogenous ones. The third advantage of this method is that the protein of interest can be overexpressed, since usually the cDNA (copy DNA) sequence in the vector is placed near a strong and controlled promoter, thus managing to get very high amounts of the protein. The prokaryotic expression has also some disadvantages. The most important one is the lack of post-translational modifications, such as glycosylation and myristylation, amongst others. If the protein, such as the one under examination, does not need any of those modifications, then a prokaryotic expression should be a good system. Another problem that one could face concerns the overexpression aspect, since some proteins upon overexpression can undergo aggregation and unfolding, thus causing them to be less active or irreversibly inactive. This parameter can be adjusted using the operator, carefully balancing the concentration of the induction factor in the media (see paragraph 2.1.1).

2.1.1 Vector description

An expression vector is an engineered cyclic double strand DNA used to express/overexpress the protein of interest. The vector is used to introduce the specific nucleotide sequence in a target cell, where the expression can be controlled by external factors, and the protein synthesis mechanism of the host cell is used for the protein expression. The nucleotide sequence coding for the protein can be inserted inside a proper section of the expression vector, in a process called cloning. The cloned vector can be used either for protein expression or physiological studies. Figure 2.1 panel A shows the vector map used for the expression of PLA1-1 in *E. coli* cells. The cDNA sequence for the PLA1-1 (named as "PLA1-1" displayed in green

color) is placed near to the tag sequence (Maltose Binding Protein, named as "MBP" in pink color), leading to the expression of a fusion protein (fusion between the tag and the PLA1-1). There are mainly two reasons why the MBP-tag is usually selected: a) to make the expressed complex more soluble, thus avoiding sometimes inclusion bodies and other difficulties that can arise without this tag; b) to facilitate the isolation of the protein of interest from endogenous ones, by affinity chromatography. The cDNA, is a double strand DNA derived from the reverse transcriptase of the mRNA (messenger RiboNucleic Acid) that codes for the protein of interest. In eukaryotic cells, the genes usually have introns and estrons, whereas prokaryotic cells lack this feature. This aspect can be problematic when heterologous expression is selected to express eukaryotic proteins in prokaryotic systems. The only way to proceed is with the elimination of the introns from the gene coding for the protein of interest, since the information of the protein amino acid sequence is contained in the estrons. Therefore, the most convenient way could be to purify the mRNA coding for the protein, since this molecule has already undergone intron elimination during its transcription process. While in the next step, using a reverse transcriptase enzyme and a DNA polymerase DNA dependent, a double strand DNA is created (cDNA) from the mRNA purified, that is ready to be cloned into an expression vector. Another aspect that needs attention on the heterologous protein expression is the codon optimization, as discussed in paragraph 2.1.2. The fusion complex expressed from the vector, has a short sequence of 7 amino acids (see in figure 2.1 as "Factor Xa site") between the PLA1-1 and the MBP-tag that can be utilised as a cleavage site to dissociate the protein from its tag, through the action of a protease (Factor Xa).

The vector employed also contains other sequences, fundamental for the normal functionality of the vector. The "ori" sequence displayed in yellow color is the origin of replication, which is important to get and maintain the right amount of vector inside the cells during its amplification and expression, process controlled by the two sequences "bom" and "rop". The next part, is a sequence named lacI, controlled by a strong promoter. This sequence is involved in the expression control, in fact LacI codes the lac repressor, a lactose binding protein, that in the absence of lactose or the analog molecule Isopropyl- β -D-1-galactopyranoside (IPTG), binds to the lac operator, right after the tac promoter before the MBP-tag sequence. This complex avoids the binding of the RNA polymerase on the tac promoter, avoiding the trascription of the downward sequences. When the IPTG is added in the medium, the lacI binds that molecule, unbinding the DNA and making the way free for the RNA polymerase. This process is called "Induction control". The over-expression of the protein of interest can be adjusted varying the amount of IPTG in the medium. As there is the promoter of transcription, a terminator is needed at the end of the fusion protein (T1 and T2 terminator sequences). The sequence between the promoter and terminators is usually named "expression cassette", as shown in detail in figure 2.1 panel B. In a vector it is also important to have a selection element, in order to be able to differentiate cells that have or have not acquired the expression vector. In this case, a sequence coding for a protein that gives the resistance against ampicillin is used as a selection element. This critical feature allows the cells containing the vector to be selected using ampicillin antibiotic, upon adding it directly to the growth media, while cells

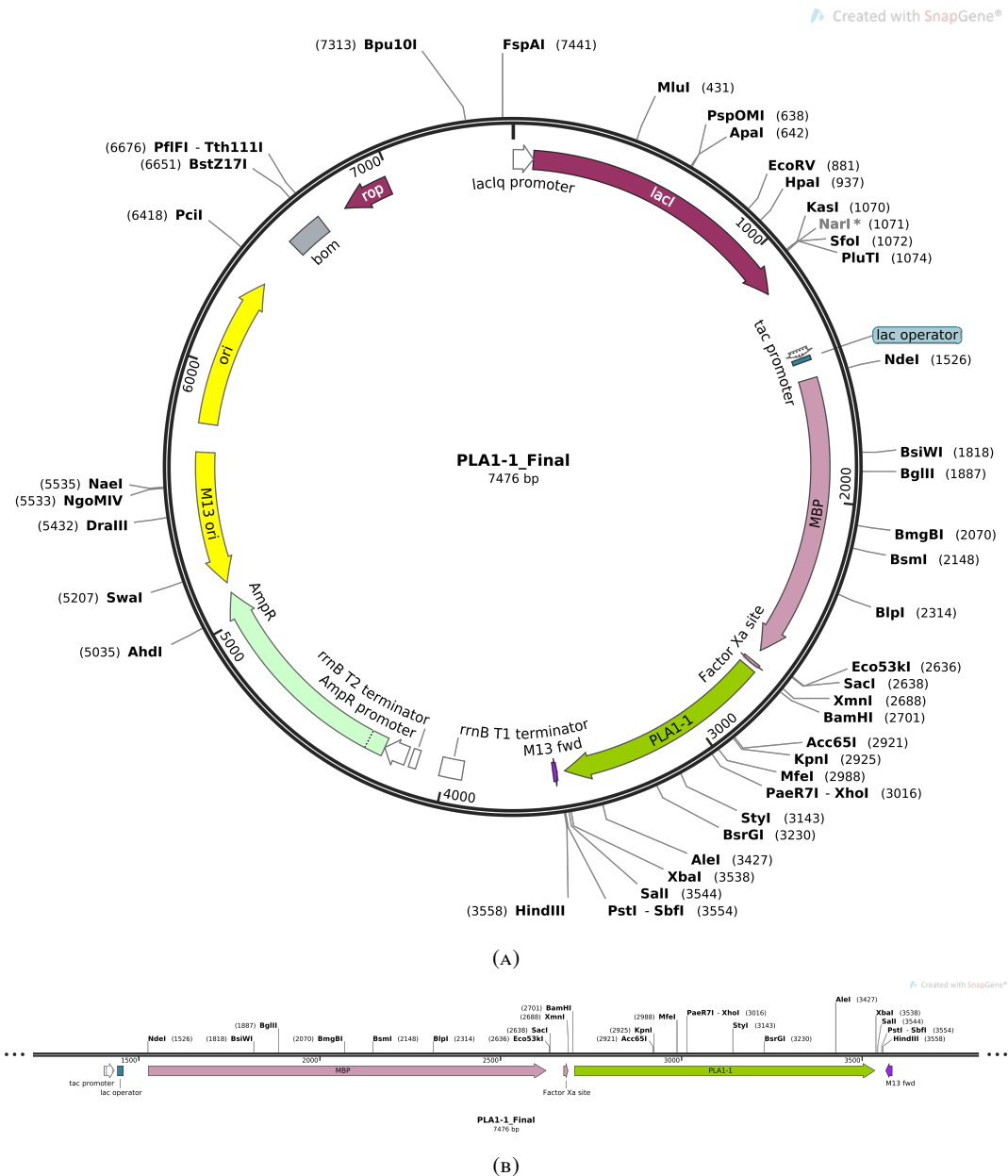


FIGURE 2.1: Map of the vector (panel A) and zoom of the expression cassette (panel B)

that do not contain the vector will not survive. In the vector there are also two sequences "M13" before and after the expression cassette, that can be used for sequencing. The vector was designed and obtained by [243].

2.1.2 Rare codons and *E. coli* strains used

Rare codons is another problem for the heterologous protein expression system, since different organisms might have different "codon usage". By codon usage we mean the phenomenon whereby synonymous codons are not used uniformly among all the living organisms, but there is a preference in the use of certain codons with respect to others for the coding of the same

amino acid. A codon is a sequence of 3 nucleotides, and since the RNA is constituted by 4 kinds of different nucleotides, the total codon combination that can be created is 61, since 3 codons are used as a stop codon for the translation process. The total number of amino acids in proteins is 20, and this overabundance of codons allows some amino acids to be encoded by several of them. The problem arises when a heterologous expression is needed of a protein (*i.e.* from *A. oryzae*) in host cells that are phylogenetically far (time of divergence) from the expression system (*i.e.* *E. coli*) that is employed. If the sequence has rare codons for the host organism, the expression can slow down or even stop, leading to a truncated product. There are basically two ways to circumvent this problem. One alternative is the codon optimization: substituting the rare codons with preferred ones for the hosting organism; the second alternative is the use of particular strains of engineered *E. coli*, capable to recognize also those rare codons. In this study *E. coli* Rosetta and Codon plus were employed. Those particular strains are engineered with additional plasmids coding for additional tRNA on the normal tRNA pool of *E. coli*, to avoid truncated and wrongly expressed recombinant proteins.

2.1.3 Expression procedures

The chemically competent *E. coli* cell strains as discussed in the previous paragraph 2.1.2 were purchase from Sigma (TOP10 and Rosetta) and from Agilent (Codon Plus), and stored at -80 °C. Chemically competent cells are cells pre-treated with salts like calcium chloride (CaCl₂), leading to the formation of pores on the plasma membrane, that facilitates the recombinant vector to enter the cells. Chemically competent TOP10 *E. coli* strain was used for the vector amplification, in order to have enough material to work with during the transformation of the *E. coli* Rosetta and Codon Plus strains. The competent cells were thawed in ice and the recombinant vector (around 40 ng) was added to the cell suspension keeping them in ice for 30 minutes to favor the diffusion and penetration of the plasmid inside the cells through the pores. To make the transformation permanent, "heat shock" was performed (45 seconds at 42 °C following by 2 minutes on ice), allowing the closure of the pores. At this point, a very rich

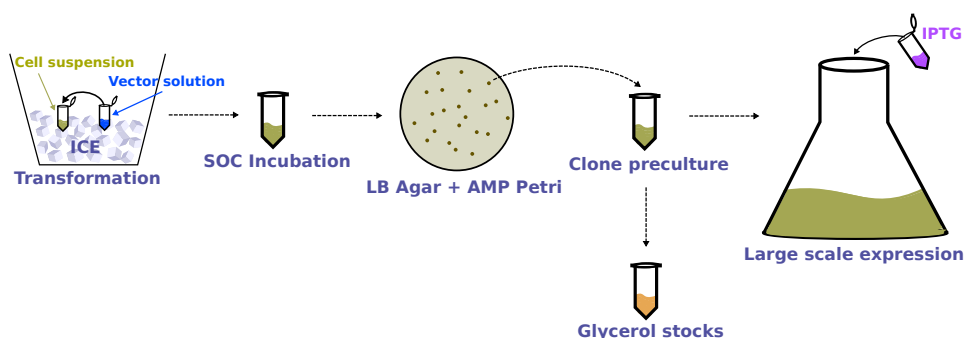


FIGURE 2.2: Scheme of the steps for cells handling

broth was added to the cells (SOC, Super Optimal Broth) 90 ul, and the culture was incubated at 37 °C for one hour. During this period, the cells recovered from the heat shock process and started the basic expression of endogenous proteins (including the antibiotic resistances used

for the selection; AMP resistance in this case, as mentioned in the paragraph 2.1.1). Then the cells were plated on a Petri dish containing LB + 1.5% agar, along with the addition of AMP in order to select the cells with the vector, followed by an o/n incubation at 37 °C. A few colonies were picked and transferred into pre-culture tubes containing liquid media for the culture (LB + AMP [final concentration in LB of 100 mg/L]) and left for O/N incubation. Next the midi-prep Wizard Plus SV DNA Purification System was performed in order to purify the recombinant vector from the pre-cultures. The midi-prep is a system of vector purification which gives very high yields. The first step of the protocol is the production of the cleared lysate, using the lysis buffer and the alkaline protease solution given within the purification kit. This step ensures the solubilization of the plasma membranes of the cells, and the deactivation of all the proteins that could damage the vector during the purification steps. Next, the binding of the vector is carried out using the proper DNA purification centrifuge filters (silica stationary phase). The washing step is then performed, where all the non-bonded molecules are washed away. The charges present in the washing buffer, mediate the binding of the DNA to the silica stationary phase of the centrifuge filters (since both are negatively charged). During the elution step, Milli-Q H₂O (18 MΩ cm at 25°C, Millipore) was added to the filter, removing the bridged salts, with the consequent elution of the DNA of interest, the amplified vector. The preps purified were then checked with the nanodrop, checking for the concentration and purity. The wavelengths used were 260 nm for the DNA, 280 nm for the proteins and 230 nm for generic organic molecule contaminates from the purification reagents. The stocks were stored at -20 °C at 20 ng/μl concentration, that were ready to be used. The transformation of the *E. coli* Rosetta and Codon Plus strains was the same as for the TOP10 cells. For the *E. coli* Codon Plus cells chloramphenicol (CLO with a final concentration in LB of 54 mg/L) was used, since this strain already has an additional selection factor, the resistance for CLO in its genome. All the steps done for the amplification were repeated for the expression cell strains. After the O/N LB + antibiotics (AMP for Rosetta and AMP + CLO for Codon Plus) liquid culture that was incubated at 37 °C, an amount of 50% sterile glycerol was added to the cell suspension, in order to be able to freeze the cells at -80 C (glycerol stocks), allowing us to have a stock of cells that could be utilised to make other liquid cultures. When a new liquid culture is needed, an aliquot of the glycerol stock or a ball, can be taken and diluted directly in the LB, and this allows to avoid the all the transformation steps. From the glycerol stocks, a preculture of 3 ml of volume is made the day before the expression. After an O/N of incubation, the pre-culture is poured into a 2000 ml glass flask with 800 ml of sterile liquid LB + AMP + CLO (only for the Codon Plus strain). When cells reach 0.6 OD₆₀₀, 1 mM (final concentration in the broth) of IPTG is added to the LB broth in order to start the expression of the interest fusion protein. The expression takes place at 25 °C O/N shaking at 120 rpm. To control the overexpression, a Sodium Dodecyl Sulphate - PolyAcrylamide Gel Electrophoresis (SDS-PAGE gel) was done. The percentage of acrylamide used was 12%, which allows a good migration for proteins with a weight of around 70 KDa. Small aliquots of the liquid culture loaded on the gel were taken at different time points during the expression. The samples between each other were normalized using

the OD₆₀₀, and cells directly diluted in sample buffer, and directly loaded in the gel after boiling step (95°C for 5 minutes).

2.1.4 Protein purification

E. coli cells expressing the protein of interest were centrifuged at 6,500 g 4 °C, using a Beckman Coulter centrifuge, in order to separate the liquid media from the cell biomass. The

Buffer name	TRIS	NaCl	CaCl ₂	Maltose	Pr. inhibitors
Lysis buffer	20 mM pH 7.4	250 mM	5 mM	None	Yes
Running or PLA1 buffer	20 mM pH 7.4	250 mM	5 mM	None	None
Elution buffer	20 mM pH 7.4	250 mM	5 mM	10 mM	None
Factor Xa buffer	50 mM pH 8.0	100 mM	5 mM	None	None

TABLE 2.1: List of the buffers used for the purification of the PLA1-1 and for its activity assays. Pr. inhibitors stands for Proteases inhibitors

supernatant was discarded and the pellet obtained was subjected to lysis using lysis buffer (20 mM TRIS pH 7.4, 250 mM NaCl, 5 mM CaCl₂ and protease inhibitors [Roche cComplete Mini EDTA-free tablets]). Mechanical lysis was carried out, first by vortexing the sample in order to resuspend the pellet in the lysis buffer followed by probe sonication (1 second ON and 1 second OFF for 2 minutes 3 times at 40% amplitude). The lysate was obtained after lysis and was centrifuged at 16,500 g at 4 °C in 50 ml polycarbonate vials in order to separate the cell debris from the solubilised component. The supernatant was then directly injected into a column coupled to the Fast Protein Liquid Chromatography (FPLC) maintained at 8 °C (cold room temperature) for the first step of purification. The 5 ml MBP-Trap (a prepacked column with dextrin sepharose, purchased from Cytiva) affinity chromatography column was used for this purpose. The dextrin stationary phase of the column allows the binding of proteins that have affinity for sugars. Since our fusion protein that is expressed has an MBP-tag, which has affinity for sugars like dextrin and in particular for maltose, a MBP-Trap column is needed for the purification. Consequently the fusion protein expressed binds to the resin of the column, whereas all the other endogenous proteins pass through it without interacting. The column was first washed with Milli-Q H₂O, to wash away the EtOH used for the storage of the column, and then equilibrated with the running buffer at 1 ml/min. The supernatant collected from the centrifugation step was injected at 1 ml/min allowing for the binding of the tagged protein. After this step, the column was washed with the same buffer used for the equilibration at 3 ml/min, in order to detach contaminants from non specific interaction with the resin. For the elution step the elution buffer containing 20 mM TRIS pH 7.4, 250 mM NaCl, 5 mM CaCl₂ and 10 mM maltose was used. The MBP-tag has more affinity for the maltose than the cyclodextrin resin, therefore by injecting the same buffer containing 10 mM of maltose, a competitive binding takes place, where the MBP binds preferentially to the soluble sugar, thus assisting to the detachment of the protein from the resin. The elution step was performed at 1 ml/min, during which fractions of 1 ml of volume

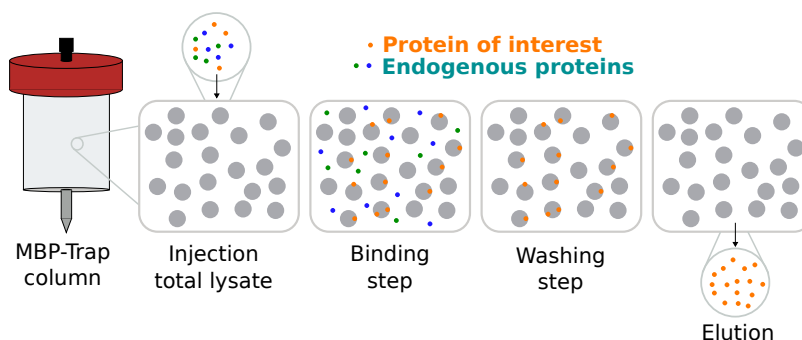


FIGURE 2.3: Scheme of affinity purification steps using MBP-Trap column coupled to the AKTA purifier

were collected. The elution buffer was injected with a gradient, starting from 0% to 100% for 3 CV (15 ml). The column then was first washed with two empty elution cycles, followed by milli-Q H₂O and then 20% of EtOH as a storage solvent. The fractions were analysed by SDS-PAGE gel to check the their purity. A brief scheme of the affinity chromatography is displayed in figure 2.3. After the affinity chromatography, a gel filtration step was needed to get purer preparations. Gel filtration allows for the separation between several components of a sample in terms of their own molecular weight. For this purpose, a HiLoad GE HealthCare 70/160 200pg coupled to the Akta pure, a highly cross-linked agarose matrix was utilized. This column permits to load up to 40 mg of protein sample with a maximum volume of 5 ml, which is ideal for large scale preparations. The key principle behind gel filtration is that smaller proteins interact highly with the matrix, since they can occupy also the smallest pores; whereas bigger proteins interact less. This means that bigger proteins or big complexes are eluted during the early fractionation, and smaller ones later (see figure 2.4). Pre-gel filtration, the affinity chromatography purified protein was centrifuged at 10,000 g in the coldroom to remove any big particles and precipitants. During the gel filtration step, 1 ml fractions were collected, and then analysed using SDS-PAGE to check for their purity.

MBP-tag cleavage

For the SAXS and the TOF-MS measurements, the protein tag was cleaved from the PLA1-1. The cleavage was carried out using protease factor Xa (Factor Xa Cleavage Capture Kit purchased on MilliPore Sigma). The purified fusion protein (MBP - PLA1-1) was first dialysed O/N in coldroom (8 °C) using GeBaFlex-tube from Gene Bio-Application with a cutoff of 8 kDa, against the Factor Xa buffer. In order to get the right ratio factor:fusion protein, a concentration dependent assay was performed adding the factor Xa from a ratio of 1:100 to 1:25 factor:fusion protein (w:w). A time dependent assay was also performed, in order to balance correctly the time of the reaction and the amount of cleaved products. The best ratio that balances the two factors was 1:50 factor:fusion protein (w:w) with a final reaction volume of \approx 5 ml. The incubation was done at room temperature, in oscillation for a continuous mixing of the solution for 4 hours. The resin Xarrest (100 μ l of slurry per 4 μ g of

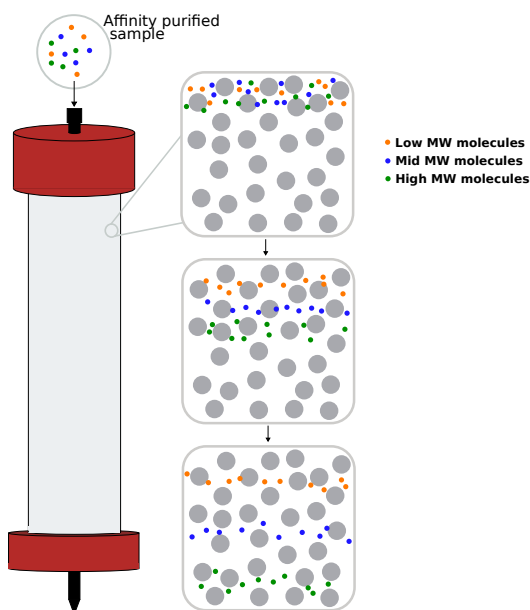


FIGURE 2.4: Gel filtration sketch, where it is possible to notice how this technique is able to separate the molecules depending on its molecular weight (MW).

Factor Xa added in the reaction tube) was loaded into supplied centrifuge filters, and washed trice with Milli-Q H₂O and the Factor Xa buffer. After the cleavage, the reaction mixture was transferred into the filters and centrifuged at 1,000 g for 2 min at room temperature in order to remove from the mixture the Factor Xa protease. After this process, the cleaved PLA1-1 had to be isolated from the cleaved MBP-tag and the residual uncleaved fusion protein, for which an MBP-Trap affinity chromatography was performed (process similar to the affinity chromatography step mentioned in the previous paragraph). The purity of the cleaved PLA1-1 was checked by SDS-PAGE before its analysis with SAXS and TOF-MS. For the SAXS measurement, the protein was dialysed again against the PLA buffer and concentrated to 2 mg/ml using the Amicon Ultra Centrifugal Filters that had a cutoff of 10 KDa. The final volume was 300 μ l, which was enough for a few SAXS measurements. In order to get the mass using the MS-TOF, the protein was dialysed against Milli-Q H₂O, and concentrated until 10 μ M (0.32 mg·ml⁻¹) in a volume of 50 μ l (16 μ g of PLA1-1). Dialysis against Milli-Q H₂O is crucial while carrying out MS-TOF analysis since existence of salts in the buffer can lead to significant noise causing MS signal loss. In addition, MS-TOF reveals only the primary structure of the protein, so the folding of the protein or its functionality is not an important factor to be maintained.

2.1.5 Sequence analysis

Analysis of the nucleotide sequence

To make sure to work with the right nucleotide sequence codifying for PLA1-1, the sequencing was performed. A midi-prep was performed using Top10 *E. coli* cells for the amplification of

the vector (like described previously in paragraph 2.1.3) and the Wizard Plus SV Minipreps DNA Purification System for the vector purification. From the MINI-Prep $\approx 1 \mu\text{g}$ of recombinant vector was purified. The purified vector was then frozen at -80°C , and lyophilized using the SpeedVac for around 4 hours, and sent to Genewiz for the sequencing. In the vector of interest, before and after the expression cassette (see paragraph 2.1.1) there are two M13 sequences that can be used for the primers design and afterwards for the Sanger PCR amplification. Those primers can be selected directly on the Genewiz site (<https://clims4.genewiz.com>) during the ordering. The analysis of the sequences was done using SnapGene software and clustalW2 (<https://www.genome.jp/tools-bin/clustalw>).

Analysis of the amino acid sequence with TOF-MS

During the expression process, it happens sometimes that the final protein has been truncated of some amino acids or the sequences are not the right ones. To ensure that the expressed and purified protein is the correct one, a mass spectrometry analysis was performed on the purified fusion and cleaved version of PLA1-1. The sample after the purification was concentrated to reach $10 \mu\text{M}$ of concentration, and it was dialysed in Milli-Q H_2O to avoid problems and noise during the acquisition of the measurements due to the salt of the buffer. The analysis was done at the Institut de Biologie Structurale (IBS) in Grenoble. The instrument used is a mass spectrometry time of flight, using a C18 column coupled to the UHPLC before the MS instrument. The TOF mass spectrometer measures basically the time of flight of ions in an electric field. The time of flight of the ions is proportionally dependent on the ratio mass/charge (m/z). The analysis was done in the "native state" and also in "reducing environment" adding TCEP 50 mM for 90 minutes at room temperature for the disulfide bridges analysis.

2.1.6 Structural and functional analysis

Structural investigation

Since no crystal structure has been deposited for the protein under analysis, a brief structural analysis was performed. The initial step was the use of "AlphaFold" ([249]), an *ab-initio* algorithm that, from a given sequence of amino acids, gives the most probable structure or structures. The cleaved protein sequence was submitted, since the fusion one has an unstructured linker that can lead to downstream problems. After getting the most probable PDB structure, a SAXS (technique described briefly in paragraph 2.5.1) experiment was performed on the beamline BM29 at the ESRF in Grenoble, France [250]. The measurements were done with 20 frames with an exposure time of 2 seconds with a sample concentrated around 2 mg/ml using a 1 mm diameter flow-through quartz capillary. The acquisition temperature was that of 22°C using a photon energy of 15 keV [see paragraph 2.5.1 for details in the data analysis].

Functional investigation

Once the sequence and structural analysis were carried out, an activity assay of the purified protein was performed. The activity of the protein was done using the synthetic DMPC lipid, purchased from Avanti Polar Lipids. A LUV solution was prepared in the PLA1 buffer following the protocol described in paragraph 2.3.2. The vesicle solution was divided across several glass vials, and various fractions eluates from the gel filtration step were tested to double check if the peak with the right MW has the expected activity. To each vial containing vesicles prepared from $\approx 150 \mu\text{g}$ of DMPC GPL in $200 \mu\text{l}$ of final solution, $\approx 2 \mu\text{g}$ of protein fraction was added. The vials were incubated at room temperature for 1 hour, followed by lipid extraction (Folch et al [251]), that was performed by adding $600 \mu\text{l}$ CHCl_3 , $300 \mu\text{l}$ MeOH and $100 \mu\text{l}$ Milli-Q H_2O , with a final ratio of 2:1:1 v/v/v (since $200 \mu\text{l}$ of H_2O were already in the sample in the form of buffer). The vials then are tightly sealed and vortexed vigorously, and incubated at room temperature for 30 min for breaking the emulsion. When two phases were clearly visible, the upper phase was discarded, while the organic phase was evaporated under an Ar stream. Thereafter the dried film was resuspended in a solution of $\text{CHCl}_3/\text{MeOH}$ [2:1 v/v] in $20 \mu\text{l}$, and after vortexing, the samples were spotted on a Thin Layer Chromatography (TLC) silica gel 60 (F₂₅₄) pre-coated with 0.2 mm layer thickness. The plate was then placed on the running chamber pre-equilibrated with $\text{CHCl}_3/\text{MeOH}/\text{H}_2\text{O}$ [110:49:1 v/v/v]. The TLC plate was then dried under an Ar stream and stained with primulene. After drying the stain, the TLC was placed under a UV-visualizer using 254 nm UV light for the visualization of the bands.

2.2 Lipid production

Synthetic GPLs for the preparation of partially deuterated PC molecules, were purchased from Avanti Polar Lipids, while natural GPL mixtures were extracted from yeast (*Pichia pastoris*, *Pp*), that was grown in collaboration with the Deuteration Lab (D-lab, ILL, Grenoble, France). Production and purification of the lipids were entirely carried out in the L-Lab (ILL, Grenoble, France).

2.2.1 Partially deuterated PC molecules

Partially deuterated PC molecules were synthesised starting from fully hydrogenous PC substrates. Those lipids (usually around 15-20 mg) were transferred into a glass vial and dried. The lipid film was dried further under vacuum for 3h to remove traces of solvent from the film. The partially deuterated PC molecule species were synthesized by esterification of lyso-phatidylcholines (LPC) and fatty acid anhydrides and then purified by normal phase column coupled to a HPLC (NP-HPLC) [252]. The fully hydrogenous synthetic PC substrate molecule, previously evaporated, was incubated with a PLA1 or a PLA2 depending on which acyl chain had to be cleaved and replaced with a deuterated FA anhydride in the vacant sn position of the prepared LPC. Anhydrides were prepared by incubating a free fatty acid with the

coupling reagent dicyclo-hexylcarbodiimide for 4-5 hours. The d-sn1/h-sn2-PC and h-sn1/d-sn2-PC species were synthesized by acylation of h-sn2-LPC with a deuterated FA-anhydride or a h-sn1-LPC with a deuterated FA-anhydride, respectively. The synthesis process involved incubating both the FA-anhydride and the LPC in a pot containing 4-pyrrolidino-pyridine (4-PP) in dry benzene that was left stirring for 5 hours leading to formation of a partially deuterated PC molecular species. The PC species prepared were finally purified using the NP-HPLC on a diol-modified silica column and their purities were confirmed by TLC and GC while their concentrations were determined based on the film mass. The various lipids synthesised are listed in table 2.2.

	Lipid name	Abbreviation	Deuteration
Saturated series	14:0 14:0 PC	DMPC	sn-1
	16:0 16:0 PC	DPPC	sn-1
	18:0 18:0 PC	DSPC	sn-1
Unsaturated series	16:0 18:1 PC	POPC	sn-1
	16:0 18:2 PC	PLyPC	sn-1
	16:0 18:3 PC	PLnPC	sn-1
	16:0 20:4 PC	PAPC	none

TABLE 2.2: List of lipids used for the NR kinetics analysis

2.2.2 Natural GPL mixtures

Cultivation of *Pichia pastoris*

P. pastoris GS115 HSA (*Invitrogen*) cells were cultured in the deuteration facility of the Institut Laue-Langevin (D-Lab, ILL), Grenoble, France, using the protocol from de Ghellinck et al., 2014 [253], described in brief in "Developing advanced models of biological membranes with, hydrogenous and deuterated natural glycerophospholipids", paper under revision.

Total Lipid extraction

GPL mixtures are extracted and purified from either deuterated and hydrogenous *P. pastoris* biomasses. After harvesting the cells, they were resuspended into 10 ml of Milli-Q H₂O and lysed by probe sonication on ice for 3 times for 5 minutes with 30 seconds intervals, 20% amplitude. The cell lysate was poured into boiling ethanol (95 °C) containing 1% butylated hydroxytoluene (BHT) to prevent double bond oxidation, while a vigorous stirring was performed in order to denature lipases. The total lipid mixtures were then extracted according to the method of Folch et al. [251], followed by the evaporation of the organic phase under a N₂ stream and their final reconstitution in CHCl₃.

GPL mixture fractionation by preparative HPLC

The various classes of GPL mixtures were separated through the two following sequential purification steps: (1) amino-bonded solid-phase extraction column, and the sequential (2)

injection of the desired GPL mixtures into a diol-modified silica stationary phase column (semi-preparative Nucleosil 100-5 OH column [10 x 250 mm], Macherey-Nagel, France) that was coupled to an Agilent chromatographic system (High Performance Liquid Chromatography HPLC 1260 Infinity II series, Agilent Technologies, France) using the SEDEX 90 Electro Spray Scattering Detector (ELSD) as the detector (Sedex Sedere, France). After the first step (1), the sample was dried under an Ar stream and the resulted film was dissolved into 1 ml chloroform before the injection into the HPLC system. The sample was injected using an auto-sampler module within the HPLC, and the various classes of GPLs were eluted by using a gradient consisting of solvent mixture A [$\text{CHCl}_3/\text{CH}_3\text{OH}$] (70:25 v/v) plus 1% NH_4OH and solvent mixture B [$\text{CHCl}_3/\text{CH}_3\text{OH} - \text{H}_2\text{O}$] (60:40:5.5 v/v/v) plus 0.5% NH_4OH at a flow rate of 1.0 ml/min. A method was programmed such that at time zero, the proportion of solvent mixture B was 5% and gradually increased to 40% at 30 min, then to 100% at 40 min and stayed at this value until 65 min after which it was again decreased to 5% at 66 min and kept there until the end of the gradient at 75 min. During the elution, fractions were collected in correspondence to chromatographic peaks. The column during the purification was maintained at room temperature, whereas the ELSD temperature was set at 60 °C. Ar was used as a carrier gas at 3.5 bars inlet pressure. All this process is explained in "Developing advanced models of biological membranes with,hydrogenous and deuterated natural glycerophospholipids", paper under revision. Data were extracted using Open Lab chromatographic workstation (Agilent Technologies, France) and analysed with home-built python program [for more details refer to Chapter 7].

Lipids analysis by high-performance thin layer chromatography (HPTLC)

In order to assess the identity and purity of each of the purified classes, 10.0 μl of the fractionated samples and standards were applied to a silica gel 60 (F_{254}) pre-coated TLC plate of 0.2 mm layer thickness. An automated instrument was utilised, CAMAG LINOMAT5 sample applicator (CAMAG, Mutten, Switzerland), in order to obtain uniform bands on the plate. Samples were subjected to a constant application velocity of 150 nl/s under a continuous stream of N_2 gas. The TLC plate was next preconditioned and then developed in a CAMAG twin-trough-chamber filled-in with a mobile phase, [$\text{CHCl}_3/\text{CH}_3\text{OH}/\text{CH}_3\text{COOH}$] (65:28:8 v/v/v). Finally, the developed plate was derivatised using a 1.5% CuSO_4 solution sprayed over it in the CAMAG derivatiser chamber following which, it was dried on a hot plate at 120 °C for 10 minutes for the development of the bands. Further, the developed spots were visualized and analysed in a CAMAG TLC scanner 3 using the winsCATS software (ver 1.4.6).

FAMES analysis by GC-MS and GC-FID

Global acyl chain composition of the total lipid extracts from *P. pastoris* were initially determined by Gas Chromatography - Mass Spectrometry (GC-MS), Agilent, 5977A-7890B, and that of the purified mixtures were carried out by Gas Chromatography Flame Ionization Detection (GC-FID). Before the GC-FID measurements, the GPLs were subjected to

the hydrolysis of the ester bond and thereafter, the released fatty acids derivatised to their corresponding fatty acid methyl esters (FAMES). 3 mL of methanolic H₂SO₄ was next added to a glass vial. The vial tube was vortexed, filled up with Argon to avoid exodation, and sealed tightly with a Teflon-lined cap. The solution was incubated at 95 °C for 1 h. Once the vial is cooled down to room temperature (≈10 min), 3 ml of MilliQ H₂O was added and the solution vortexed following which 3 ml of hexane was added and vortexed vigorously to create an emulsion. The supernatant phase of ≈ 2.8 ml was then transferred into a fresh vial, evaporated under a stream of Ar and the resulted dried film was reconstituted in 250 μl of hexane and transferred into a GC auto sampler vial that was then loaded into the GC's automatic liquid sampler. The GC instrument (GC 2010 Plus, Shimadzu) was equipped with a SGE BPX70 70% Cyanopropyl Polysilphenylene-siloxane column (25m by 0.22mm ID and 0.25 μm film thickness). Helium was used as a carrier gas at a flow rate of 1.04 ml/min with a linear velocity of 35 cm/sec and a purge flow rate of 1 ml/min. The column was allowed to equilibrate for 3 minutes at 155 °C before injection and then the temperature was ramped up to 180 °C at a rate of 2 °C/minute and then to 220 °C at a rate of 4 °C/minute and finally held at 220 °C for 5 minutes resulting in a 27.5 minutes total run time. Samples (5 μl) were injected into the column at 250 °C using an AOC-20i auto injector. Detection was done using a FID operating at 260 °C with 40 ml/min H₂, 400 ml/min compressed air and 30 ml/min He make-up flow. Global fatty acid methyl esters were identified by their mass spectrum and retention time and quantified by Mass Hunter Quantification Software (Agilent) while for the purified GPL mixture data analyses were carried out by LabSolutions software (Shimadzu). The relative abundance was obtained by GC peaks integration, using an in house python code for more details refer to Chapter 7.

2.3 Sample preparation

In order, to analyse the interaction and the kinetics of the PLA1-1 with the lipid substrate molecules, model membranes were prepared. This section will show all the procedures that were employed to prepare model membranes for this study. All the lipid powders and lipid stock solutions in a solvent solution - CHCl₃/MeOH [9:1 v/v], were stored at -20 °C. Here CHCl₃ ensures and keeps the GPLs soluble and the MeOH helps to avoid the oxidation of the sample through stabilising the CHCl₃ molecule. All the lipids stock solutions were stored at a concentration of 10 mg/ml, whereas the solutions for the Langmuir Blodgett lipid preparation were diluted to 1 mg/ml.

2.3.1 Crystals for NR and QCM-D, description and cleaning procedures

The crystals used for the NR experiments are made of silicon (crystallographic direction 111) with a top layer of silicon oxide with variable thickness and roughness. The crystals used for QCM-D measurements are made by a silica layer deposited by sputtering on the top of gold and of crystalline AT-cut quartz. The supports used have dimensions of 8 x 5 cm² with a

thickness of 1.5 or 2 cm and polished on one face with a roughness of $\leq 5 \text{ \AA}$. The QCM-D crystals are thin small quartz crystal disks with metallic electrodes on both sides. On the top of the crystal, a layer of silicon oxide is deposited, with a roughness that is usually higher than that of the crystals used for the neutron reflectivity. For a full description of the techniques see paragraph 2.5.1 and 2.4.2 for NR and QCM-D techniques respectively. Before use both supports were cleaned and activated in order to get the polished surface polar for vesicle interaction. Crystal cleaning was done using a specific teflon holder, that fits into a glass beaker. Solvents were poured in the beaker and the holder with the supports was placed in it. The solvents used for the cleaning were in the following order: (1) CHCl_3 , (2) Acetone, (3) EtOH and (4) H_2O , from the most apolar to the most polar. In order to increase the cleaning capability of each solvent, the beaker was placed in a bath sonicator for 15 min per solvent. After every solvent change, the supports were dried using a N_2 stream. After the whole solvent cycle, the supports were activated using a plasma cleaner Harrick (for NR supports) for 2 min and a UV Ozone cleaner BioForce (for QCM-D supports) for 30 min. This process allows to make the surface hydrophilic, with a deep cleaning from organic molecules that could be deposited on the surface. The supports were then cleaned with N_2 stream to get rid of dust particles that may have been deposited, and lastly flushed with Milli-Q H_2O . Finally, the supports were kept in Milli-Q H_2O until use.

2.3.2 Solid supported model membranes preparation

In order to prepare solid supported model membranes that can be used for NR, two methods were employed depending on the type of lipid used (saturated vs unsaturated chains).

Langmuir-Blodgett Langmuir-Schaefer method

The Langmuir-Blodgett Langmuir-Schaefer (LB-LS) technique was used to prepare solid supported bilayers from partially deuterated saturated PC molecules which have a transition temperature above room temperature (i.e. DSPC and DPPC). The trough used was the Langmuir Trough NIMA 611, equipped with a dipper for the first monolayer deposition. This instrument was also used to perform lipid monolayer analysis, deriving the compressibility of the layer as well as interaction between lipid layer/peptides or layer/organic molecules. The instrument consists of a teflon reservoir filled with an aqueous solution (buffer or Milli-Q H_2O), with a barrier that can be used to compress the surface area. A precise balance is also present, equipped with a properly dimensioned filter paper, in order to measure the surface tension. The surface pressure can be calculated considering the standard surface tension of the water at $22 \text{ }^\circ\text{C}$ $\Pi_0 = 72.8 \text{ mN/m}$. The difference $\Pi_0 - \Pi$, where Π is the read value from the balance during the experiment, is the surface pressure π , that must be zero after a good calibration with water. The trough before use was cleaned using the same solvent cycle mentioned before for the crystal cleaning process ((1) CHCl_3 , (2) Acetone, (3) EtOH and (4) H_2O). In the last step, the trough was filled with Milli-Q H_2O until the reservoir was completely full and aspirated with a peristaltic pump. The process was repeated twice,

followed by filling the reservoir with degassed Milli-Q H₂O. To make the deposition, a cleaned and activated support for NR experiments is clamped on the dipper and submerged under the level of the solution in the trough, while paying attention to avoid touching the water surface with the clamp. To double check the cleaning of the surface, a fast isotherm was performed, to see if there was any increase in the pressure during the compression. If the pressure registered was under 1 mN/m, the barrier was set open to perform the lipid spreading. The spreading was done using a 100 μ l Hamilton syringe previously cleaned 3 times with CHCl₃. A volume of 45 μ l from a stock lipid solution (1 mg/ml), was spread on the surface of the water drop by drop, making sure to touch the drop on the top of the needle to the water surface. During this process the surface pressure was recorded and saved. An incubation of 20 minutes was performed with the ventilation switched on to evaporate the CHCl₃ from the surface. Then the isotherm was performed with a barrier speed of 25 cm²/min until a pressure of 35 mN/m was reached. During the compression, the lipids rearrange from the gas phase to the solid-liquid phase, since the area available per lipid decreases during the compression. After the isotherm was recorded, the support was raised at 10 mm/min while the barrier maintained a constant pressure of the monolayer during the whole deposition, thus causing the formation of a monolayer on the silicon support (Langmuir-Blodgett method). To make the complete bilayer, a second deposition was performed using the Langmuir Trough NIMA 1212D. This trough was cleaned as mentioned for the previous one. Before the spreading, the PEEK portion that is important to close the NR cell, (for details see paragraph 2.5.1 and appendix A.4.1) was placed under water in an appropriate space. After carrying out the three steps of (1) spreading (2) incubation and (3) isotherm recording, the silicon support with the previous monolayer deposited on it, is placed horizontally with respect to the level of water in the trough. Then the support was carefully lowered down until it touched the monolayer in the trough (Langmuir-Schaefer method). The support was placed in contact with the PEEK portion under the water, thus closing the cell. The assembly was then taken out from the water and screwed with the metal part of the cell, where the thermo-controller is located. The sample was then ready for the measurement.

Vesicle fusion method

The vesicle fusion (VF) method was used to prepare supported lipid bilayers composed of unsaturated GPLs, or saturated ones with a transition temperature below room temperature (i.e. DMPC). The method requires the direct injection of a vesicle solution into the QCM-D or NR cell, that was prepared starting from dried lipids. Generally 1 mg for a NR cell and for four QCM-D cells, was taken from the stock solution of the lipid stored at -20 °C into an empty and clean vial using an Hamilton syringe. The solvent was evaporated under Ar until a lipid film was obtained. The vial was then placed in the vacuum for at least 3 hours, and secondly hydrated with 1 or 1.5 ml of vesicle fusion buffer (0.5 M NaCl). The idea behind such a high amount of salt, is to increase as much as possible the osmotic shock during the deposition, in order to have uniform and high coverage bilayers. The vial was then

filled with Ar gas and then vortexed in order to solubilise the lipid film, with the consequent creation of multi lamellar vesicles (MLVs) in solution which led to an opaque solution. To make large unilamellar vesicles (LUVs), the tip sonication was used with 20% amplitude, 1 second ON and 6 seconds OFF for 5 min and twice, in ice and under a continuous stream of Ar. The ice and the Ar helps the preservation of the double bonds of the unsaturated lipids. The obtained solution was finally ready for injection in the QCM-D or NR cell. During the experiments the flow rate used for the injection was set to 1 ml/min for QCM-D and 2 ml/min for NR experiments. The cells were first equilibrated with 0.5 M NaCl for 5 min at the flow rate previously mentioned, and then the vesicle solution injected. After an incubation of 20 min, Milli-Q H₂O was injected for 20 min to wash the vesicles that did not interact with the support and to start the osmotic shock. In these conditions, since inside the vesicles a buffer with high salt content is present, the water has the tendency to move through the membrane to inside the vesicles, which leads to the pop of the vesicles on the support with the consequent bilayer formation. At the end the cell was equilibrated with the experimental buffer, except for the characterisation of the natural lipid model membranes, that was done in Milli-Q H₂O.

2.3.3 LUV preparation for activity assays and MS kinetics analysis

Large unilamellar vesicles (LUVs) were used for mass spectrometry (MS) kinetic analysis. LUVs were prepared in PLA1 buffer following the protocol mentioned in paragraph 2.3.2. PC molecules are zwitterionic phospholipids in nature, leading to a charge on the surface of the vesicles that is equal to zero. This could lead to aggregation of the vesicles, leading to a non-homogeneous solution and causing problems with the PLA/vesicle interaction. To avoid such problems, a negatively charged lipid in the form of PA (DPPA) was added to the PC mix pool. The lipids used and their concentrations are described in paragraph 2.5.2.

2.4 Pre-characterisation studies by physico-chemical techniques

In order to assess the protein/lipid ratio for neutron experiments, some pre-characterisation experiments were carried out mainly through the use of ellipsometry and QCM-D.

2.4.1 Ellipsometry

Ellipsometry is a non-destructive optical technique widely used for the study of surfaces and thin films. It is based on the determination of the polarisation changes that light undergoes when it is reflected at an interface (Δ). Each layer that forms the sample has a different refractive index, and this profile (perpendicular to the plane of incidence) has an impact on the Δ variation. Ellipsometry experiments were performed on a Picometer Light ellipsometer (Beaglehole Instruments, Kelburn, New Zealand) using a He-Ne laser with $\lambda = 632$ nm. A fixed single angle closed cell was used for this experiment. The cell shown in appendix A.4.3, is made of PEEK material, with two glass windows through which the laser passes. The silicon support was screwed using a metal base to the PEEK with a O-ring ensuring a tight

closure. The angle of the incidence beam from the first window to the silicon support is 68° , close to the Brewster angle of silicon in water (72°). It is to be noted that with this system it is not possible to resolve structural information of the sample under examination, since only one angle is available with only one wavelength.

2.4.2 Quartz Crystal Microbalance with Dissipation monitoring

The Quartz Crystal Microbalance with Dissipation monitoring (QCM-D) is a surface sensitive instrument, measuring the mass changes on the crystal surface as well as the dissipation (viscoelastic properties) of the adsorbed layer. This technique is useful especially for interaction analysis and it is largely used in membrane biophysics. The fundamental working principle consists of detecting the resonance frequency over time applying an alternative current on the quartz silicon crystals, inducing them to a physical deformation. The alternating current causes the crystals to oscillate at their characteristic resonance frequency, that is directly dependent on the mass (correlated to the thickness and the mass density) of the layer deposited on the crystal, as also shown in the Sauerbrey equation 2.1. The oscillation of the crystals generate a shear wave that propagates perpendicular to the crystal through the sample. For the sensor used, the resonance frequencies are in the order of MHz.

$$\Delta m = -C \frac{\Delta f_n}{n} \quad (2.1)$$

From equation 2.1, C is the Sauerbrey constant ($17.7 \text{ ng}\cdot\text{Hz}^{-1}\cdot\text{cm}^{-2}$ [254]) and Δm is the absolute mass variation expressed in ng of the material on the crystal. This equation can be used only with rigid films, with a dissipation ΔD values of ≈ 0 . 7 harmonics (n) are measured simultaneously per each crystal used during the experiment (Fundamental $n = 0$, 3rd $n = 3$, 5th $n = 5$, 7th $n = 7$, 9th $n = 9$, 11th $n = 11$ and 13th $n = 13$). Each harmonic is more sensitive to a particular zone of the sample along the z axis (axis perpendicular to the crystal), for which reason usually all the 7 harmonics are used during an experiment. The resonance frequency of the crystal (F_{0_n}) measured in the buffer used in the experiment is taken as zero in ΔF ($F_{0_n} - F_{t_n}$; where F_{t_n} is the resonance frequency found at the time t). When there is a variation in the material deposited on the crystal, the resonance frequencies (F_{t_n}) vary, and this variation is shown as a negative ΔF_n (with positive mass variation). The dissipation is also measured during an experiment, providing information on the energy loss and therefore on the viscoelasticity of the soft layer deposited on the crystal, that is calculated measuring how fast the frequency pulses are dissipated. For instance in soft layers with complex structures that develop along the z axis respect to the crystal, the energy loss is higher, resulting in high ΔD values. The dissipation is measured per harmonic, in order to have a more complete overview of the sample.

QCM-D measurements were performed with an E4 instrument (Q-Sense, Biolin Scientific AB, Sweden), using SiO_2 -coated 5 MHz quartz sensors in the PSCM labs at the ILL. The crystals were cleaned as explained in paragraph 2.3.1. The experimental setup consists of four QCM-D cells with an inlet and outlet each. The outlet is connected through tubes to

a peristaltic pump, where the operative flux is set to 0.1 ml/min. The inlets are connected to tubes with the same length, for the injection of solutions. The cells are mounted inside a thermostatic chamber controlled directly by the QCM-D software. The temperature was kept constant at 22 °C. For the kinetics measurements, when the bilayer formation using the VF method was done, the protein was injected and the incubation started. During the incubation, all the harmonics in frequencies and dissipation were monitored.

2.5 Experimental setup

2.5.1 Scattering techniques

Neutron and X-ray scattering are powerful techniques, useful to obtain the structure of matter in solution or at interfaces at high or low spatial resolution. They have been widely used in biophysics, for the determination of structure and dynamics of biomolecules. In the present study, we have employed scattering techniques to obtain information on the factors that regulate the substrate specificity of the PLA1-1 isoform. Such techniques also help shed light on the structure of the membrane bilayers during the course of the kinetics.

NR

Specular reflection is a mirror reflection of an incident beam from an interface, consequently the angle of the reflected beam respect to the sample is the same as the incident beam ($\theta_{in} = \theta_{refl}$). The reflected beam is the result of the reflection and refraction caused by the intrinsic features of the interfaces that form the sample. The neutrons interact with interfaces depending on the difference in refractive index or scattering lengths and roughness of the materials forming them. According to the Bragg law, performing measurements varying the angle or the wavelength of the incident beam, different inter-lamellar distances (interface distances) d can be seen (see equation 2.2).

$$n\lambda = 2d \cdot \sin(\theta) \quad (2.2)$$

Bigger θ angles or lower wavelengths lead to smaller inter-lamellar distances, and vice versa. Neutron Reflectivity (NR) is a reflection technique that uses a neutron beam from a nuclear reactor or spallation source, to analyse thin layers with a thickness in the order of few Å. The technique measures the specular reflection $R(q_z)$ as a function of the momentum transfer q_z , shown in equation 2.3

$$q_z = \frac{4\pi \cdot \sin(\theta)}{\lambda} \quad (2.3)$$

where θ is the angle of incidence and λ is the wavelength of the neutron beam. Consequently q_z can be also defined as $q_z = k_{in} - k_{out}$, where k is the wave vector of the incident "in" and of the reflected "out" beam, figure 2.5. In order to measure a "full q-range" reflectivity of a sample, two approaches can be employed: (1) vary the angle of the incident monochromatic beam; (2) fix angle and vary the wavelength of the beam. For X-rays a monochromator crystal

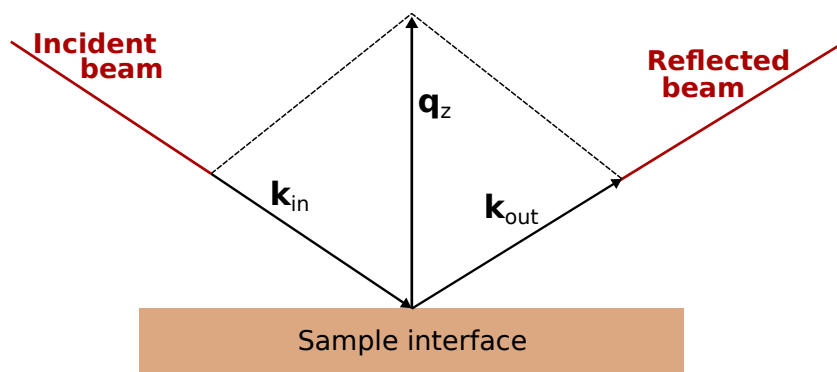


FIGURE 2.5: Scheme of the geometry during reflection of a beam from a surface

is usually used in order to obtain a monochromatic beam, but seeing that a very large amount of flux is lost during this process, it is less preferable for a neutron beam, since the flux is already quite low from the source. In order to control the wavelength of the neutrons in a neutron beam, mechanical velocity selectors can be used, that allow to obtain an higher flux compared to what could be achieved from a crystal monochromator system at the expense of wavelength resolution. A mechanical velocity selector works in time of flight (TOF), where only the neutrons with a specific speed (specific energy and wavelength) can pass through. Nevertheless, this method leads to q -resolution ($\lambda \pm \Delta\lambda$), that is directly correlated with the parameters of the mechanical velocity selectors (for instance the aperture). Therefore, there is always an uncertain in the q value using neutrons, that is expressed usually as $\Delta\lambda/\lambda$ and $\Delta q/q$. With neutron reflectivity the TOF is usually used to obtain pulses constituted by a range of neutron wavelengths (for example 2-30 Å wavelength on the ILL reflectometers), in order to acquire with one or two angles a wide q -range. The velocity selector compartment of FIGARO reflectometer at ILL is made by choppers (see in details figure 2.6) placed in a row, where the aperture, the rotational speed and the distance can be tuned to obtain the desired q -range, q -resolution and flux depending on the sample under analysis. For instance, thick interfaces in the sample generate a very high number of fringes in the reflectivity profile, and for those samples a high q -resolution is needed, or else the fringes can not be probably resolved, which will negatively impact the data analysis. In the case of supported lipid bilayers, the relatively small amount of features in the reflectivity profile, permits to work with a lower q -resolution that corresponds to a higher aperture of the choppers and consequently an higher flux of the neutron beam, leading to shorter acquisition times. [For more details on the q -resolution see chapter 6]. The main advantage of using the TOF method *versus* the monochromatic, with NR consists in the higher speed of the acquisition at lower resolution, due to the higher neutron beam flux and, since more q points are measured at the same time, the possibility to measure fast kinetics. The reflected intensity is dependent on the chemical composition of the interfaces within the sample, *i.e.* their coherent neutron scattering length density (SLD) of the materials. The SLD of a molecule is defined as the sum of the coherent scattering lengths of

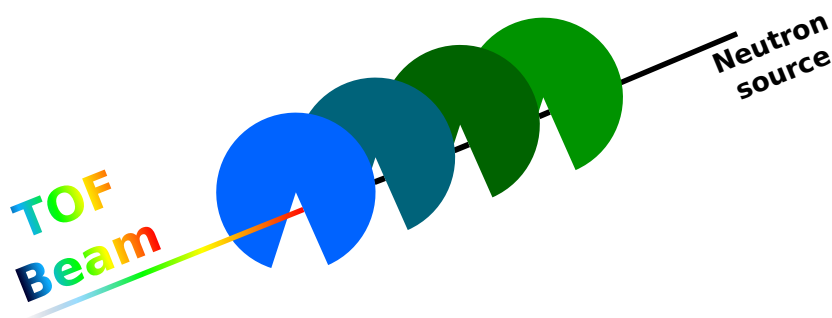


FIGURE 2.6: Scheme of the choppers used on FIGARO instrument for the TOF beam

all nuclei divided by its molecular volume. By modelling the structure of the sample, in this study a supported membrane, as a series of layers corresponding to the molecular constituents, it is possible to determine the one-dimensional structure described with the SLD profile along the z -axis of the sample, which is optimised to the experimental data. Neutrons also permit the use of so called "contrast variation" consisting of varying the percentage of deuterium content in the material measured (see details in Chapter 6). In NR, the lipid bilayers are usually measured in different solvent contrasts, differing for the amount of heavy water (% D_2O). By using different contrasts, the signal originating from different sample components can be selectively enhanced or matched out (a condition where the SLD of the molecule is equal to the SLD of the bulk solution). Also, the sample components can be selectively labelled with deuterium, like deuterated lipids or proteins/peptides, in order to hide or expose a certain molecule inside the sample. This method enables the analysis of the interaction between bilayers and organic molecules/peptides/proteins with higher accuracy.

NR measurements were carried out on the FIGARO (Fluid Interfaces Grazing Angles Reflectometer) neutron reflectometer at the ILL [255] using a neutron wavelength spectrum from 2 Å to 20 Å at two incident angles (0.8° and 3.2°) and constant wavelength resolution of $\Delta\lambda/\lambda = 7\%$. This instrument setup (see figure 2.7) allowed covering a q -range from 0.009 to 0.35 \AA^{-1} with reflectivity signals typically measurable above the incoherent sample background up to 0.25 \AA^{-1} . The sample cell used for the measurements was a closed flow cell consisting of a 1.5 or 2 cm thick single crystal silicon wafer (8 cm x 5 cm) mounted against a polyether ether ketone (PEEK) trough (1 ml internal volume) sandwiched between hollow aluminium holders to allow temperature control by means of water circulation. An inlet and outlet from the cell were used for the injection of samples and for buffer exchange (full description and pictures of the cell can be found in appendix A.4.1). The cell was connected through the inlet and outlet to a preparative HPLC pump for mixing and injection of water contrasts totally controlled by the instrument software. Four solvent contrasts (with their neutron scattering length densities SLD given in brackets) were used: 100% D_2O (SLD $6.35 \times 10^{-6} \text{ \AA}^{-2}$ from now on D-PLA-buffer), TMW, (59% D_2O , contrast matched to the partially deuterated tails SLD $3.5 \times 10^{-6} \text{ \AA}^{-2}$), CMSi or SMW (38% D_2O , contrast matched to the

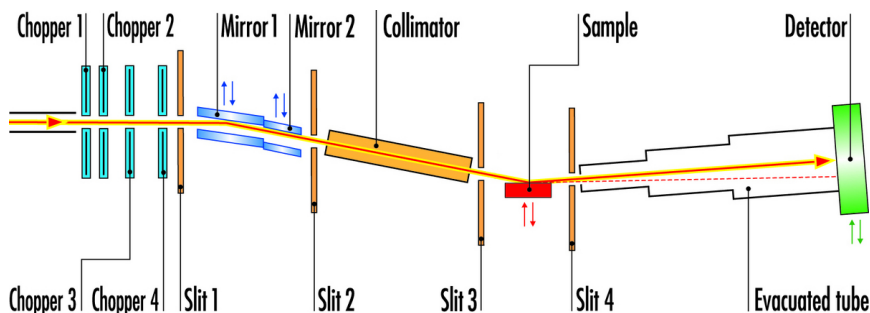


FIGURE 2.7: FIGARO instrument setup scheme

silicon substrates, $SLD\ 2.07 \times 10^{-6}\ \text{\AA}^{-2}$), and 100% H_2O ($SLD\ -0.56 \times 10^{-6}\ \text{\AA}^{-2}$ from now on H-PLA-buffer).

The measurements were carried out as following: after the bilayer preparation, data from supported lipid bilayers were collected in 3 or 4 contrasts to obtain the membrane parameters before the PLA1-1 injection. After the complete characterisation of the SLB, the enzyme was injected (1.5 ml at different concentration values depending on the type of lipid substrate used), and the measurement started as quickly as possible after the opening of the beam. The first measurements were done using the first angle at $\theta = 0.8^\circ$ with 5 minutes of exposure repeated for 1 hour, then with 10 min exposure for 2 hours. This enabled the monitoring of the kinetics of the membrane - PLA1-1 system. A full curve was measured at the two angles every now and then in order to get the complete q -range for a good estimation of the model. At the end of the reaction, once it was observed that there were not relevant variations in the reflectivity profile, the cell was washed to remove proteins and membrane debris, and measurement of what was left on the support in 3 or 4 contrasts was carried out. Most of the kinetics were measured in H-PLA-buffer contrast. The lipids used for the NR kinetics are listed in table 2.2. The solid supported bilayers from natural lipids were measured also in 4 contrasts using pure H_2O/D_2O combinations. Detailed description of the model used and of the algorithm behind CoruxFit can be found in Chapter 6.

Small Angle Scattering

Small angle scattering (SAS) is a powerful technique that is been used in different fields for the past 50 years, from fundamental physics to biology. The technique measures small and very small scattering angles, where the q -range can be tuned, depending on what the user wants to observe in the sample. In a colloidal solution, a high amount of the beam passes through the sample, whereas the rest of it is absorbed and scattered from the particles, where this latter contains the small angle signal that can be analysed to obtain information about overall shape and the nanoscale structure of the system. The particle size that can be resolved is in the range of 10 - 1000 \AA using a typical set-up, but it can be extended using higher angles (Wide angle scattering - WAS) or smaller angles (Ultra small angle scattering - USAS). The range of angles employed can be selected varying the sample to detector distance or the wavelength used. The small angle signal from a sample depends on the tri-dimensional SLD profiles (see

equation 2.4) of the scattering particles (scatters), which contain information on the SLD and dimension.

$$I(\vec{q}) = V^{-1} \left\langle \left| \int_{r^3} \delta\rho(\vec{r}) \cdot e^{i\vec{q}\cdot\vec{r}} d\vec{r} \right|^2 \right\rangle \quad (2.4)$$

The scattering intensity \vec{q} (from now on q in the text for simplicity) dependent is $I(q)$, where V is the averaged volume of the scattering particles; r is the radius in each 3D direction; $\delta\rho$ is the 3D electron density of the system subtracted with the solvent; and $i^2 = -1$. The experimental $I(q)$ came from the radial mean of the 2D image given by the detector. This process can be performed if the sample under examination is isotropic, where all the particles are randomly orientated, giving similar signals in all the radial directions on the 2D image. After the radial average, a SAS curve ($I(q)$ vs q) can be achieved and analysed by a model. SAS can be used to acquire low resolution structure of proteins in solution, and this aspect is essential in biology, since crystallography, which is a very high resolution technique, needs the protein to be crystallised, which is definitely a non-native environment. In addition SAS can also be used to get information about protein-protein and protein-lipid association, giving a good estimation on the ratio between the bound/unbound, and on the final low resolved structure of the complex.

Small Angle X-ray Scattering - SAXS In this study, SAXS was used to obtain the low resolution structure of the PLA1-1 protein, since no crystal structure was available in the PDB data bank. The sample was prepared as mentioned in paragraph 2.1.4 with the set-up described in paragraph 2.1.6. Data were analysed using the model #15 [256] of Genfit program [257]. This model takes into consideration a PDB file of the protein under examination, and in this case the predicted PDB structure of PLA1-1 was loaded. All the atomic coordinates were taken into account by the model as shown in equation 2.5.

$$A(\vec{q}) = \sum_{k=1}^N a_k(\vec{q}) e^{-i\vec{q}\cdot\vec{r}_k} \quad (2.5)$$

r_k corresponds to the distance of a k atom with respect to a given central one, $A(q)$ is the amplitude small angle signal and $a_k(q)$ is the atomic scattering length that takes into account the electron radius, the Thomson scattering and the real/imaginary part of the anomalous scattering. The hydration shell is also taken into account in this model, by "simulating" solvent atoms using "dummy" atoms with a spherical Gaussian distribution of scatters. From this last step, the hydration shell can also be displayed within the protein PDB structure using spheres. Details on how the shell is created can be found in [256]. The two amplitude contributions can be summed and averaged on the rotational factor ω_q (for the randomly oriented protein in solution) to get the theoretical form factor of the protein ($P(q)$). From the $P(q)$, with a inverse Fourier transform, the $p(r)$ can be calculated, that is by definition the probability to find two points in the shape of the protein within a length r . Then the final scattering intensity, physically defined as macroscopic differential scattering cross section is

calculated as shown in equation 2.6,

$$\frac{d\Sigma}{d\Omega}(q) = nP(q)S_M(q) + B \quad (2.6)$$

where $S_M(q)$ is the "effective" structural factor, that includes the form factor and the structure factor $S(q)$ derived from protein-protein interactions and n is the number of scatters (protein/complexes) in solution.

This model was used to analyse the SAXS profile of the PLA1-1 in solution taken on BM29 instrument. In order to estimate the amount of aggregation of the protein, the theoretical and the experimental curves were then subtracted, and this second curve was analysed separately using a second model within Genfit program.

Small Angle Neutron Scattering - SANS In order to obtain the match point of the purified deuterated natural GPLs, SANS measurements were performed on the instrument D22 at the ILL. The measurements were done using Hellma quartz 120-QS cells of 1 mm pathway and were measured over a q -range of $2.5 \cdot 10^{-3} - 0.6 \text{ \AA}^{-1}$ at a single wavelength of 6.0 \AA (FWHM 10%) with 3 sample-to-detector distances of 1.5 m, 5.6 and 17.6 m. The samples were measured at $22 \text{ }^\circ\text{C}$. Data were subtracted using the attenuated direct beam, and data correction was performed using the software GRASP (<https://www.ill.eu/users/support-labs-infrastructure/software-scientific-tools/grasp>) and merged using an IGOR macro. In order to get the match point, the average intensity of the points at $q < 0.005 \text{ \AA}^{-1}$ and at $0.2 < q < 0.4 \text{ \AA}^{-1}$ was performed calculating the $\sqrt{\Delta(I)}$, that corresponds to the squared difference of the $I(\approx 0)$ and the intensity at high q . Fitting with a straight line to the point plotted as "%D₂O" vs $\sqrt{\Delta(I)}$, it was possible to obtain the %D₂O at which the signal from the deuterated GPL vesicles is equal to zero, leading to the % of deuteration of the sample.

SANS measurements were also performed to vesicles with and without the incubation with the PLA1-1 under examination, utilising the same instrument and set-up described above. The samples were kept at $22 \text{ }^\circ\text{C}$ during the acquisition.

2.5.2 High-throughput lipidomic analysis (MS analysis)

High-throughput lipidomics and the PLA1-1 kinetic analysis were done using the 6470 Triple quadrupole LC/MS Agilent.

General physics behind the instrument

Mass spectrometry is an analytical method useful to determine the mass of the compound being analysed, the formula and the structure. A mass spectrometer employs ionization of the molecules under analysis, in order for them to be accelerated and investigated through the components of which the spectrometer is made. After ion formation from the sample, the mass analyser separates all the ions based on the charge to mass ratio, and outputs them to the

detector, where the ions create an oscillation on the output current of the detector that can be converted on a digital output. Several types of mass spectrometers exist, working with different components and different principles. The main ones used are the following: Quadrupole mass analyser, Time of Flight mass analyser (TOF), Magnetic sector mass analyser, Quadrupole Ion Trap mass analyser and Ion Cyclotron Resonance. In our study, a triple quadrupole MS was employed to carry out high-throughput measurements.

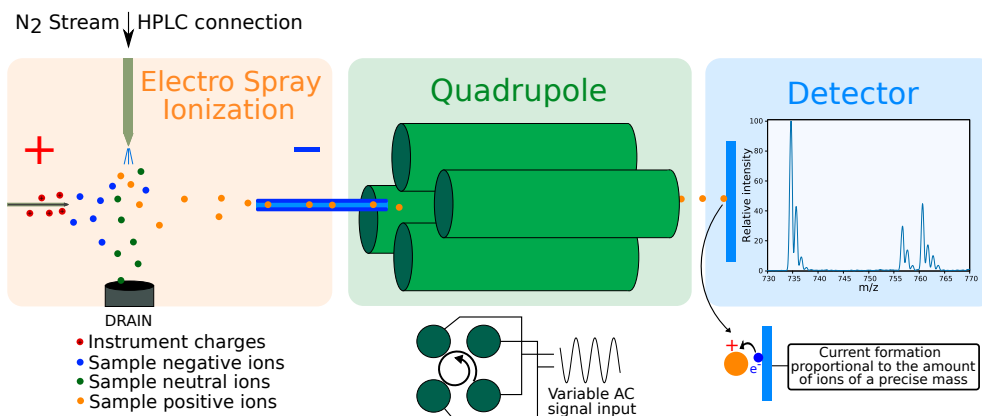


FIGURE 2.8: Single quadrupole scheme.

Single quad mass spectrometry - Figure 2.8, displays a scheme of a single quadrupole mass spectrometer (Q-MS), the simplest version of the triple quadrupole. Usually these instruments are coupled to an HPLC or an UHPLC (Ultra High Performance Liquid Chromatography) for a very precise and controlled injection of the samples in the instrument, and for an automated injection of several samples. If the sample needs to be purified before the mass analysis, a column can also be installed. The first module of the mass spectrometer displayed in figure 2.8 is the Electro Spray Ionization (ESI), where the sample is nebulised (process helped by the pressure from the HPLC/UHPLC) followed by employing an N_2 stream to dry the small drop created through the spraying process. The sample usually is solubilised using a solvent (ACN, $CHCl_3$, MeOH, ect), as to improve and speed up the drying process of the drops. In this chamber a strong electric field is applied in order to accelerate the dried molecules towards the analysis module. There are mainly two types of analysis controlled by the ESI section: positive and negative mode. The positive mode (shown in the figure 2.8) is when the positively charged molecules are pushed toward the analysis part, whereas the negative mode is the other way round. All the zwitterionic and positively charged lipids can be seen in the positive mode, while all the negatively charged lipids are seen in the negative mode.

Next, the accelerated ions pass through the quadrupole for the mass versus charge separation (m/z). This element acts like a filter, permitting the passage of only certain m/z ions depending on the alternative current (AC) signal in input. Every ion with a different m/z ratio, resonates with a certain AC signal frequency. Thanks to this property, the AC signal can be adjusted in order to scan between a preferred m/z range. The speed of the scan cycle depends on the range and on the Δr (resolution of the m/z scan). In our experiment, the cycle

is around 2 seconds, with a Δr of 0.05 m/z. The ions coming out of the quadrupole module are, therefore, separated (in m/z) in time. So different m/z ions hit the detector in a different part of the scan cycle. The analyser measures the electric current variation when an ion hits the detector, giving a spectra over m/z. The intensity of the electric current variation depends on the absolute amount of ions hitting the detector.

Triple Quad-Mass Spectrometry - For our experiment a triple quadrupole (QQQ) was used, in order to have clearer and less noisy spectra to work with. The first part of this QQQ-MS works as mentioned in the section above, with the addition of two quadrupoles in a row after the first one. The third quadrupole acts like the first one, analysing ions coming from the second. The second quadrupole, also known as the "Collision Cell", is where the fragmentation happens. Under specific conditions of the collision cell (voltage of the quadrupole, pressure of the collision gas, etc), the molecules under analysis (parents) can be fragmented, realising daughter molecules as a finger print of the parent ones. For instance, if there are two different molecules with the same m/z ratio in the same sample, there is no way to distinguish them without using a column for a physical separation; whereas, with the fragmentation method, it is likely the two molecules release different daughter molecules, that can be identified using the third quadrupole. The third quadrupole method can be in scan mode or single ion monitoring. With the first method the quadrupole scans all the m/z in a given range; whereas with the second one the quadrupole is fixed to one or N possible m/z. The resulting scan from the Q1 can be also filtered consequently with the result from the Q3. For instance, if only the spectra from the Q1 of a single chemical species is needed, the Q1 spectra can be filtered in order to have the signals on the Q1 that give a proper value m/z of the daughter molecule in the Q3. In this study, such a method was used to get very clear and low noise spectra, using the parent 184 m/z protocol. This method consists of the fragmentation of the choline from the polar head of the lipid used (phosphatidyl choline) giving a signal in the Q3 of 184 m/z. At the end of the measurement, it was possible to get all the peaks in the Q1 that give the 184 m/z signal in the Q3.

Kinetic assay protocol for MS analysis

The lipid mixtures used for the MS kinetics experiment are reported in table 2.3 and 2.4 for the PC kinetic mix (A) and (B) respectively. Mix (A) consists of a number of saturated and unsaturated PC molecule species while mix (B) contains only unsaturated species. Both these mixtures were employed to investigate the contribution of (a) the efflux and (b) the active site accommodation, in regulating the activity of the enzyme. Since, when MS measurements of mix (A) were carried out, we had faced difficulties in the assessment of the degradative kinetics of the selected unsaturated species (for instance POPC, PLyPC, etc), we had to prepare another simpler mixture *i.e.* mix (B) that contained only unsaturated series. This was needed to investigate if the hydrolysis rates of such species were influenced by the presence of certain long chained saturated species. Also such a mixture will allow us to precisely study

the kinetics of such unsaturated species. The lipid stocks that were stored at 10 mg/ml at -20 °C were used to make mixtures in solution: 1 ml of volume with a lipid concentration of 2000 nmol/ml per each PC GPL. Such mixtures were used to prepare a second stock mixture at a concentration of 200 nmol/ml per lipid. From this stock 10 μ l was taken into an empty and clean vial to make LUVs for the MS experiment, allowing us to have an amount of 2 nmol per lipid for the kinetics experiment. The sample was evaporated under Ar and placed under vacuum for at least 3 hours. The LUV solution for the MS kinetics experiment were prepared as described in paragraph 2.3.3 using for the hydration 500 μ l of PLA buffer.

The kinetics were performed at 37 °C in a thermo-bath. The protein prep and the LUV solution were incubated in the same thermo-bath for 20 min before mixing them, as to make sure that the start of the reaction was at 37 °C. The protein concentration across all the experiments was of \approx 0.7 mg/ml, in a volume of 500 μ l resulting in a final amount of 350 μ g of PLA1-1. The two solutions (LUV and PLA1-1) were mixed together to get a final reaction solution volume of 1 ml. Upon incubation, a number of aliquots at regular intervals (time points - tp) were pipetted out (60 μ l) into glass vials containing 2 ml MS-Grade MeOH + 0.5% HCl followed by a vigorously vortexing and maintained on ice. The action of this solution is the immediate stop of the hydrolysis reaction, since the MeOH destroys the structure of the vesicles, while the cold temperature slows down the reaction following the denaturation of the protein caused by HCl.

A modified lipid extraction protocol as described by Folch et al [251] was performed. 4 ml MS-Grade CHCl_3 followed by 2 ml Milli-Q H_2O were added to each sample. All the samples were tightly capped, vortexed and incubated at RT for one hour to allow the emulsion to settle down and two phases to clearly separate. The upper phase is the aqueous phase, where the protein and salts are, whereas the bottom phase is the organic one, where the lipids are dissolved. The upper phase was discarded using a 1000 μ l pipette, and the theoretical upper phase solution ($\text{CHCl}_3/\text{MeOH}/\text{H}_2\text{O}$ [3:48:49 v/v/v]) was added to each vial for a second wash of the organic phase. This second step was essential, since salts like Na^+ may bind to the polar head of the PC molecules, giving a shift in the MS spectra by a difference of +23 m/z, causing consequent problems while interpreting the data. The vials were again vortexed for 10 second and incubated for one hour. The upper phase was again discarded and the lower phase evaporated under Ar. The invisible film created was then resuspended in the MS running solvent (ACN:IPA: H_2O) and transferred into vials containing conical inserts, and were finally ready for the MS measurements.

Method for the PLA1-1 MS kinetic assays

MS measurements were carried out by direct infusion into the triple quad MS. Samples after lipid extraction were resuspended in 150 μ l of MS running solvent solution (ACN:IPA: H_2O), that was transferred into vials with conical inserts and stored at -20 °C until analysis. The samples were then vortexed and heated up before placing them in the sample rack of the uHPLC, that was maintained at 16 °C. The uHPLC was programmed to inject the samples into

	Lipid name	Abbreviation	Mol. mass [Da]	[nmol]	[mg]
Saturated series	18:0 - 18:0 PC	DSPC	790.145	2000	1.58
	16:0 - 16:0 PC	DPPC	734.039	2000	1.47
	14:0 - 14:0 PC	DMPC	677.950	2000	1.36
	12:0 - 12:0 PC	DLPC	621.826	2000	1.24
	16:0 - 18:0 PC	PSPC	762.076	2000	1.52
Unsaturated series	16:0 - 18:1 PC	POPC	760.076	2000	1.52
	16:0 - 18:2 PC	PLyPC	758.060	2000	1.52
	16:0 - 18:3 PC	PLnPC	756.060	2000	1.51
	16:0 - 20:4 PC	PAPC	782.082	2000	1.56
	16:0 - 22:6 PC	PDPC	806.100	2000	1.61
Charged lipid Internal std	18:0 - 18:0 PA	DPPA	670.873	3800	2.55
	24:0 SM	SM	815.240	3570	2.91

TABLE 2.3: Lipid mixture (A) [PC kinetic mix (A)] used for the MS kinetic analysis.

	Lipid name	Abbreviation	Mol. mass [Da]	[nmol]	[mg]
Unsaturated series	16:0 - 18:1 PC	POPC	760.076	2000	1.52
	16:0 - 18:2 PC	PLyPC	758.060	2000	1.52
	16:0 - 18:3 PC	PLnPC	756.060	2000	1.51
	16:0 - 20:4 PC	PAPC	782.082	2000	1.56
	16:0 - 22:6 PC	PDPC	806.100	2000	1.61
Charged lipid Internal std	16:0 - 16:0 PA	DPPA	670.873	2000	1.34
	24:0 SM	SM	815.240	2000	1.63

TABLE 2.4: Lipid mixture (B) [PC kinetic mix (B)] used for the MS kinetic analysis.

the QQQ-MS in a sequence. A volume of 2 μ l per sample was injected with a flow rate for the measurements of 0.04 ml/min, in order to obtain a good signal within a sufficient time. Each sample was measured trice in order to test the reproducibility. The first quadrupole (Q1) range scan was 435 - 835 m/z, in order to get the signal of all the phospholipids molecules within the mixture and the lysophospholipids formed during the PLA hydrolysis reaction. The fatty acids were not detected, but their amount could be determined by integrating the normalised total count chromatograms [for more details see Chapter 7] and plotting the integrated values (exponential decay of the signal due to the loss of material during the kinetics). As mentioned in the paragraph 2.5.2, in order to get a more accurate and less noisy spectra, the precursor ion scan was used. To perform that, the collision cell (second quadrupole Q2) was set in order to get the fragmentation of the polar head of the phospholipids, and the Q3 for the analysis of the fragments. The parameters for the collision cell are: 15 eV for the collision energy, 5 V the electric potential with a capillary accelerator voltage of 3500 V. The Q3 was set to 184 m/z single ion monitoring, precursor ion of the phosphatidylcholine lipids. The Q3 acts like a filter, so that the final spectra measured on the Q1 displays only the peaks giving the 184 m/z signal in the Q3. For every 5 samples, a blank was run, in order to clean the instrument thus ensuring that there was no carry over from the sample previously measured.

A second method for the MS analysis was developed, to allow us to do the analysis of

the kinetics carried out using the total lipid extracts (TLE) from *Pichia pastoris*. The TLE utilised for the kinetics experiment, contains all the classes of phospholipid molecules as follows: PS, PG, PI, PA and PE. In order to obtain more detailed information on all the lipid species inside each class, a "dynamic multiple reaction monitoring" (DMRM) was set up. The method consists in the use of a C18 column, for the separation of all the lipid species inside the sample before their injection in the MS for the analysis. In principle, every lipid species has a certain retention time through the C18 column, leading to the "spreading" of the samples in different peaks during the MS analysis. Consequently, a table describing the list of the expected lipids under examination can be applied, describing each molecule per its retention time (RT), mass (m/z), fragmentation (for instance parent 184 for PC, or neutral loss, etc) and the polarity of the analysis (positive or negative to scan different charged lipids). The "spreading" of the lipids contained into the sample leads to a less complex mixture that is consequently even more ionised within all the molecular species from the ESI of the MS, since, during this step, the competition of the lipids for the ionization normally occurs. This competition is an important factor to take into consideration, especially when the amount of the various molecular species contained into the sample is different. Accordingly, a more reliable and stable signal can be achieved. This method is useful also for quantitative determinations of a set of known lipid species. The experiment was performed using an already existing DMRM method, in order to determine the quantity of the most popular lipids.

Data analysis

The total count chromatograms (TIC) outputs generated by the instrument, were integrated using the MassHunter software in order to get the MS spectra of each sample injected (including the technical replicates). After the integration process, all the spectra were subtracted utilizing the blank measured, in order to have a baseline ≈ 0 intensity in all the spectra. The data were then exported and normalised by an in-house built python program [see details in chapter 7], using the signal of the standard SM (non degraded by the PLA1-1). The ratio between the area of the SM at time point 0 minutes (tp0) and the area of the same SM at the other time points, gave a multiplication factor per tp, that was used to normalise the spectra directly. After normalisation, all the peaks in every tp spectra were integrated and normalised using the same peaks in the tp0, in order to generate the degradation profile (between 0 and 1). These profiles were then fitted using an ad-hoc python program with a first exponential decay model, that directly gave the speed of the degradation of each lipid species as well as the final amount of degradation.

Chapter 3

Results: Protein and lipids production

To study the PLA1-1 - model membrane interactions and the hydrolysis kinetics, PLA1-1 and phospholipid molecules were produced in the ILL laboratories. This Chapter is focused on the results obtained for the (a) protein expression and purification, (b) lipid extraction and purification from biomass and (c) chemical synthesis of partially deuterated phospholipid molecules.

3.1 PLA1-1 production

In this section, the expression and purification of the *Aspergillus oryzae* PLA1-1 isoform, is discussed including results emanating from its structural and functional investigation.

3.1.1 Expression and purification

The recombinant expression of the PLA1-1 protein, as mentioned in Chapter 2 (paragraph 2.1), was performed in *Escherichia coli*, a prokaryotic system. The purification of the protein was done sequentially first by affinity chromatography and then by gel filtration. In order to explore the best conditions for the MBP - PLA1-1 overexpression (MBP - Maltose Binding Protein), an expression test was performed using different temperatures and expression times. The amount of IPTG (Isopropyl β -D-thiogalactopyranoside) utilised was kept constant at 1 mM (final concentration in the culture medium). As shown in the gel in figure 3.1, where only few conditions were run, there was not much difference between 3h at 37 °C and O/N at 25 °C. Consequently, the expression at 25 °C, O/N was chosen, in order to slow down the expression, thereby decreasing the probability of an incorrect folding of the protein of interest. By comparing, the "non-induced" and the induced lanes displayed in figure 3.1, it is clear that the protein of interest is correctly overexpressed, since a very strong band appears at the level of ≈ 72.5 KDa, that corresponds to the molecular weight of the fusion protein MBP - PLA1-1 (≈ 42.5 KDa and ≈ 30 KDa for the MBP and PLA1-1 respectively). Once the expression conditions were identified, a large culture was started, in order to produce a large protein batch. The clear lysate obtained from the O/N culture was directly injected in the MBP-Trap column coupled to the FPLC (Fast Protein Liquid Chromatography). In figure 3.2, is shown the chromatogram obtained from the affinity purification step. The graph displays the time of the purification, (and if multiplied by the flow rate, the ml of running buffer [PLA1-1 buffer]

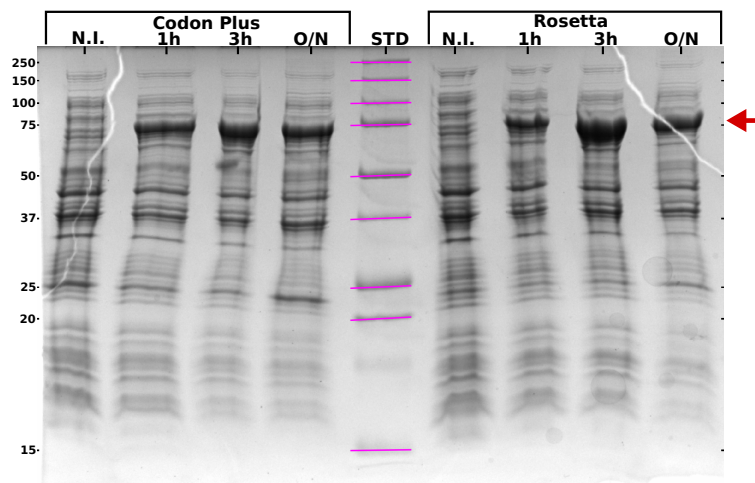


FIGURE 3.1: Time dependent expression test, performed for Codon Plus and Rosetta strains. The lane "N.I." is the non-induced cells; 1h, 3h at 37 ° and O/N at 25 ° are from induced cells. The two strain expressions resulted in similar protein expression (as indicated by the red arrow).

passed through the column), versus the absorbance at 280 nm (expressed in mAU), that is usually used to detect proteins. The orange line corresponds to the gradient of elution buffer used. The first broad peak appearing at the beginning of the chromatogram, is the result of the non-bonded proteins washed from the resin of the column using the running buffer. For the elution step, a gradient (between PLA-Buffer and Elution Buffer) was set, and at $\approx 20\%$ of the elution buffer, we assisted to the elution of the MBP - PLA1-1, within the typical sharp peak of an affinity chromatography. During the elution step, fractions of 1 ml were collected

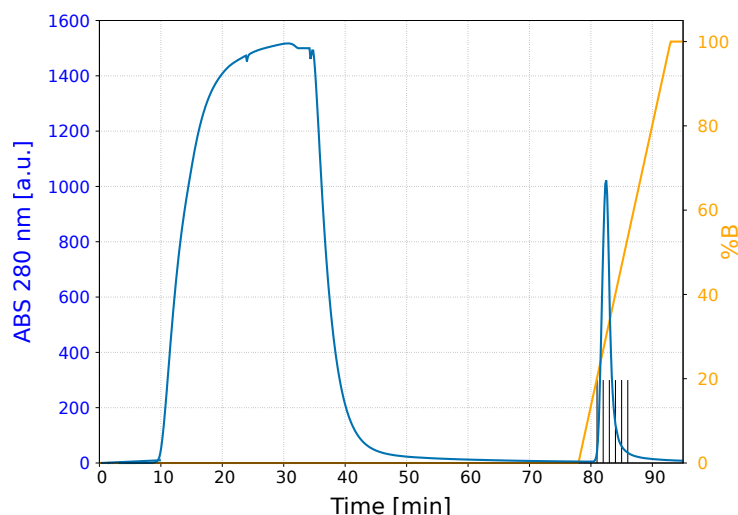


FIGURE 3.2: MBP Trap chromatogram. The black straight lines represent the fraction collected, from the N°7 to the N°11. The "%B" displayed in the second y-axis corresponds to the ratio between the PLA-Buffer (used as running buffer) and the Elution Buffer.

(displayed in figure 3.2 as straight black lines), obtaining the eluted protein in 5 fractions that were checked using an SDS-PAGE gel (figure 3.3). The fraction tested were from 7 to 11

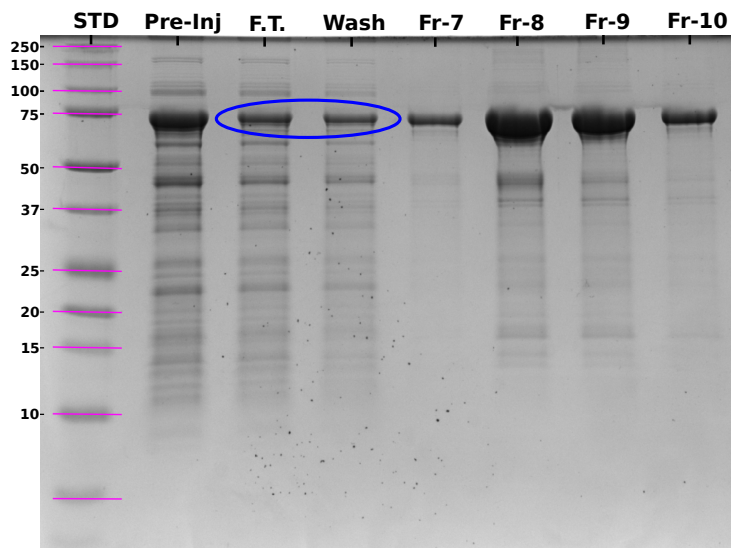


FIGURE 3.3: SDS-PAGE gel of the affinity purification step. Where STD is the standard; Pre-Inj is the sample before its injection into the column; F.T. is the flow through (non-bound proteins); Wash is the washing step of the column; and the last 4 lanes are the 4 eluted fractions. The blue circle represent the protein lost during this purification, as mentioned in the text.

(where the fraction 1 starts with the start of the gradient), but only four of them were loaded in this gel (figure 3.3). Following the description of the lanes: (1) STD the standard; (2) the clear lysate before the injection in the column; (3) the flow through from the column; (4) the wash fraction; and finally, in the last four lanes, the elution fractions (from 7 to 10). As noticed from the flow through (F.T.) and the wash lanes, some of the fusion protein was lost during these steps. This depends on the saturation of the column, since the stationary phase has an upper limit in the binding of MBP tagged proteins. The amount of protein injected was then optimized, in order to obtain the maximum protein yield from the clear lysate (for instance see figure 3.6). From the elution fractions, a large (because of its high concentration) and clear band appeared ≈ 72.5 KDa in the gel in figure 3.3, that corresponds to the MBP - PLA1-1. The purified fractions contained also other small bands corresponding to proteins with lower molecular weights. The most abundant protein in the eluate fractions was the endogenous MBP (≈ 45 KDa), since *E. coli* normally express it, resulting in the final contamination of the eluted fusion protein (coelution of MBP and MBP - PLA1-1). This first purification step was performed twice starting from 3 g of cell pellet resuspended in 30 ml lysis buffer, in order to avoid the saturation of the MBP-Trap column. From this process, 55 mg in 10 ml of purified protein was obtained, constituted by MBP endogenous protein + MBP - PLA1-1. In order to procure a more pure solution of MBP - PLA1-1, a gel filtration step was performed. 2 ml of the purified MBP - PLA1-1 pool was injected into a gel filtration column coupled to an FPLC. The low volume injected allows a higher peak resolution during the purification. Fractions of 1 ml were collected starting from ≈ 30 min after the injection of the sample in gel filtration (0.25 CV). A large peak appeared at the very beginning of the gel filtration

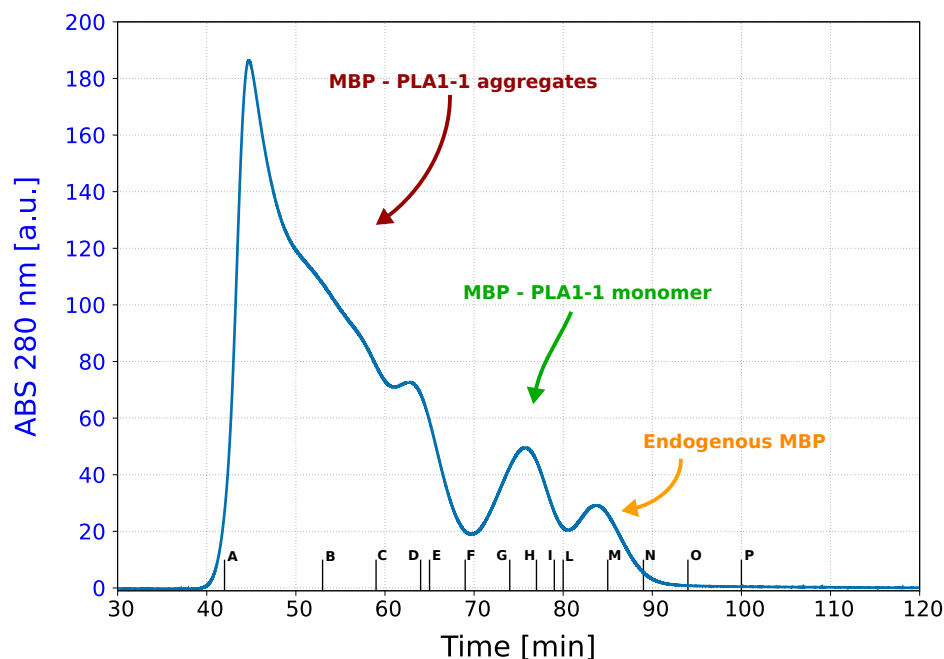


FIGURE 3.4: Gel filtration chromatogram. The black straight line represent the fraction taken for the SDS-PAGE gel shown in figure 3.5

chromatogram (44 min, 0.37 CV) as displayed in figure 3.4, that corresponds to aggregated complexes since it eluted with the void volume of the column. A second peak right after the aggregation one eluted around 75 min, and corresponds to the MBP - PLA1-1 (≈ 75 KDa), according to the calibration curves on the manual of the column. The third peak appeared at 84 min corresponds to the endogenous MBP, that coeluted during the affinity chromatography step. The fractions shown in the chromatogram were then loaded into an SDS-PAGE gel displayed in figure 3.5. As shown in figure 3.5, the first peak corresponds to the aggregation

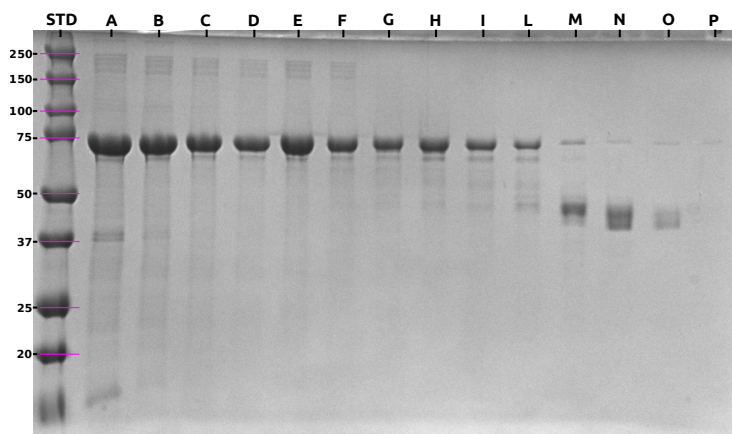


FIGURE 3.5: SDS-PAGE gel of the gel filtration purification. The fraction loaded are displayed in figure 3.4

status of the MBP - PLA1-1, since the gel shows clearly the right molecular weight of the MBP - PLA1-1 protein. The second peak corresponds to the right monomer of MBP - PLA1-1, since its molecular weight is the same in its "native" condition (gel filtration, from the

calibration curve) and in its denatured state (SDS-PAGE gel). The last peak, as supposed, is the endogenous MBP protein. The gel filtration chromatogram, was then deconvoluted using 5 gaussian functions, in order to obtain the purity of the pool collected from this step. The result and the process are explained in Appendix paragraph A.2.3 and in figure A.1. From this process, a purity of 96.3% of the pool collected (71 - 79 ml) was found, and an efficiency of purification of 10% was achieved (ratio between integrated peak of the MBP - PLA1-1 and the total chromatogram integration). The entire process resulted in a final amount of 5.5 mg of MBP - PLA1-1, from 3 g of cell pellet. In figure 3.6, a gel of the entire process of purification is shown. In this gel only the fractions of the MBP - PLA1-1 gel filtration peak were loaded. As mentioned before, the protocol for the affinity purification was optimised,

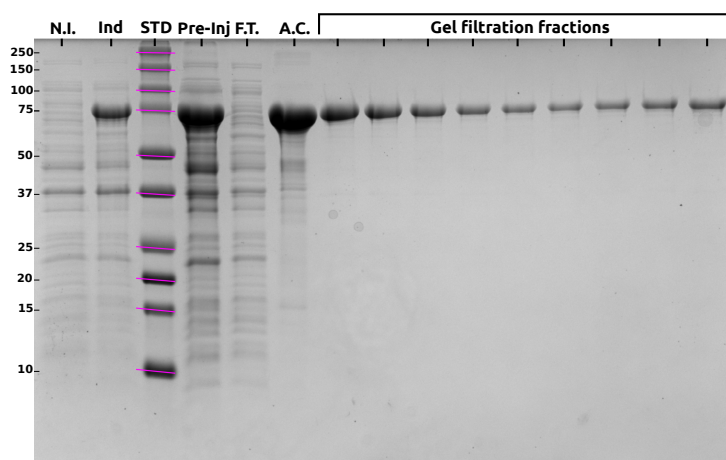


FIGURE 3.6: Entire purification process SDS PAGE gel. Where N.I. is the non-induced cells and Ind represent the induced cells; STD is the standard; Pre-Inj is the protein sample before its injection into the MBP-Trap; F.T. is the flow through of the non-bonded proteins; A.C. is the affinity chromatography purified sample; and finally the last lanes represent the gel filtration fractions.

as the MBP - PLA1-1 does not appear in the flow trough lane (figure 3.6 lane "F.T."), since all the injected MBP - PLA1-1 bonded to the resin of the column. In summary, all the peaks from the gel filtration were checked using calibration curves and SDS-PAGE gels, thereby confirming the purity and the identity of the collected MBP - PLA1-1 pool.

An activity assay was performed for all the fractions as shown in figure 3.4, in order to spot in which fraction the active protein was located. DMPC as substrate was utilised for this purpose, and a TLC was performed as shown in figure 3.7. In the TLC displayed in figure 3.7, only the first two peaks were tested, since the last peak corresponds to the MBP, that has no activity on phospholipid substrates (data not shown). The first lane of the TLC corresponds to the blank (LUV solution without the addition of the protein), followed by LUV + gel filtration fraction and the last two lanes are the standards (PC and LPC standard). The LPC migrates on the silica TLC at a slower rate compared to DMPC, due to its higher polarity (higher interaction with the matrix) since it contains only one acyl chain, resulting in a good separation between PC and LPC. The FFA migrates to the top of the plat (along with the running buffer), since their hydrophobicity does not allow any interaction with the

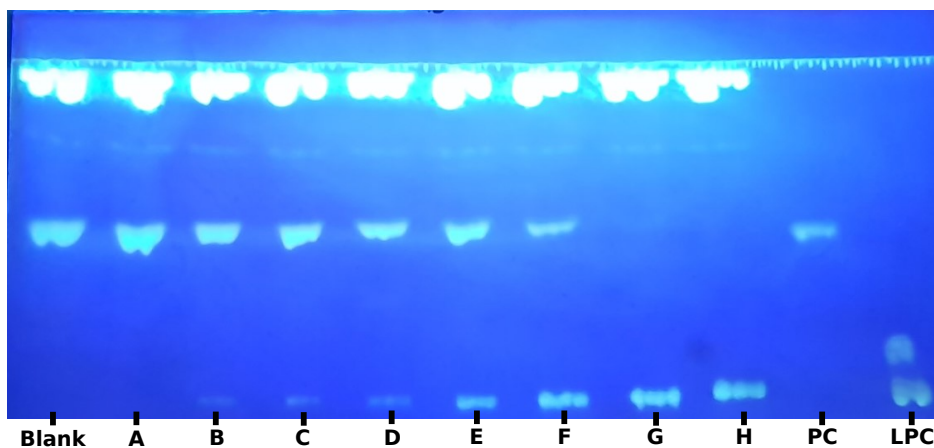


FIGURE 3.7: TLC representing an activity assay performed on the fractions displayed in the gel filtration chromatogram in figure 3.4. In this experiment, the FFAs released from the reaction are not visible, since the TRITON used covers their signal, migrating in the same spot.

matrix of the TLC. In this example the FFAs are not visible, since the band of the Triton used for this assay, covers that region. From the TLC in figure 3.7, it can be observed that the first peak fractions have no hydrolysis activity on the DMPC composed LUVs, since no LPC is released, whereas the activity is observed for the fractions in the second peak, since the LPC band appears in those lanes.

In summary, from 800 ml of LB liquid culture, ≈ 3 g of cell pellet can be achieved, which allows to obtain 5 mg of purified fusion protein. The integrated peak of the gel filtration was 10% with a contamination from the other peaks of 3.7%, where the aggregated proteins and the endogenous MBP correspond to the remaining part (90%). The efficiency of the purification (in terms of the yield) was not very high, even after the various optimisations, but the protein achieved was enough for the NR, SAS and MS experiments.

3.1.2 MBP tag removal, cleavage mediated by Factor Xa

In order to get sequence and structural information for the expressed PLA1-1, MBP-tag removal was carried out, to perform those analysis only for the protein of interest. As mentioned in Chapter 2 paragraph 2.1.1, between the MBP-tag and the PLA1-1 sequence in the vector, a small sequence coding for 10 amino acids exists. This sequence can be recognized by the protease Factor Xa. In order to get the correct balance between amount of cleaved products and reaction time, a small scale time-dependent assay was performed, and shown in figure 3.8 through a SDS-PAGE gel. As seen from the gel SDS-PAGE in figure 3.8, the cleavage reaction, with a ratio of 1:50 factor Xa:fusion protein (w:w), reached the plateau after 4 hours, since the intensity of the bands between 4 and 6 hours did not change much. Short reaction times reduce the possibility of protein degradation, that may occur since the reaction was carried out at RT (≈ 22 °C). A large scale cleavage (4 hours at RT) was next performed, followed by the factor Xa arrest, in order to stop the reaction by removing the Factor Xa from the reaction solution. After this step, an MBP-Trap affinity chromatography

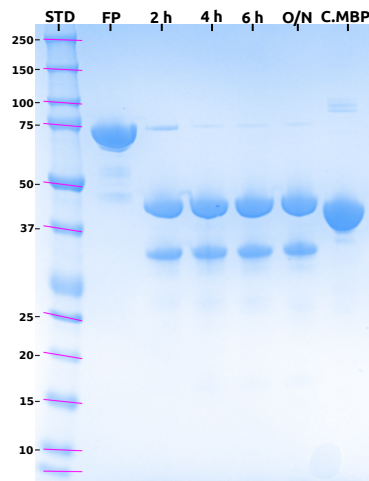


FIGURE 3.8: Time dependent Factor Xa cleavage assay. Where STD is the standard; FP is the fusion protein; following the different timings where O/N is the over night digestion; and finally C.MBP is the MBP protein used as control.

step, was carried out in order to separate the MBP-tag and the uncleaved MBP - PLA1-1 from the cleaved PLA1-1. Figure 3.9 shows the chromatogram resulting from the affinity chromatography step, and the figure 3.10 shows the SDS-PAGE gel carried out to check the correct course of the purification. Figure 3.9 depicts the purification of PLA1-1 through the MBP-Trap affinity chromatography after the cleavage reaction. The first peak, which is the F.T., corresponds to the cleaved PLA1-1, whereas the second peak (during the elution step) corresponds to the MBP-Tag and the uncleaved MBP - PLA1-1 fusion protein. Next, the activity of the cleaved PLA1-1 was tested, using the same lipid substrate along with the conditions used for the MBP - PLA1-1 assays, resulting in a functional protein.

3.1.3 cDNA sequencing

The sequencing of the expression cassette was performed in order to check if the theoretical sequence corresponded to the one used for the recombinant expression. The vector solution was prepared as mentioned in Chapter 2, and sent to "Genewiz". Figure 3.11 shows the alignment between the theoretical vector sequence (query) and the sequence obtained from Sanger sequencing (forward). The selected sequence corresponds to the theoretical nucleotide sequence coding for PLA1-1, resulting in a 100% of match between the two. Sanger sequences are characterized by problems at the beginning and at the end of the reaction, resulting in gaps and mismatches at the beginning and end of the alignment. The PLA1-1 sequence is located exactly in the middle of those sequences, and none of those problems occurred.

3.1.4 Mass spectrometry analysis of the uncleaved and cleaved PLA1-1

Since the nucleotide sequence for PLA1-1 is not optimized, even if Codon Plus cells were employed, a control of the amino acid sequence of the protein after the purification was

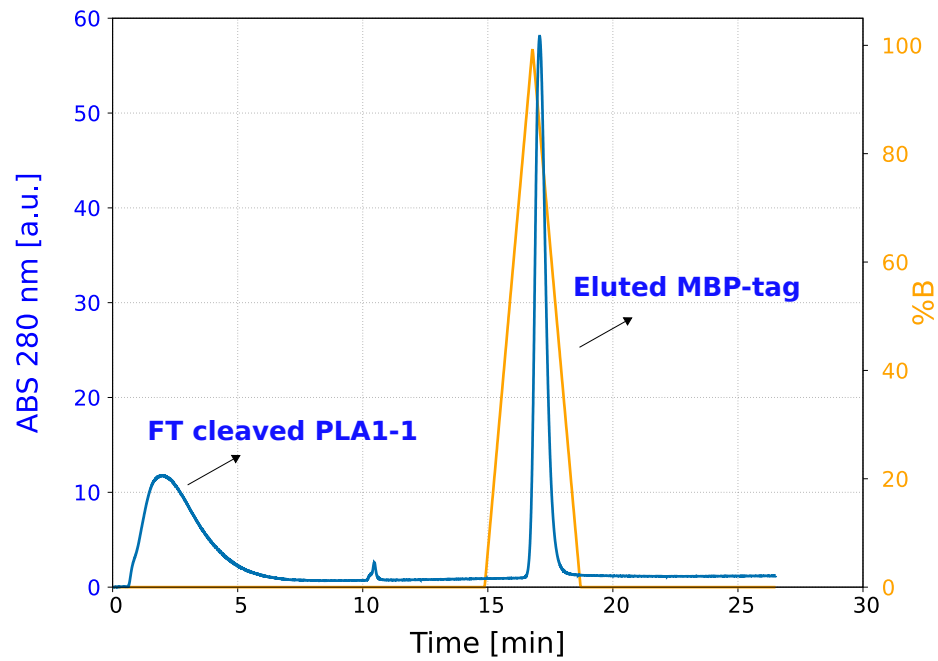


FIGURE 3.9: Affinity chromatography separation between MBP-tag and cleaved PLA1-1.

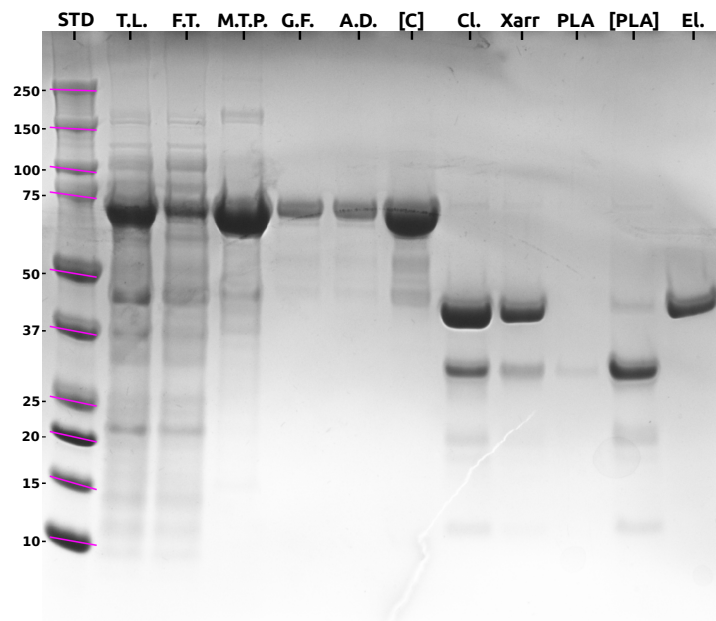


FIGURE 3.10: Entire process of purification. Where STD is the standard, T.L. is the total lysate, F.T. is the flow through, M.T.P. is the MBP-Trap purified protein, G.F. is the gel filtrated protein, A.D. is after the dialysis, [C] is A.D. concentrated, Cl. cleavage, Xarr is after the Xarrest, PLA is the PLA1-1 purified from the second MBP-Trap step and its concentrated version [PLA] and finally El. that is the eluate from the MBP-Trap



FIGURE 3.11: Alignment of the theoretical sequence of the vector (query) and the sequence obtained from the Sanger sequencing (forward). The selected sequence is the query coding for PLA1-1, and there is a clearly perfect match between the two.

carried out with mass spectrometry. The analysis was performed on the fusion protein (MBP - PLA1-1) and for its cleaved version (PLA1-1). The sequences used to compare the masses obtained from the MS-TOF analysis are shown in Appendix paragraph A.2. Figure 3.12 "Raw spectrum", shows the raw data from the MS-TOF measurement, whereas in panel "Deconvoluted spectrum" displays the deconvolution of the raw data. The theoretical mass calculated from the sequence of the MBP - PLA1-1 reported in Appendix paragraph A.2, corresponds to 72565.83 Da for the oxidized form (3 disulfide bridges), and to 72571.88 Da for the reduced form. Disulfide bridges are covalent bonds occurring between cysteine amino acids within the protein. This amino acid exhibit a free -SH group, that can be oxidized forming the -S-S- (disulfide bond) with another cysteine. This type of covalent bond is important for the stability of the tertiary structure of the protein. The mass obtained by MS is 72556.90 Da, which deviates 8.9 Da from the oxidized form and 14.9 Da from the reduced one. We have noticed some differences on the nucleotide sequence of the MBP-tag, that could explain this shift in mass. In order to have a clear scenario of the PLA1-1 protein, the same analysis was repeated for the cleaved version (PLA1-1), see figure 3.13 From figure 3.13 panel "Deconvoluted spectrum", the experimental mass was found to be 30103.70 Da, whereas the theoretical mass corresponds to 30101.82 Da for the oxidised form, and to 30107.87 Da for the reduced form. The mass found from the analysis is therefore placed between the two expected theoretical masses. The PLA1-1 protein has 6 cysteins, since between the oxidised and reduced -SH groups in the protein, a shift of 6 Da was found (the mass of 6 H atoms). However, a difference of 2 Da was found instead, therefore we supposed the PLA1-1 protein to have in its native form 2 disulfide bridges. In order to support this hypothesis, a third analysis was carried out, using the TCEP as reducing agent used to break down all the disulfide bridges. Figure 3.14 shows the mass spectra of this last experiment, and from the deconvoluted spectra, a mass of 30107.72 ± 0.15 Da was found, that corresponds to the PLA1-1 full length in its

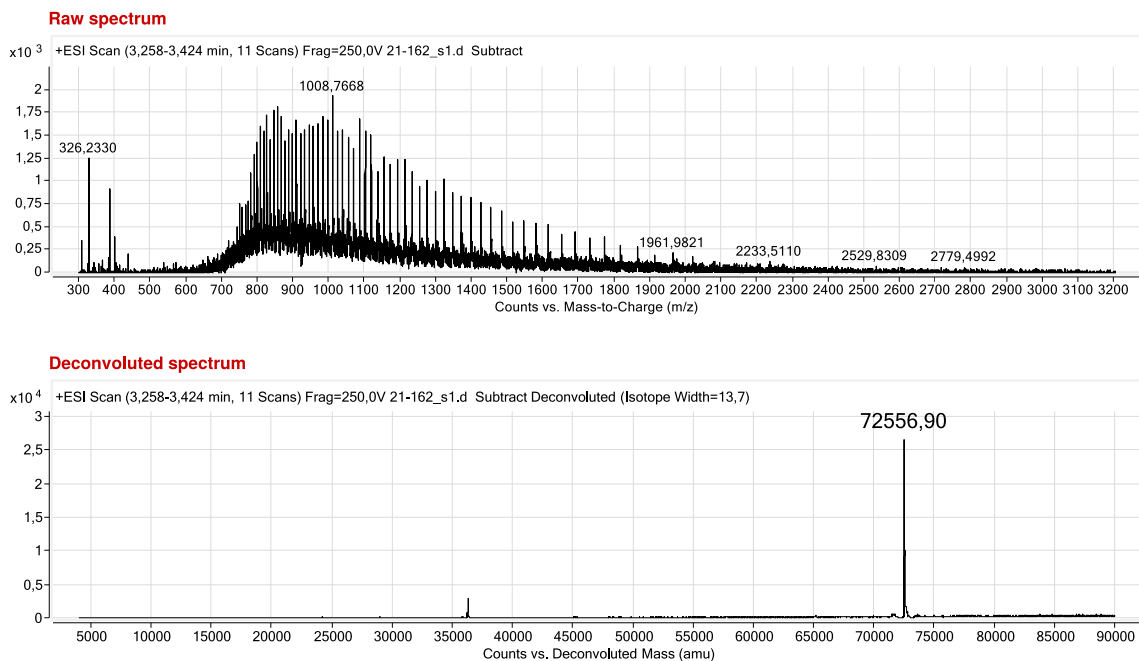


FIGURE 3.12: MS-TOF analysis of the MBP - PLA1-1. From the deconvoluted spectra it can be noticed a single peak corresponding to 72556.9 Da, which lead to a high purity sample eluted.

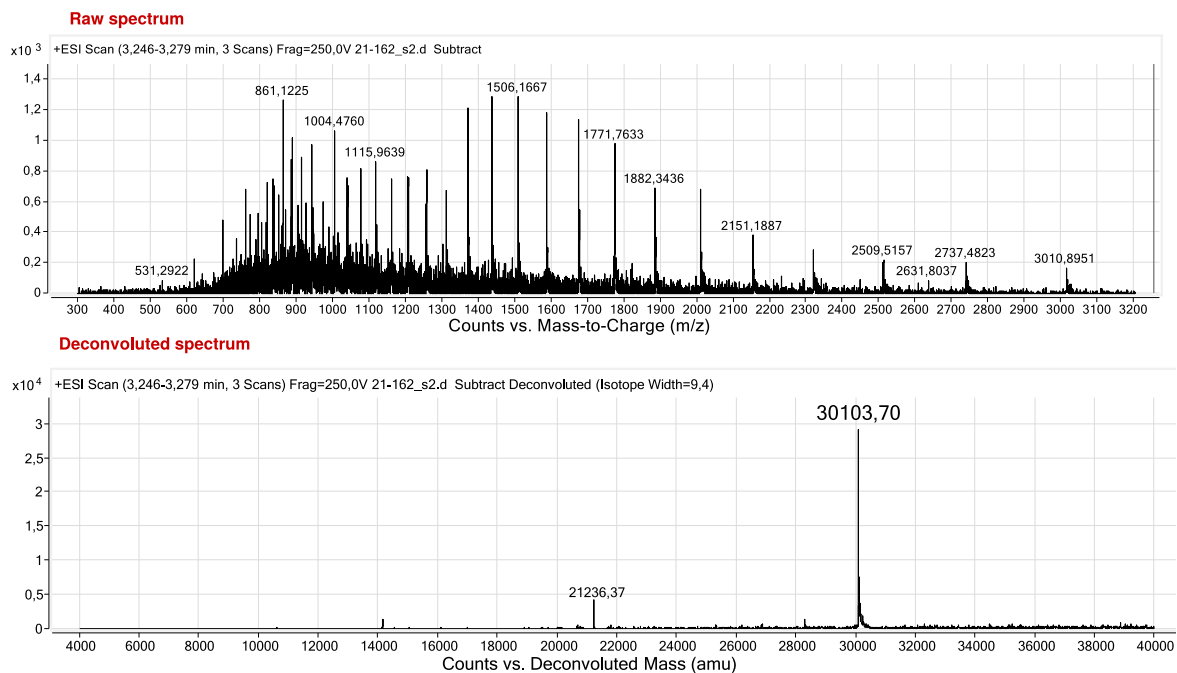


FIGURE 3.13: MS-TOF analysis of the cleaved PLA1-1. Also in this case mainly one peak was found. Its mass was found to be between the oxidised and reduced protein.

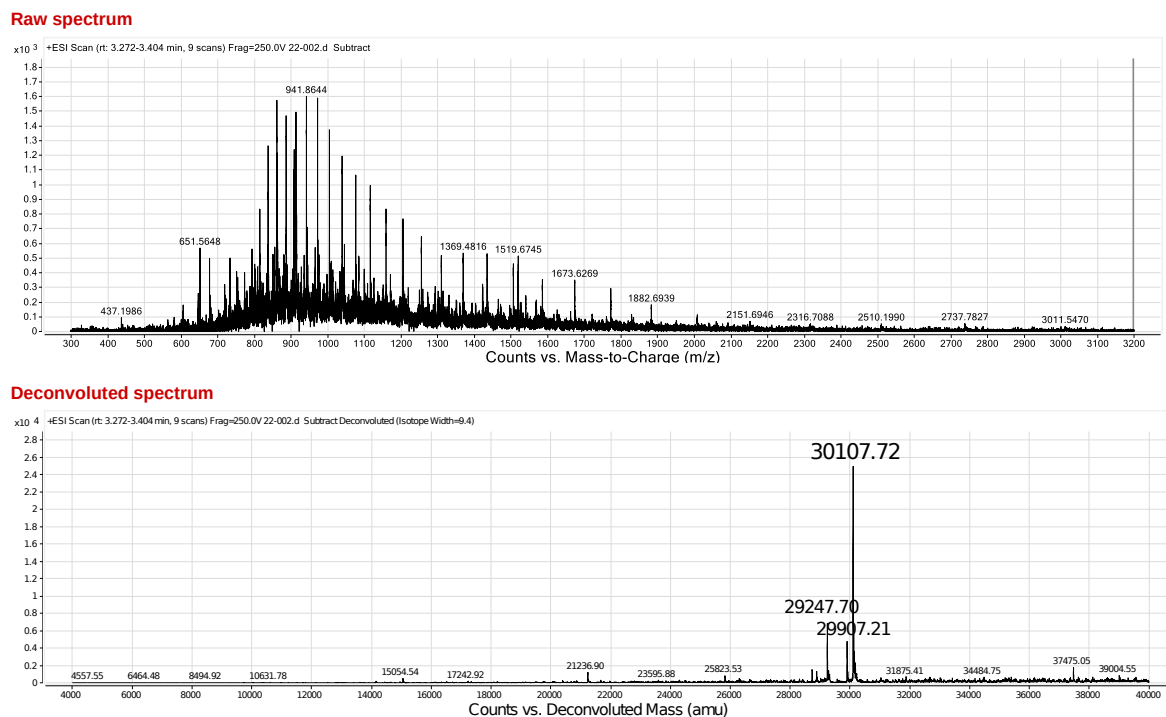


FIGURE 3.14: MS-TOF analysis of the cleaved PLA1-1 in the presence of TCEP. In this case the mass corresponds to the totally reduced protein. Therefore, 2 disulfide bridges exist in its active form.

reduced form, confirming the presence of only 2 disulfide bonds and two free -SH of the cysteins in the native form of the protein.

3.1.5 PLA1-1 structure prediction

Since no crystal structure for PLA1-1 exists in the Protein Data Bank (PDB) an investigation at lower resolution of its structure was carried out. First, homology modeling was performed to obtain a rough structure. Homology modeling by definition is the modeling of an unknown protein starting from a structure of a known protein that has already been deposited in the PDB, with a similar amino acid sequence. The similar proteins sequences were found using BLAST, searching through the PDB databank. The theoretical primary sequence was taken from SnapGene software, and then uploaded on BLASTp. The most similar protein was found to be the chain A of 6UNV, a lipase from *Rasamsonia emersonii* (see details in figure 3.15). The identity between the PLA1-1 and 6UNV is around 53% with a similarity of 66%. Results from the sequence analysis showed that, a point mutation exists in the active site sequence, GHSLG instead GHSYG, where Serine is the most important amino acid for the reaction (NS [Nucleophilic Substitution] reaction), whereas the other residues are important for specificity. The PDB structure of this protein was downloaded from the PDB database, and using Swiss PDB viewer tethering was performed, in order to thread the PLA1-1 sequence inside the Lipase 6UNV structure. A refinement was performed to avoid atom clashing and not permitted structures. Figure 3.16 depicts the structure obtained. Since, the model

Chain A, Lipase [Rasamsonia emersonii]

Sequence ID: [6UNV_A](#) Length: 301 Number of Matches: 1Range 1: 44 to 301 [GenPept](#) [Graphics](#)[▼ Next Match](#) [▲ Previous Match](#)

Score	Expect	Method	Identities	Positives	Gaps
234 bits(596)	9e-76	Compositional matrix adjust.	138/259(53%)	171/259(66%)	3/259(1%)
Query	20	FAQYSAAAYCDENLN-STGTKLTCVGNCPLEAASTQSLDEFNESSSYGNPAGYLADE			78
Sbjct	44	F QYSAAAYC N S GT ++CS GNCPLV+ A L FN S G+ G+LA D			102
Query	79	TNKLVLVLSFRGSADLANWVANLNFGLDASDLCSGCEVHSGFWKAWSEIADTITSKVESA			138
Sbjct	103	TN+L+VLSFRGS L NW+A+L L DAS +CSGCE H GF +W+ +A T+TSK+ SA			162
Query	139	LSDHSYSLVLTGHSYGaalaalaatalRNSGHSVELYNYGQPRLGNEALATYITDQNKG			198
Sbjct	163	+++H Y LV TGHS GAALA L A +LR SG++++LYNYG PR+GN ALA +IT Q+ G			222
Query	199	GNYRVTHTNDIVPKLPPTLLGYHHFSPEYYISSadeatvt-ttdvtevtgidatggndgt			257
Sbjct	223	NYRVTH++D VPKLPP GY SPEY+I+S + TV + G +			282
Query	258	dgtsidAHRWYFIYISECS 276			
Sbjct	283	G IDAHRWYF IS CS 301			

FIGURE 3.15: BLAST Protein alignment PLA1-1 vs the Lipase 6UNV chain A

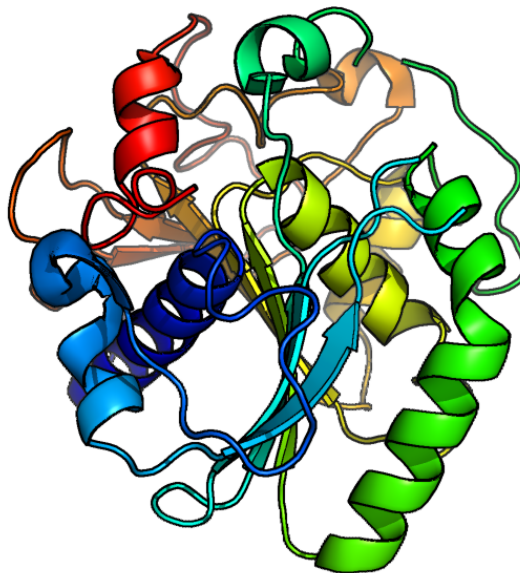


FIGURE 3.16: Homology modeled structure for PLA1-1 with 6UNV

protein used for this process was 53% identical with respect to the PLA1-1, and since there exists a point mutation inside the active site, the structure obtained could be an artifact. Thereafter, another method was employed to obtain the structure of the fusion and the cleaved protein, AlphaFold [249]. In figure 3.17 and 3.18, are shown the PDB structures with the hydrophobic surface for the fusion protein and the cleaved version respectively. In the fusion

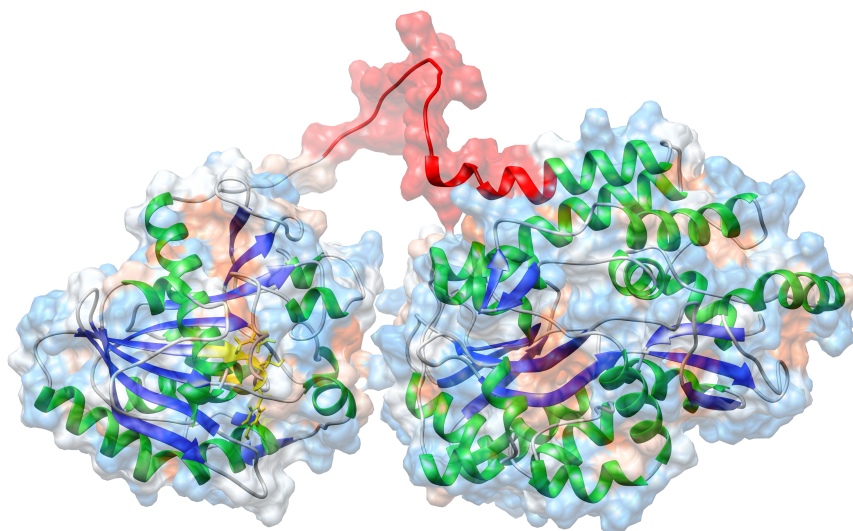


FIGURE 3.17: AlphaFold prediction of the MBP - PLA1-1

protein structure predicted which is displayed in figure 3.17, the linker (displayed in red color) between the tag and the PLA1-1 does not have a defined structure, as expected. Active site of the PLA1-1 is displayed in yellow. The two structures (from the homology and the ab-initio modeling) were overlapped and displayed in figure 3.19. From this figure, it can be noticed that the two structures are almost identical, giving a very good example of the molecular evolution, since usually proteins with the same function, have a similar structure. Next, in order to confirm the structures obtained, SAXS measurements were performed on the PLA1-1 protein, and analysed through Genfit [257]. Figure 3.20, displays the SAXS data collected for the PLA1-1 protein and its analysis. In the graph in panel (A), the blue dataset corresponds to the experimental measurement of the protein in solution and the red line is the form factor obtained from the fit using the model #15 of Genfit [256], performing the theoretical form factor of the protein from the PDB file given as input to the program. As can be noticed, in the low q region, an important shift appears between the experimental and theoretical curves, indicating the presence of aggregated PLA1-1 in the sample prepared. The theoretical curve was then subtracted from the experimental one, obtaining the green colored dataset. This was analysed using Genfit with a cylinder model, since it was the best model that could interpret this dataset. The aggregates can be model as cylinders in the solution, for

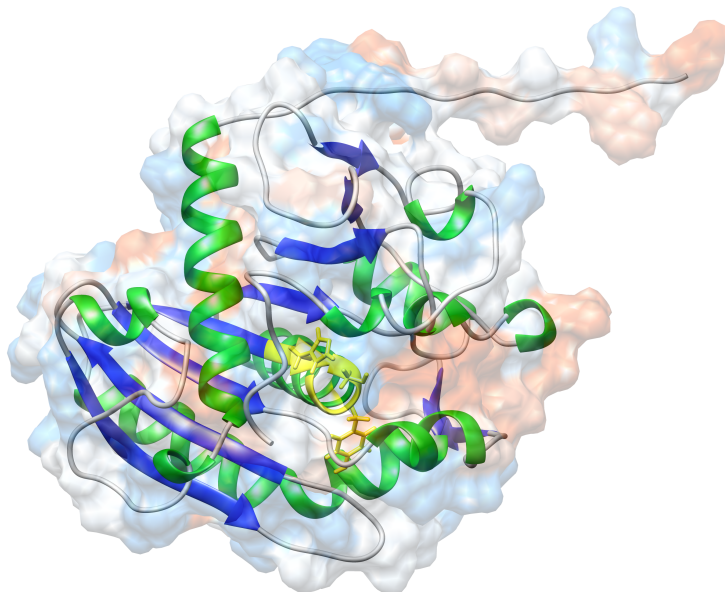


FIGURE 3.18: AlphaFold prediction of the cleaved PLA1-1

which the parameters are listed in table 3.1. Summing then the theoretical red curve with the theoretical black curve, the pink curve was obtained, for a perfect interpretation of the data. In panel (B) is displayed the $p(r)$ calculated from the red colored theoretical curve from which

	Parameter	Value
Protein	$[C]_{th}$ [$\text{mg}\cdot\text{ml}^{-1}$]	0.82
	MW [$\text{g}\cdot\text{mol}^{-1}$]	30103
	Vol [\AA^3]	81280
Cylinder	r [\AA]	42
	d [\AA]	300

TABLE 3.1: Parameters from the SAXS data analysis using the model #15 and the cylinder model of Genfit software. $[C]_{th}$ corresponds to the theoretical concentration calculated from the intensity of the SAXS profile, the MW the molecular weight inserted as fixed parameter for the scale factor calculation, Vol is the volume of the protein, r is the radius of the cylinder and d its length.

a gyration radius of $\approx 25 \text{ \AA}$ was found.

3.1.6 Summary of the results on protein production

MBP - PLA1-1 and its cleaved version PLA1-1, were produced as described in this section. The expressed and purified fusion protein MBP - PLA1-1, before the kinetics experiments, was checked using different techniques, to ensure we had produced the enzyme molecule

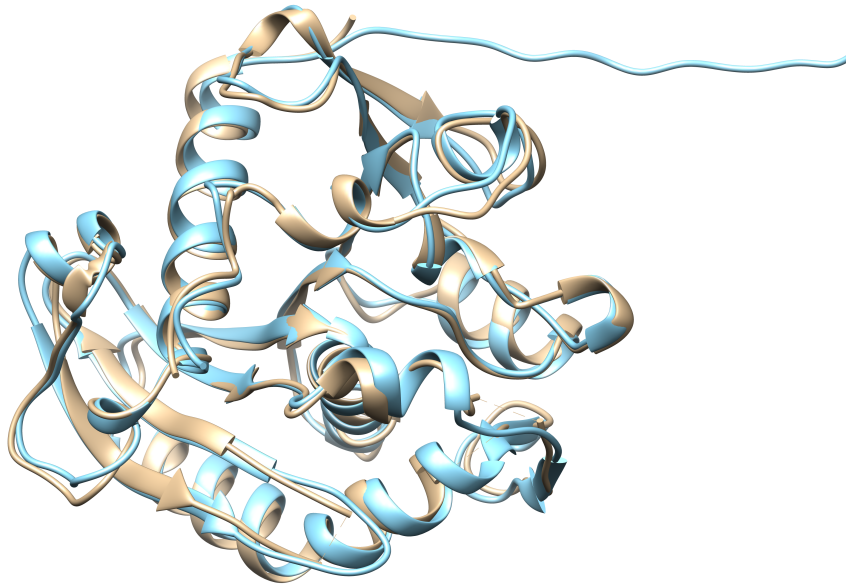


FIGURE 3.19: Superimposition between Predicted and Homology modelled structure

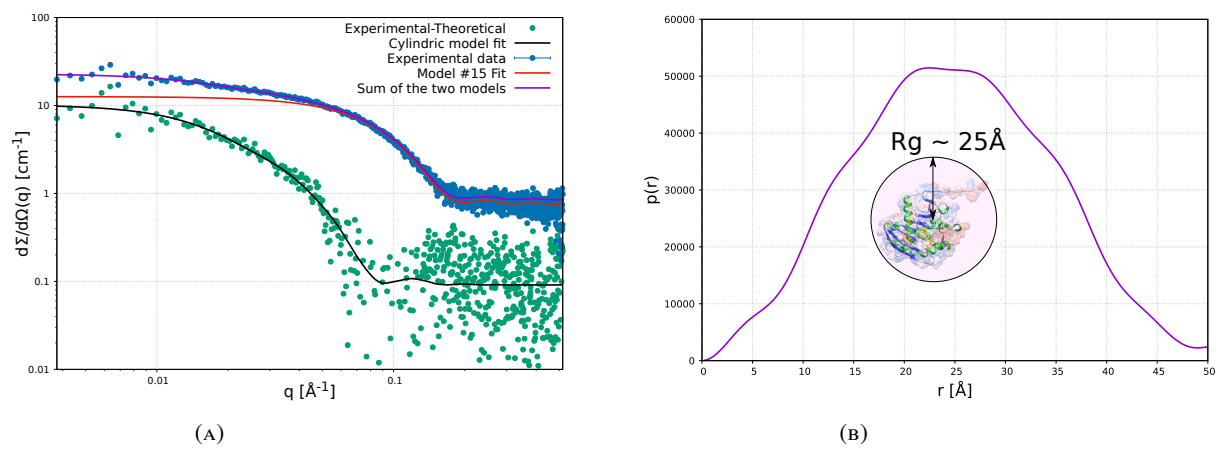


FIGURE 3.20: In panel (A) the fit of the experimental curve with the model #15 of Genfit and a cylinder (for aggregates); in panel (B) the $p(r)$ from the fit displayed in (A)

with the expected amino acid sequence. First the cDNA was sequenced in order to verify the nucleotide sequence coding for the PLA1-1, subsequently the protein was checked during the purification steps. Using gel filtration for the purification, an estimation of the molecular weight of the protein purified can be obtained through the calibration curves. Then, using an SDS-PAGE gel, the molecular weight and the purity of the purified product was further assessed. In order to acquire with higher accuracy the molecular weight of the protein, MS-TOF was performed, providing a very good match with the calculated molecular weight from theoretical sequences. An activity assay was carried out in some of the fractions of the gel filtration, in order to verify that the peak with the expected molecular weight was the one that also showed the expected activity. A structural analysis was also performed on the cleaved PLA1-1 protein, providing a good match with the ab-initio predicted PLA1-1 structure and the SAXS curve.

3.2 Lipid production

In this section, the main results related to the production and lipid characterisation are explained and discussed. We firstly assessed and optimised a protocol for the extraction and purification of the different classes of polar lipids from biomass, especially from *Pichia pastoris*. Next, we focussed on the synthesis of partially deuterated GPLs that were used for the PLA-membrane interaction studies. Using natural lipids, more biologically relevant membrane bilayers can be obtained (with properties closer to the natural cellular membranes). The main classes of phospholipid molecules utilised for the PLA1-1 kinetics analysis, were PC and PS, but also PG was purified and characterised. The characterisation consisted of (a) the lipidomics profiling, finding the relative abundance of the acyl chains for the three classes of GPL molecules purified, and (b) the structural characterisation of flat membranes containing the purified GPLs. Profiling the lipid component, is a fundamental step in order to have more controlled system to work with, allowing also to calculate the SLD values from the composition of the acyl chains. Membranes constituted of pure PC, and PC/PS, PC/PG with a ratio of 80:20 (w/w) were characterised using NR. PC class of phospholipids are zwitterionic molecules, uncharged at physiological pH, needed for the formation of a charged flat membrane onto the silicon support (i.e. containing charged GPL molecules as PS and PG). For that reason the PC class was utilised as a "carrier" molecule to deposit membranes composed by those charged GPL molecules (PC/PS and PC/PG). Differently, the charges between the silicon support and the polar head region of the lipids would not allow the fusion and the formation of an high coverage membrane.

3.2.1 Natural lipids production and characterisation

The cultures of *Pichia pastoris* were carried out in collaboration with the Deuteration-lab (D-Lab) within ILL, where the protocols to grow cells in deuterated conditions were optimised.

Extraction and purification

From the biomass, the total lipid extraction was carried out as explained in Chapter 2. Upon lysis of the cells, the first step of the extraction consisted of the formation of a double phase, caused by the different polarity and mass density of the solvents used. This system can be formed only with a precise ratio between the solvents (CHCl_3 , MeOH and H_2O). During the formation of the two phases, the polar molecules move into the upper phase (polar fraction) where they are more soluble, whereas the apolar molecules are located in the bottom phase (apolar fraction). This results in the fractionation of the proteins and metabolites (polar molecules) from the apolar molecules as phospholipids, neutral lipids, sterols and apolar metabolites. In order to recover only the phospholipid fraction, an SPE procedure was performed, and the eluate was injected into the normal phase column coupled to an HPLC. This step of purification allows the separation of each class of phospholipids using the protocol described in Chapter 2. The purification was performed for both the hydrogenous

and deuterated biomass, in order to obtain both the H and D lipid mixtures respectively. Figure 3.21 shows a typical chromatogram that can be achieved from the HPLC purification step. As can be noticed, the two chromatograms have a similar trend, and the amount of lipids

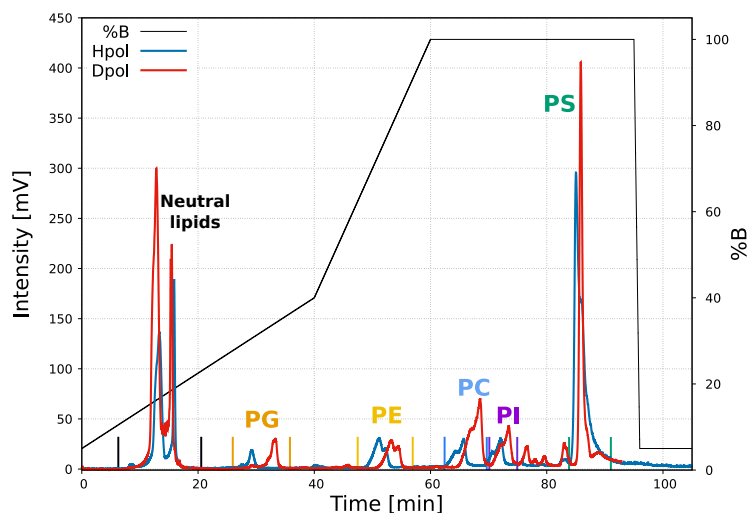


FIGURE 3.21: HPLC chromatograms H versus D.

per each class is approximately the same. The order of the GPL classes purified with this method is as follows: PG, PE, PC, PI and PS. The initial peak (around ≈ 15 min) corresponds to the neutral lipids, resulting in a non-100% removal of those lipids from the SPE step, that were then separated during this purification step. Each class of purified phospholipids was determined with an HPTLC, in order to assess the identity and purity of the fractions (figure 3.22).

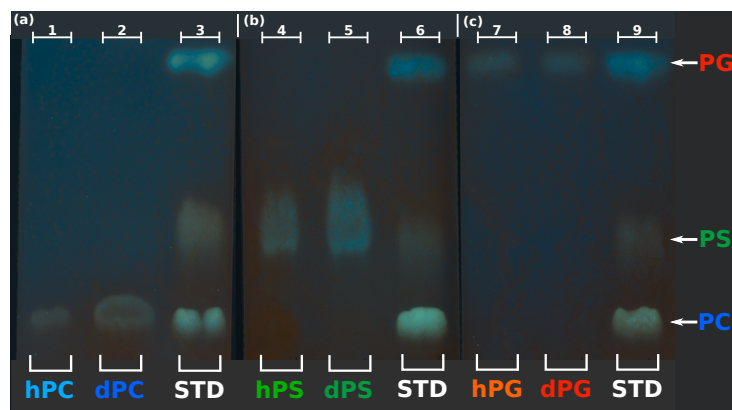


FIGURE 3.22: TLC analysis of the three purified classes of phospholipids purified. This step is fundamental for the assessment of the identity and purity of the purified fractions.

Molecular compositional analysis by Gas Chromatography (GC)

Since these purified mixtures were used for the neutron experiments, the profiling of the acyl chain composition was carried out for each of the purified classes. This step is fundamental for the proper and accurate calculation of the acyl chain region-SLD of these

phospholipid mixtures (the details on the calculation are shown later in this section [paragraph *Scattering techniques*]). The advantages of using natural lipids, lie in the fact that more natural-mimicking model membranes can be achieved, making the experiments more relevant; and secondly perdeuterated GPLs can be used, which gives a large advantage for neutron scattering experiments, since usually the chemical deuteration is expensive and not always available. The profiling of the acyl chain composition for the total polar lipid extract was performed using GC-MS, for both the H and D extracts. Figure 3.23 shows the GC-MS Total Ion Chromatogram (TIC) of the total lipid extract. The sample injected in the instrument went first through the GC column, separating all the Fatty Acids Methyl Esters (FAMES) with respect to their hydrophobicity, resulting in the chromatogram shown. The TIC signal came from the total ion counts in the MS detector, which is coupled right after the GC column. Using MS, information regarding the mass of the molecules separated by the GC column can be achieved. Integrating each peak in the TIC, the MS spectra per each lipid species can be extrapolated, for identification purposes. As observed, the TIC chromatograms for the H

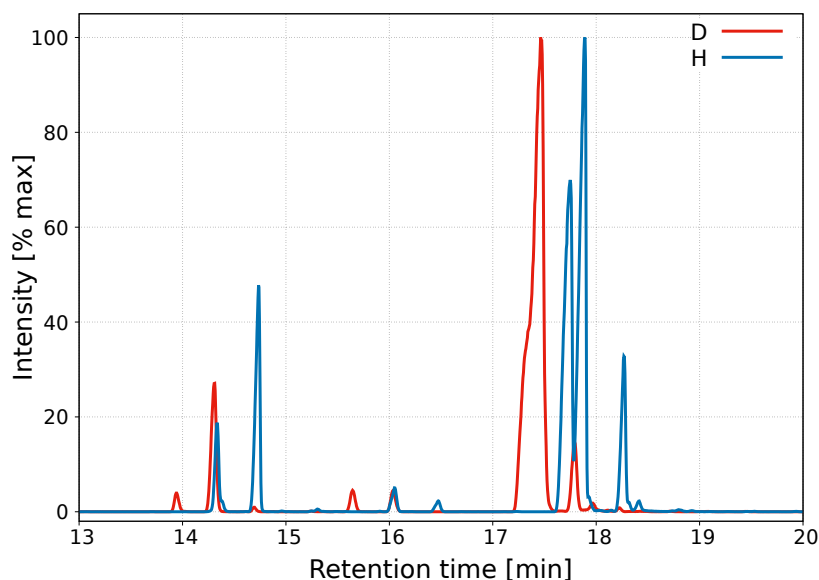


FIGURE 3.23: H *versus* D lipid extracts GC-MS chromatograms. It can be noticed a consistent shift of the peaks in low time ranges for the D lipids. The chromatograms are normalised to the highest peak for a better view.

versus D, are shifted on time. This behavior is derived from the fact that the hydrophobic interaction between D/H material and the GC column is different. From the TIC, the relative spectra of each peak can be achieved (an example is shown in figure 3.24). As can be noticed, the spectra between H and D are also shifted in mass, since the D atom weight is "+1 Da" with respect to its more popular isotope H. From the spectra it is also noticeable that the shape of the peaks in H and D spectra are different. The peak shapes of the D spectra are more similar to a Gaussian function, whereas the peaks in the H spectra do not contain any shoulder on the left side. This behavior can be explained by the fact that the deuteration level of natural lipids and consequently of the FAMES, is not 100%, giving to the molecules different amount of D contained, spreading the MS signal in a Gaussian shape. From the

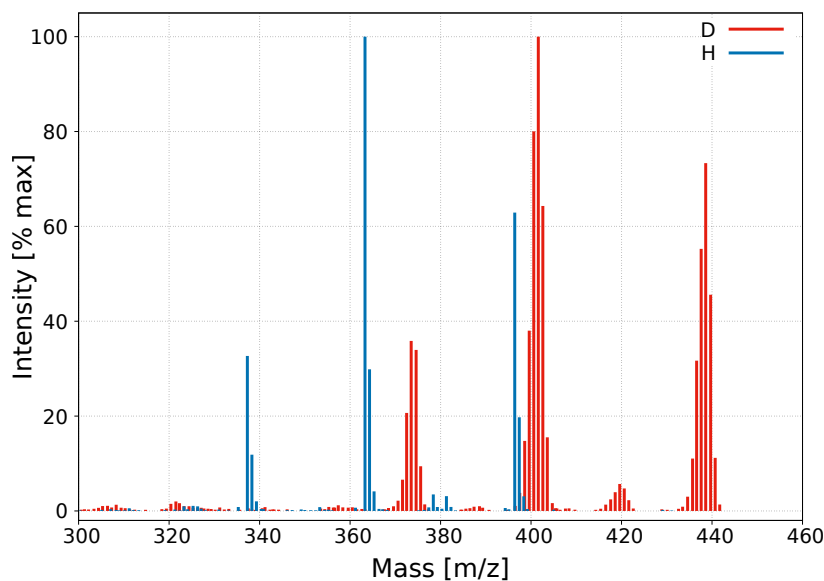


FIGURE 3.24: MS spectra of the peak corresponding to 25:0, taken as example because of its symmetric shape. The first peak on the right corresponds to the m/z of the 25:0 FAME, whereas the other signals are fragmentation products. The shift seen in the spectra is caused by the deuterium content.

MS spectra, the Extrapolated Ion Chromatogram (EIC) can be computed. The EIC is the GC chromatogram of the ions that gave that certain signal on the MS detector. For instance, by taking a GC peak of one FAME, and by integrating it, a specific mass from the resulted related MS spectra can be selected. From this process, the GC EIC chromatogram can be achieved for that particular ion with that particular m/z selected. In the D measurements, each GC peak contained different masses due to the different deuteration level of the FAMEs. The signal of each GC peak, can be described with different EIC peaks, that corresponds to different MS signals within the main GC peak. An example is given in figure 3.25, where the peak for the FAME D-25:0 contains different EIC peaks, one from each signal of the related TIC-MS spectra (varying from one to another on the D atom content). It is confirmed also with this experiment (in figure 3.25) that deuterated molecules elute earlier than hydrogenous ones, as the EIC chromatograms are shifted on to the left increasing the D atoms content in that molecule. Once the peaks of the GC were identified (where each GC peak corresponds to a precise FAME), each purified GPL class was run using the GC-FID, in order to be able to calculate the acyl chain distribution as shown in figure 3.26. The process utilised for the peak integration is explained in Chapter 7, section 7.2. It is evident a large difference in the acyl chain abundance between the H and D extracts, as seen in all the three classes analysed, specifically the acyl chain 18:1 increases considerably in the D extracts compared to the H, whereas a decrease in the 18:2 and 18:3 contents is observed. The hydrophobic interaction between lipids is different if the material is H or D, as can be also explained by the shift in the D/H GC-MS TIC chromatograms seen before. It follows accordingly that the cells adjust the contents of double bonds in order to keep the membrane fluidity constant between D and H conditions. This effect was systematically found also in other works [258], although further

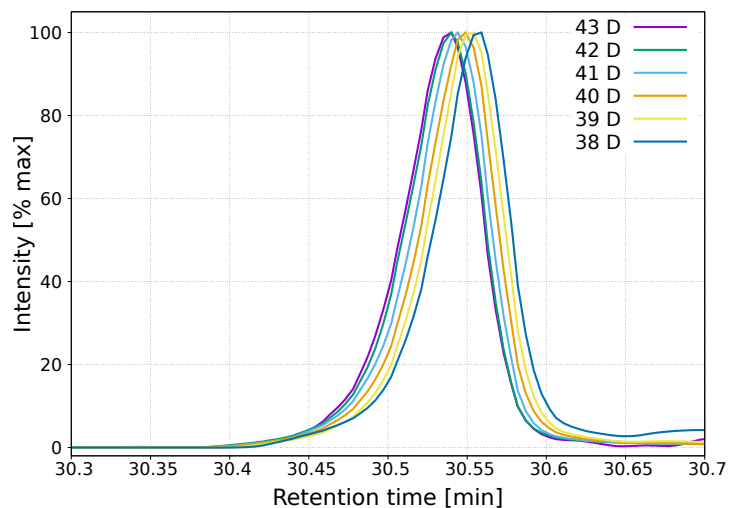


FIGURE 3.25: Effect of deuteration on the GC column retention time. Figure shows the EIC of the same molecule with different deuterium atom content. More deuteriums causes an early elution, whereas lower content gives later elution.

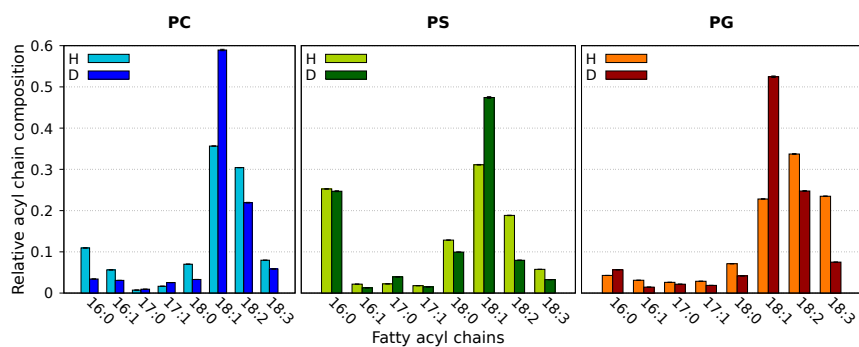


FIGURE 3.26: Acyl chain profiling of each purified GPL class. Can be noticed a large difference in the acyl chain profile between H and D lipids.

analysis needs to be carried out in order to assess how the process is actually controlled.

NL-SLBs structural characterisation

QCM-D and NR experiments were carried out to characterise the structure of the produced model membranes. The optimisation of the SLB formation protocol was performed utilising mainly the QCM-D technique, with the aim to obtain high coverage SLBs (as explained in Chapter 2 paragraph *Vesicle fusion method*).

QCM-D The protocol for the deposition of the lipids was optimized using QCM-D technique before proceeding to NR experiments. Figure 3.27 shows the measurement performed on the purified deuterated PC mixture (dPC). After the recording of the baseline, the buffer

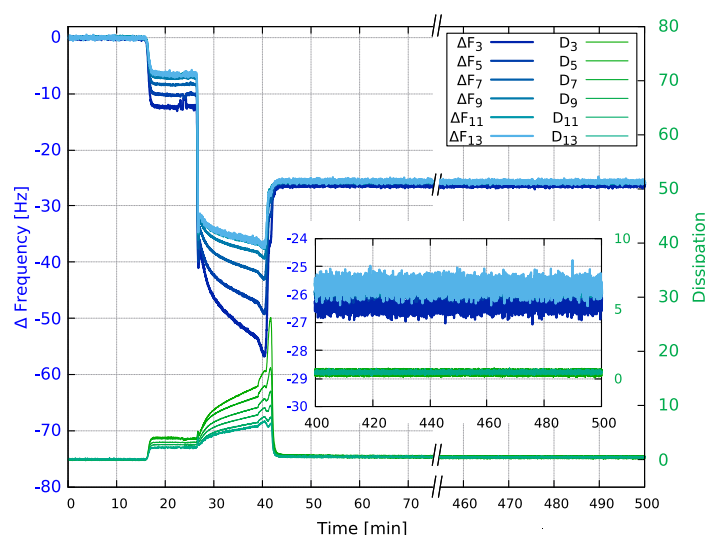


FIGURE 3.27: QCM-D measurements of the dPC mixture. As noticed, the frequency of ≈ -26 and the dissipation of ≈ 0 , shows the good formation and coverage of the lipid bilayer.

solution was injected to equilibrate the cell before the injection of the vesicle solution in the same buffer. This step caused a drop of the ΔF and an increase of the ΔD , since the density and viscosity of the solvent are different with respect to Milli-Q H_2O which was used to record the baseline. Next, the vesicle solution was injected into the cells, giving a large drop in the ΔF signal and an increase in the ΔD . This drop is caused by the interaction of the vesicles with the crystal in the QCM-D sensor, thereby increasing the mass on the crystal itself and the consequent drop of the resonance frequency. The increase in the ΔD is caused by the soft structure of the adsorbed vesicles, consequently dissipating vibrational energy from the crystal. This step is followed by Milli-Q H_2O rinsing, which produces an osmotic shock, which help the vesicles to pop on the surface of the crystal and in the meanwhile washes away the vesicles/debris excess. After this step the ΔF signal was stable at -26.0 ± 0.5 , which is the expected value for a lipid bilayer (for instance -25 is the ΔF signal for a POPC membrane

with high surface coverage). The correct formation of the SLB can also be extrapolated by the ΔD , since the signal is stable between 0 and 0.2.

Scattering techniques Once the protocol for the deposition was established, the NR experiments were performed on the following mixtures: PC, PC/PS and PC/PG in their H and D versions. The molecular volumes, for the acyl chain and polar head region were calculated in order to obtain the SLD values for the lipids under examination. The acyl chain volumes were calculated taking into consideration the GC acyl chain relative abundance, by employing the following volumes for lipids in the fluid phase (22°C and 37°C): $V_{CH_2} = 27.5 \text{ \AA}^3$, $V_{CH_3} = 55.1 \text{ \AA}^3$, $V_{CH} = 22.2 \text{ \AA}^3$ [259]. The polar head volumes were calculated by employing the relative mass density (PC-PH_{vol} = 318 \AA^3 , PS-PH_{vol} = 263 \AA^3 , PG-PH_{vol} = 288 \AA^3). The SLDs for the hydrophobic and polar head region for the H lipids were calculated by summing all the scattering lengths of each atom in the polar head or acyl chain region and by dividing for the corresponding volumes. Since the level of deuteration of the D lipids was not 100%, the NR SLDs were fitted during the data analysis. In order to obtain a good estimation of the amount of deuteration, SANS measurements were first performed. As mentioned before, neutrons are strongly sensitive to the level of deuteration of the material under analysis. The principle behind the SANS measurements performed consists in matching out vesicles constituted of the purified deuterated GPLs, by varying the amount of D₂O where the lipid vesicles are solubilised. The absolute value $I(\approx 0)$ of the small angle signal is correlated to the SLD variation between solvent and lipids ($\delta\rho$ [$\rho - \rho_0$], where ρ is the SLD of the sample and ρ_0 the SLD of the solvent). For that, five samples were prepared, ranging between 20 and 100% of D₂O, consequently scanning different $\delta\rho$ and seeing how the small angle signal changes (figure 3.28). As noticed, the small angle signal decreases upon increasing the amount of

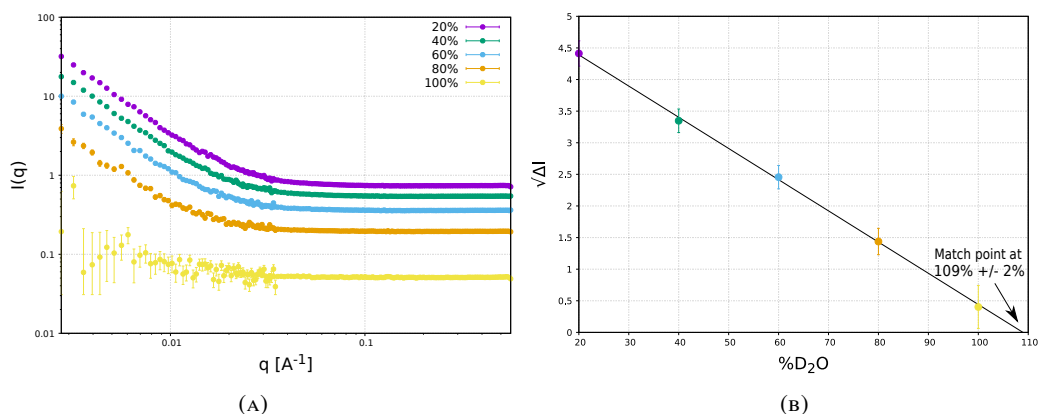


FIGURE 3.28: Panel (A) displays SANS experimental data for the dPC vesicles suspended in mixtures of D₂O and H₂O with different D₂O content as reported in the legend. In panel (B) is plotted the $\sqrt{\Delta I}$ as function of the D₂O content. The plot was used to extrapolate the match point for the dPC lipids analysing the data with a straight line.

D₂O, since the $\delta\rho$ decreases due to the fact that the SLD of the lipids is similar to the SLD of the pure D₂O, switching off the signal in this contrast (as sketched in figure 3.29). Next,

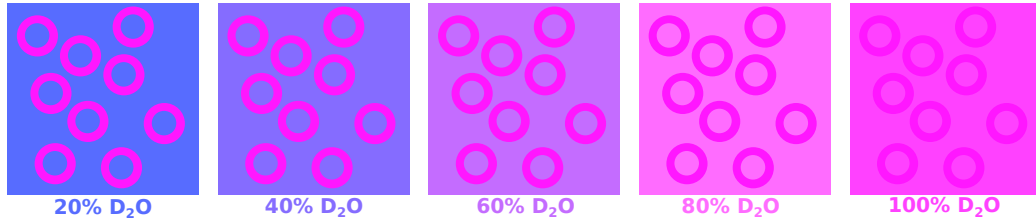


FIGURE 3.29: Sketch explaining the contrast variation of the vesicles solubilised in solutions containing different amount of D_2O

the match point can be calculated, integrating the q -points before 0.005 \AA^{-1} and the point between 0.2 and 0.4 \AA^{-1} as shown in table 3.2. Figure 3.28 panel B shows the plot of the

$\%D_2O$	Int $q < 0.005$	Int $0.2 < q < 0.4$	ΔI	$\sqrt{\Delta I}$
20	20.21	0.74	19.47	4.4 ± 0.2
40	11.75	0.54	11.21	3.3 ± 0.2
60	6.39	0.36	6.03	2.5 ± 0.2
80	2.26	0.19	2.07	1.4 ± 0.2
100	0.21	0.05	0.16	0.4 ± 0.3

TABLE 3.2: Scattered intensity corresponding to different q -ranges for the investigated vesicle suspension. The square root ($\sqrt{\Delta I}$) of the difference between the calculated values (ΔI) was used to extrapolate the match point for the dPC lipids (see also Figure 3.28)

$\sqrt{\Delta I}$ calculated, where ΔI is the intensity (I) at low q subtracted by the background (taken at high q ranges). It can be noticed that there is a good alignment between the points in the plot, that can be fitted using a straight line. The intercept of the straight line to the x axis corresponds to the match point of the D lipids (where the SANS signal would be equal to 0, where the SLD of the solvent equals the SLD of the material under examination), which was found to be $109 \pm 2\%$. From this value the overall scattering length density of the dPC lipids mixture was calculated as $6.92 \pm 0.15 \cdot 10^{-06}$ ($SLD_{D_2O} \cdot 109 \pm 2\%$). By comparing this value to the overall theoretical scattering length density of the fully deuterated PC lipids, *i.e.* $7.15 \cdot 10^{-06}$, a deuteration level of $97 \pm 1\%$ was estimated.

NR experiments were then performed, using the protocol optimised with the QCM-D technique. The SLB characterisation was carried out using different contrasts (similar to what was done for the SANS experiment, usually with 3 or 4 contrasts for NR), in order to obtain more accurate structural information of the membrane. The data were analysed using CoruxFit with the error function fraction volume distribution approach, as extensively explained in Chapter 6. Briefly, the NR technique allows to obtain information along the z -axis of the sample, consequently the sample under analysis can be modeled using a layer model, where in CoruxFit each layer is described through error functions. The physical parameters of the lipids in the outer and inner leaflets were considered to be the same, since the membrane has a flat structure. The area per lipid was used to constrain the polar head and the acyl chain region thicknesses. The hPC and dPC data analysed as described are shown in figure 3.30. NR experiments confirmed the correct formation of the SLB in both cases

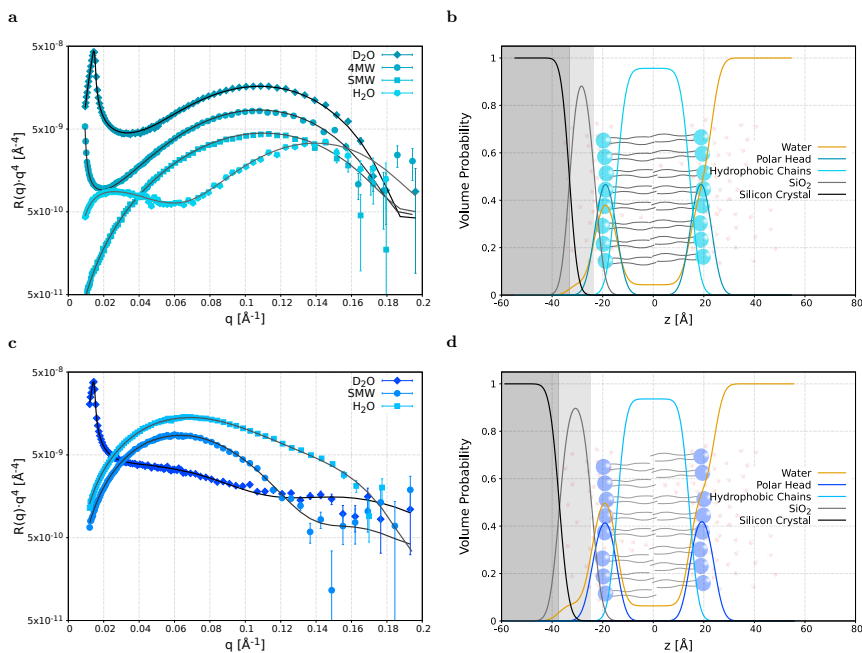


FIGURE 3.30: NR measurements and analysis of the PC SLBs. Panel A and C show the NR datasets and its analysis, panel B and D shows the related model. The formation and the good coverage of the lipid membrane can be noticed already by observing the model, since very low amount of solvent was found in the acyl chain region.

of hPC and dPC (figure 3.30a and 3.30c). In figure 3.30b and 3.30d the minimised model corresponded to the theoretical curve calculated. The structure of the two SLBs created was very similar, despite the large change in the fatty acid distribution between H and D lipids (the fitted parameters are displayed in Appendix A.5.1). The SLDs for the polar head and acyl chains region was optimised to the experimental data only for the D lipids, giving an amount of deuteration of $94.5 \pm 0.5\%$ (for both polar head and hydrophobic chain region), which is similar to the overall SLD found with SANS ($97 \pm 1\%$).

PS and PG-GPL molecules, are the most abundant negatively charged class of GPL molecules in biological membranes [260]. In order to obtain more biologically relevant model membranes, those lipids have to be included in the mixture, in order to simulate the structure and the surface charge of a real lipid membrane. For this purpose, lipid membranes constituted of PC/PS and PC/PG from the extracted and purified fractions, were also characterised using NR.

SLBs constituted by PC/PS were analysed in their H and D forms. Such mixtures were produced and purified first from the total GPL, and subsequently recombined together in a solution constituted of PC/PS 80/20 w/w. The SLBs for these mixtures were prepared using the protocol employed for the PC mixtures. Figure 3.31 shows the NR data analysed with a similar model compared to the one used for the PC mixtures, adjusting the various SLDs due to the different polar head composition and the different acyl chain distribution. The analysis displayed in figure 3.31 shows the correct formation of the SLB also with these

mixtures, resulting in a high coverage lipid membrane. This result allows us to confirm that the vesicle fusion protocol developed can be also used for the deposition of charged lipids on silicon substrates. The structure resulting from the analysis did not change much with respect to that found for the PC mixtures and, also in this case, the deuteration had no effect on the structure of the membrane. Analogous experiments were performed with mixtures of

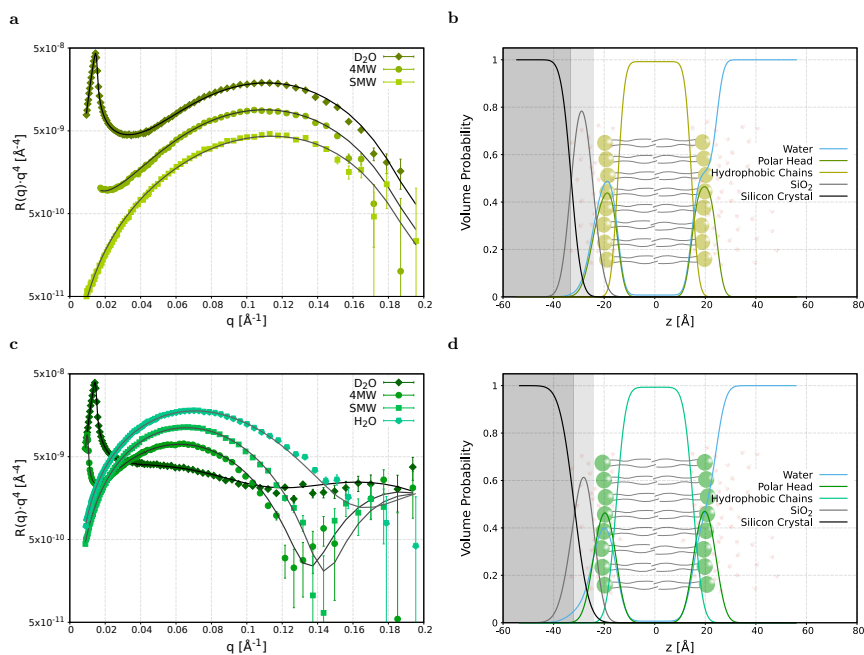


FIGURE 3.31: NR measurements and analysis for the mixture PC/PS in its hydrogenous and deuterated form. Also in this case the formation of the lipid bilayers and the coverage were found to be quite good.

PC/PG in their H and D form, by utilising the same protocol, SLBs with this lipid mixture were carried out. As in the case of PC/PS, the concentration of PG in this mixture was 20% w/w. Figure 3.32 shows the NR data analysed with the same model described briefly above. Also in the case of PC/PG, a good coverage lipid bilayer for H and D form was achieved, with comparable parameters obtained for PC/PS and PC SLBs. Interestingly, (a) the structure between the different mixtures tested does not change much and (b) the structure of H and D model membranes remains comparable. These two characteristics of the natural lipids can be an enormous advantage for lipid and lipid-proteins interaction experiments.

3.2.2 Partially deuterated lipids production

Partially deuterated PC molecules were synthesised in order to assess the substrate preference of the PLA1-1 using neutron scattering and to analyse how the structure of the membrane changes during the hydrolysis reaction. The strategy of the experiment is based on the contrast variation, where deuterated and hydrogenous material possess a totally different SLD. The PLA1-1 enzyme, as mentioned before, cleaves preferentially the first acyl chain (sn1), in the first position, thereby damaging the membrane structure and changing its composition due

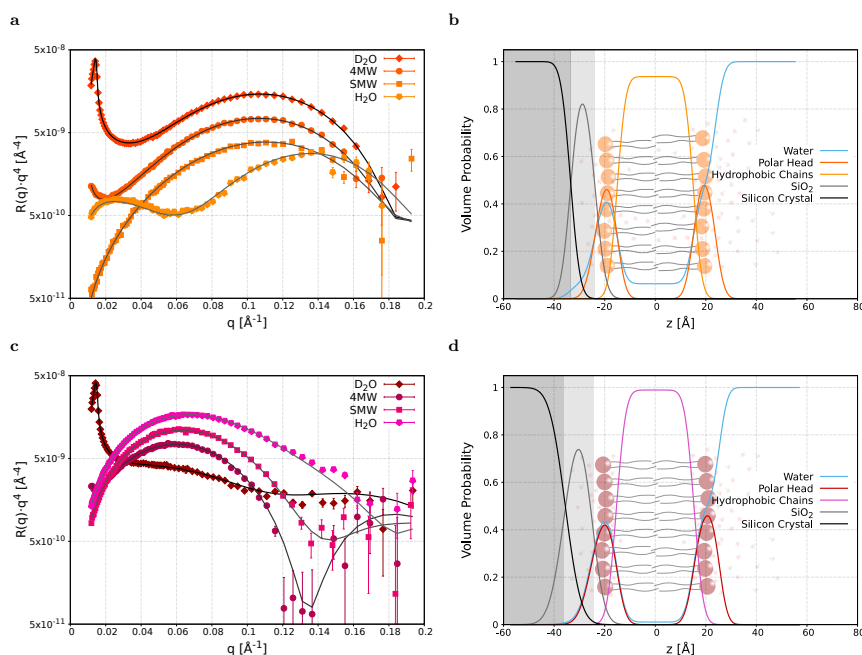


FIGURE 3.32: NR measurements and analysis of the mixture PC/PG. As well as the other two mixtures, the coverage found was very high.

to the release of material. Therefore, using partially deuterated phospholipids, with the sn1 chain deuterated and the sn2 hydrogenous, it is possible to track where the FFA or the lyso go during the course of the kinetics, since the two have a different SLD value. Once, the FFA or the lyso leaves the membrane, its SLD will vary over the hydrolysis reaction. With neutron scattering technique it is also possible to follow structural changes of the membrane during the cleavage activity of the enzyme. In order to assess the substrate preference of the PLA1-1 under examination, different phospholipid substrates (varying the acyl chain length and the number of double bounds), were synthesised, and different model membranes constituted of one of these synthesised PC molecule species each, were prepared.

Synthesis and purification

Partially deuterated PC molecules were synthesised as described in Chapter 2, and purified afterwards using a normal phase column coupled to an HPLC. After the cleavage of the first acyl chain residue mediated by the PLA1 enzyme, the lipid molecules were extracted and purified in order to separate the lyso, FFA and the uncleaved molecules. Next, the deuterated fatty acid was prepared with coupling agents and mixed with the purified lyso PC, in order to obtain the complete partially deuterated PC molecule. A second purification was carried out to purify the synthesised molecule. The purified fraction was collected and checked with TLC, in order to assess the correct condensation of the coupled deuterated fatty acid. To confirm the correct condensation of the correct fatty acids, GC-FID measurements were carried out. Figure 3.33 shows the GC chromatograms of 3 of the synthesised lipids. From the chromatograms, the successful deuteration of one of the two FAMES in each sample can

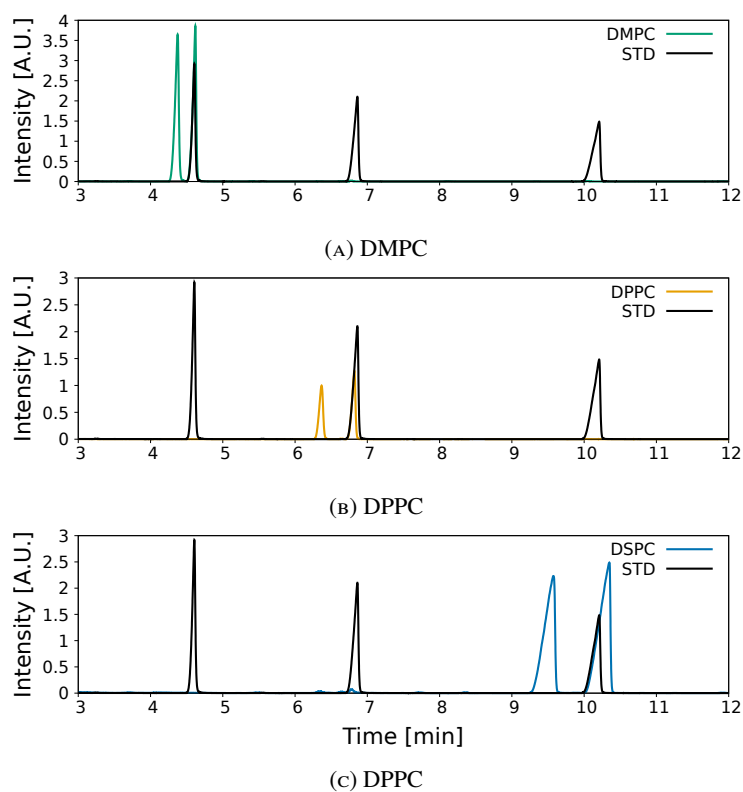


FIGURE 3.33: GC chromatograms of the partially deuterated PC molecules synthesised. The standard (shown in black color) used to compare the peaks was constituted by a mixture of FAMES such as 14:0 (R.T. \approx 4.3), 16:0 (R.T. \approx 6.8) and 18:0 (R.T. \approx 10.2) [where R.T. corresponds to the retention time].

be seen. The standard used was a mixture of hydrogenous 14:0 (R.T. ≈ 4.3), 16:0 (R.T. ≈ 6.8) and 18:0 (R.T. ≈ 10.2) lipids.

Structural characterisation

Partially deuterated PC molecules are characterized by having an SLD of the acyl chain region collocated between 3.2 and $3.6 \cdot 10^{-6} \text{ \AA}^{-2}$, which corresponds to an averaged SLD between a deuterated and hydrogenous acyl chains. Those PC molecules, were deposited using the vesicle fusion protocol described above, used for the natural lipids deposition. Figure 3.34 shows the reflectivity profiles in 4 contrasts of the partially deuterated 16:0|18:2 PC molecule, displayed now as an example. The model used to analyse the data is the one used also for the natural lipids. Figure 3.35 shows the SLD profile of the sample. As mentioned before,

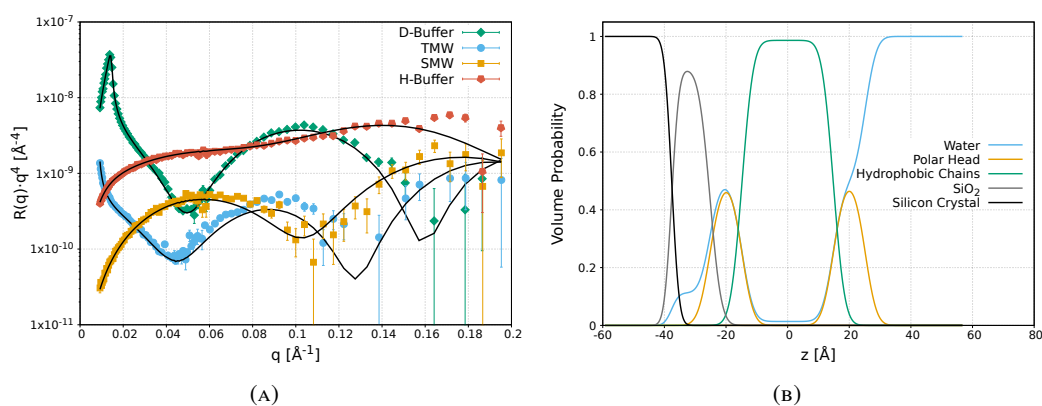


FIGURE 3.34: NR data and analysis of the synthesised partially deuterated 18:2 PC molecule. In panel A the data and the fit is shown in the 4 contrasts used and in panel B the related model is displayed.

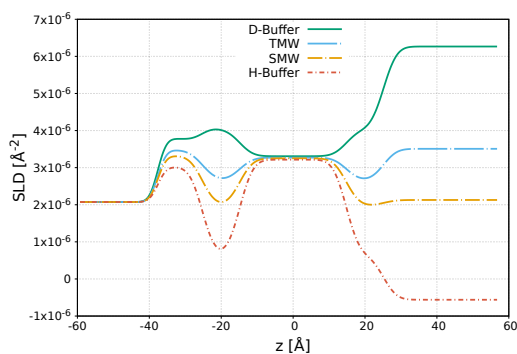


FIGURE 3.35: SLD profile calculated from the model shown in figure 3.34.

the SLD of the acyl chain region is around $3.2 \cdot 10^{-6} \text{ \AA}^{-2}$, confirming the success of the synthesis. During the reaction, if only deuterated material is removed, the SLD of this region shall decrease over time, thus approaching the hydrogenous one. This system allows us to follow the kinetics of the PLA1-1 with different model membranes constituted of different lipid molecules, by following the SLD variation. The second advantage on using these lipids,

consists of having a good view on the released material, for instance if there is a rearrangement leading to the formation of other structures.

Deposition of the saturated partially deuterated PC molecules

Some of the synthesised partially deuterated molecules, have a transition temperature above 37 °C, temperature that was used for the neutron experiment. Since for the vesicle fusion, a fluid state lipid has to be utilised in order to obtain high coverage SLBs, another technique for the deposition had to be employed. The Langmuir-Blodgett (LB) technique was used for the deposition of the lipids d18:0 | h18:0 PC and d16:0 | h16:0 PC, since their transition temperature is respectively 41 and 55 °C. The deposition was performed in gel phase of the lipids, at 22 °C. After cleaning the trough and the silicon support, the support was placed vertically under the level of water, that was degassed and added to the trough after the cleaning (as displayed in figures in Appendix A.4.2). Next, the PC molecule solution was spread onto the surface of the liquid using an Hamilton syringe. The stock solutions per each lipid used for the LB depositions were concentrated 1 mg·ml⁻¹. For the first deposition, an amount of 45 μl were used for the spreading. After the evaporation of the CHCl₃ from the liquid surface, the isotherm was performed, until a target pressure of 35 mN/m was reached. Figure

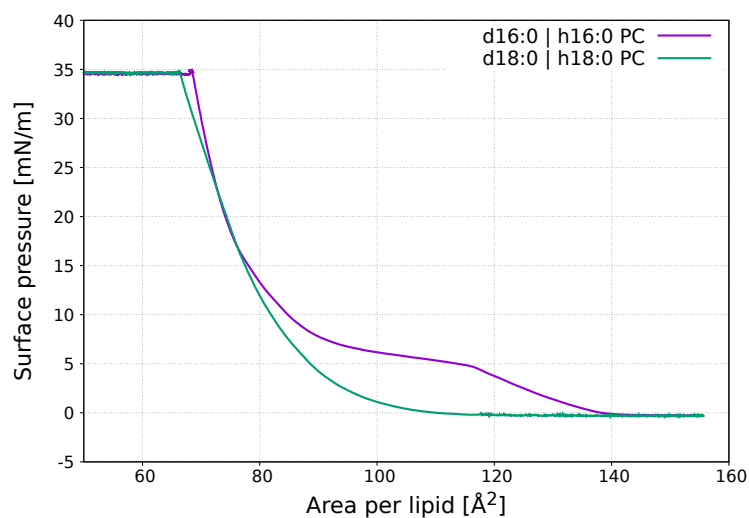


FIGURE 3.36: Isotherm and deposition of the lipids d18:0 | h18:0 PC and d16:0 | h16:0 PC

3.36 shows the two isotherms for the d18:0 | h18:0 PC and d16:0 | h16:0 PC. It can be noticed as the two monolayers behave differently during the isothermal compression. The d16:0 | h16:0 PC constituted monolayer has a intermediate step, that corresponds to the change of phase of this lipid, whereas this plateau is not present for d18:0 | h18:0 PC lipid monolayer. From amount of lipid utilised for the spreading, the average topological area per lipid can be achieved during the compression, as shown in the x-axis of the plot in figure 3.36. Once the pressure reached the target, the deposition was carried out. The silicon support was slowly raised up while the barrier moved maintaining a constant pressure. The deposition step can be seen in the plot as a straight line. In this step the topological area per lipid is not changing,

but the area of the trough changes due to the deposition of the monolayer onto the silicon support, giving the plot shown. The deposition can be also plotted as displayed in figure 3.37,

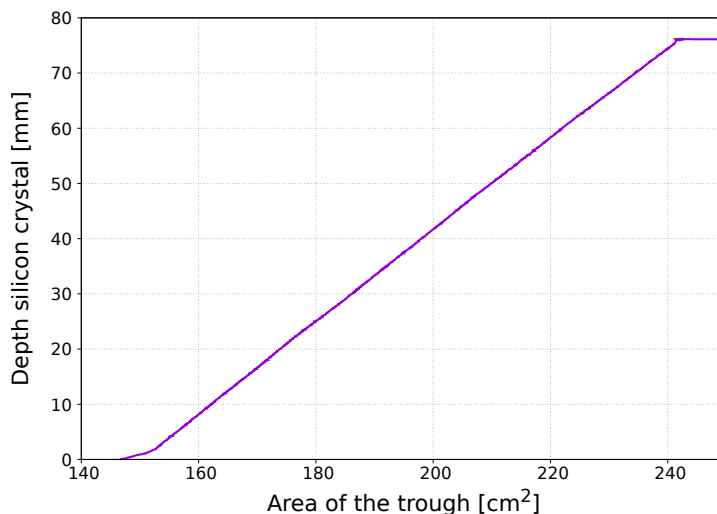


FIGURE 3.37: Efficiency of the deposition for the lipid d16:0 | h16:0 PC, that it was found to be in this case to 100%

where the area of the trough and the depth of the silicon crystal are compared. From this plot the efficiency of the deposition can be calculated, since the ratio between the variation of the depth and the variation of the area of the trough, gives how much of the monolayer went onto the support. In this exceptional case, an efficiency of 100% was reached. Next, the deposition

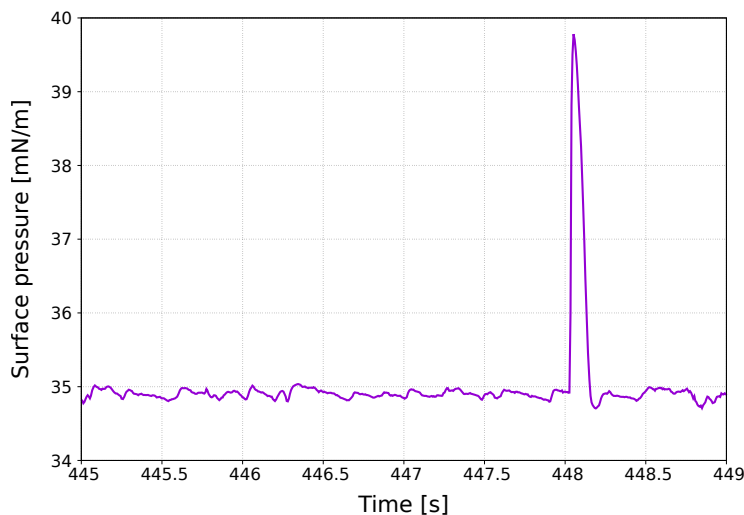


FIGURE 3.38: Deposition of the second leaflet via Langmuir-Schaefer, in order to obtain the complete bilayer.

of the second leaflet needs to be performed, in order to obtain a bilayer. A second trough was utilised, as shown in figure in Appendix A.4.2. In this case the PEEK cell is placed under the water, and the silicon support with the already deposited monolayer, placed horizontally on the top of the level of the liquid. Also in this case the isotherm was carried out, in order to reach the same target pressure. Next, the silicon support is slowly lowered down, until the two monolayers touch each other, giving the peak in pressure shown in figure 3.38. The cell

then is closed under the trough liquid, and screwed with the metal cover, giving at the end of the process the NR cell ready for the measurement (as shown in figure in Appendix A.4.1). The same process was performed also for the d18:0 | h18:0 PC bilayer.

3.2.3 Summary of the results for the protein and lipid production

In this section the lipid production results are shown and discussed. Natural lipids are an excellent alternative to synthetic ones, in order to produce more biologically relevant model lipid membranes. The second fundamental advantage consists in the fact that those lipids are now available in their deuterated form, enabling to design experiments with techniques where the deuterium labeling is an important factor (for instance neutron scattering, NMR or infrared spectroscopy). The experiments performed found a deuteration level of $\approx 95\%$. The lack of structural changes despite the difference in the acyl chains profile, between different mixtures in both H and D forms, is a valuable point for lipid and protein-lipid interaction studies. This behavior comes from the fact that the hydrophobic interaction in D and H material is different (demonstrated also with the GC measurements), and the cell adjusts accordingly the composition of the acyl chains (as displayed and discussed above) in order to have the same membrane fluidity in H and D conditions. This aspect explains the lack of structural differences between H and D membranes. With the protocol described in Chapter 2 and above in this section, the purification of different classes of GPL molecules can be achieved, resulting in a controlled environment for the experiments. In order to obtain an accurate SLD calculation, GC-MS and GC-FID was carried out to obtain information on the acyl chain distribution. The SLBs created show a high coverage using the vesicle fusion method at room temperature with the protocol discussed. As shown, this optimised protocol can be used for the deposition of both uncharged and charged lipids.

Partially deuterated PC molecule species were also synthesised, in order to assess the kinetics of the PLA1-1 under analysis using neutron scattering techniques. These PC molecules are characterised by the first position acyl chain being deuterated, whereas the other parts of the molecule were in their hydrogenous form. This configuration is useful since the two products of the reaction created after the PLA1-1 - lipid membrane interaction hydrolysis, have different deuteration level (deuterated FFA and hydrogenous lyso PC). With this system, the differentiation of the two products of the reaction can be achieved and the structural changes of the membrane during the hydrolysis reaction can be recorded, and the preferred substrate can be determined. Natural lipids were used to study the kinetics of the interaction of the PLA1-1 under examination with biologically relevant model membranes. PC and PC/PS flat membranes were used with the PLA1-1, to assess if charged membranes change the velocity of the reaction. Partially deuterated PC molecules were used for the assessment of the kinetics, using the advantage of having two different SLDs for the two reaction products, and analyse the substrate specificity making flat lipid membranes with the lipids synthesised.

Chapter 4

Results: Protein-lipid interaction studies

The study of the PLA1-1 - model membrane interactions and kinetic process involved the use of two main techniques. Firstly NR, that provided information on the substrate preference and the structural changes of the model membrane upon reaction, by utilising mono-species SLBs constituted by the synthesised partially deuterated PC molecules. Secondly, MS experiments were carried out, where the substrate specificity was achieved by using vesicles constituted by a multitude of PC molecules in the same vesicle sample. More natural like model membranes were tested with this technique, where each molecule can be distinguished and analysed. From these experiments, the preference of the PLA1-1 for different substrates can be determined without any bias on the different packing of the membrane, which is an important factor in mono-species SLBs. Natural lipids were also utilised in both techniques, in order to perform kinetics through more biologically relevant model membranes. Finally, other physico-chemical techniques were employed, in order to obtain further complementary information on the systems and strengthen the interpretation of the results.

4.1 NR analysis

In this section, the kinetics results emanating from the NR measurements are presented. Partially deuterated PC molecules were employed to assess the substrate preference of the PLA1-1. Such lipids varied from one another in terms of their acyl chain length and number of double bonds. Employing such PC molecules, helps understanding structural changes within the bilayer and the distribution of the reaction products over time. NR measurements were performed firstly on mono-species and successively on natural lipid extracts SLBs. The latter were used in order to record kinetics on more biologically relevant lipid membranes. Nevertheless, by using these lipids, less information can be achieved on the kinetics, since they are either fully H or D, and no specific site deuteration can be utilised. After the deposition of the SLBs followed by their structural characterisation, a certain amount of PLA1-1 was injected into the cell, to achieve a pre-determined stoichiometry, depending on the different lipid membrane composition used. The right amount of protein per lipid was assessed by employing ellipsometry, as explained later in this section. This step is fundamental, since

with the NR set-up used in this work kinetics faster than 5 minutes could not be recorded, without large experimental errors. Consequently, the shortest time resolution of 5 minutes in the kinetics measurements was achieved, by only measuring the first angle, where not all the structural information can be extracted. Accordingly, the amount of protein needs to be well calibrated in advance in order to obtain slow enough kinetics for each lipid. The right amount of protein was diluted to 1 ml of final solution, and directly injected into the cell to start the reaction.

4.1.1 PLA1-1 kinetics with partially deuterated PC molecules

As mentioned in Chapter 3, partially deuterated PC molecules were synthesised for the analysis of the PLA1-1 kinetics. SLBs were made through the various PC molecules synthesised, in order to obtain several lipid membranes. The principle behind the experiment is based on testing membranes composed of different lipids, that allowed assess to the substrate preference of the enzyme under examination, and also to understand how the structure of the system changed over time.

NR studies on saturated series SLBs In this study, we first started measuring kinetics using saturated PC molecules, such as d18:0 | h18:0 PC, d16:0 | h16:0 PC and d14:0 | h14:0 PC. The first two lipids mentioned are both in the gel phase at 22 and 37 °C, whereas the last lipid is in its fluid phase at 37 °C, since its transition temperature is around 22 °C. As explained in Chapter 3, the deposition of the d18:0 | h18:0 PC and d16:0 | h16:0 PC, was performed using the Langmuir-Blodgett Langmuir-Schaefer technique, that allows better lipid depositions from saturated long chain species. After the deposition and the characterisation with NR of the SLBs, the PLA1-1 was added into the cell, and the kinetics measurements were started. The amount of protein used per each lipid is listed in table 4.1. Figure 4.1

PC molecule	PLA1-1 added [μg]
d18:0 h18:0 PC	300.00 *
d16:0 h16:0 PC	60.00 *
d16:0 h18:1 PC	10.00
d16:0 h18:2 PC	0.25
d16:0 h18:3 PC	0.22
h16:0 h20:4 PC	0.20
d14:0 h14:0 PC	0.05

TABLE 4.1: Absolute amount expressed in μg of PLA1-1 injected into the NR cell after the complete SLB characterisation. The * values were not experimentally calculated, since for technical reasons linked to the sample cell available, it was not possible to use the ellipsometry technique with layers deposited via the LB-LS method. Consequently those values were estimated from the ellipsometry results from the other PC molecules.

shows the analysis of the SLB composed of d18:0 | h18:0 PC, and as can be noticed, the SLD of the hydrophobic region is $\approx 3.3 \cdot 10^{-6}$, that confirms the successful synthesis of

the partially deuterated PC molecule. The fit displayed is non-perfect, since some difficulties arose during the analysis of the silicon support. In this case the crystal has a very thick oxide, that disturbs the signal from the lipid bilayer, resulting in difficulties in the fitting using the model described. Nevertheless, the parameters of the SLB could be determined, and upon PLA1-1 injection, the kinetics performed. Figure 4.2 shows the analysis of the degradation, where the green colored curve is the DSPC SLB before the PLA1-1 injection, and the purple curve is after 12h of incubation and wash. It is evident that a certain degree of degradation

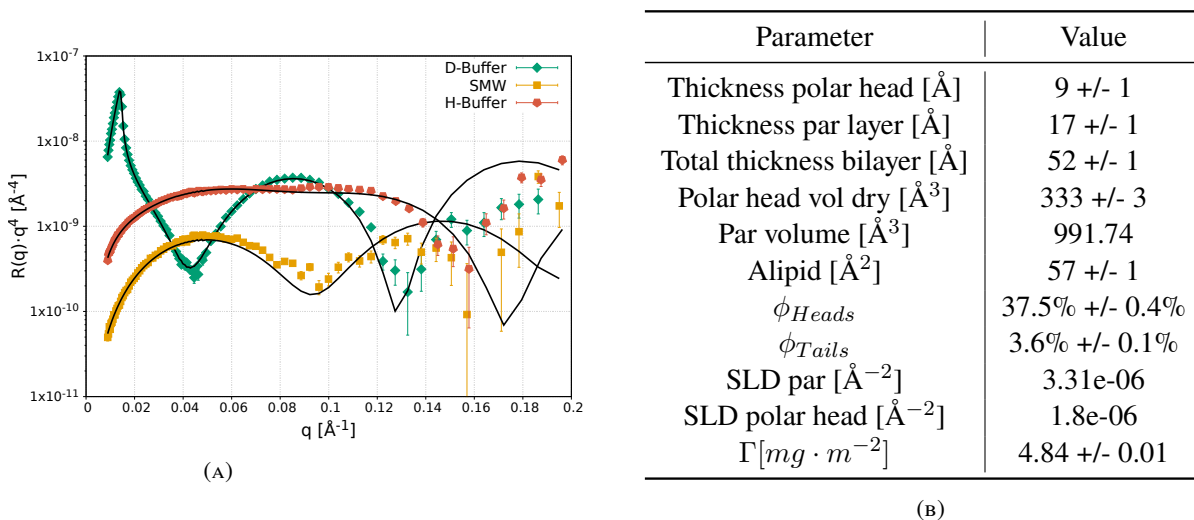


FIGURE 4.1: DSPC SLB structure profile in 3 different contrasts (A) and parameters used to fit the data in panel (B)

of the lipid bilayer was recorded. The speed of the reaction is very slow and the resulting degradation barely noticeable. Figure 4.2 panel B shows the SLD profiles resulted from the NR analysis, where the asymmetry of the membrane after the hydrolysis is clearly visible. This behavior, which will be explained in Chapter 6, is directly related to the structure of an SLB. The SLB, as mentioned in Chapter 2, are lipid membranes supported by, in this case, a silicon support, from which they are separated by a few Å water layer. This space is not enough to host a protein, resulting in the non-availability of the inner leaflet (leaflet facing the silicon support) of the membrane to the PLA1-1 injected. Therefore, the hydrolysis of the SLB, is mainly performed by the protein on the outer leaflet (leaflet facing the bulk solution). This behavior is shown experimentally, as mentioned, in figure 4.2 panel B, where the SLD of the outer leaflet decreases, whereas the inner leaflet remains unaltered.

Flip-flop mechanism - In a plasma membrane, the process of flip-flop of GPLs is an important factor for the normal life of a cell. This process is based on the movement of some phospholipid molecules from one leaflet to the other of the lipid bilayer, needed to maintain a homogeneous phospholipid composition along its perpendicular axis. Such a process is thermodynamically favored due to the entropy increase. In fact, since often the homogeneity of the plasma membrane is correlated to apoptosis processes [261], the cell has to spend energy to contrast this phenomena, given that usually plasma membranes are strongly asymmetric. In the case of DSPC flip-flop was not observed, as expected since this kind of

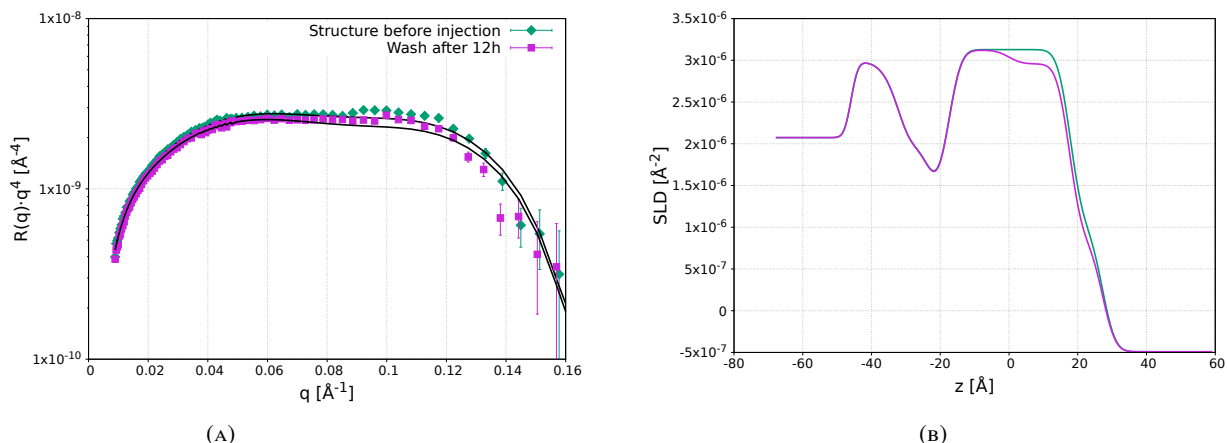
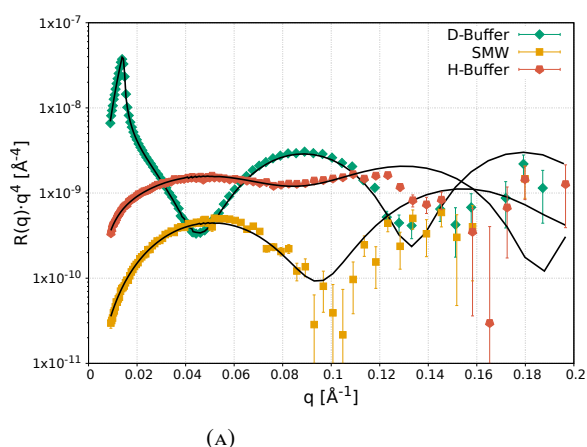


FIGURE 4.2: Kinetics recorded using DSPC SLB in incubation with PLA1-1. In panel (A) the NR data and analysis and in panel (B) the correlated SLD profiles are displayed. A slight decrease of the SLD of the outer leaflet only can be noticed, since that leaflet is the only one available for the attachment of the enzyme.

lipid molecule creates very rigid membranes, which limits the movement of PC molecules. Additionally, because of this rigidity, the efflux of the PC molecules is very low, leading to the low rate of the hydrolysis reaction recorded.

A slightly different scenario was observed with d16:0 | h16:0 PC-SLB, which structure is shown in figure 4.3. In this case the SLB was found to have a $\approx 90\%$ of coverage, a lower value than that found in the d18:0 | h18:0 PC case. Also in this case, the silicon support had a thick oxide layer, that complicated the analysis. The area per lipid in this case was lower, thus resulting in a higher thickness of the bilayer and a similar surface excess (Γ) to the d18:0 | h18:0 PC-SLB. The SLD found was consistent with a successful synthesis of partially deuterated chains. SLBs containing shorter acyl-chain PC molecules, leading to a



Parameter	Value
Thickness polar head [Å]	10 +/- 1
Thickness par layer [Å]	18 +/- 1
Total thickness bilayer [Å]	56 +/- 1
Polar head vol dry [Å ³]	330 +/- 2
Par volume [Å ³]	880.54
Alipid [Å ²]	49 +/- 1
ϕ_{Heads}	39.7% +/- 0.3%
ϕ_{Tails}	15.8% +/- 0.2%
SLD par [Å ⁻²]	3.3e-06
SLD polar head [Å ⁻²]	1.82e-06
Γ [mg · m ⁻²]	4.90 +/- 0.01

FIGURE 4.3: DPPC SLB structure analysis in 3 different contrasts (A) and its fitted parameters in panel (B)

lesser packed membrane, since the hydrophobic interactions are less intense. This behavior

is directly correlated to the rate of the hydrolysis reaction, that in fact was found to be faster compared to the d18:0 | h18:0 PC SLB case. This meant that the shorter lengths of the acyl chain, contained in the d16:0 | h16:0 PC molecules, lead to a faster efflux of the molecule from the membrane, as well as more free fluctuations within the membrane. In figure 4.4 the kinetics measurements, analysed with the kinetic plug-in inside CoruxFit program (see details in Chapter 6), are shown. The fit could be further refined, although the signal from the silicon

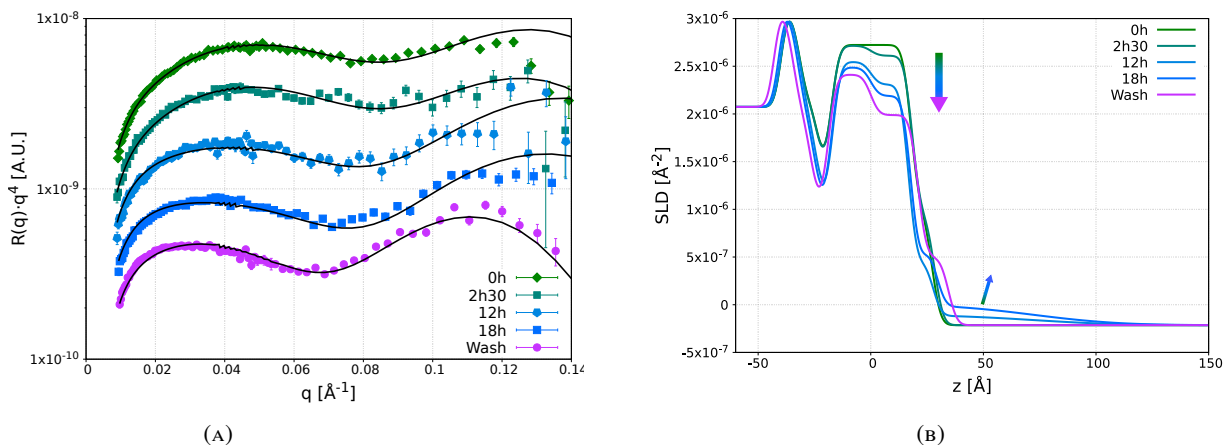


FIGURE 4.4: Kinetics recorded on DPPC SLB in incubation with PLA1-1. In panel (A) the NR data and their analysis, in panel (B) the SLD profiles. The degradation is clearly visible from the decrease of the SLD values, where an increase of the SLD occurs around 50 Å from the center of the bilayer (micelle layer).

oxide complicates the task. However, useful information can be obtained from this analysis. All the reflectivity curves are shifted vertically, for clarity. It is clear in figure 4.4 panel A, that the curve changes during the reaction. Since the lipids used are partially deuterated PC molecules, formation of defects and the removal of deuterated material from the lipid membrane leads to a decrease of its SLD (measurements were performed in H-Buffer). The removal and the defects formation are constrained as explained in Chapter 6. The decrease of the SLD of the lipid membranes resulted in the decrease of the signal from the sample, as shown in the plot in figure 4.5, where the integration of each dataset was performed between $0.1 < q < 0.14 \text{ \AA}^{-1}$, thus ignoring the noisy points at high q . Taking into consideration once more the figure 4.4 panel A, it can be noticed that the minimum of the reflectivity profile that lies between 0.06 and 0.08 \AA^{-1} , shifts during the hydrolysis reaction. In principle, this behavior can be correlated to the increase of the total thickness of the sample. In fact, as explained later, the area per lipid decreases over time, giving an average increase of the lipid bilayer thickness. The depth of this minimum also changes, becoming much stronger over degradation, because of the different level of contrast inside the sample due to the decrease of the SLD and the formation of defects. Figure 4.4 panel B shows the SLD profiles calculated from the analysis displayed in figure 4.4 panel A. In comparison to the d18:0 | h18:0 PC-SLB, a different trend was observed for the d16:0 | h16:0 PC-SLB, where the outer leaflet of the lipid bilayer undergoes degradation first followed by degradation of the inner leaflet. As mentioned before, this behavior is related to the flip-flop of the PC molecules from the inner to the outer

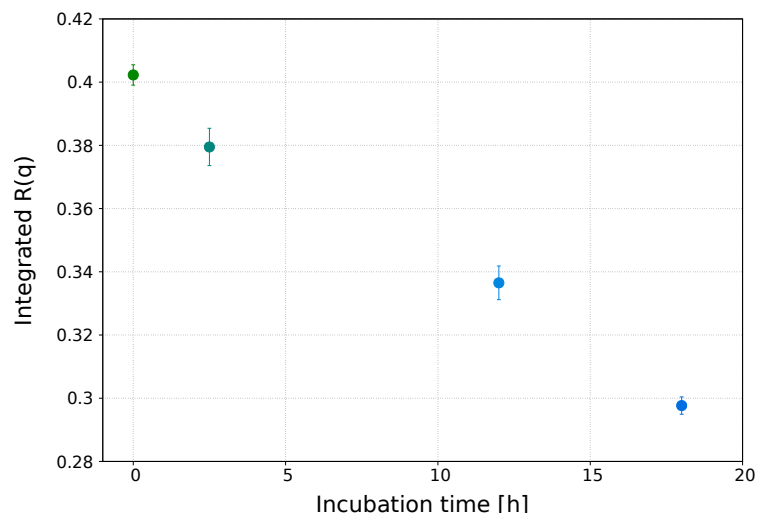


FIGURE 4.5: Integrated $R(q)$ intensity over the hydrolysis reaction time. The integration was carried out between $0.1 < q < 0.14 \text{ \AA}^{-1}$

leaflet, and in this example this process is visible. In fact, the SLD of the inner leaflet also decreases, although at a lower speed compared to the outer leaflet. Upon degradation, the lipids from the inner leaflet moved to the outer one, in order to compensate for the defect formation of that leaflet, where the lipids can be hydrolysed. Such a process occurs in 16:0 | 16:0 PC-SLB, due to the shorter acyl length that leads to a faster degradation, causing the membrane to become more fluid over time. From the SLD profiles, it can be also noticed that there is an increase of the SLD right above the bilayer structure (as indicated by the small arrow). This feature will be discussed later in this section. From the analysis with the kinetics plug-in in CoruxFit program, the degradation graph can be obtained as shown in figure 4.6. In this figure, the plotted parameter f_{kin1} represents the amount of degradation of the sn1 acyl

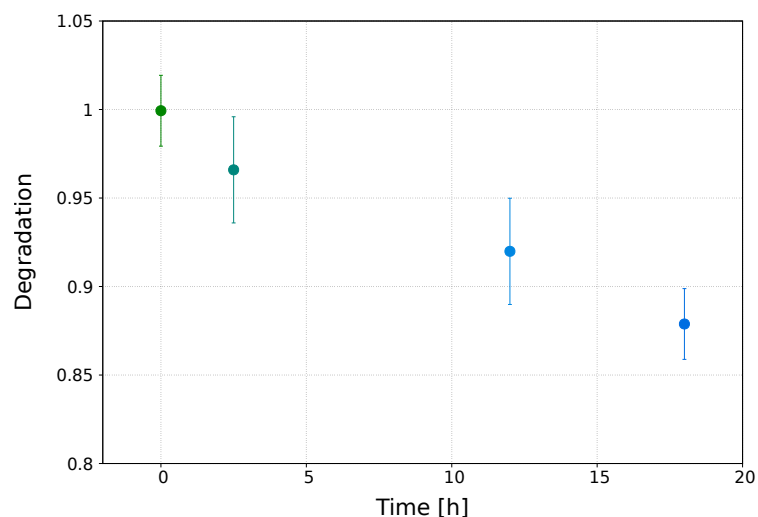


FIGURE 4.6: Degradation level from the d16:0 | h16:0 PC SLB kinetics analysis, using the kinetics plug-in for CoruxFit

chain (see for more details the model in Chapter 6). It is clear that degradation occurs over time, even though the process is slow, since $\approx 0.87\%$ of the bilayer remains after 18 hours of

incubation. From the degradation graph, it is clear that the reaction did not reach the plateau, but unfortunately the measurements were stopped as we reached the end of our beamtime. Unfortunately, some data points are missing, especially those between 2.5 hours and 12 hours measurements (caused by problems to the instrument during the night). From this analysis, the flip-flop that has accrued, can be also calculated, as it is shown in figure 4.7. A flip-flop equal

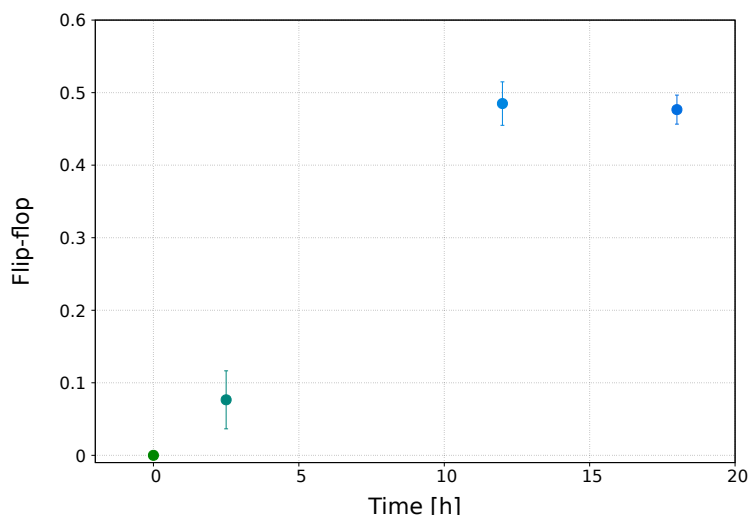


FIGURE 4.7: Extent of flip-flop determined from d16:0 | h16:0 PC SLB calculated from the kinetics plug-in analysis.

to ‘0’ corresponds to a totally asymmetric bilayer, where all the degradation is considered only occurring in the outer leaflet, whereas ‘1’ indicates a fully symmetric bilayer. The first point was set to zero manually, since the parameter for that dataset is not relevant, due to the fact that the degradation (f_{kin1}) is 1, and every value of the flip-flop (between 0 and 1) results in the same SLD profile. Upon hydrolysis, the asymmetry of the lipid membrane decreases, until it finds an equilibrium. Hypothetically, the flip-flop process can reach a certain level such that the speed of degradation and the speed of the flip-flopping are equal and lead to the plateau displayed in figure. More points would be needed for a correct interpretation and confirmation of the proposed mechanism. As mentioned before, the topological area per lipid (A_{lipid}) changes upon degradation as shown in figure 4.8, since the thickness of the bilayer slightly increases. As it will be explained in Chapter 6, the parameter A_{lipid} is constrained to the f_{kin1} through the fitted global parameter $A_{lipid\ factor}$, which is common for all the datasets of the same experiment. The A_{lipid} per time point is calculated by using an empirical equation that includes the f_{kin1} parameter and the initial A_{lipid} . This constrain is one of the fundamental ones to avoid the over-parameterisation of the model.

Micellar formation - The final kinetics study taken into consideration is related to the reaction products released from the lipid membrane bilayer. As mentioned earlier, an increase of the SLD on the top of the lipid bilayer was found to occur upon reaction, which is correlated to structures forming over time above the SLB. It was found that these structures are correlated to the material that is released from the bilayer upon its degradation. We interpret this behaviour with the formation of micelles from the deuterated palmitic FFA,

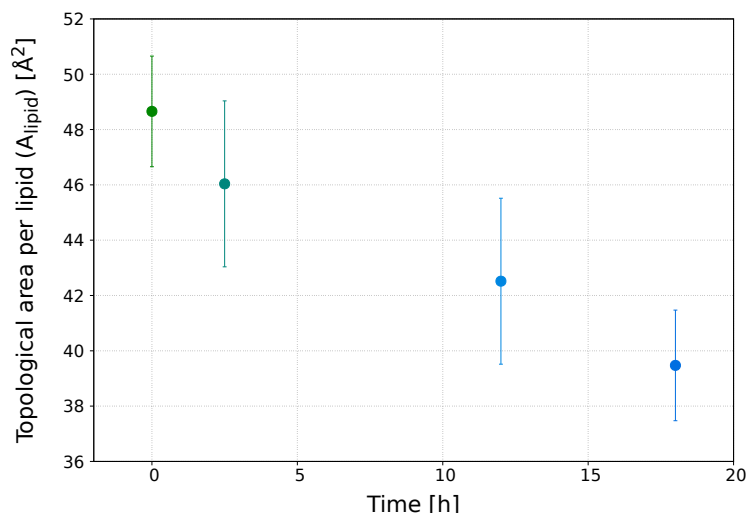


FIGURE 4.8: Topological area per lipid variation upon degradation for the d16:0 | h16:0 PC kinetics

since an SLD of a deuterated acyl chain for this structures was found to fit correctly all the datasets. Nevertheless, within these micelles formed by the palmitic FFA, the presence of other lipid species such as lysos and phospholipid molecules as well as proteins might occur. The parameter f_{kin1} previously described, is correlated to the amount of degradation as well as to the amount of deuterated material released into the bulk solution. The SLD of the bulk solution is corrected by employing f_{kin1} , even though the correction normally is small. FFA molecules are not soluble, and after reaching a certain concentration level, they start to rearrange and interact, forming a more thermodynamic stable system: micelles. The concentration level mentioned corresponds to the critical micellar concentration (CMC), which varies between different FFAs. Above the critical micellar concentration (CMC) of the palmitic FFA corresponding to $4 \mu\text{M}$ [262], the formation of micelles occurs in the bulk solution. Micelles can be compared to solid spheres as shown in figure 4.9. The parameter

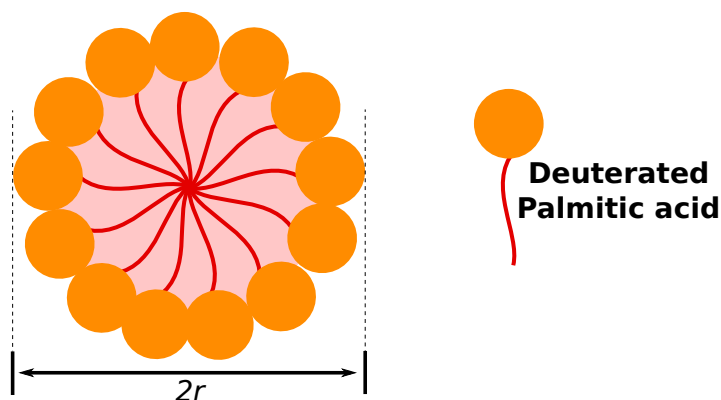


FIGURE 4.9: Sketch representing a palmitic acid micelle

r , the radius of the sphere, equals or is less than the thickness of the palmitic FFA, that was taken from the DPPC fit ("Thickness par layer"). The calculated maximum volume of the

described micelle corresponds to $\approx 18,300 \text{ \AA}^3$. The volume of a single FFA was taken by the "Par volume" shown in the table of figure 4.3B, divided by a factor 2, giving a volume of 440 \AA^3 . The number of FFA molecules within a micelle was obtained by dividing the volume of the sphere with the volume of the FFA, found to be ≈ 40 . Therefore, a palmitic fatty acid micelle contain a maximum of 40 molecules. In order to form micelles, the concentration of the palmitic acid in solution has to be, as mentioned, above the CMC. Starting from this concentration, the corresponding amount of molecules can be calculated, and corresponds to $2.4 \cdot 10^{18}$ molecules per liter of solution. The volume inside the used NR cells is $\approx 1 \text{ ml}$ and leads to $2.4 \cdot 10^{15}$ molecules per ml of solution. Next, the amount of lipid molecules was calculated, taking into consideration the surface excess Γ , that for the d16:0 | h16:0 PC is $4.9 \text{ mg} \cdot \text{m}^{-2}$. From this value, the actual amount in mg from a silicon support surface of $8 \times 5 \text{ cm}^2$ corresponds to 19.6 \mu g . Taking the molecular weight of the d16:0 | h16:0 PC ($765 \text{ g} \cdot \text{mol}^{-1}$), the number of molecules deposited on the crystal can be calculated as $1.6 \cdot 10^{16}$ molecules. Next, in order to assess at which amount of degradation the CMC value is reached, the number of molecules needed for the micelles and the total amount of lipids in the cell are divided, giving the result of 0.15. Consequently, when the lipid bilayer has been degraded by more than 0.15 (that corresponds to 0.85 in the degradation graph), the micelles start appearing in the bulk solution. Considering the values calculated, an amount of $6 \cdot 10^{13}$ micelles (considering the aggregation number calculated above) should appear in the bulk solution just above the CMC of the palmitic acid. It was found experimentally with NR, that those micelles, over time, attached back to the lipid membrane, creating a diluted layer on the top of the lipid membrane. It was also found that the degradation after which the micelles appear is around 0.1, that is in good agreement with the calculations discussed. The aggregation number was utilised as a fixed parameter in the kinetics plug-in, in order to calculate the amount of micelles using the variable parameter f_{kin1} . The layer interpreting the "micellar layer" is described with a volume fraction distribution (details in Chapter 6) as shown in figure 4.10, where '0' is the center of the lipid bilayer. The fraction volume distributions are sharp near the lipid bilayer, and diffuse into the bulk solution, in order to describe a layer that is diluted over the z-axis. The fraction volume distributions per time point was then multiplied by an SLD of 7, that corresponds to a fully deuterated FFA, giving the SLD profile shown in figure 4.4. The micellar layer is highlighted with the small arrow, indicating the orientation of this signal upon the reaction. It can be observed that this layer was not found for the time point at 2.5 hours, because the amount of FFA in the bulk is below the CMC of the palmitic acid. An example of the model for time point 18h is shown in figure 4.11. The volume fraction distribution for the micellar layer is placed near the polar head, in order to obtain a layer on the top of the membrane. Figure 4.12 summarizes the events through a sketch of the kinetics recorded with NR. Finally, it is worth mentioning that we also experimented with SLB composed of d14:0 | h14:0 PC (DMPC) (results not shown). Unfortunately, we could not track the kinetics for this SLB due to its very fast reaction. Even the addition of a very small amount of protein led to a very fast kinetics, where even from the first measurement after the injection of the protein, the signal from an empty silicon support

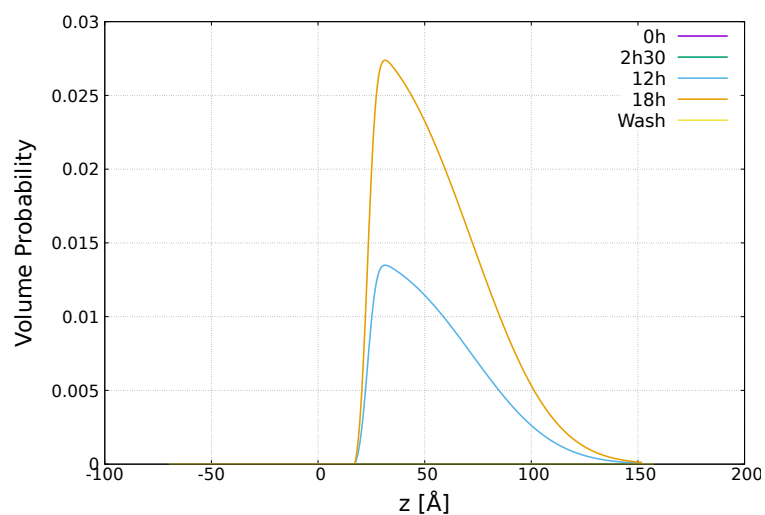


FIGURE 4.10: Plot of the fraction volume distribution of the ERF representing the micellar layer upon degradation.

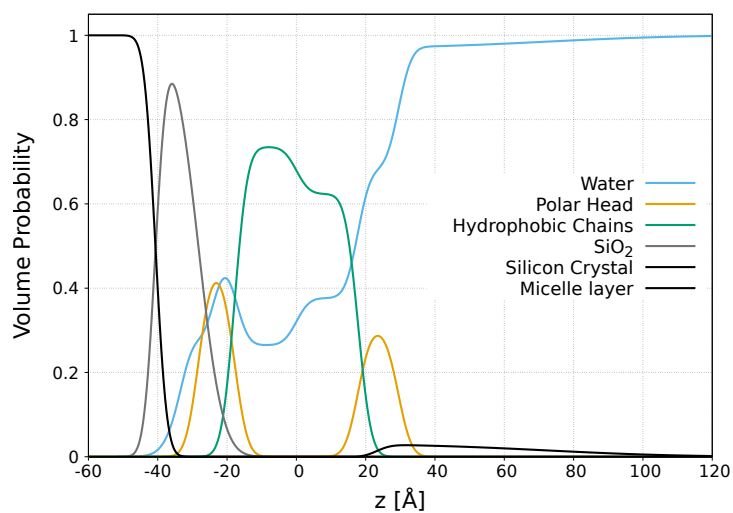


FIGURE 4.11: Model for the time point 12h of the kinetics recorded for d16:0 | h16:0 PC SLB.

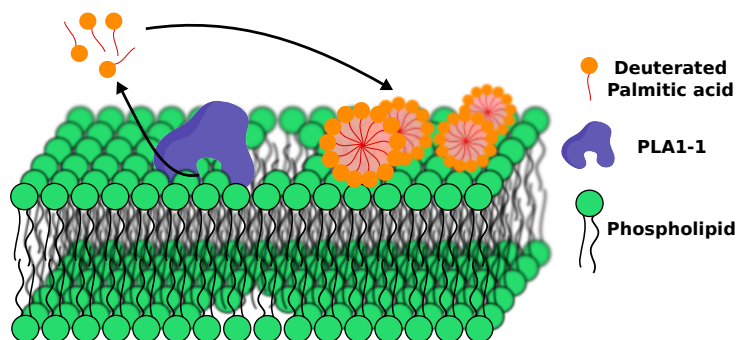


FIGURE 4.12: Sketch representing the course of the kinetics recorded with NR for the d16:0 | h16:0 PC SLB

was observed. These experiments on the saturated series SLBs support our assumption of the acyl chain length playing a role on the degradation. Specifically, longer acyl chains lead to a lower efflux propensity, giving slow kinetics. Also the fluidity of the membrane is an important factor, since only DMPC-SLB was in the fluid phase within the saturated series employed, giving more chances to the phospholipid to efflux.

NR measurements of the unsaturated series SLBs - Next, unsaturated PC molecules were employed, in order to assess the preferred substrate within the unsaturated series. Unsaturated PC molecules have a transition temperature below room temperature (some of them even below zero), therefore they are in fluid phase, and consequently vesicle fusion can be used to prepare the supported bilayers. After the characterisation of the "empty cell" (silicon support measured in at least two contrasts), the vesicle solution composed by the lipid 16:0 | 18:2 PC was injected and vesicle fusion performed. Next, the bilayer was characterized as is shown in figure 4.13. The thickness of the oxide of the silicon crystal

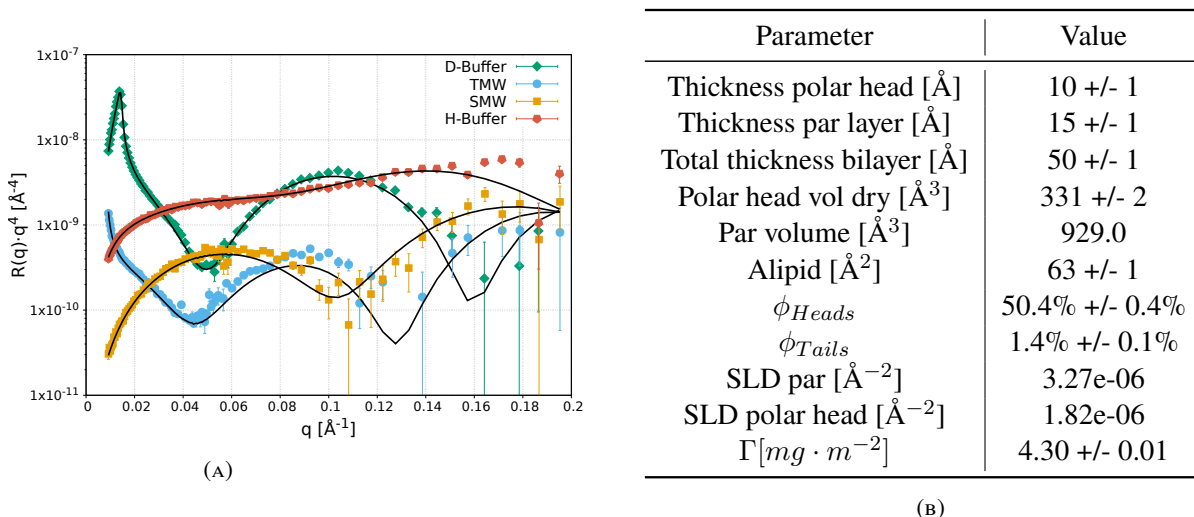


FIGURE 4.13: d16:0 | h18:2 PC SLB reflectivity data in 4 different contrasts (A) and fitted parameters in panel (B)

used for the above sample, was lower compared to the previous cases. This led to a better and simpler analysis and more accurate results as well as a to a high bilayer coverage. The area per lipid was higher compared to the saturated series, which is the consequence of a more fluid lipid membrane (less packed). Also in this case the SLD of the hydrophobic part suggests the successful synthesis of the partially deuterated PC molecules. The thickness of the total bilayer is lower, and it is due to the higher topological area per lipid, correlated to the higher fluidity. Unfortunately we were not able to successfully utilise this SLB to measure the PLA1-1 kinetics, due to occurrence of some technical issues with the HPLC pump controlled by the instrument. Thereafter, another SLB composed of the same molecule was recreated. This sample d16:0 | h18:2 PC-SLB had a coverage of 92%, which leads to an SLD of the hydrophobic part of $\approx 3 \cdot 10^{-6} \text{ \AA}^{-2}$, as displayed in figure 4.14 panel A, where all the other parameters are retained. The structure was measured in only 2 contrasts, since structural

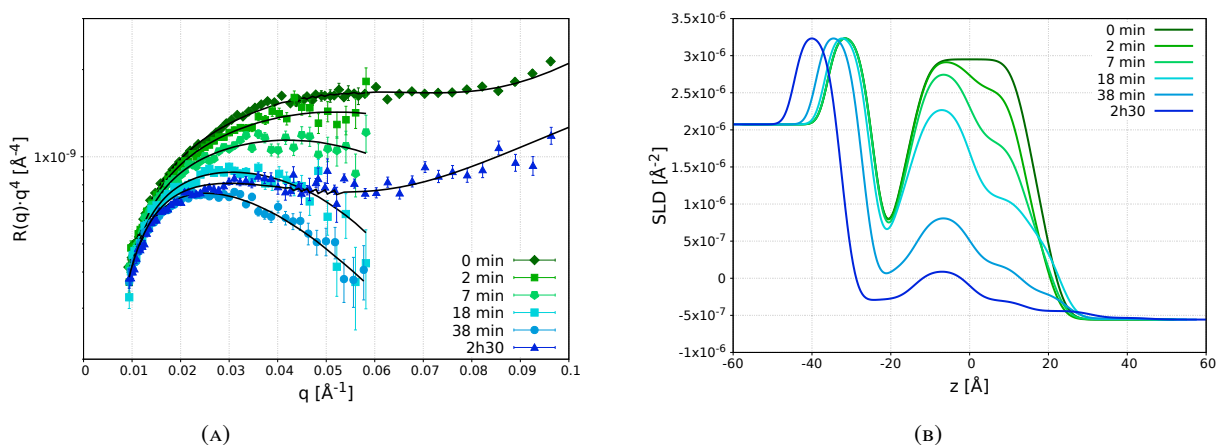


FIGURE 4.14: Kinetics recorded on d16:0 | h18:2 PC SLB. In panel (A) the NR data and their fitted curves, in panel (B) the related SLD profiles. The degradation of the lipid bilayer is clear from the shift to lower values of the SLD profiles.

parameters were found precisely using the first SLB. After the bilayer characterisation, an amount corresponding to $0.25 \mu\text{g}$ (see table 4.1) of PLA1-1 was injected into the NR cell, and the kinetics recorded as explained before. The kinetics, as it can be noticed, is faster compared to the kinetics recorded for d18:0 | h18:0 PC and d16:0 | h16:0 PC. This can be explained by the presence of the two double bonds in the sn2 chain of the PC molecule (16:0 | 18:2) leading to a more fluid lipid membrane. The double bonds behave as kinks in the acyl chain [263], disrupting the close interaction and packing of the acyl chains in phospholipid molecules, resulting in a more disordered membrane (fluid membrane). In fact, acyl chains contained in phospholipid molecules with more than 18 carbons and 1 or more double bonds (16:0 | 18:1 PC, 16:0 | 18:2 PC, etc), lead to phospholipids with transition temperatures below room temperature. For instance, taking into consideration the lipid under analysis, its transition temperature is below zero, giving a fluid phase membrane for both 22 and 37 °C. Given this scenario, the efflux propensity of phospholipid molecules is theoretically faster compared to that shown and discussed for the saturated series, since the packing parameter is lower. Faster efflux propensity could lead to a faster hydrolysis reaction, since the speed of the first "bottle neck" (the efflux of the phospholipid from the membrane) of the reaction increases upon the "membrane disorder". As noticed in figure 4.14 panel A, for the time points between the '0' and '2h30', the reflectivity profiles were recorded only in the first angle, due to the higher speed of the reaction. These "cropped" profiles contain less structural information since data at high q , where details of small and very small features in the sample are measured, is not present. The lack of the minimum of the reflectivity profile also led to problems in the exact quantification of the defects in the lipid bilayer, and thicknesses variations. But these parameters can in any case be obtained from the low q , given the high constrained model in use. Also the flip-flop has an effect on the minimum shape, and also on the 'low q ' profile shape. In conclusion, all these parameters can be obtained given the profiles recorded, but the errors of the fitted parameters are higher compared to an analysis with the complete profiles.

The flip-flop was found to be present in this sample, as shown in figure 4.14 panel B. After 2h30 of reaction, the amount of the lipid membrane deposited is small, giving almost the reflectivity signal of a clean silicon crystal. All the SLD profiles are centered to the '0', which corresponds to the center of the lipid bilayer. Since the area per lipid also in this case decreases upon hydrolysis, the thickness increases, and this mathematically causes the increase of the distance between what is left on the silicon support and the silicon support itself. In this experiment, no micellar layer was found, probably due to the fast speed of the hydrolysis reaction, and so the micelles do not have time to deposit on the bilayer. Figure 4.15

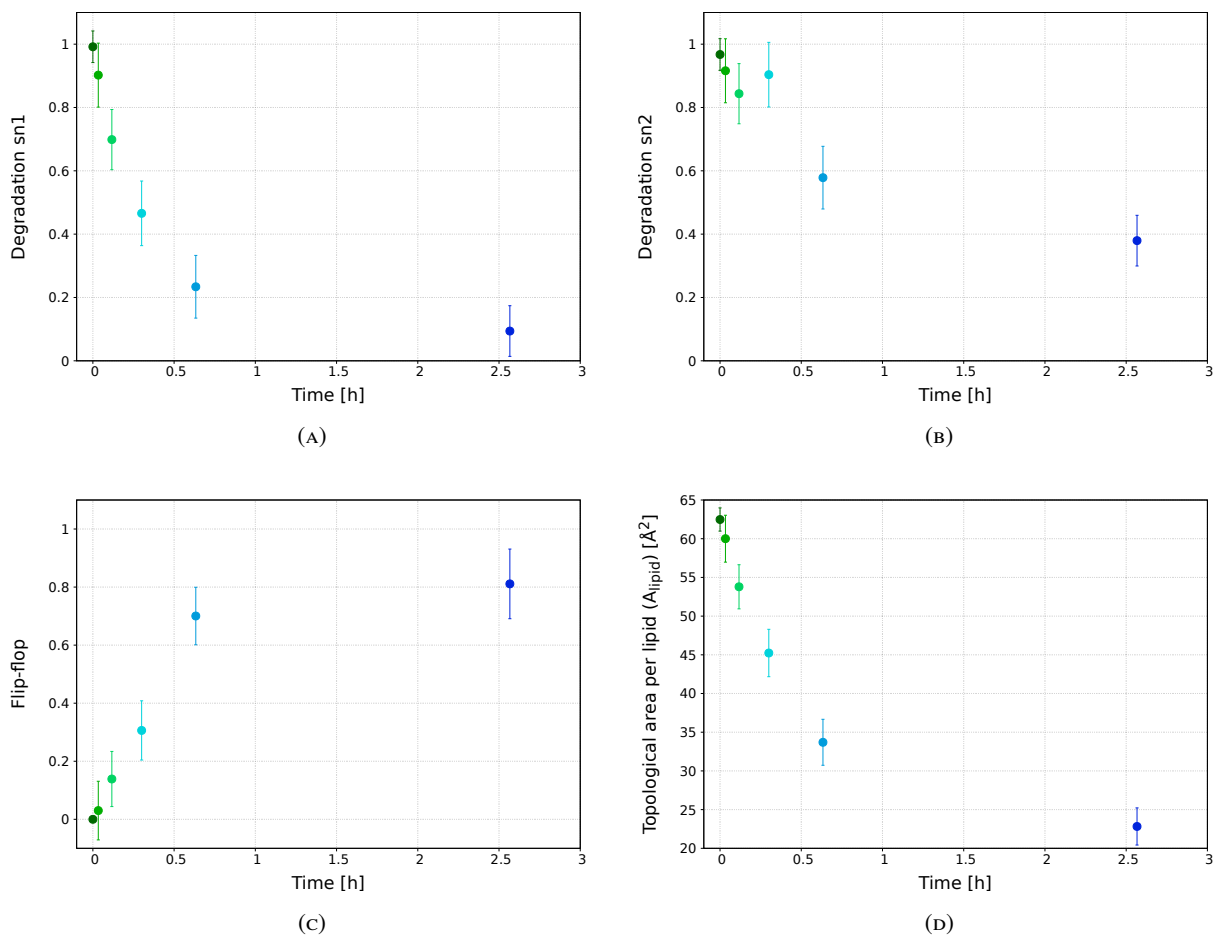


FIGURE 4.15: Graphs from the analysis of the kinetics of d16:0 | h18:2 PC SLB. In panel (A) the sn1 degradation is displayed, in panel (B) the sn2 degradation, in panel (C) the flip-flop profile and finally in panel (D) the topological area per lipid profile. With sn2 degradation we mean the sn2 acyl chain that is hydrolysed when the shift from sn2 to sn1 position occurs.

displays the parameters for the kinetics under discussion. The degradation of the sn1 acyl chain is displayed in panel A, where we can see that the trend follows an exponential decay, typical of the hydrolysis reaction mediated by PLA1-1 (see next section). Contrarily to the previous cases, also the sn2 degradation can be extrapolated, as this parameter does not remain constant for all the duration of the kinetics as before. PLA1-1 is an A1 phospholipase, where the sn1 acyl chain of the phospholipid molecules is the preferred acyl chain to be cleaved. Nevertheless, the degradation of the sn2 chain takes place, although the rate of degradation is

slower compared to the sn1 chain degradation. There is no conclusive evidence in literature that the PLA1-1 has any affinity for the sn2 acyl chain. Our results make us confident to suggest here that the migration of the sn2 position acyl chain to the sn1 occurs after the hydrolysis reaction takes place on the intact phospholipid. The non-enzymatic migration is most probably due to the instability of the sn2 lyso PC, where an equilibrium between sn1 and sn2 lyso then takes place. Once the sn1 lyso forms, it becomes again a substrate for the enzyme under examination (since a lyso phospholipase activity was recorded by lab and MS experiment, as explained later in this paragraph 4.2). In panel C the flip-flop is shown, and also in this case a plateau is reached nearby the end of the reaction. In panel D the area per lipid variation upon reaction is displayed, and reaches a plateau near the end of the reaction. We also carried out studies on other SLBs not mentioned in this section, such as 16:0 | 18:1 PC, 16:0 | 18:3 PC giving similar results as shown and discussed for the other lipids except for the rate of the reaction, that was found to be very different (slower) for the 16:0 | 18:1 PC compared to 16:0 | 18:2 PC.

The last kinetics experiment from the synthetic phospholipids involves the h16:0 | h20:4 PC molecule. Figure 4.16 shows the structural analysis of this PC molecule, which was found to be strongly different compared to the other PC molecules presented above, where the

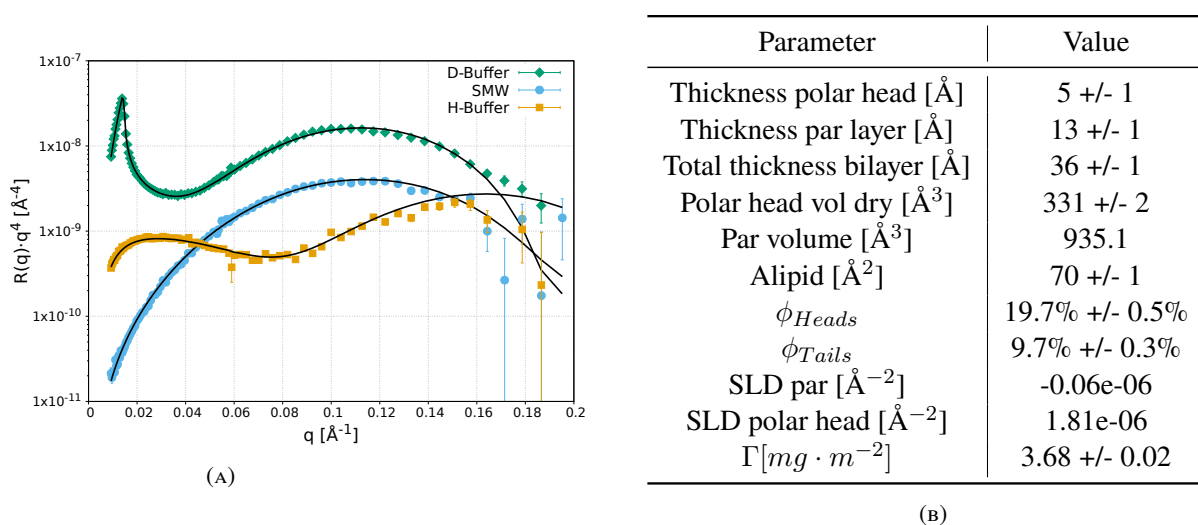


FIGURE 4.16: d16:0 | h20:4 PC SLB structure analysis in 3 different contrasts (A) and its fitted parameters in panel (B)

hydration water of the polar head region is lower and the area per lipid larger. This is probably due to the higher number of double bonds, since, as mentioned, the higher the unsaturation, the higher the number of kinks that lead to higher disorder of the lipid membrane. In this case, the whole lipid is in its hydrogenous form, giving an SLD of the hydrophobic region of $-0.06 \cdot 10^{-6}$. Since the contrast between the acyl chain region and the bulk solution is not as high as for the other samples described, the kinetics was carried out in D-Buffer. Figure 4.17 panel A, shows the fits of the reflectivity data collected at different time points. As it can be seen, upon degradation, the position of the minimum of the reflectivity profiles changes, as well as the intensity at higher 'q' ranges. In this experiment, since a very little

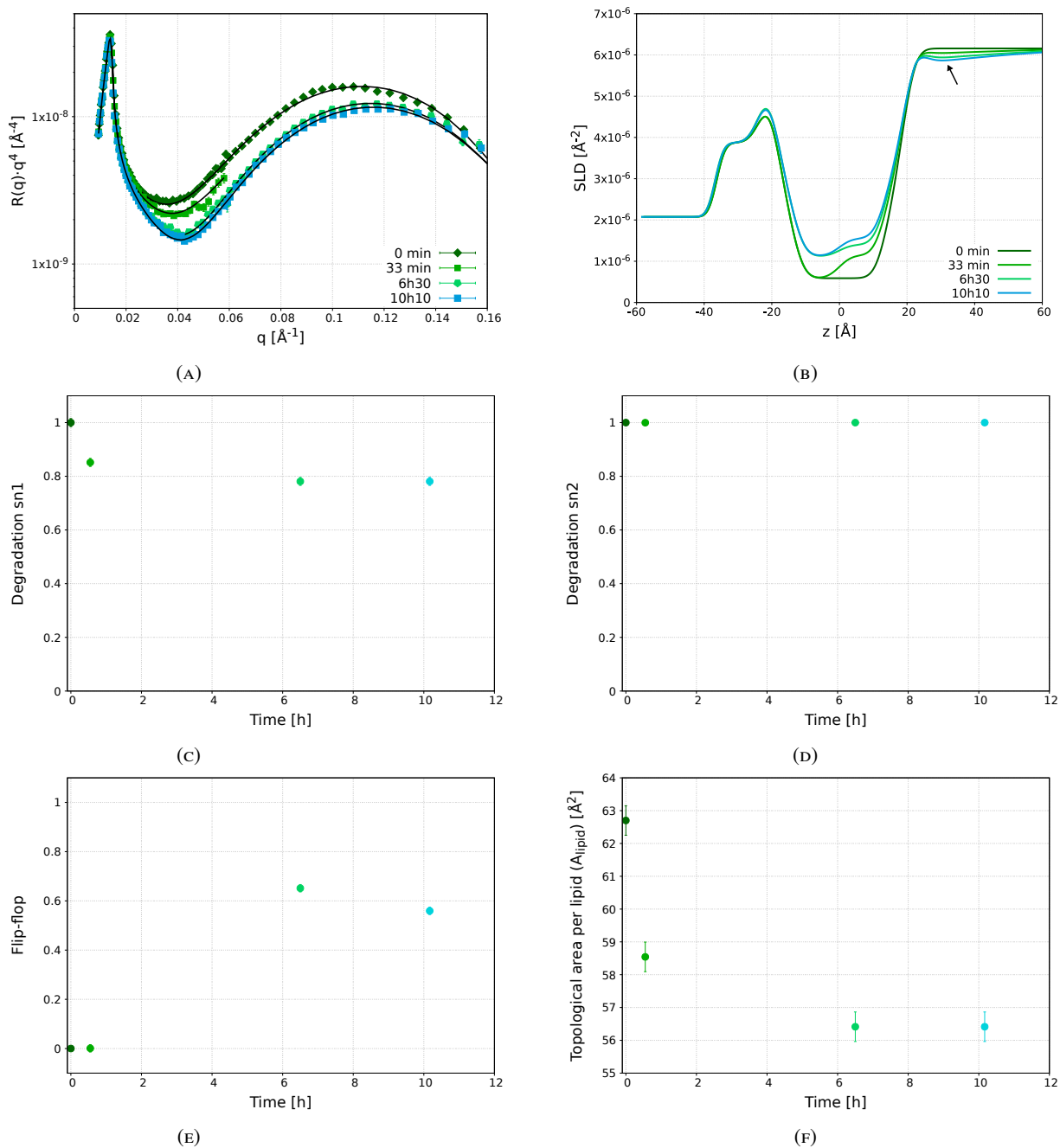


FIGURE 4.17: Graphs resulting from the analysis of the kinetics performed on the h16:0 | h20:4 PC SLB. In panel (A) the NR data and the fitted curves, (B) the correlated SLD profiles, (C) the sn1 degradation, (D) the sn2 degradation, (E) the flip-flop profile and finally (F) the topological area per lipid profile.

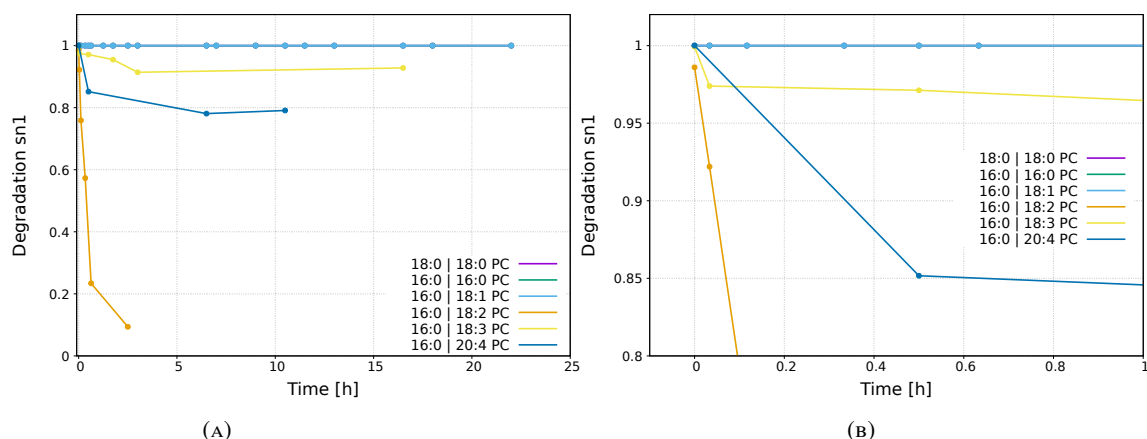


FIGURE 4.18: Panel A: Degradation parameter as determined from NR data fitting; panel B: zoom of the graph displayed in panel A. The errors of the points are omitted for clarity.

amount of protein was injected, the degradation was slower compared to the previously discussed d16:0 | h18:2 PC case. The plateau of the reaction was not reached, since the time allocated was not enough to cover it entirely. The previously mentioned micellar layer appeared also in this sample. Since the micelles are hydrogenated in this sample, they are very visible since the bulk solution is 100% deuterated (D-Buffer). The micellar layer on the top of the lipid membrane is highlighted with an arrow in figure 4.17 panel B. The presence of the micellar layer causes a shift of the critical angles at lower q ranges, and it can be easily analysed by the kinetics plug-in. Since the PC molecules under examination is totally hydrogenous, the discrimination between the degradation sn1 and sn2 chains cannot be used without large errors. Consequently, the degradation of the chain sn2 was fixed to 1 for all the datasets, and the $f_{solvent\ pol}$ (fraction of solvent in the polar head which is correlated to the sn2 degradation, details in Chapter 6) was exceptionally constrained to the sn1 degradation. The other parameters were found to have the same behavior of the parameters discussed for the other PC molecules tested.

Degradation graphs and summary - After performing the analysis of the NR data for all the partially deuterated PC molecules synthesised, a normalised degradation graph can be calculated, as shown in figure 4.18. The normalisation between all the PC molecules was carried out using the amount of PLA1-1 injected into the NR cell. It can be noticed that the lipid 16:0 | 18:2 is degraded much more compared to the other lipids tested, whereas initial speed of the reaction, between 0 and 0.2 hours, is comparable within the unsaturated series tested (except for the 16:0 | 18:1 PC which was found to be slower). All the other lipids, after the normalisation, are shifted to 1, where if the amount of protein would have been as the amount injected for the 16:0 | 20:4 PC (taken into account for the normalisation of all the other kinetics profiles), their degradation would have been null. The large difference towards the end of the hydrolysis reaction, is probably due to the amount of initial protein injected. The higher the protein amount, the higher the degradation, correlated to a decrease on the

formation of the micellar layer. This layer probably plays a crucial role by leading to a non availability of the lipid membrane surface for the degradation to take place. In fact, the layer is not present for high speed reactions. In the case of the 16:0 | 20:4 PC and 16:0 | 18:3 PC, the amount of protein injected was lower with respect to the amount injected for the 16:0 | 18:2 PC. This led to the formation of the micellar layer in those samples (not shown in this section), and the reaction slowed down. The amount of protein does not change in any case the initial speed (after the normalisation), that can instead be changed by the initial coverage of the lipid membrane, that in our case was found to be similar for those 3 lipids. Also, as mentioned earlier, the lipid 14:0 | 14:0 PC was tested with NR, but no kinetics could be measured since, even injecting a very low amount of protein, the membrane degraded much faster than NR can record, leading to data corresponding to a removal of lipids from the surface already during the first measurement after the injection of the PLA1-1.

4.1.2 Natural lipids

In order to obtain kinetics with more biologically relevant lipid membranes, natural lipids extracted and purified from *Pichia pastoris*, were utilised. The structure of the membranes constituted by these mixtures, has been discussed in Chapter 3. The mixtures dPC and hPChPS (80/20 w/w), were utilised to study the degradation mediated by PLA1-1. After the deposition that was carried out with the vesicle fusion method and the characterisation in 3 or 4 contrasts, an amount of 7 μg and 0.3 μg of PLA1-1 was used for dPC and hPChPS respectively. These values were taken arbitrarily, since for those mixtures no ellipsometry analysis were performed. A lower amount of enzyme was injected since it is known that PLA2 phospholipases have a faster kinetics in the presence of charge in the lipid membrane [264]. The recorded kinetics data and the results from the analysis are displayed in figure 4.19. The panel A in the figure shows the reflectivity profiles, where the last two are offset for clarity. Panel B shows the SLD profiles calculated from the analysis, and no micellar layer was found in these kinetics, probably due to the reaction being too fast for the layer to form, as discussed above. The hydrolysis was found to be slower compared to the lipid 16:0 | 18:2 PC, probably due to the higher amount of 18 carbons in the acyl chains, as from the analysis discussed in Chapter 3. As it will shown in the next section, the high amount of 18 carbons acyl chains leads to an abundance of various lipid species such as 18:0 | 18:1 PC, 18:0 | 18:2 PC, 18:0 | 18:3 PC, 18:1 | 18:3 PC, etc. This higher number of unsaturated over the saturated lipids, leads to a fluid state membrane. In order, to analyse the data collected with the dPC, the sn2 degradation parameter was fixed to 1, since the discrimination between sn1 and sn2 is not possible without large errors in the parameters (same as discussed for h16:0 | h20:4 PC). The amount of lipid deposited onto the silicon support after 3h of incubation is almost 0, indicating a high reaction speed. This is probably the reason for the lack of the micellar layer. Additionally, as it will be discussed in the next section, saturated FFA can inhibit the hydrolysis reaction mediated by the PLA1-1 under examination. Since the dPC mixture contains mainly unsaturated PC molecules, saturated FFA are at very low concentration in the bulk solution, leading to a higher final degradation of the SLB. The flip-flop was also recorded, displaying a similar trend compared to the synthetic lipids. For the last point the error has been removed, since at the end of the kinetics the reflectivity data come from a bare substrate where all lipids have been removed and where the flip-flop parameter has no effect on the SLD profile. Also the area per lipid was found to have similar behavior.

So far, in this thesis, only zwitterionic lipid (PC) systems were utilised for the NR kinetics experiments. The charge, as well as other parameters of the lipid membranes are fundamental for the normal life of the cell. Consequently, kinetics with the PLA1-1 was carried out using the natural lipid mixture hPChPS, where the two mixtures PC and PS were mixed in the ratio 80/20 w/w. After the bilayer characterisation, an amount of 0.3 μg PLA1-1 was injected and the kinetics recorded with the same protocol used before. The sample was measured in H-Buffer, which sadly led to a low contrast between the lipid membrane and bulk solution. This problem especially affected the flip-flop parameter as well as the precise characterisation

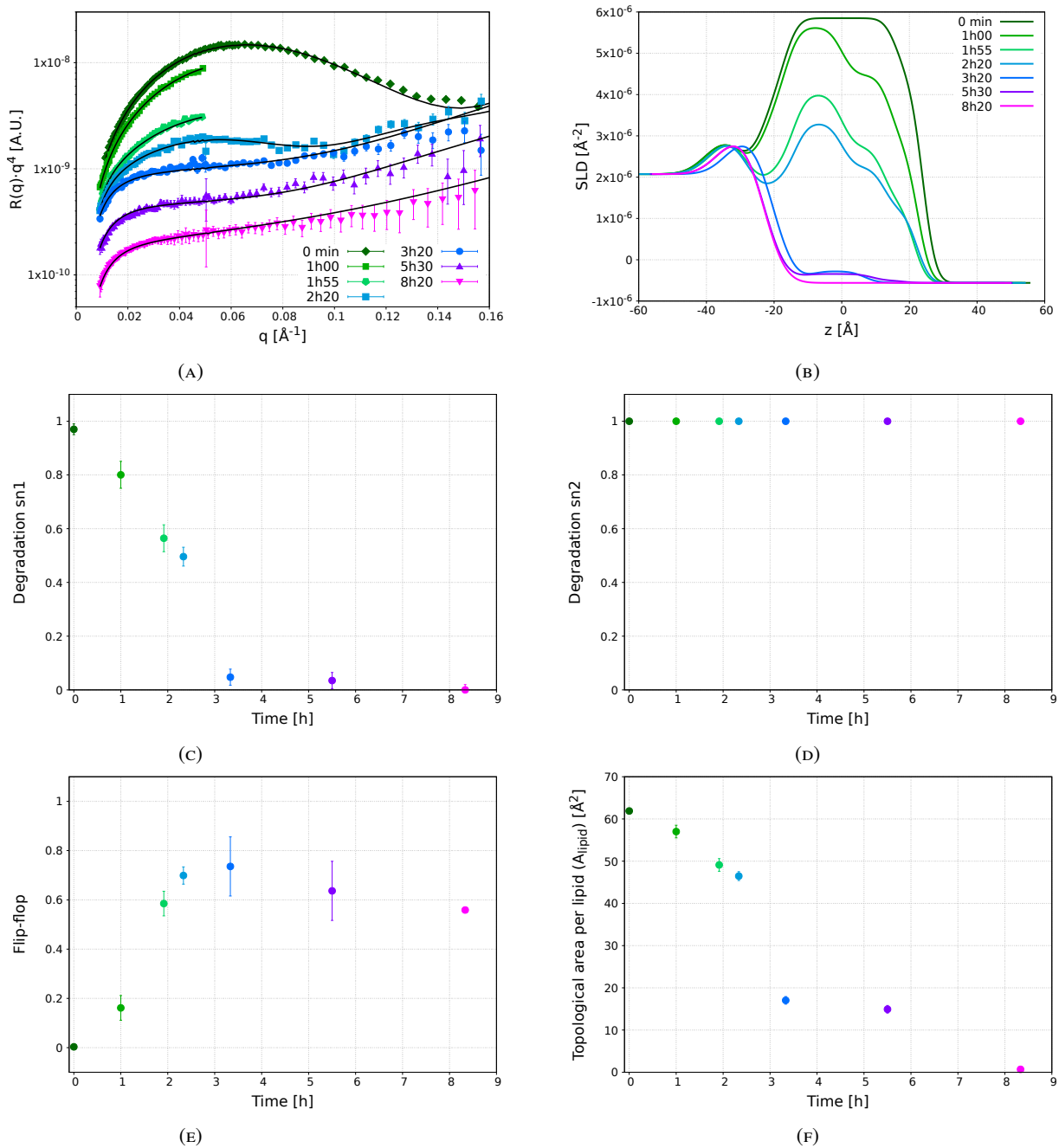


FIGURE 4.19: Graphs obtained from the analysis of the kinetics measurements performed on the dPC SLB. In panel (A) the NR data and the fitted curves, (B) the correlated SLD profiles, (C) the sn1 degradation, (D) the sn2 degradation, (E) the flip-flop profile and finally in panel (F) the topological area per lipid profile. Data collected at 5h30 and 8h20 in (A) are offset for clarity.

of the area per lipid during the kinetics. Consequently, the sn2 degradation and the flip-flop were fixed to 1, in order to determine the remaining parameters with reasonable uncertainty. But in any case, a degradation profile was obtained, as displayed in figure 4.21.

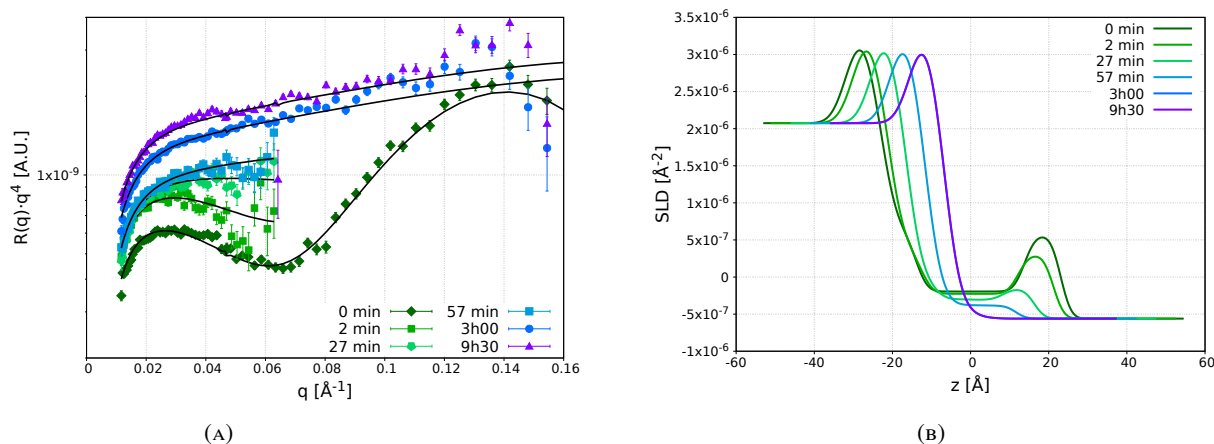


FIGURE 4.20: Graphs obtained from the analysis of the kinetics measurements performed on the hPChPS SLB in H-buffer. In panel (A) the NR data and the fitted curves, (B) the correlated SLD profiles.

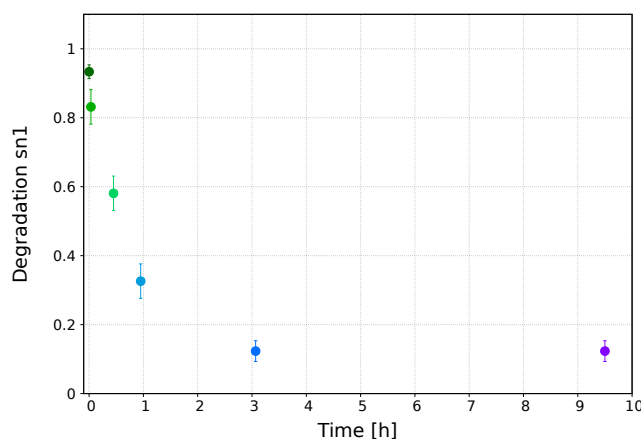


FIGURE 4.21: sn1 degradation obtained from the analysis of the kinetics measurements performed on the hPChPS SLB in H-buffer.

Also in this case the micellar layer was not detected, as it can be seen in figure 4.20. It is clear that the speed of degradation is faster compared to the dPC hydrolysis, even though a very low amount of protein was injected ($7 \mu\text{g}$ for the dPC and $0.3 \mu\text{g}$ for the hPChPS). The difference in the amount of protein was high enough to avoid the formation of the micellar layer, allowing then to compare the two datasets without the added complication of this additional layer. Additionally, lab experiments using bulk vesicles and TLC (data not displayed), showed a similar preference of the PLA1-1 *versus* hydrogenous and deuterated substrates, but more experiments need to be performed in order to obtain a more precise view into this argument. In summary, this experiment proves that the charge on the membrane increases the hydrolysis rate of the PLA1-1.

4.1.3 Appearance of a Bragg peak

During the last NR experiments of the thesis, smaller silicon crystals were used ($5 \times 5 \text{ cm}^2$), since the instrument was already calibrated for sample cells accommodating this size sample at that time. For this experiment, some of the previous experiments were repeated. During the measurements of these lipids, the protocol as well as the amount of PLA1-1 injected were maintained from the previous experiments on the same sample. After a certain amount of degradation, an initial small Bragg peak started appearing in all the lipids in different cells tested, increasing its intensity upon hydrolysis. Figure 4.22 shows the measurement of a washed cell, where the reflectivity profile is comparable with an empty silicon surface, with the addition of a strong Bragg peak in the profile. The peak is also visible in the H-Buffer

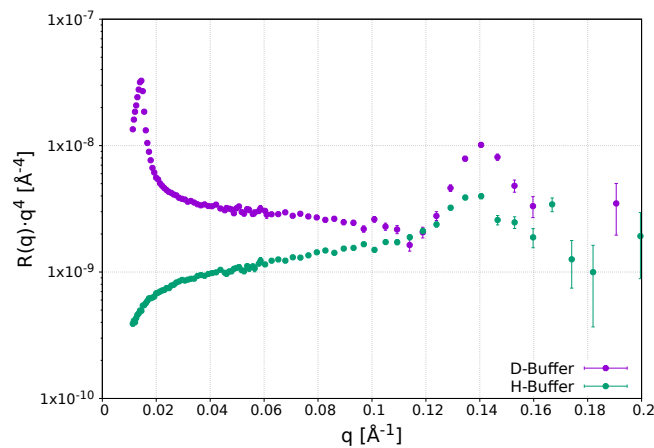


FIGURE 4.22: Bragg peak of a dataset after the wash

contrast, and it was analysed using a series of stacked layers, where one layer is characterised by a thickness of 15 \AA , an SLD of $-0.2 \cdot 10^{-6}$ with a fraction of water ϕ_{solv} of 0.9. The distance between layers was found to be 28 \AA . The intensity of the peaks suggests a number of stacked layers ≈ 7 . Along with the strong Bragg peak, a small angle signal was found from

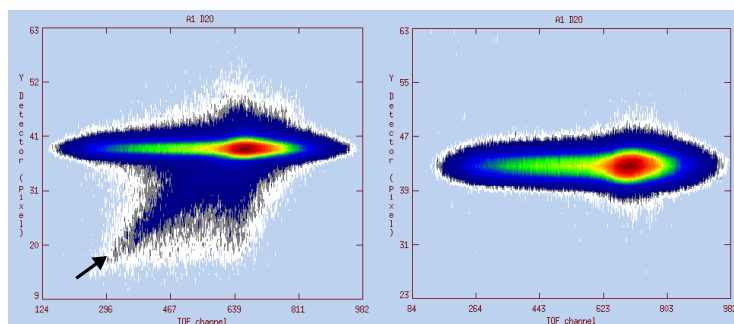


FIGURE 4.23: Two-dimensional image NR from the detector, where in y-axis is represented the pixel position of the image in the detector, the x-axis represent the TOF channel (energy of the neutrons detected, from which the scattering vector q is calculated)

the two-dimensional image from the detector. An example is given in figure 4.23, where on the right a normal signal from an empty silicon, and on the left the signal from the sample

described above. The small angle signal is highlighted with the black arrow. Small angle signals are usually from large structures formed on the top of the silicon crystal, that in this case could be related to cubic phases of the lipid products from the hydrolysis reaction. But an open question correlated to the formation of this signal remains, since this behavior does not appear in any of the previous experiments.

In order to assess the structural characterisation of this deposition onto the lipid membrane, a diffraction experiment could be performed. The micellar layer explained and used for the analysis, is an assumption, since using NR only the information on the z-axis are available. The formation of a micellar layer is the most reasonable interpretation of the NR experiments results. But in this case, the experiments performed on smaller crystals lead to the formation a layer with an unknown structure on the top, which it can be resolved with other techniques such as the mentioned diffraction (work in progress).

4.1.4 Summary of the NR results

NR measurements were performed using SLB constituted by synthesised one-chain deuterated PC molecules, in order to obtain information on the structural changes and kinetics of the interactions between model membranes and the enzyme PLA1-1. Different species varying from one another in terms of their chain length and number of double bonds were utilised, to assess the specificity of the PLA1-1 interaction. The substrate preference is dependent on the ability of the PC molecules to efflux from the membrane, since shorter chain length and higher number of double bonds in the acyl chain lead to higher degradation. The unsaturated series utilised starting from 16:0 | 18:2 PC, have similar initial degradation, but after a certain level of the SLB degradation, the different lipids starts to deviate between each other. In fact, the speed of the reaction can be determined from the first 1 or 2 hours of kinetics, since after that, for some lipids, the formation of a micellar layer on the lipid bilayer inhibits the hydrolysis reaction, leading to a plateau of the degradation curve. This layer was found to be formed when the reaction is 'slow enough', where this exact speed value was not precisely determined, because of the limited time of the NR experiments. This layer is created most probably by the deuterated acyl chains (palmitic acid) released from the lipid membrane during the course of the hydrolysis reaction. The micelles covered the surface of the SLB, decreasing the physical space for the attachment of the protein onto the membrane surface, thereby slowing down the reaction. Both the sn1 and sn2 positioned acyl chain degradation can be followed by NR, using partially deuterated PC molecules, since their SLD is very different. It was found that the acyl chain at the sn1 position was initially degraded (since the enzyme under examination is an A1 group phospholipase) followed by a degradation of the sn2 positional acyl chain (upon migration to the sn1 position), although at a lower rate compared to the sn1 acyl chain degradation. This result consequently proves that PLA1-1 harbors lyso PLA activity as well. Structural changes of the SLB were also recorded, in particular existence of a flip-flop mechanism of the phospholipids from one leaflet to the other. This parameter shows the membrane asymmetry, balancing the amount of degradation

between the two leaflets. The leaflet near to the silicon crystal, is not subjected directly to the hydrolysis from the protein, since the space between the support and the leaflet is not large enough to physically host the protein. In fact, it was found that, the degradation started first in the outer leaflet, and only later the degradation of the inner leaflet occurred. The defects formed on the membrane upon hydrolysis lead to a more fluid membrane, where the exchange of PC molecules from one leaflet to another one can occur more easily. The area per lipid also changed during the hydrolysis, since one of the two acyl chains was removed, leading to a different volume of the lyso and consequently a different structure of the molecule. The flip-flop parameter was found to decrease over time. Charged SLBs appear to have a faster kinetics, since the degradation of hPChPS sample happens at a higher speed compared to the dPC bilayer.

4.2 MS analysis

In this section, the kinetics results recorded through employing a mass spectrometer (MS) technique are shown and discussed. MS analysis was performed on bulk vesicle solutions, in order to assess the preferential interaction of PLA1-1 with the various phospholipid species present in the same vesicle sample. During the NR experiments, only mono-species SLBs were utilised to record the kinetics. Nevertheless, the cell membrane is composed by several phospholipid molecular species (and other compounds), that give specific physical and chemical properties to the plasma membrane itself. The MS technique allows for the discrimination between the different molecular species within a sample, consequently, the tracking of the kinetics using more biologically relevant lipid membranes can be performed, thus helping assessing the substrate preference of the enzyme under examination.

Lipid vesicles (LUVs) were formed by hydrating in PLA-Buffer the lipid film composed of a mixture of phospholipids molecules (synthetic or natural extracts). Next, the PLA1-1 was incubated with the vesicle solution at 37 °C, and samples were taken from this reaction mixture at different time points, and directly added into a solution of ice MeOH + 0.5% HCl, in order to stop the reaction. Next, lipid extractions were carried out for each sample, and after evaporation and reconstitution of the resulted films, the samples were injected into the QQQ-MS for the analysis. The kinetics plots of the hydrolysis reactions were obtained upon integrating the peaks of the normalised spectra. The normalisation was carried out by utilising the signal of the non-degradable sphingomyelin (SM, specifically 24:0 SM) (added to the lipid mixture).

4.2.1 Kinetics assays - synthetic PC molecule mixtures

Synthetic PC molecules were utilised to investigate the factors determining the activity of PLA1-1 towards LUV bilayer substrates composed of a multitude of GPL species. Lipids employed were combined in equal amounts (2 nmol/lipid) in order to make mixtures that were thereafter utilised to form lipid films. Following sample measurements by MS, the kinetics plots of the hydrolysis reactions were obtained upon spectra normalisation. An example of two normalised spectra (0 min and 75 min) obtained from the MS measurements, is displayed in figure 4.24. From this plot it can be noticed that some of the PC molecules in this mixture were hydrolysed at a faster rate than the others, allowing us to get an initial understanding of the substrate preference of PLA1-1. The m/z displayed in the figure corresponds to the mass window utilised during the MS analysis, which allowed us to measure also the lyso products within the hydrolysis reaction. While the signal of the PC molecules decreased upon hydrolysis, the signal from the lyso products started emerging between 400-600 m/z. Consequently, lysos emanating from each of the PC species used in the mixtures were also detected and tracked upon reaction. The FFAs were not scanned in these experiments, since a higher scan range could lead to a lower sensitivity of the instrument towards the intact phospholipid molecules. Next, peaks corresponding to each of the PC molecules under examination, were integrated, in order to obtain the degradation plots as shown in figure

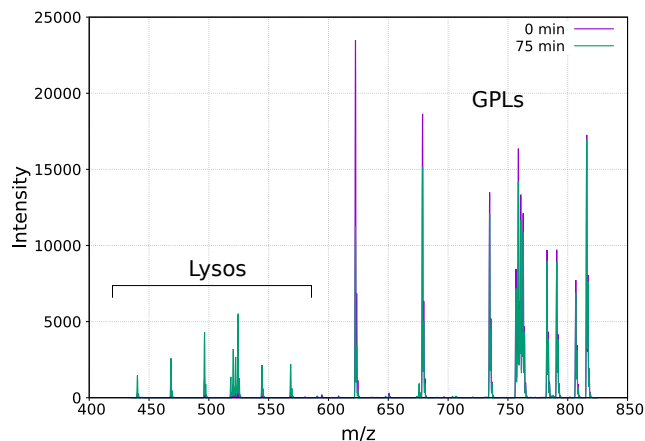


FIGURE 4.24: Example of normalized spectra, where the spectra of the time point "0" is superimposed to the time point "75"

4.25. Finally, such plots were analysed using a first exponential decay function (details in Chapter 7), from which the hydrolysis rates of each phospholipid species under examination were calculated. Two PC mixtures were utilised for this experiment, as shown in figure 4.25. Figure 4.25 panels (A) and (B) depict the degradation plots achieved from the spectra analysis of the mix A and B respectively. As mentioned in Chapter 2, the difference between

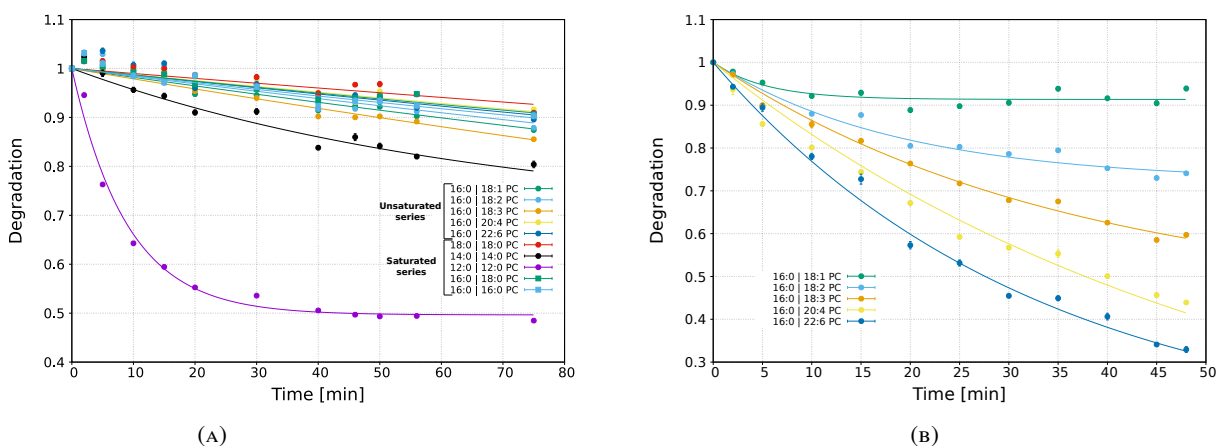


FIGURE 4.25: MS degradation graphs of the Mix A in panel (A) and Mix B in panel (B)

the two mixtures is based on the presence and absence of saturated phospholipid molecules (mix A and B respectively). The idea behind these two samples is to understand singularly the role of saturated phospholipids on the hydrolysis reaction mediated by PLA1-1. On the other hand, mix B, permits a better analysis of how lipids containing double bonds behave and play a role in the substrate preference of the enzyme under examination. The kinetics performed using mix A and displayed in figure 4.25 (A) show that when the purified PLA1-1 is incubated with the LUV solution composed of the saturated, unsaturated and polyunsaturated phospholipid molecules, the short-chained saturated series up to 14:0 | 14:0 PC (DMPC) are easily hydrolysed. Specifically 12:0 | 12:0 PC (DLPC), looked to be the best substrate for PLA1-1 in this mixture, followed by DMPC. DLPC was hydrolysed faster with respect to

the other PC molecules in this mixture, where around 50% of degradation at the end of the reaction appears, and at 40 min of reaction the profile reaches a plateau, after which no drop was observed. The hydrolyses of almost all the other PC molecules were observed to be around 10% after 75 minutes. DMPC was degraded faster than the other PC molecules, but with a similar trend. The reaction for those PC molecules, except for the DLPC, did not reach the plateau, but the time range used was enough to obtain information on the reaction speeds. The rates of the enzyme per PC molecule, displayed in table 4.2, can be achieved from the first exponential decay fit that was carried out on the degradation profiles. Specifically, from the fit, the ‘degradation units’ (D.U.) per minute are obtained, describing the amount of lipid degraded per minute. This value is then multiplied by the amount of lipid used for the sample (2 nmol), thus obtaining the degradation expressed in nmol/min. From these rates, the fold

Lipid name	Rate of reaction [nmol/min]
12:0 12:0 PC (DLPC)	0.110 ± 0.002
14:0 14:0 PC (DMPC)	0.010 ± 0.002
16:0 22:6 PC (PDPC)	≈ 0.002
16:0 20:4 PC (PAPC)	≈ 0.002
16:0 18:3 PC (PLnPC)	≈ 0.002
16:0 18:2 PC (PLyPC)	≈ 0.002
16:0 18:1 PC (POPC)	≈ 0.002
16:0 16:0 PC (DPPC)	≤ 0.001
16:0 18:0 PC (PSPC)	≤ 0.001
18:0 18:0 PC (DSPC)	≤ 0.001

TABLE 4.2: Table of the rates calculated from the Mix A experiment

difference between the hydrolysis rates of the DMPC and DLPC can be estimated, and it was found to be 0.09, where the speed of degradation of DMPC is 9% of the DLPC. All the other saturated PC molecules, were found to have a lower degradation rate, where it was difficult to obtain an accurate rate (that it was found to be $\approx 1\%$ compared to DLPC velocity).

Mix B, that excluded all the saturated species, resulted in a vesicle solution composed of only the unsaturated and polyunsaturated phospholipid molecules. In this case, as shown in figure 4.25 panel (B), the hydrolysis kinetics depicts a contrasting result, where the unsaturated series undergoing degradation were detected. The preferred substrates in this mixture appear to be those with a higher number of double bonds. The reaction rates per GPL molecule are listed in table 4.3 for this experiment. The 16:0 | 18:1 PC (POPC) kinetics reached a plateau at

Lipid name	Rate of the reaction [nmol/min]
16:0 22:6 PC (PDPC)	0.052 ± 0.002
16:0 20:4 PC (PAPC)	0.044 ± 0.002
16:0 18:3 PC (PLnPC)	0.032 ± 0.002
16:0 18:2 PC (PLyPC)	0.028 ± 0.002
16:0 18:1 PC (POPC)	0.026 ± 0.004

TABLE 4.3: Table of the rates calculated from the Mix B experiment

≈ 10 minutes with a total hydrolysis of $\approx 92\%$, whereas the other substrates did not reach the plateau in the time range employed in the experiment. In any case, also for this experiment, data were analysed with the first exponential decay function, resulting in values as shown in the table discussed. Figure 4.26 displays the plot of the velocity rates of the molecular species undergoing hydrolysis vs the number of double bonds. As discussed, an increase in rate of

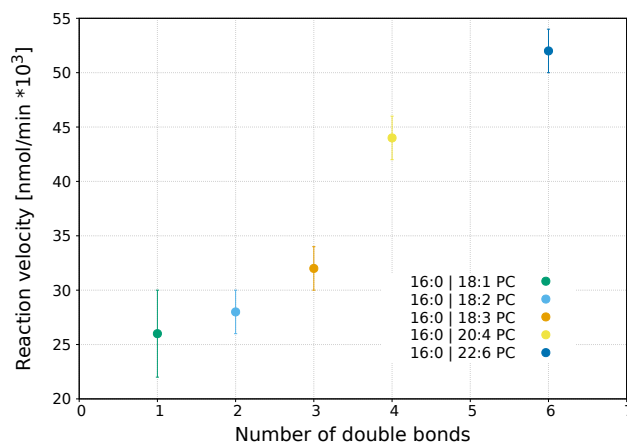


FIGURE 4.26: Plot of the velocity rates of the hydrolysis reaction vs number of double bonds

the reaction was noticed upon increase in the number of double bonds. The hydrolysis rates appear to follow a sigmoidal behavior, where the first 4 points follow an exponential profile, after which a plateau in the rates occurs.

It has been found that long acyl chain containing phospholipid molecules are subjected to a very low degradation, whereas the degradation for the other saturated phospholipids appears to be proportional to their acyl chain lengths. Unsaturated molecules appear to have a speed of reaction proportional to the number of double bonds harbored within them, where 16:0 | 22:6 PC seems to be the most preferred substrate when saturated phospholipid molecules were not included into the mixture. In fact, the presence of saturated molecules appears to cause a sort of inhibition on the hydrolysis reaction, since only DLPC and DMPC have a speed above $1 \text{ pg} \cdot \text{min}^{-1}$.

Lysos profiling - As mentioned earlier, the recorded MS m/z range was large enough to measure the lyso products upon GPL hydrolysis. Consequently, from the MS spectra, the lyso peaks were also integrated, in order to profile them during the reaction. Figure 4.27 displays the trend of the lyso products during the course of the reaction for the Mix A in panel (A) and Mix B in panel (B). It can be noticed that the trend of the lysos is different, contrasting our expectations, since the signal of the products did not increase during the whole course of the reaction. An analogous behavior was also recorded with neutron reflectivity as well as during the biochemical assays that were visualised by TLCs, that showed an increase in lyso production upon phospholipid degradation, up to a certain level, above which they remain constant or decrease over time. For the experiment with Mix A, taking into consideration the range between 0 to 20 min of the reaction, the highest lyso increase can be correlated to the

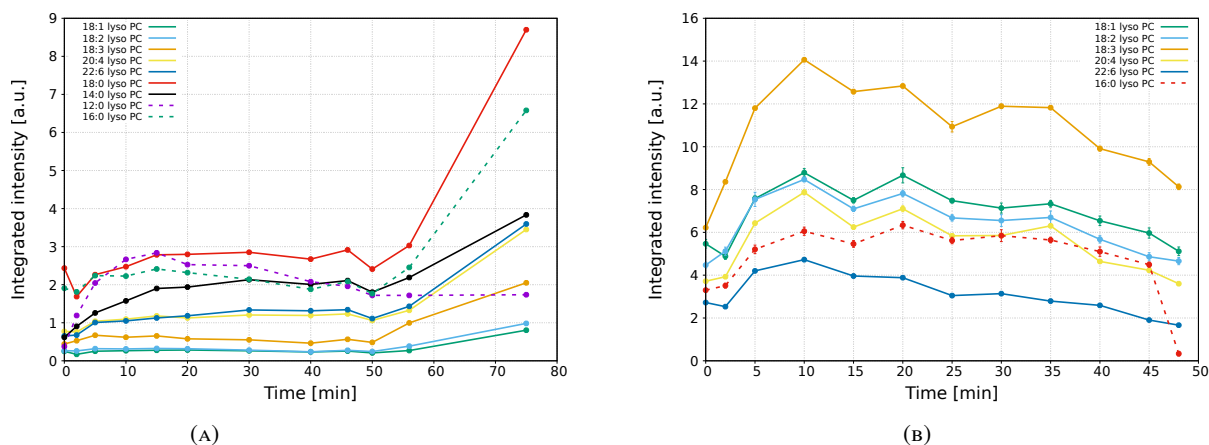


FIGURE 4.27: Lyso products profile over reaction time: Mix A in panel (A) and Mix B in panel (B)

phospholipids which have the highest hydrolysis rates (*i.e.* DLPC and DMPC), whereas the other lyso signals remain almost constant during this period of time. After the first 20 minutes of the reaction, the lysos signals remain stable except for the 12:0-lyso PC, that decreased over time. This is probably correlated with the plateauing of the degradation curve of the DLPC, as shown in the graph in figure 4.25 panel (A), since no more lysos were produced upon degradation of this lipid. After 50 minutes of the reaction, the amount of lysos increased, except for the 12:0-lyso, reaching a maximum at 75 min. A different scenario was recorded for Mix B, where all the lyso signals increased during the first 10 min of the reaction, followed by a gradual decrease. The maximum signal recorded for the lysos corresponded to 10 minutes, that is when the POPC degradation curve plateaued. The lyso 16:0 PC was also found and recorded, but theoretically, since 16:0 FA existed at the sn1 position in all the lipids used, and considering that the PLA under examination belongs to the A1 group, it should not appear as a product of the reaction. It is to be noted that, synthetic phospholipids (*Avanti*) have a certain amount of regioisomers, that could be $\approx 5\text{-}10\%$. Consequently, taking as an example the 16:0 | 18:1 PC species, it can be assumed that 5-10% of the molecules utilised were actually 18:1 | 16:0 PC. This can probably explain why the lyso 16:0 PC appears within the other lysos during the hydrolysis reaction using mix B. The difference between the starting point and the maximum signal reached for each lyso profile is different between all the lysos tracked. This lead to a different amount produced upon reaction, but it can be also caused by the different sensitivity of the MS detector within the lipids tested. In order to obtain the precise amount of lysos produced upon reaction, a standard curve needs to be performed, but it was not carried out in this thesis work. The lysos tracked, for the two experiments shown, did not start from a signal equaling 0, since some of those lysos were already present in the initial vesicle solution. This is probably due to the process used for the sample preparation, during which the ester bond can be ruptured, since no lysos were recorded running the stock mixture solutions in CHCl_3 .

PLA1-1, a lysophospholipase? - As mentioned earlier, the FFAs produced during the course of the reaction were not scanned for during the MS measurements (400-850 m/z), since higher scan ranges could lead to a drop in signal sensitivity of the other lipids. Since the FFAs were not taken into account during the measurements, a decrease of the TIC chromatogram intensities was observed, caused by the loss in material detected (less counts on the detector caused by less ions), that can be directly correlated to the FFAs released upon reaction. Specifically, when one PC molecule is hydrolysed, the initial ion is transformed into another, the LPC and also a FFA ion with the latter not being scanned. Consequently, the total ions during the measurements should be retained since ions are transformed upon hydrolysis, thus remaining in the same amount. As mentioned, our results showed that PLA1-1 has a lyso PLA activity as well, where the LPCs were, after a certain point, also hydrolysed. In this case, the total number of ions were no more retained, since the LPC ions were transformed into the FFA ions, that were not scanned during the kinetics measurements. Consequently, this variation of the FFA contents during the reaction can be determined by utilising the drop in signal of the TIC chromatograms. Accordingly, the profiling of the FFAs can be then determined by integrating the TIC chromatograms after their normalisation. The normalisation was carried out using the SM intensity from the spectra obtained integrating the related chromatograms. The normalisation value obtained (which is the same used for the spectra normalisation), was taken into account and used as a multiplication factor for each TIC chromatograms. Next, the integration was performed on those normalised chromatograms, and the data plotted as a function of time. Figure 4.28 shows the profile of the integrated chromatograms *versus* time

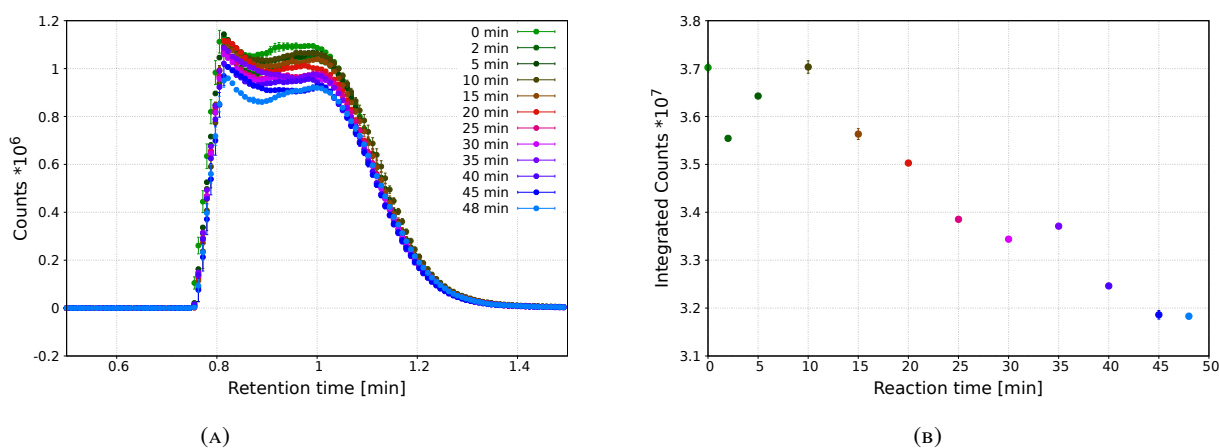


FIGURE 4.28: TIC chromatograms (panel (A)) and its integration plotted as function of time (panel (B)).

of the mix B experiment, and a decrease in the signal takes place upon hydrolysis is clearly observed. This signal corresponds to the sn2 FFA released, since the variation is correlated as mentioned to the lyso activity of the enzyme. In fact, as it can be noticed in figure 4.28, the signal at the beginning, although fluctuating, does not decrease as it decreases after 10 min. This result can be compared to the lyso graphs displayed in figure 4.27 panel B, where after 10 min, the degradation of the lysos started to be visible by the change of the lyso profiles. The reaction was found to be not plateauing, in fact the measurements done were not long

enough to cover the entire kinetics. This result confirms the lyso activity of the PLA1-1 under examination, as previously found through lyso integration as well as from the use of other techniques.

Does vesicle size influence substrate specificity or the rate of degradation? - Within the preliminary experiments performed, during the optimisation of the protocols, different extrusion membranes were utilised in order to obtain vesicles with uniform distribution. The extrusion was performed at the beginning (prior PLA1-1 injection), in order to try to avoid the fluctuations of the signal between samples. The fluctuation problem was then solved by heating up and vortexing the samples before placing them into the injection module of the MS instrument. Consequently, measurements with different sized vesicles were carried out. It was noted already, through the assays TLC and other lab experiments, that the vesicle size was critical for the rate of the hydrolysis reaction. This is probably due to the different superficial membrane frustration, that is different within different sized vesicles. A second effect, could be correlated to the maximum curvature that the enzyme under examination can tolerate for its attachment and reaction. Figure 4.29 shows the degradation plots of the

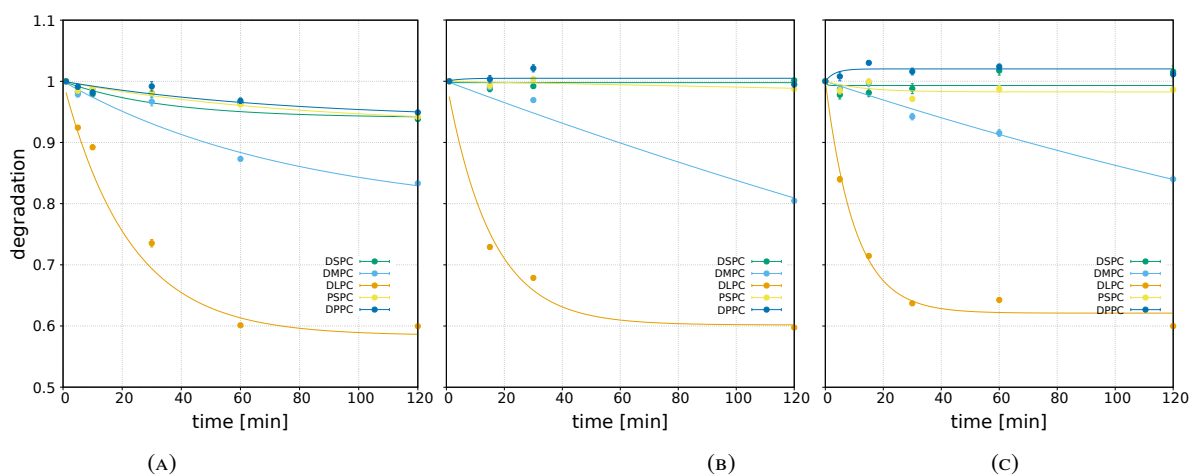


FIGURE 4.29: Degradation plots using different sized vesicles, where panel (A) displays the degradation graph for the non-extruded vesicles, panel (B) vesicles extruded at 1000 nm and finally panel (C) vesicles extruded at 400 nm

non-extruded, extruded 1000 nm and extruded 400 nm vesicles, respectively. It can be noticed that the degradation profile differs upon vesicle extrusion. With non-extruded vesicles (panel A), the high chain length saturated PC molecules were degraded, while surprisingly, with extruded vesicles (panel B and C), the same PC molecules underwent a very low rate of degradation over time. The low degradation of the long chained saturated PC molecules, is accompanied by a higher degradation of the 12:0 | 12:0 PC (DLPC), which remains in any case the best substrate. In fact, for both the extruded vesicles, at 20 min, the DLPC was found to be degraded by 30%, whereas for the non-extruded the value was 20%. The unsaturated PC molecules were not plotted for more clarity of the plots, and no much changes occurred in those lipids in any case. Table 4.4, shows how the hydrolysis speeds change upon vesicle

PC molecule	Non-extruded	1000 nm extruded	400 nm extruded
Long chained saturated	≈ 0.001	≈ 0	≈ 0
14:0 14:0 PC	0.003 ± 0.001	0.002 ± 0.001	0.002 ± 0.001
12:0 12:0 PC	0.018 ± 0.001	0.024 ± 0.001	0.034 ± 0.001

TABLE 4.4: Rates of the analysed lipids at different vesicle sizes.

extrusion. It is clear that the reaction of saturated phospholipid molecules was slowed down except for the 12:0 | 12:0 PC (DLPC) which speed increases upon vesicle extrusion.

Summary of the MS results with the use of synthetic PC molecules The kinetics of interaction of PLA1-A1 with two different lipid mixtures, named mix A and mix B, composed by synthesised lipids were analysed by MS. The hydrolysis reaction recorded using mix A, showed a different profile compared to the mix B. Efflux propensity seems to play a key role in the selection of the phospholipid molecule to be cleaved. Additionally, it seems that the saturated FFA released upon cleavage had some sort of inhibitory effect on the reaction mediated by PLA1-1. The degradation plots shown, never reached 100% of degradation, that is probably correlated to the amount of saturated FFA released, since even in the mix B, 16:0 PC is in any case released although in a slightly lower quantity with respect to the mix A. The result on the kinetics recorded with different vesicle sizes seems in a way correlated with the previous finding, where the slowing down of the hydrolysis of the long saturated acyl chains contained into the PC molecules used, increases the speed of the reaction for the DLPC. Additional experiments need to be carried out in order to confirm this hypothesis. The decrease of the TIC chromatogram intensities confirms the lyso activity of the PLA1-1, since also the second acyl chain is degraded after a certain point in time.

4.2.2 Kinetics assays - natural mixtures

Experiments investigating the factors regulating the activity of the enzyme in the presence of a substrate composed of natural lipid mixtures (extracted from *Pichia pastoris*) were carried out as well. Similarly to the NR results, this allowed us to obtain information on the class preferences for the PLA1-1 and to use a more biologically relevant membrane system. The total lipid extract (TLE) utilised contained all the various classes of phospholipid molecules within the membranes of *Pichia pastoris*, *i.e.* PC, PS, PG, PE, PI and PA. An internal standard, SM 24:0 was added to the TLE enabling us to normalise the data during the analysis. The analysis of the PC class was carried out as mentioned earlier, through using the precursor ion scan 184 m/z, scanning from 400 to 850 m/z). Figure 4.30 shows the spectra of the identified peaks. It can be noticed that, there are still a few peaks that have not been identified yet. Further analysis has to be carried out in order to identify the molecular species contained in such natural mixtures. The highest intensity peak at 787.8 and the peak 801.9 were not identified, since they do not correspond to any of the known PCs (as listed in Lipid Maps database). The lipids detected in the mixture were used to track the kinetics of the PLA1-1.

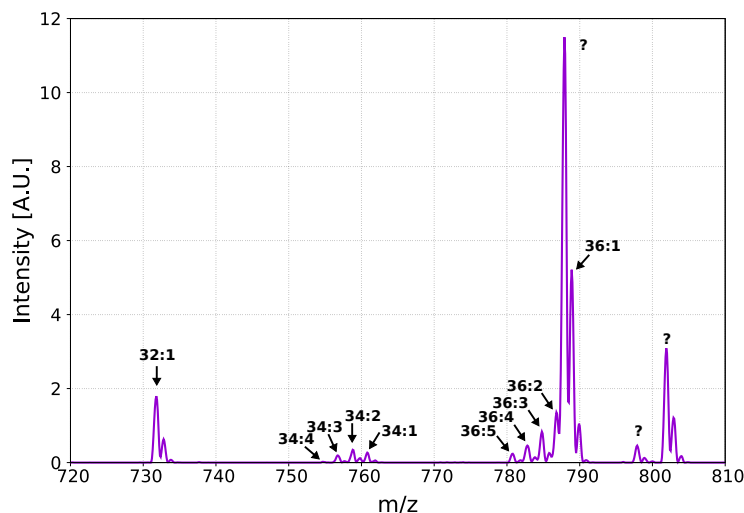


FIGURE 4.30: MS spectra of the parent 184 m/z to scan PC molecules from the TLE utilised. The question marks indicates unknown lipids found in the sample.

Figure 4.31 shows the degradation rates of the lipids identified. Two groups of degradation

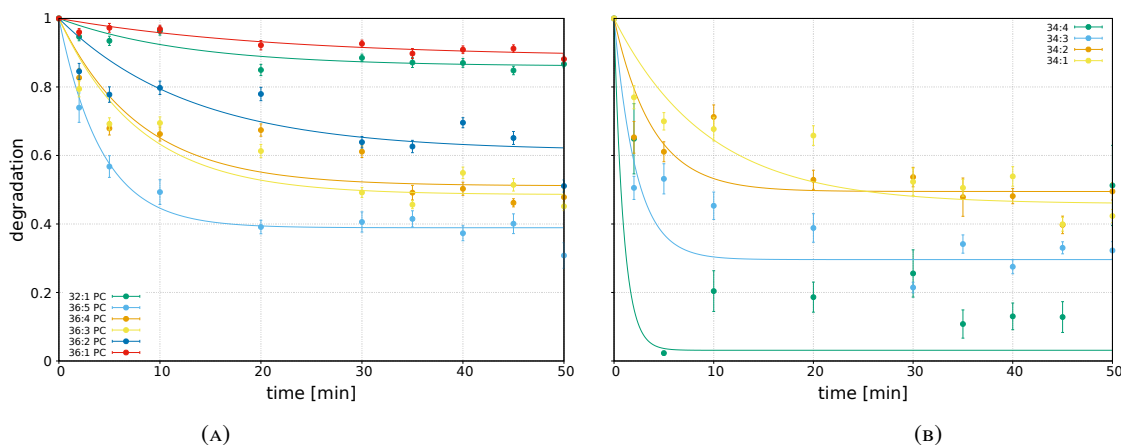


FIGURE 4.31: Degradation graphs achieved from the kinetics analysis of the TLE.

plots were produced for clarity. As can be noticed in figure 4.31, the higher the number of double bonds harbored in the acyl chain of a phospholipid, the higher its hydrolysis rate. For instance, within the 36C series, the hydrolysis of the phospholipid 36:5 PC is significantly higher compared to 36:4 PC, 36:3 PC, etc. Also for the 34C series, an analogous behavior was found, as could be noticed from figure 4.31 panel (B), where the phospholipid species with an increasing number of double bonds undergo to a faster degradation. Table 4.5 shows the relative hydrolysis rates of the PC molecules tracked for the kinetics described. The table displays the speed of the reaction in "degradation unit", that represent the total amount per lipid species, undergoing degradation over time (per minute). In this case, this unit was utilised since it was not possible to precisely determine the absolute amount of the lipid species present in the mixture utilised. For the experiments, where synthetic PC molecules were employed, the degradation unit was multiplied by the absolute amount of lipid species

Phospholipid	Possible lipids	Speed of the reaction (D.U./min)
32:1 PC	16:0 16:1 PC	0.0109 ± 0.0003
34:1 PC	16:0 18:1 PC	0.058 ± 0.005
34:2 PC	16:0 18:2 PC	0.130 ± 0.005
34:3 PC	16:0 18:3 PC	0.31 ± 0.01
34:4 PC	16:0 18:4 PC	0.98 ± 0.02
36:1 PC	18:0 18:1 PC	0.0052 ± 0.0002
36:2 PC	18:0 18:2 / 18:1 18:1 PC	0.0293 ± 0.0007
36:3 PC	18:0 18:3 / 18:1 18:2 PC	0.0641 ± 0.0008
36:4 PC	18:1 18:3 / 18:2 18:2 PC	0.0609 ± 0.0006
36:5 PC	18:2 18:3 PC	0.1438 ± 0.0005

TABLE 4.5: Table representing all the lipids tracked during the kinetics with the TLE of *Pichia pastoris*. "D.U." is the "degradation unit", since for this experiment was not possible to obtain the precise amount for each lipid specie present into the mix utilised. The sn1 and sn2 position acyl chain displayed in the column 'Possible lipids', can be assumed to be also specular.

used for the vesicle formation, obtaining the unit "nmol/min". As noticed, the general amount of degradation is higher with respect to the synthetic mixtures utilised previously, probably due to the higher averaged amount of double bonds.

Next, lipid classes degradation profiles were analysed using the DMRM method discussed in Chapter 2. In order to obtain the degradation graph displayed in figure 4.32, an ad-hoc

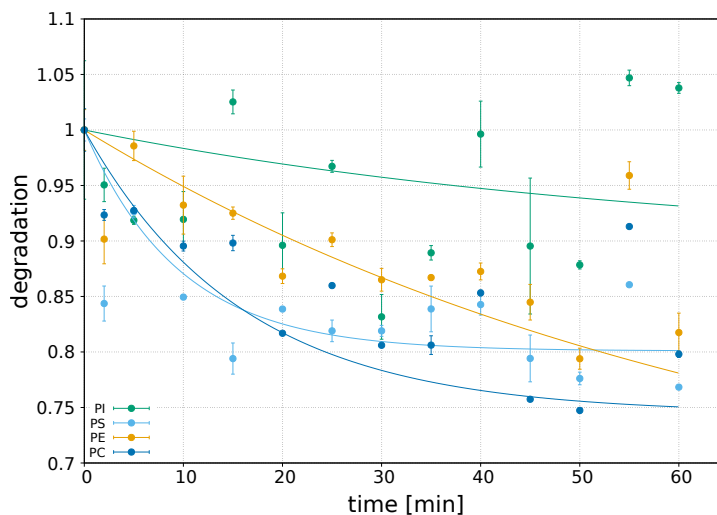


FIGURE 4.32: Analysis of the degradation of 36:1 species from various PL classes recorded through DMRM

python program was written for the treatment of the data. The degradation graphs were then analysed as shown before. The signal from the various lipid classes is conspicuously fluctuating, since the signal of the SM 24:0, used for the normalisation, came from different parameters compared to those used for the detection of the other classes (PS, PG, PI, PE and PA). Therefore, more experiments need to be performed with the right standards, in order to obtain more stable degradation profiles. Figure 4.32 shows the degradation profiles of

the molecular species with a variable head group (36:1). It can be noticed that a variable behavior within all the different classes of lipids monitored existed. Specifically, PC and PS had a similar preference by the PLA1-1, while PE was also degraded but at a lower rate, and finally PI was found to be the least preferred substrate for the enzyme. PA and PG were also tracked for in these experiments, but their signals were found to be conspicuously fluctuating, with large errors bars that led to the inability of calculating their rates. Accordingly, the data for these two lipid classes are not shown in plot in figure 4.32. Despite the fluctuations, the degradation profile of the PA class appeared to be below the PC and PS profile, suggesting the preference of this enzyme for the PA class. However, more experiments need to be performed to prove this finding with better signals. Due to the very large signal fluctuation of the PG

Lipid class	Reaction rate (D.U./min)
36:1-PI	0.0008 ± 0.0005
36:1-PS	0.021 ± 0.007
36:1-PE	0.005 ± 0.002
36:1-PC	0.016 ± 0.007
36:1-PA	PA > PC and PS
36:1-PG	N/D

TABLE 4.6: Reaction velocities vs. different lipid classes

class, the degradation plot could not be determined. Table 4.6 shows the degradation rates of the lipid classes taken into consideration. Unfortunately, because of the signal fluctuations of the lipids under examination, a good fit was not achieved, leading to higher errors for the calculated rates. Despite all these hurdles faced, a good estimation of the substrate preference could be obtained as has been discussed earlier.

Additional data obtained from the DMRM analysis - The advantages of using a column for the MS measurements consists in having a much reliable signal and in measuring physical/chemical properties. Lipids, as mentioned before, have different hydrophobicity, depending on the acyl chain length, number of double bonds, polar head, etc. Usefully, with this method, two different molecules characterised by the same m/z, can be separated and analysed separately. An example is given in figure 4.33, where the chromatograms are displayed for the lysos 16:0 and 18:0. It can be noticed that the profiles of these two lysos have a double peak, which lead to two different structured molecules characterised by the same mass, since the chromatogram displays only the molecules with a certain m/z. In the case shown in figure 4.33, probably the two peaks correspond to the two positional isomers of the lysos (sn1 and sn2). The first block of chromatograms displayed corresponds to the profile of the lyso 16:0, and the second to that of the lyso 18:0. It can be noticed that there exists a different behavior for the two isomers upon hydrolysis: the first peak of the two types of lysos increases while after 10 min time starts to decrease probably due to its degradation; moreover the peak on the right of each chromatogram starts to decrease immediately after the start of the reaction. A similar behavior was also recorded for some phospholipid molecules, as displayed in figure

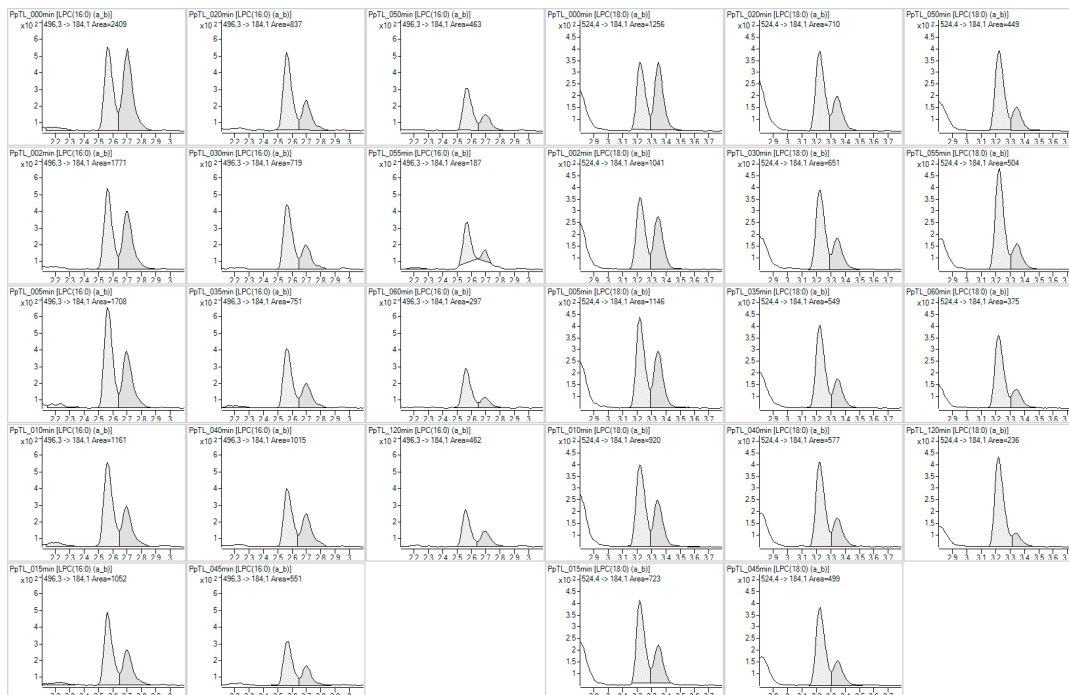


FIGURE 4.33: Lyso profiling MS intensity vs. retention time (RT)

4.34. It can be noticed as, also in this case, a different behavior along the reaction of the two peaks was found. Unfortunately, these double peaks are not yet identified, leading to difficulties in extrapolating conclusions out from those data. Nevertheless, the two positional isomers of these lysos and phospholipids have a different profile during the reaction. Also, all the other PC lysos show this kind of behavior, except for the 18:1, 18:2 and 18:3, where only a low and broad shoulder from the principal peak appears. A large amount of information can be still achieved from the MS analysis, and more experiments need to be performed in order to solve the mystery behind the reaction mediated by phospholipases using the systems described and discussed.

4.2.3 Summary of the MS results

Mass spectrometry analysis given a good view of the system that until now was analysed using biophysical techniques through tracking only one lipid at the time. The large advantage of such MS experiments is based on the fact that a multitude of lipids species can be simultaneously studied at the same time, also creating a more natural membrane composition. The data obtained from this technique matches the data already obtained from other experiments, where the efflux propensity of the phospholipid is the most important selection factor for the PLA1-1 with the lipid mixtures employed. The lysos were also tracked upon the hydrolysis reaction, where at the beginning of the reaction their quantities increased, due to the degradation of the phospholipid molecules, but at a later stage of the reaction, the lyso products were degraded as well. This result proves the lysophospholipase activity of the PLA1-1 under examination. FFA release from the reaction can be also achieved, although they were not scanned during

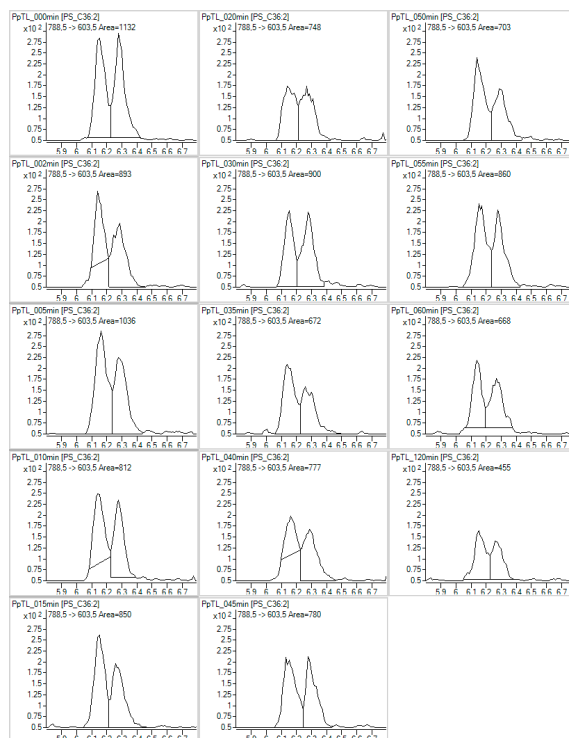


FIGURE 4.34: PS 36:2 profiling MS intensities vs. retention time (RT)

the MS measurements. The decrease of the intensity of the TIC chromatograms led to the loss of ion counts to the detector, giving a good estimation of the FFA released from the hydrolysis of the lysos. Experiments with differently sized vesicles were performed, where the PLA1-1 appears to be vesicle size-dependent. Small vesicles lead to low hydrolysis rates of the saturated lipids tested, except for its preferred substrate molecule (DLPC), whose hydrolysis rate was found to be higher. The lower amount of degradation of the saturated phospholipid molecules in this experiment, caused by the small vesicle size compared to the non-extruded vesicles, confirms that the saturated lysos or saturated FFA plays a key role in the hydrolysis reaction mediated by the PLA1-1. This point was also confirmed by employing natural lipid extracts, where the higher number of unsaturations leads to an increase in the final amount of degradation. Using the DMRM method, additional data were collected, where, for instance, we could show that two positional isomers for the lysos exist as well as also for some other phospholipid molecules. There is a difference on the kinetics between the two different isomers, and more experiments and measurements need to be performed in order to have an in-depth understanding about this complex system.

4.3 Additional biophysical characterisation studies

4.3.1 QCM-D

QCM-D measurements were also performed in order to obtain additional information on the system under examination. Complementary data to those from NR were obtained by

using this technique, which is sensitive to the mass of material deposited onto the crystal, as opposed to the monitoring via SLD determination of structural variations in the system. Additionally, further data can be obtained to better understand the micelle layer mechanism, that was characterised using NR. This technique, as explained in Chapter 2, is a mass sensitive technique, where the signal is directly dependent on the mass deposited onto the quartz-silicon crystal. After performing the deposition of the lipid bilayer onto the crystal, the protein was injected into the cell in order to start the kinetics. The concentration of the protein used was about the same amount as utilised for the NR measurements, since the ratio between the crystal surface and the cell volume (bulk solution) is comparable to the one of the NR cells used. For the measurements explained in this paragraph, the lipid used was the h16:0 | h18:1 PC (POPC). The protein was injected in 1 ml of volume, and the kinetics was recorded in two different ways: (a) after the injection, the flux was stopped and the measurement taken until ≈ 700 minutes; (b) after the injection, the outlet of the cell was connected to the inlet, and the flux was set to $0.1 \text{ ml}\cdot\text{min}^{-1}$ during the kinetics measurement. The idea behind

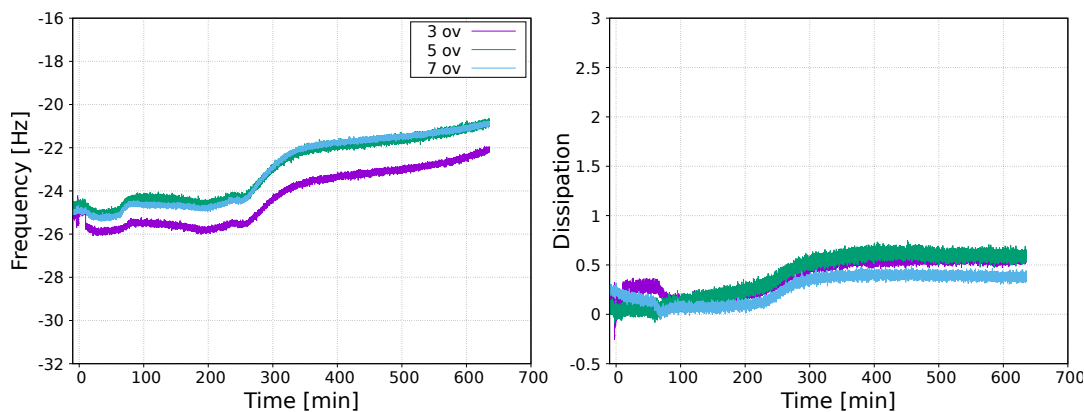


FIGURE 4.35: Cycled flow QCM-D kinetics measurement

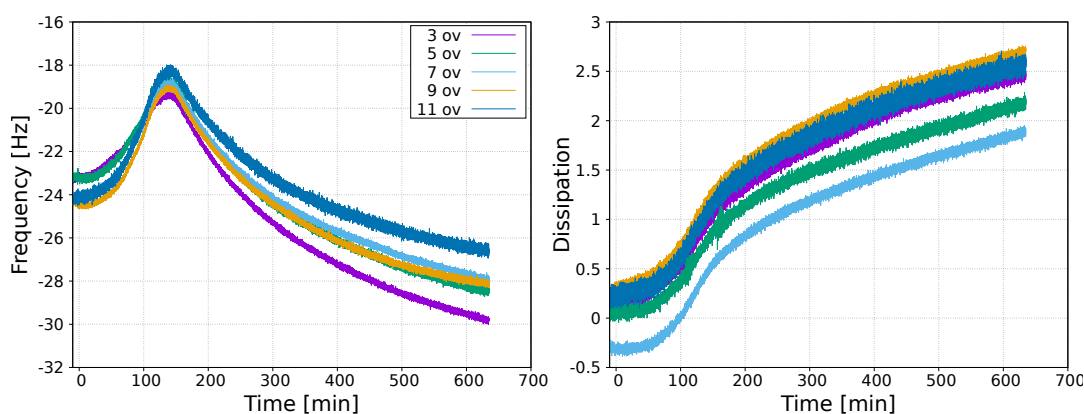


FIGURE 4.36: Normal QCM-D measurement

the experiment (b) consists in the analysis of the system, when a stress is applied on the surface of the SLB. The stress in this experiment is related to the flow passing on the top of the SLB, washing continuously the cell. Figure 4.35 shows the kinetics measurements of the experiment (a), where no flow is applied. The "0 min" is the time when the PLA1-1 was

injected into the cell after the successful deposition of the lipid bilayer. It can be noticed that the frequencies remained constant in the first period of the reaction, and after a certain point the frequencies increased, that led to the removal of material from the crystal. The dissipation profiles of the lipid bilayer slightly increased at the beginning, with higher increase in value when there was the change in frequency. Surprisingly, very different results were obtained with the experiment (b), where a constant flux was applied to the cell during the kinetics measurement. After the protein injection, the frequencies start to immediately increase, due to the removal of material. At a certain point during the reaction, the frequencies started to decrease again, as rapidly as the initial increase. While the described behavior of the frequencies occurred, the dissipation increased all the time until the end of the measurement. The change of the frequencies in the experiment (b), could be correlated with the formation of the micellar layer as described for the NR. In fact, considering -25 Hz the frequency shift of a POPC bilayer with 100% coverage, a value of -18 Hz corresponds to the POPC bilayer with a degradation of 22% (78% still deposited onto the lipid membrane). This value was also discussed when the NR data were described. At 22% of degradation, considering the same ratio of surface of the crystal and volume inside the cell as in the NR cell, one obtains the CMC of the palmitic acid, where the conditions for the micelle formation are satisfied. In fact, beyond the CMC value, the mass deposited onto the crystal starts to increase (decreasing of the frequencies recorded), supporting the possibility of a deposition of micelles onto the bilayer. The frequencies were found to decrease even lower than the starting point, that could be explained with the deposition of the protein, since an amount of 10 μg was injected into the cell (with a sensitivity of the QCM-D of ng of material). Probably this step is not visible with the QCM-D measurement on experiment (a), because the degradation, micellar deposition and protein attachment could occur at the same time, and this could mask the decrease of mass seen in the experiment (b). Probably also the orientation of the crystal plays a role, since in NR the silicon support is placed on the top of the PEEK cell, whereas in this case the crystal is at the bottom of the cell, where by gravity, particles can sediment. Consequently, the stress applied in the experiment (b) could help avoiding the deposition, simulating the NR cell experiment. Measurements with this technique allow us to understand better what has been hypothesised with NR experiments, where (1) the micellar layer formation occurs above the CMC of the FFAs released, and (2) removal of material occurs during the kinetics. It is still not clear how the signal behaves differently after the CMC, since in experiment (a) it is increasing over time whereas in (b) it is decreasing. Therefore, more analysis has to be performed, in order to fully understand the system under examination. The experiments were performed twice, in order to check the consistency of results.

4.3.2 Ellipsometry

Ellipsometry measurements were performed before carrying out NR experiments in order to obtain the right amount of protein to be injected in the cell with different PC molecules composed SLBs. The amount of protein to be injected is a fundamental parameter, since the

speed of the reaction, as mentioned before, needs to be tuned in order to measure it by NR. Due to the low flux of the neutron beam utilised, the exposition time needs to be at least 5 minutes (only for the first angle), which lead to a time resolution of that time. Since the data collected using only the first angle, contains less structural information compared to the full q-range profiles normally used, it is fundamental to slow down the reaction in order to be able to perform measurements in the full q-range. Figure A.6 in Appendix A.4.3 shows the picture of the cell employed for this experiment. The silicon crystal used is the one employed for NR experiments. The SLBs were formed using vesicle fusion technique, employing PC molecules with transition temperatures below room temperature. The laser beam angle was set to 68° , near to the Brewster angle of the silicon in water (72°). In this configuration the laser passed through the first window, reflected from the silicon support through the second windows, going directly to the detector for the analysis. The measurement was performed at an interval of 5 seconds, and it was recorded continuously from the empty silicon to the end of the hydrolysis reaction. Figure 4.37 displays an example of the measurements performed

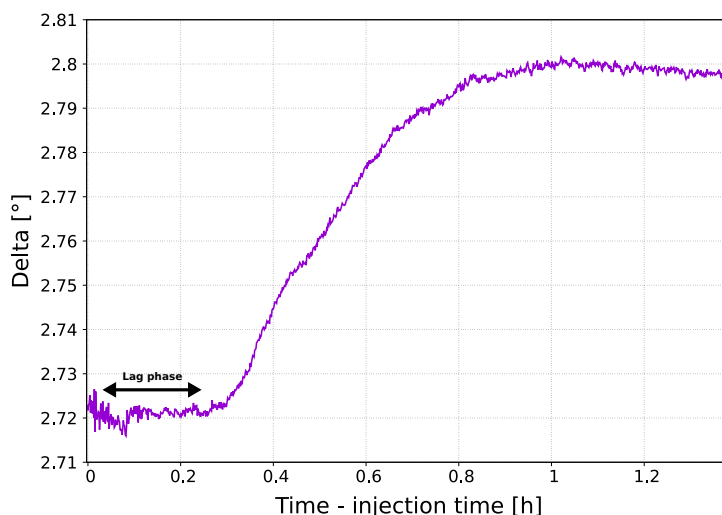


FIGURE 4.37: Ellipsometry measurements

using ellipsometry technique. As it can be noticed from the plot, an initial lag is present, similar to what was found using NR. This initial lag of the reaction is probably due to the diffusion in the bulk solution of the protein injected. In fact, this lag, taking into consideration the same lipid constituting SLB, is larger in ellipsometry measurements compared to the NR, since the bulk volume in the ellipsometry cell (≈ 5 ml) is bigger than the volume of the NR cell used (1 ml). The delta parameter, upon hydrolysis, increases, getting closer to the delta of the silicon support. It can be noticed as after 1 hour, that the kinetics have plateaued. The delta measured for the empty silicon crystal was $\approx 2.95^\circ$, whereas with the lipid bilayer deposited was $\approx 2.72^\circ$. The surface excess is proportional to the difference of refractive index between the bulk solution and the lipid bilayer. An increase of delta is correlated to a decrease of this difference, leading to a bilayer with more defects. Since only one angle was used for the measurements, the assessment of the thickness was not carried out, since higher resolution measurements are needed for that kind of an evaluation. Using the equation 4.1,

an idea about the degradation can be achieved.

$$Deg = \frac{\Delta Deg}{\Delta Delta} \cdot (Delta - Delta_{Bilayer}) \quad (4.1)$$

In equation 4.1 Deg represents the amount of degradation of the SLB; $Delta_{Bilayer}$ is the Delta of the lipid bilayer; ΔDeg is maximum and minimum amount of degradation (0 and 1) and $\Delta Delta$ is the difference between Delta measured on an empty and an occupied silicon support. It was found, taking into account the data displayed in figure 4.37, that the degradation was 35% for 16:0 | 18:2 PC. In summary, an amount of protein in the order of μg was found to be ideal to analyse the kinetics of the SLBs under analysis utilising NR technique. This amount of protein is a compromise between the micellar layer and the rapidity of the reaction, permitting the analysis of the kinetics without structural formation on the top of the reaction and at the same time perform measurements in two angles. It was also found using ellipsometry technique, after the plateauing of the reaction, a decrease of the Delta value, as the figure 4.38 displays. This behavior is probably due to the re-deposition of the

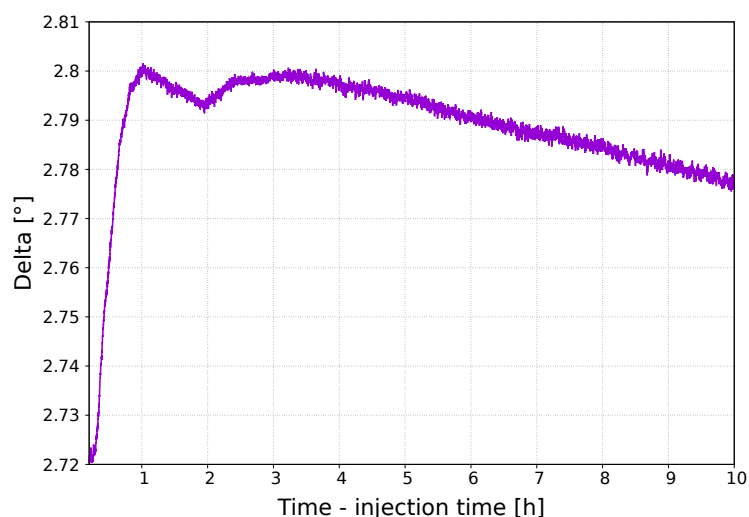


FIGURE 4.38: Ellipsometry measurement

material released from the SLB during its hydrolysis. In our experiments on the FIGARO reflectometer, NR cells were placed in the instrument 'upside down', where the silicon support is placed on the top of the PEEK cell, and the reflection is performed as 'reflection up'. In the case of the ellipsometry measurements, the PEEK cell was placed on the top of the silicon support, where the material released into the bulk solution, can be re-deposited due to the gravity.

4.3.3 SANS

During the kinetics assays performed right after the purification of the PLA1-1, multilamellar vesicles of 14:0 | 14:0 PC (DMPC) were utilised in order to assay the functionality of the enzyme. Figure 4.39 depicts a picture of the vials used to perform the kinetics assay. The enzyme fractions from the gel filtration step were aliquoted into each vial, in order to assess

the activity profile of each one of them. It can be noticed that, after 20 min of reaction, the fractions where the active protein is located became transparent, whereas the others remains opaque (due to the large size of the lipid vesicles). This led to a change in the structure of the vesicles, where the light is scattered differently. In fact, from DLS measurements (data not shown), there was a clear shift of the average dimension of the vesicles. Smaller structures appear upon reaction, probably due to the rearrangement of the vesicles into smaller ones, caused by an increase in the products of the reaction (such as LPC and FFA). Figure 4.40



FIGURE 4.39: Picture representing the kinetics using DMPC

shows the end point of the reaction, where on the left can be seen the reaction vial, and on the right the blank, that has no protein injected, used here as a visual control. It can be seen that, in the reaction vial, a precipitation occurs. It was found, in fact, that the solution becomes clear upon reaction as explained before, and after a certain level of degradation (≈ 1 hour), the solution recovers the initial opacity. By using a TLC, it was confirmed that this opacity is



FIGURE 4.40: Blank (right) and end reaction (left) of DMPC + PLA1-1

caused by FFAs aggregation. The precipitants have a bigger dimension and they can be seen by eye. Since structural changes were found to occur upon reaction of this system, SANS measurements were also performed, in order to analyse the kinetics in this system. In order

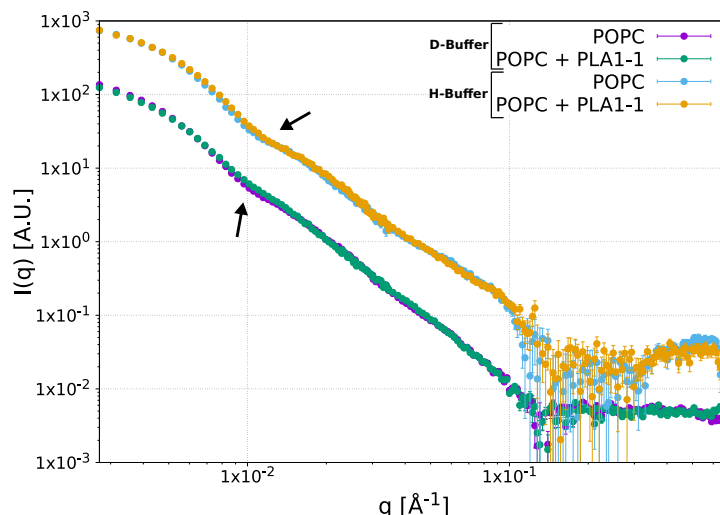


FIGURE 4.41: Kinetics SANS data, where the two black arrows indicate the differences between

to have an initial clear signal from the blank, the vesicle solution was extruded using a 100 nm membrane, leading to mono-dispersed vesicles (LUVs). The lipid used in this case was the synthesised d16:0 | h18:1 PC. From the SANS measurements, a different phenomenon was noticed. Figure 4.41 depicts the data collected in H and D-Buffer with the blank and the vesicles incubated with the PLA1-1 for 2 days. The shape of the SANS signal has not changed much compared to the blank, implying the absence of detectable structural changes in the vesicles. The only evident change that can be noticed in both H and D samples, is related to the low q (0.01 \AA^{-1}) indicated by the two black arrows, where there is a reduction of the small bump that is clearly present in the blank. This behavior could be related to the polydispersity or flexibility/fluidity of the vesicle or both factors together, where either polydispersity and flexibility/fluidity lead to the disappearance of this bump. A TLC was performed after the SANS experiment, in order to analyse the amount of degradation, and it was found to be only 40% (estimation carried out visually) even after 2 days of incubation. The increase of the polydispersity is correlated to the degradation carried out by the enzyme, where the LPC and FFA remains embedded within the lipid membrane (we could not record any deposition on the surface of the vesicles, since no major shifting of the bumps were recorded) or no evidence of them being released in solution, leading to a more disordered membrane. We suspect that the vesicle size has a direct influence on the activity of the enzyme, since experiments on this front have been carried out using MS technique (section 4.2) and other lab experiments through the use of TLCs. Probably, this could be explain the very low degradation after an incubation of 2 days. The above described are preliminary investigations, and further work needs to be carried out for a complete analysis including, for instance, experiments with bigger sized vesicles and different lipids such as d14:0 | h14:0 PC (as hydrogenous DMPC was used for the functional assays).

4.3.4 Summary of the additional biophysical characterisations

Other chemical/physical techniques were utilised in order to obtain complementary data of the systems under examination. Ellipsometry measurements were carried out in order to determine the right amount of protein to be used for NR measurements. These experiments were a fundamental step, since the speed of the reaction has to be tuned in order to perform NR kinetics measurements, due to the low neutron flux utilised. QCM-D measurements were also performed. Two different experiments were carried out, stopped and continuous flow, that led to two different behaviors of the system. Using the stopped flow, a lag in the reaction was found, whereas it was not found with the continuous flow. The lag is hardly explainable, since the information on the structure of the SLB is not seen by the instrument. The most probable hypothesis relies on a compensation between the material released and the attachment of the protein onto the SLB. In fact, the dissipation recorded slightly increased in that time range, leading to a less packed system. Measurements performed with the continuous flow, show an initial increase of the frequencies, leading to a loss of material from the crystal, and a subsequent drop in frequencies. The peak corresponds to a degradation of the SLB of 22%, a value leading to an amount of FFA in bulk solution above the CMC of the palmitic acid. This value was found also with NR measurements, where above that degradation (in some of the lipids tested), the micellar layer occurs. The change recorded for the frequencies with QCM-D leads to the same micellar layer, that occurs only if the surface of the SLB is flushed. The flushing probably helps the visualisation of this micellar layer, since the crystal, as also for the ellipsometry, is placed at the bottom of the cell, where due to gravity, the deposition of the material can occur. SANS measurements were also performed on a vesicle solution, in order to obtain information on structural changes of vesicles upon hydrolysis reaction. SANS profiles acquired were not very different, since the structure of the vesicles did not change upon hydrolysis (hydrolysis found to be around 40%), even after 2 days of incubation of the vesicles with the PLA1-1. Small vesicles were found to have a slow hydrolysis kinetics, and a higher structural stability. The presence of the LPC and FFA mostly within the lipid bilayer (since no extra-structures were found to exist in the bulk solution) caused only a higher polydispersity or a higher fluidity of the vesicles, clearly seen by SANS measurements.

Chapter 5

Discussion

The aim of this thesis work was to develop novel tools for investigating the underlying factors that regulate the activity of the PLA1-1. The developed tools involve NR and MS methods, synthesis of novel substrate molecules as well as sample preparations, and software to analyse the data collected from some of these experiments. All such approaches help in the study of enzymes, especially lipases and their interactions with membrane bilayers. Glycerophospholipids (also called phospholipids or GPLs) are amphiphilic molecules constituted by a polar head and hydrophobic chains (that can be discriminated as sn1 and sn2). Phospholipid molecules are involved in several pathways such as inflammation, signal transduction, etc. Their chemical-physical properties also allow them to rearrange themselves into complex structures when they are in an aqueous environment. The structure of these complexes is directly dependent on the physical properties of the lipid that forms them (cylindrical, conical shape, etc). One of the most important structure that phospholipid molecules assume is that of lipid bilayers which are involved in the formation of the cell membrane for instance, fundamental for the containment of the cell itself as well as of its organelles. The function of lipid bilayers does not stop in the physical containment of cells, but they mediate molecular exchanges, vesicles exchange, transduction of the signals and other very important functions. In order to maintain its functionality, the lipid membrane has to be constituted of other lipids also, such as neutral lipids (triglycerides, etc), glycolipids, sterols, as well as proteins, sugars and other minor compounds. All these compounds assure the functionality, structural resistance and help mediate the signaling exchanges as well as material exchange between the cytoplasm and the external environment or the cytoplasm and sub-cellular organelles. Another fundamental parameter of the lipid membrane is its fluidity, that has to be retained over time, in order for the lipid membrane to maintain its normal functionality. For instance, the membrane fluidity is a fundamental parameter for the vesicle/micelle fusion.

In order to conserve this fluidity, several pathways are actively engaged. These pathways can be divided into 3 different metabolic processes: (a) synthesis, (b) remodeling and (c) degradation. Synthesis is the process where phospholipid molecules are actively synthesised from their basic components. PA class is the precursor of all phospholipid molecules, in fact, an adequate PA amount in the cell is fundamental for the maintenance of a proper homeostasis of various phospholipid molecules [226]. The pool of PA is directly synthesised from G-3-P (glycerol 3-phosphate), where two acyl chains are then condensed to form the complete PA

phospholipid molecule. This precursor PA molecule then undertakes different pathways in order to condense a proper polar head chemical group to the PA allowing for the all the other classes of GPLs. When the phospholipid molecules are present in the right amount in the cell, and no more synthesis is needed for the normal functionality of the cell, many phospholipid species undergo to the process of acyl chain remodelling. This process involves mainly two different types of enzymes: (i) phospholipase As and (ii) acyl chain transferases or transacylases. The first group (i) mediates the removal of an acyl chain from the sn1 or sn2 position of a phospholipid molecule, dividing the group into PLA1 and PLA2, while the second group of enzymes (ii) mediates the reacylation of an acyl chain with a different one. These processes are fundamental for maintaining the GPL within the various compartments in a cell. Besides that, acyl chain remodelling is also required for other different processes such as (1) arachidonic acid release for signalling, (2) activation of enzymes the in mitochondrial inner membrane, (3) functional alveolar surfactant, (4) replacement of oxidised acyl chains [226]. The last bioprocess (c) concerns the degradation of phospholipid molecules, and this is considered to be a key process in maintaining lipid homeostasis. Degradation normally occurs in living cells, and the process can be tuned depending on the different stimuli given by the external environment. Phospholipases are the most important enzymes in this process, which can further be divided in three groups depending on the bond they cleave. PLAs, have the ability to cleave acyl chains from the glycerol moiety (sn1 and sn2, PLA1 and PLA2 respectively) through a hydrolysis reaction on the ester group; PLCs hydrolyse the bond between the phosphate and glycerol backbone to produce DAG (diacyl-glycerol); PLDs hydrolyse instead the bond between the phosphate group and the polar head chemical group, thus generating PA class; finally PLBs, phospholipases are enzymes that contain both PLA1 and PLA2 activities simultaneously. All these groups of phospholipases are thought to be involved in GPL homeostasis, although mainly members of PLA family are considered to be key players. PLAs have been found to form a large protein superfamily of 15 different groups, and it has been identified that 24 different genes encode for mammalian PLAs [265]. PLAs are found to be involved in a multitude of cellular phenomena, such as lipid metabolism [186, 266, 209, 84, 157, 267]. Besides, different studies have shown that the majority of the GPL turnover is mediated through PLAs [268, 269]. PLAs in these pathways need to be carefully regulated in their activity, in order to maintain the functionality of the cell membrane. Several studies have been proposed that membrane fluidity and elasticity play a role on the regulation of some enzymes. Membrane fluidity is a fundamental property of the cell membrane that needs to be conserved in order to maintain its normal functionality. It has been proved that the activity of the CT (enzyme directly involved in the PC synthesis), is regulated by membrane elasticity, as proved by Attard and colleagues [270]. However, no literature has been published describing the interaction between GPL homeostasis and membrane elasticity. A second model that has been developed for the PLAs regulation is the so-called "superlattice model". This model assumes that when the concentration of a phospholipid exceeds a critical value, membrane packing rafts appear on the lipid membrane itself, since the additional molecules cannot be adjusted in the existing super-lattice (where

lipids are theoretically evenly laterally distributed onto the membrane). Some phospholipases could be activated by these membrane packing defects [271, 272, 273] and once the lipid in excess is degraded, the packing defects disappears, resulting in the same initial membrane, thus decreasing the activity of the related phospholipases. These mechanisms described play a key role on the highly demanding tasking of lipid homeostasis, and are a fundamental point to be regulated. A malfunctioning in one of those pathways could lead to the dysfunction of the lipid membranes or signalling cascades, causing diseases or syndromes.

Phospholipases as mentioned, have a key role in membrane lipid homeostasis, a process where in a specific PLA is activated by one of the models mentioned earlier, in order to digest a certain pool of phospholipid molecules. The reaction mediated by the phospholipase enzymes is characterised by the following steps: (1) phospholipase - membrane association, (2) efflux of the GPL molecule, (3) active site accommodation of the molecule and finally (4) cleavage of the substrate. The selection of the proper substrate to be cleaved is mediated mainly by step (2) efflux and step (3) active site accommodation, that appears to be the two bottlenecks of the reaction. The efflux propensity of a phospholipid molecule is its ability to escape from within the lipid membrane where it lies. This property is directly correlated to the lateral interaction between different phospholipid molecules in the membrane. For instance, taking into consideration the same lipid class, longer acyl chained phospholipid molecules have a lower efflux propensity compared to a molecule with shorter acyl chains. Thus, hydrophobic interactions in this case play an important role, since longer carbon chains lead to a higher hydrophobic interaction, involving a higher energy required for the phospholipid to leave the membrane. In addition, double bonds in a GPL molecule play a fundamental role, since these chemical groups behave as kinks, causing disorder within the membrane, thus leading to a higher fluidity (decreasing the hydrophobic interactions, increasing the efflux propensity). Next, active site accommodation (2) describes how well a phospholipid molecule fits inside the active site pocket of the enzyme. The volume of the active site cavity could play a role in the selection of the phospholipid molecules to be cleaved in some phospholipases. All this proves that selection could be mediated by either the ability of the GPL molecules to efflux or the active site accommodation of the effluxed molecules, or both. Therefore, the substrate preference depends on the phospholipase under examination (for instance, lipid homeostasis, signalling cascades, etc). In fact, it is known that phospholipases in a venom, such as the one from bee, have a preference to degrade phospholipids that have a high rate of efflux propensity, specifically the unsaturated acyl chains containing phospholipids. In fact, the aim of these phospholipases is both the demolishing of the target tissue and at the same time to cause the release inflammation factors, such as arachidonic acid, that gives all the symptoms related to an inflammation of a tissue [234]. Accordingly, every phospholipase has a preferred set of phospholipid molecules, that are the target of the enzyme when it is expressed in a cell. Phospholipases A can be divided in two main groups, A1 and A2 as mentioned, depending on which of the two positional acyl chains the PLA preferentially cleaves. A1 group preferentially cleaves the first position acyl chain (sn1) whereas A2 the sn2 position. Over the past decade, a large amount of work has been carried out in order to

understand PLA2s, while a few studies have focused on characterising members of the PLA1 family, although they have not led to a detailed understanding of these enzymes specifically in terms of their regiospecificity, substrate preference, cellular localisation, and physiological functions. A recent study was carried out to understand the headgroup specificity of the *Aspergillus oryzae* isolated PLA1 isoforms (PLA1-1 and PLA1-2). Results emanating from that study show that PLA1-1 displayed a higher degree of affinity towards PC and PE while it also had the ability to hydrolyse other classes of GPLs and meanwhile no lipase activity was observed. On the other hand, PLA1-2 showed a tendency to degrade only, thus making it very different from PLA1-1. Taking it from there, we in this work, employed techniques including neutron reflectivity and mass spectrometry in order to investigate the key factors regulating the substrate specificity of PLA1 in lipid bilayers and in parallel obtain structural information on the membrane during the hydrolysis kinetics. Specifically, the aim was to investigate the factors that can have an effect on the regulation of the activity of the enzyme thus influencing the substrate specificity of the PLA in the presence of various macrosubstrates composed of a wide range of different molecular species within a specific GPL class. Such an approach lends deeper insights into the relationship directly between the action of a PLA1 and the fate of its potential substrate *i.e.*: a specific GPL molecule while it undertakes different bioprocessing pathways.

Structural and functional characterisations were performed in order to assess the identity of the enzyme upon expression and purification before carrying out NR and MS experiments. NR experiments were performed to analyse the substrate preference employing mono-species SLBs. From this technique information on the structure of the sample during the kinetics was obtained. NR helped in the understanding of the complexity of the system, although the lipid membranes used for the kinetics were far from a natural system, since a plasma membrane for instance, contains a multitude of phospholipids, other lipid molecules and fundamental compounds. In parallel, MS was utilised, in order to perform kinetics in bulk using vesicles constituted of a wide range of phospholipid molecules, thus leading to a more natural membrane in terms of its physical properties and allowing us to record the substrate preference as well. In addition, natural lipids were utilised for these experiments, to analyse how PLA1-1 behaves in the presence of a bilayer composed of such lipids.

NR pioneering experiments with one-chain deuterated and one-chain hydrogenous lipids were performed by Wacklin and coworkers [247] using PLA2 enzymes. NR experiments on porcine pancreatic PLA2 showed a long lag phase of several hours, after which the degradation started. The asymmetry in the lipid bilayer during the course of degradation appeared as well as the asymmetry in the distribution of the reaction products. Also a preference for POPC over DPPC was found, since POPC has a higher efflux propensity due to its higher fluidity.

Similarly, MS measurements were carried out in the past by Haimi, Batchu and colleagues [234, 233], that demonstrated the substrate specificity on PLA2s. Specifically, cPLA₂α and some secretory phospholipases of the group A were studied, to understand the factors determining their activity. cPLA₂α was studied in the presence of vesicles composed of different regioisomers of phospholipid molecules, where for instance the first position was

maintained constant and the second position was condensed with different acyl chain lengths, and specular isomers were also synthesised. It was found that chain lengths higher than 17 carbons lead to a drop in the degradation of such phospholipid molecules, leading to the assumption that the length of the active site cavity was equivalent to an acyl chain consisting of 17 carbons. In any case the preference of the protein for the arachidonic acid (20:4) contained in phospholipid molecules was observed for cPLA₂ α . In fact, it was found from other studies [274, 275] that arachidonic acid is the main precursor of prostaglandins and other eicosanoids, playing a fundamental role in signaling in mammals during inflammation. In fact, cPLA₂ α plays an important role in this regard [276, 277], since its preference for phospholipid molecules containing arachidonic acid.

In this regard, we have employed MS and NR techniques, in order to understand the importance for the PLA1-1 and factors such as active site accommodation and efflux propensity in regulating this enzyme and also to analyse the structural changes of the system upon hydrolysis. All the methods and protocols developed, can be employed to better understand the principles underlying the substrate specificity of other unknown phospholipases.

We have started assessing the substrate specificity and analysing the structural changes of the membrane during the PLA1-1 kinetics using NR technique. The strategy adopted for these experiments was initially through the use of partially deuterated phospholipid molecule (*i.e.* one deuterated chain and one hydrogenous), where mono-species SLBs were formed and used to analyse the PLA1-1 kinetics. Since neutrons are very sensitive to the deuteration level of the sample, this approach helped us to follow the PLA1-1 kinetics over time, tracking the SLD variation of the lipid bilayer and to assess the structure variation as well as the distribution of the products of the reaction upon hydrolysis.

Kinetics measurements on bilayers by NR - NR analysis on the various SLB systems prepared from partially deuterated GPL molecules showed that longer chained GPL molecules possess a lower rate of hydrolysis compared to shorter chained ones. In fact, GPL molecules containing shorter acyl chains were observed to be the most preferred ones, where practically no hydrolysis was observed with the long-chained ones. Taking into consideration the fully saturated series, the preference pattern of PLA1-1 was observed to be as such: 18:0 | 18:0 PC < 16:0 | 16:0 PC < 14:0 | 14:0 PC, thereby indicating that efflux propensity is a key determinant of PLA1-1-mediated GPL hydrolysis. These results were in good agreement with previous studies on both non-homeostatic secretory PLA2s [234] as well as the soluble iPLA2 β [233]. In those studies, a similar kind of preference for substrates within bilayers was observed and, based on such observations, it was concluded that hydrolysis rate specially those of saturated PC series decreased strongly and monotonously with increasing acyl chain lengths, due to the fact that longer acyl chain-length GPL molecules have stronger hydrophobic lateral interactions with adjacent GPL molecules. Previous studies, also collected data on the interactions of PLA2s with GPL micelles containing detergents, in order to reveal the effect of the differences in the packing order and intermolecular interactions in different macro-substrates, on the specificity of the enzymes under study. In micelles, PLA2-mediated

hydrolysis resulted in a contrasting specificity and faster kinetics, probably reflecting the importance of two major factors: (1) specific interactions of the substrate molecules with the substrate binding site on the enzyme and (2) the intermolecular packing, that is quite loose compared to bilayers as proved by NMR studies [278] and MD simulations [279]. Collectively, all these results indicate that for both PLA1 and PLA2-mediated hydrolysis of saturated GPL molecules embedded within bilayers, efflux is the rate-limiting step, since efflux propensity is largely determined by the acyl chain length.

Another important aspect to consider is the SLB phase behavior. Generally, at a given temperature, a lipid bilayer composed of certain GPL can exist in either a gel or a liquid phase. Almost all GPLs, undergo a transition phase from an ordered gel phase to a liquid phase. Within the gel phase, the hydrocarbon chains are fully extended while in the liquid phase they are randomly oriented and fluid. GPL molecules that we have employed as part of the saturated series in these experiments such as 18:0 | 18:0 PC and 16:0 | 16:0 PC occur in gel phase at 37 °C, while 14:0 | 14:0 PC exists in a fluid phase at that temperature. In this context, it is to be noted that a fluid phase allows for a higher membrane fluidity (less packed membrane) [280], thus causing a further increased propensity of short-chained GPL molecules to efflux from the bilayer. Finally, the efflux is then considered as the first "bottleneck" of the reaction mediated by PLAs, where GPL molecules with high efflux propensity passes to the second "bottleneck" of the reaction faster than the other GPLs. The second bottleneck that determines the regulation of a PLA has been speculated to be the active site accommodation of a GPL molecule within the catalytic active site. Past interaction studies on cobra PLA2 and GPL substrate molecules with a bulky acyl chain demonstrated the importance of accommodation of GPL acyl chains. In fact, adding a detergent onto the lipid mixture, in order to obtain micelles, all the lipids have theoretically a similar efflux propensity [234, 233], allowing the analysis of the active site accommodation. Next, it was noticed that in vesicle bilayers, an increasing unsaturation leads to an increase in the rate of degradation, again reflecting the fact that ability of the GPL molecule determines the substrate specificity of the enzyme. Double bonds contained in acyl chains of GPL in a lipid membrane, behave as kinks, leading to a more fluid and consequently more disordered membrane. In this system the hydrophobic interactions between acyl chains are comparatively loose, thus requiring a lesser amount of energy to pull a phospholipid molecule out from the membrane (in comparison to a membrane composed of saturated acyl chained GPLs). Accordingly, the efflux propensity of a GPL molecule depends on the fluidity of the membrane, and on the number of double bonds in its acyl chain region as well as its acyl chain length. Significantly, higher number of double bonds results in higher efflux propensity. Similarly, it was found during the characterisation of the natural lipid extracts, that higher number of double bonds are characterised by a lower retention time in the GC-FID measurements, leading to their lower hydrophobicity. Therefore, high number of double bonds lead to less lateral hydrophobic interactions, leading to a more easy efflux of those GPLs from the membrane. The results suggested that the PLA1-1 has the preference for phospholipid molecules with high efflux propensity, since within the saturated series, 14:0 | 14:0 PC was the preferred substrate, and between the unsaturated series 16:0 |

18:2 PC, 16:0 | 18:3 PC and 16:0 | 20:4 PC appear to have similar degradation profiles, taking into consideration the normalised degradation profiles within the first 1h of kinetics.

Lyso-phospholipase activity - Further, from our NR studies, we were able to extract the degradation profiles for both the sn1 and sn2 positioned acyl chains in the GPL molecule due to their difference in SLD. Interestingly, upon cleavage of the sn1 positioned acyl chain, a progressive release of the sn2 positioned chain was also noticed. Such marked changes in the SLD profiles of the SLB were possible to track by NR using the partially deuterated phospholipids synthesised. Since, PLA1-1 does not possess any PLA2 activity and based on earlier investigations on PLA2 isoforms, it is believed that post PLA activity, the sn2 lyso-GPL molecule becomes unstable, thus leading to an equilibrium between the two positional isomers of sn1/sn2 lyso-GPLs, where the sn1 lyso-GPL again becomes a substrate for the enzyme. The removal of the second acyl chain, after its migration to the sn1 position, was found to be happen at a slower rate in comparison to the originally positioned sn1 acyl chain, since probably, first the sn1 has to be degraded in order to create the second product/substrate (sn1 lyso PC) for the enzyme. Such a migration of either the sn1 acyl chain to the sn2 position or vice-versa was evidenced from an earlier study as well [281]. In agreement, our studies emanating from NR, MS and other biochemical assays have demonstrated that PLA1-1 harbors lyso-PLA activity as well.

The phenomenon of GPL flip-flop during the interfacial kinetics - Analysis of the NR measurements, leads to a very interesting revelation on the ability of a GPL molecule to diffuse transversely from one leaflet to the other, within the same bilayer, during the course of PLA1-1 hydrolysis. Previous studies by Liu et al (2005) on PLA2 activity of SLBs, have shown that the membrane composition changes on both the leaflets of a supported bilayer which implies the occurrence of flip-flop of GPLs. Such assumptions were based on using the scooting model of interfacial hydrolysis. SLBs are supported lipid bilayers as already described, consequently the two leaflets can be divided into an inner and an outer leaflet, where the inner leaflet faces and interacts with the silicon crystal, and the outer leaflet faces the bulk solution of the PEEK cell used for the NR measurements. The space between the inner leaflet and the support is normally in the order of Å, leading to the non-availability of that leaflet for the attachment of the injected protein. Consequently, only the outer leaflet can be degraded by the enzyme, since only its surface is available. Initially the membrane is considered asymmetric at the start of the reaction (since mathematically at the beginning of the reaction this parameter is not relevant) and during the course of the activity of the PLA, the flip-flop increases, resulting in a more symmetric membrane. Results from our studies showed that the flip-flop phenomenon in 18:0 | 18:0 PC (DSPC) containing SLBs was practically either quite slow that was not noticeable or non-existent, while it is far more evident coming to shorter acyl chained and unsaturated series.

NR reveals formation of micellar aggregates that adsorb to the surface of the SLB -

Analysis of our NR data shows that, surprisingly, lyso-PC molecules released after PLA1-1 activity preferred to stay within the bilayer and probably only a small portion of the total amount released does not stay within. Therefore, lyso molecules containing only one of the two acyl chains within the SLBs lead to a decrease in the average volume of the lipids. This resulted in an average decrease in the area per lipid, causing a slight increase in the thickness of the SLB. During the course of the PLA1-1 mediated hydrolysis, peculiar structures were formed on the surface of the SLBs; upon analysis it was found that such aggregates were micellar in nature and were formed from the released D-labeled free fatty acids. Additionally, contrast variation of the lipid membranes also confirmed the release of free fatty acids into the aqueous phase, thereafter forming micellar structures that adsorbed to the SLB surface. Such a phenomenon was unexpected since a free fatty acid is hydrophobic in nature and less likely to prefer the release in aqueous phase like the lyso-GPLs. These results are also in contrast with findings from other studies that found lyso-lipids being released into the aqueous phase and leaving on the surface a layer composed of FFAs [247, 248]. In addition, such earlier studies have not evidenced formation of additional structures on the surface of the SLB. The discrepancy can be explained by the fact that the liquid volume above the bilayer used in those previous studies was much higher than that used here (22 ml vs 1 ml here), which would lead to a concentration of lyso release largely distant from its CMC. The contrasting result obtained could probably be correlated to the different enzyme (PLA2) previously studied. We would like to highlight here that, such micellar structures formed, were observed to exist only while experimenting with SLBs composed of certain poor substrates, specifically, when the reaction was found to be "slow enough". This indicates that, hypothetically, when the reaction is slow, micelles have more time to interact with lipid membranes, thus allowing for them to cover a large surface of the SLB over time and be detected by neutrons. From the normalised degradation profiles, it was noted that the micellar layer appears when the plateau of the reaction occurs after the first 1h of kinetics. The presence of the adsorbed layer appears to lead to an inhibition of the reaction mediated by the PLA1-1, most probably due to the lack of physical space where the enzyme can attach the lipid membrane. This layer does not affect the initial speed of the reaction, since it does not exist below a certain level of degradation, that was calculated to be around 15-20% of membrane degradation (considering 1 ml of volume of NR cell). In fact, from the normalised degradation graphs, it is notable that, for the lipids where the micellar layer is present, the reaction plateau occurred before the total degradation of the SLB.

Effect of the SLB charge on the hydrolysis kinetics - NR experiments were performed using also natural lipids, and a similar trend to the synthetic ones was found. Although not all the information obtained with partially deuterated PC molecules was available with natural lipids, since their either full-H or D labeling. Also in the case of dPC the micellar layer was not found, most probably due to its fast kinetics, since its fluid state due to the high number of unsaturations. Next, the mixture hPChPS was also tested, which lead to a charged SLB.

It is known already, from other studies [282], that a more charged lipid membrane leads to a higher speed of the reaction. Specifically, the interactions between phospholipases and lipid membranes are not driven by electrostatic charges, but by hydrophobic interactions [264]. The charge in the bilayer can in some cases increase the amount of protein deposited, but not the speed of attachment. Studies [264] prove that non-hydrolytic membrane disruption is an important factor for the kinetics of phospholipases. The lateral phase separation is defined as the physical separation of phospholipid molecules into the membrane, creating rafts or defects. This phase separation induced by the protein attachment, is correlated with the charge of the lipid bilayer. With anionic membranes, this effect is higher compared to zwitterionic membranes [283]. Higher defects onto lipid membrane, lead to a less packed membrane, with higher disorder, leading to a higher efflux propensity of the phospholipid molecules forming the membrane. The charge added using the natural mixture hPChPS falls into this point, where higher number of defects formed due to the charge of the membrane, increases drastically the speed of the reaction.

Mass spectrometry reveals that efflux propensity is the key determinant for PLA1-1 activity - MS measurements were performed on LUVs constituting a multitude of PC molecules, in order to assess the substrate preference of PLA1-1. Two different PC mixtures (A and B) were employed to assess the contributions of efflux propensity and active site accommodation in determining the specificity of PLA1-1. MS analysis of the PC mix A, showed that within the saturated series, shorter acyl chain GPL molecules were degraded with faster kinetics while an increasing chain length seemed to have an inhibitory effect on the activity of the enzyme. The preferred substrates were in the following order: 12:0 | 12:0 PC > 14:0 | 14:0 PC > 16:0 | 16:0 PC > 18:0 | 18:0 PC. Next, PLA1-1 in the presence of vesicles composed of species that contained molecular species of varying chain length and double bonds (Mix B), preferred to hydrolyse exclusively species that contained the highest number of double bonds, where the velocities appeared to follow a sigmoid function as a function of the number of double bonds. All these observations confirm the results obtained from NR analysis of the various PLA1-1 hydrolysed SLBs employed earlier. Data from other studies on substrate specificities of PLA1 isoforms are also in good agreement with our findings [243]. Analogous results were achieved when a natural lipid composed vesicular macro-substrate was employed in this study. Natural lipids extracted from *Pichia pastoris* provided us with an opportunity to recreate a more biologically relevant lipid membrane since they contain GPL molecular species similar to those that exist in mammalian cellular membranes. Such mixtures are relevant for this study since they contain GPL molecular species containing double bonds ranging between one and five in total. A high-throughput MS method was developed to identify a wide range of molecular species within each class of GPL. MS data showed similar trends within each class, increasing acyl chain length lead to an increasing rate of inhibition while an increase in the degree of unsaturation was found to cause an increase in the rate of PLA1-1 catalysed rate of hydrolysis. For instance: within the series of species that contained 36 carbons in total, the preference was in the following order: 36:5 > 36:4 > 36:3 > 36:2 > 36:1

and similar was the case with the series that contained 34 carbons ($34:4 > 34:3 > 34:2 > 34:1$). Species containing similar number of double bonds with varying acyl chains had an effect on the hydrolysis rate. For example, 34:4 PC seemed to be a preferred substrate over 36:4 PC since the former has the ability to efflux at a faster rate compared to the latter due to it being lesser hydrophobic. Analogous results emerged across all the different classes of GPLs, which again showcases the importance of substrate efflux propensity in determining the specificity of PLA1-1. Studies by the Somerharju group on secretory PLA2s [234] and human cPLA2 α [233] led to different results. They showed that efflux is the main key in regulating enzyme activity specifically in the case of saturated GPL molecules (shorter the acyl chain, more the rate of hydrolysis) which is kind of similar to what we have observed with PLA1-1 but it was not the case with the unsaturated series. For instance, PLA2 from bee venom or cPLA2 α when interacting with SUV bilayers composed of several molecular species, indicated that GPL molecules containing either 4 (arachidonic acid) or 6 (docosahexaenoic acid) double bonds, independent of the chain length, were the most preferred substrates indicating that active site accommodation is a key determinant in regulating their specificities. Contrasting results emerged when micellar substrates were employed, the preference for species containing 4 or 6 double bonds was much more pronounced, which indicates that, apart from active site accommodation, efflux propensity is also a major contributor. On the other hand, the homeostatic phospholipase (iPLA2 β) has been shown to be regulated through a combination of both efflux propensity as well as active site accommodation. Given these observations from earlier studies, it would be interesting to see how PLA1-1 responds when in contact with micellar substrates, probably the rate of hydrolysis would be several times higher than that observed with bilayer systems. Further, MS analysis through performing dynamic multiple reaction monitoring (DMRM) measurements helped us in looking at the effect of head group structure on the rate of hydrolysis in LUVs composed of natural GPL mixtures. PLA1-1 showed affinity for mainly PC and PS both of which were hydrolysed at similar rates followed by PE. The least preferred substrate was shown to be PI. These results are in good agreement with results from studies by Arioka et al [243]. In contrast, in the same study it was shown that the PLA1-2 isoform showed affinity only for PG. These findings indeed show that the structure of the headgroup has an effect on substrate specificity of the enzyme, resulting from the charge that it possesses or the active site accommodation of the molecule. Unfortunately, we were not able to reliably quantify PA and PG owing to their low signals and high fluctuations.

MS analysis shows that PLA1-1 harbors lyso-activity - Surprisingly, MS analyses of the m/z region corresponding to lyso-PC molecular species, showed an increase in the lyso production during the initial period of PLA1-1 activity, followed by the plateauing or even decrease in the abundances of some of the molecular species. For instance, analysis of the MS-lyso profile obtained from PLA1-1 hydrolysis of the PC mix B showed an initial increase of the peaks corresponding to lyso species followed by a subsequent decrease in their abundances. Such a phenomenon validates the lyso-GPL activity of PLA1-1 that was earlier observed by NR. A similar kind of behavior was earlier attributed to other PLA2s as well [189,

216]. These observations demonstrate that PLA1-1 is a true phospholipase, although it also harbors lyso-PLA1 ability, albeit it can cleave an sn-1 positioned fatty acid from lyso-lipid at a slower degradative rate compared to its PLA activity. For instance, we noticed that 12:0 | 12:0 PC (DLPC) in Mix A (which was the most preferred substrate) after 10 minutes into PLA1-1 mediated degradation, no further changes were observed and similar was the case with 16:0 | 18:1 (POPC) in Mix B. In fact, after this 10 minutes, the PLA1-1 stopped exhibiting its phospholipase activity (for the mentioned PC molecules), and we noticed it displaying its lyso-PLA activity which lead to a decrease in the lyso-lipid content. Although, the PC and lyso molecules were not hydrolysed in their entirety (plateau of the reaction before the digestion of the totality of the molecules in the mixtures used). The most accredited hypothesis for such a phenomenon is that saturated acyl chains has an inhibitory effect on PLA activity. Through previous studies it is already known that some PLA2 reactions are slowed down by the presence of FFA in the bulk solution [284]. The lyso-activity was also confirmed by integrating the normalised TIC chromatograms, where a drop in the TIC signal was recorded due to the loss of signal from the second acyl chain cleavage. In fact, after the plateauing of some PC molecules degradation profiles (10 min for the DLPC in mix A), the signal started to drop, confirming the cleavage of the second acyl chain. Another feature observed during the DMRM measurements, was the existence of stereo-isomers in the reaction mixture. Split lyso peaks detected represent the presence of fatty acid in its two possible positional isomers, where the peak on the left of center corresponds to the lyso sn2 and the peak right of center is the lyso sn1 (information taken on <https://metabolomics.baker.edu.au/method/>). The left peak corresponding to sn2 lyso released upon cleavage of the fatty acyl chain at the sn1 position was seen to increase at the beginning of the PLA reaction with a gradual decrease until the end point on expected lines. The right peak corresponds to the sn1 lyso, formed upon sn2 - sn1 FA migration, and it was found to decrease during the hydrolysis reaction. This migration hypothetically is slower than the initial rate of production of the lyso sn2, causing the increase of its peak upon reaction. After 10 minutes, when the hydrolysis profiles started to plateau, slowing down also the production of the sn2 lyso, the migration takes over the sn2 lyso production, causing the decrease in amount of this product, producing sn1 lyso. This latter was found to decrease, probably because of the fact that the lyso activity rate and the migration rate speeds are comparable. Earlier studies [281] have shown that such acyl chain migration occurs in aqueous phases compared to solvent systems. It is assumed that such events could be captured through freezing the sn1-sn2 lyso equilibrium by extraction of the reaction mixture into CHCl₃:CH₃OH followed by preservation of the sample in ACN. Further, investigations need to be carried out to prove these assumptions.

Vesicular size impacts PLA1-1 hydrolysis rate – We next looked at the aspect of how vesicle size influences the activity of PLA1-1. Vesicles of varying sizes composed of synthetic GPL mixtures were extruded and subjected to PLA1-1 following which the hydrolysis kinetics of each species were measured. Analysis shows that vesicle size mainly influences the hydrolysis rate of saturated PC molecules with 12:0 | 12:0 being an exception. We had

hypothesized different possible explanations for this phenomenon: (a) Curvature of the membrane which probably plays a crucial role in the attachment of the membrane to the PLA1-1, (b) the packing of the phospholipid molecules is very different, due to the frustration of the lipid bilayer, causing different substrate preferences; (c) Lower degradation of the saturated GPL molecules therefore no major amount of saturated FFAs are released thus causing an increase in the activity of the enzyme leading to a faster degradation of the most preferred substrate (12:0 | 12:0 PC). Nevertheless, further analysis is necessary to be carried out to prove such assumptions.

Biophysical experiments to characterise PLA - bilayer interactions - QCM-D measurements through two different formats were performed: (1) stopped flux and (2) active flux. We employed 16:0 | 18:1 (POPC) and studied its interaction with PLA1-1 by injecting an amount that was similar to what was injected into a NR cell. Taking into consideration the measurements performed using the active flux, an initial degradation was recorded. The frequencies increased (going toward "0") due to the removal of material from the lipid membrane. Next, the frequencies plateaued with a sequential drastic decrease. As mentioned earlier, the peak recorded corresponds to a point where the micellar layer conditions are met, thus probably leading to the re-attachment of these structures to the surface of the bilayer. Such structures as mentioned earlier, might contain other chemical species such as lyso and protein. The fact that the entire cell is placed upside down compared to the NR cell, it is possible that gravity could play a role in the deposition of such structures. In any which case, such a behavior was analogous to what was found during the NR experiments. The decrease of the frequencies below the starting point at the end of the reaction, could probably be due to the gradual deposition of the PLA1-1 upon reaction. Different measurements were recorded with the stopped flux, where a quite long lag phase was observed. This lag phase is probably caused by the gradual deposition and degradation of the lipid membrane and the PLA injected, that occur at the same time, resulting in an approximately equal mass being deposited onto the crystal. In fact, the dissipation recorded, slightly increased in that range, which could be attributed to a minor change in the structure of the membrane. The final state of the reaction is not very well understood, since for the fluxed experiment the frequencies decreased (probably for the PLA1-1 and micelles deposition) while for the stopped flux experiment, they increased. Therefore, further experiments will need to be conducted to obtain a better understanding.

Additionally, ellipsometry measurements were performed on similar kind of SLBs that were employed for NR analysis. These measurements helped assess the hydrolysis kinetics of each of those SLBs (composed of varying mono-species) employed over time. Further, such an approach also allowed us to well calibrate the amount of enzyme to be injected into the cell accordingly. This should allow us to capture slower kinetics for each substrate condition by NR. Upon completion of the reaction, a decrease of the delta was subsequently observed, probably due to the re-deposition of all the products released into the bulk solution over the course of the reaction or alternately it could be possible that it is the injected protein deposited on the surface. Such a behavior can be attributed to the orientation of the crystal with respect

to the gravity, albeit this was not visible during the NR measurements in which case the silicon crystal was placed on the top of the PEEK cell. Ellipsometry measurements did not detect the formation of any kind of micellar layer on the surface of the SLB upon PLA1-1 hydrolysis. In fact, hydrolysis kinetics of POPC measured by ellipsometry (data not shown) were almost similar to the 16:0 | 18:2 kinetics with an almost equivalent amount of final degradation in both the cases. The absence of the micellar layer in the case of POPC could be directly attributed to the volume of the cell utilized in the case of ellipsometry measurements, where the volume was ≈ 5 ml. At this volume the CMC is not reached and therefore no micellar formation takes place. In addition, earlier studies [247, 248], were able to determine through employing NR and ellipsometry, the binding of the protein to the surface of the SLB. In contrast, in our investigations, this behavior was not found. It is known that, some secretory PLAs, [285, 248, 247], have a variable lag phase, where the protein needs to first interact with the model membrane thus allowing it to disrupt the structure thereafter triggering GPL hydrolysis. We noticed that with PLA1-1, the lag phase was very short, which can be probably correlated to the diffusion of the protein into the cell. In fact, it was found to be longer during the ellipsometry experiment, where the volume cell is 5 folds larger than the cell used for the NR measurements. Hypothetically, the attachment equilibrium of the PLA1-1 to the SLB seems to be quite slow, during which period the protein starts to bind to the SLB and at the same time initialises the degradation of the GPL molecules, and in parallel the other enzyme molecules are in the process of binding onto the SLB. Hydrolysis kinetics obtained from PLA1-1 interaction with 18:0 | 18:0 PC containing SLB (data not displayed in this thesis), showed an increase in the SLD of the bulk solution over a period of 8 – 10 hours although no or very little degradation occurred. Therefore, we were not able to reliably analyze those data sets. We suspect that the increase of the SLD that we had noticed corresponds to the protein binding (since for this lipid-SLB an higher amount of PLA1-1 was injected - 300 μg), even if this increase was found to take place to the whole bulk solution. Additional experiments in this regard, need to be carried out, for instance by using analogous lipid molecules (where the ester bond is replaced with an ether group that is non-hydrolysed by the PLA1-1), in order to analyse specifically the protein-membrane kinetics interaction.

Moreover, kinetics using vesicles were recorded also with SANS measurements. Change in the structure of multi lamellar vesicle (MLV) were found during the activity assays, where the solution made by 14:0 | 14:0 PC (DMPC) from opaque became transparent. LUVs of partially deuterated d16:0 | h18:1 PC (POPC) were used for SANS measurements, and it was found that even after 2 days of incubation with the enzyme, the structure of the vesicles remains almost unaltered. Similar experiments were performed by [283], where they found that the LUVs structure remains unaltered even if the outer leaflet is completely degraded. These findings prove that LUVs are much more stable than SLBs, where the lipid bilayer can rearrange maintaining similar structures. Additionally, it was found from SANS measurements an increase of the polydispersity or fluidity of the lipid membrane due to the plateauing of the bump related to the form factor of vesicles. More experiments need to be performed, in order to assess whether the polydispersity is what changes in the system, or

the fluidity. SANS experiments employing a lower q range can be performed to find if is the polydispersity that changes; whereas the more fluidity of the system can be assessed by utilising neutron inelastic techniques.

Conclusive remarks - The possible explanation on the behaviors of the PLA1-1 studied, is related to its function in *Aspergillus oryzae*, that remains unknown. Nevertheless, few hypothesis have been formulated by [243], where they found that this phospholipases is actually secreted in the environment where the fungi grows. Since it was not found any phospholipid specificity (efflux propensity is the key selecting factor), it may be involved in the degradation of phospholipid molecules in the extracellular media so that the cells can uptake the FFA or lysos as nutrients. A second PLA1 was found in the same microorganism, which seems to be a paralog of PLA1-1 (named PLA1-2, as second isoform) [243]. PLA1-2 was found to have some preferences within the PG class of phospholipids, and it is mainly located in the mycelial fraction, and it is probably important in the signaling, since lyso-PGs are involved in diverse cellular activities such as the intracellular calcium increase, kinase phosphorylation, cellular migration, and so on [243]. Also this aspect needs additional work in order to be fully understood.

Maintenance of Natural GPL homeostasis – A number of studies have demonstrated that PLAs are involved in a plethora of lipid homeostatic pathways, for instance, the membrane remodeling or GPL degradative processes. GPL homeostasis is a cellular process that has been postulated to exist in order to maintain steady-state GPL compositions within certain limits in biological membranes. Lipid compositions have been shown to adjust in response to external stimuli/conditions. For example, micro-organism cultures that were maintained at different temperatures, resulted in varying lipid compositions in their membranes, where in the ratio between lipid classes and the species are consequently adjusted accordingly so as to tune the fluidity of the membrane at that particular temperature [286]. The compensation of the membrane fluidity is carried out by incorporating either saturated or unsaturated acyl chain constituted GPL molecules to the membrane or by varying the ratio between classes. For instance, cell cultures upon being maintained at 22 °C resulted in a higher amount of unsaturated acyl chain containing GPL molecules in comparison to cell cultures maintained at 37 °C. Saturated acyl chains lead to higher hydrophobic interactions, thus lending more rigidity to the lipid membrane while unsaturated acyl chains lead to a more disordered membrane. Consequently, cells adjust the GPL acyl chain compositions within their membranes, in order to obtain a similar membrane fluidity at varying temperatures. In this context, a similar behavior was noticed in *P. pastoris* cultures from which natural GPL mixtures were extracted. A significant difference in the relative abundances of various GPL species was noticed when cells growing under normal (H) media conditions were adapted to deuterated conditions. GC analysis revealed that deuteration supposedly induced an increase in the oleic acid content in the GPLs in comparison to their hydrogenous variant. Such a phenomenon can be considered to be a compensatory step adapted by the cell in

response to the deuteration effect and this could be correlated to membrane fluidity. In fact, a previous study showed [287] the isotopic effect of deuterium labeling on organic molecules, where hydrogenous variants have higher hydrophobic interactions compared to its deuterated version. Hydrophobic interaction describes the interaction between hydrophobic molecules and water, where hydrophobic molecules have the tendency to aggregate between each other, thus increasing the entropy of the system. Consequently, GPL molecules have the natural propensity to form these complex structures, where the hydrophobic part of the GPL molecules are hidden from water molecules through their polar heads. Higher hydrophobic interaction led to a higher hydrophobicity, leading to a stronger interaction between hydrophobic molecules as well as stronger repulsion with water molecules. In support of these observations, our HPLC and GC analyses showed that upon separation, the natural deuterated lipid molecules eluted much earlier (faster retention time) compared to their hydrogenous counterparts. Accordingly, the higher amount of 18:1 fatty acid in the deuterated grown cells can be attributed to the fact that cells decrease the number of double bonds harbored in their acyl chains in their membranes, in order to retain the hydrophobic interactions (packing), thereby increasing the saturated acyl chain compositions thus helping confer more order and packing of the lipid membrane. Thus, under such conditions, cells manage to retain the same membrane fluidity and functionality of their lipid membranes in these two conditions.

GPL molecules extracted from *P. pastoris* cells, grown under hydrogenous and deuterated conditions, were utilized to obtain SLBs, followed by their structural analysis analyze by NR. Different classes of the purified GPL classes were utilized (PC, PC/PS, PC/PG) in both their hydrogenous and deuterated versions to prepare and characterize SLB systems. NR analysis showed that the structure between deuterated and hydrogenous GPL bilayers was retained. We hypothesise here that membrane fluidity has a major influence on the membrane structure as well, where the difference in the chemical composition of the acyl chain is compensated by the different hydrophobic interactions of deuterated and hydrogenous material. All this indicates that the complete process that controls the membrane composition of cells is a very is quite complex, within which a number of pathways play an important role for the membrane remodeling. Natural lipids have become a powerful tool to recreate more biologically relevant model lipid membranes. Given that both hydrogenous and deuterated membranes display similar structural characteristics, which is quite advantageous, since the same experiment can be performed using the same membrane (in terms of the structure), but in both deuterated or hydrogenous version. This by changing the deuteration level thus maintaining the same structure under analysis. This advantage has a direct connection on the membrane/protein or peptide or organic molecule interaction. The deuteration level is fundamental for some techniques, such as neutron scattering, FT-IR, NMR, where the deuteration level can be used for the change of the contrast in the system. For example, SLBs are employed for the analysis of protein interaction using NR. A protein usually has an SLD that is very similar to the polar head SLD of hydrogenous GPLs. Consequently, the system can be measured using the same protein, and making two different lipid bilayers (H and D). In this configuration, more details

can be achieved, through increasing the contrast in the polar head region. A second advantage of employing these lipids constitutes the use of a more natural lipid membrane for the such interaction experiments.

5.1 Conclusions and Perspectives

The PLA1-1 - lipid membrane interaction was found to be an extremely complex phenomenon, and despite the large number of experiments and analysis carried out in this work, many more are needed to reach a full understanding. Structural changes were recorded on SLBs with NR, with the formation of a micellar layer that plays a key role in the final part of the kinetics profile. The efflux propensity and the active site accommodation are the two bottlenecks of the phospholipase reaction, but here only the first one appears to be fundamental for the model enzyme utilised. The lyso-activity was found to exist in this enzyme, where also saturated FFA appears to have an inhibition effect on the hydrolysis reaction. The preference for the PC and PS classes were found, where PE and PI are not the best substrates for this enzyme. As mentioned at the beginning of this conclusive section, this is not the end of the study. Additional work need to be performed to fully understand this amazing and very complex system.

As a perspective, it would be interesting to validate the findings of the last experiment of this thesis where conditions of preparation were such that, on $5 \times 5 \text{ cm}^2$ surfaces, multilayer formation was found. These multilayers could be further studied by using a small angle diffractometer, such as D16 at ILL. The structure as mentioned in the results section, appears to be as series of layers with a certain amount of polydispersity along the z-axis. This actually could lead to cubic phases that the lipid formed upon the end of the hydrolysis reaction. Diffractometry could help us in the understanding of the properties of this layer, and what experimental conditions lead to their formation. Additional MS experiments need to be performed as mentioned above. Furthermore, MS measurements on the micellar layer can be carried out as well. We have planned to perform kinetics inside NR cells in the lab, washing them at a certain point in order to analyse what is the composition of this micellar layer found by NR. NR and QCM-D experiments need to be performed to understand the kinetics of attachment of the PLA1-1 to the SLBs, that it was found to be very slow and without any attachment layer formation on the top of the SLB before the start of the degradation (only a very large layer using DSPC-SLB only after several hours upon the injection).

PLA1-1 was employed for both analysing its kinetics and as a model enzyme to design protocols to study other phospholipases. In this line, iPLA2 β was expressed in insect cells with the aim to use the same techniques described above and similarly study the kinetics of interaction with model membranes. The vector was designed (pFastBac) and Sf9 as well as Hi5 insect cell strains utilised. Figure 5.1 represents the Petri dish with the white/blue scan, needed to pick the right colonies with the recombinant bacmide. Figure 5.2 displays the fluorescent microscopy of the cell, performed to asses the amount of expression of the protein inside insect cells. The DH10-Bac *Escherichia coli* cell strain utilised, has a fluorescent

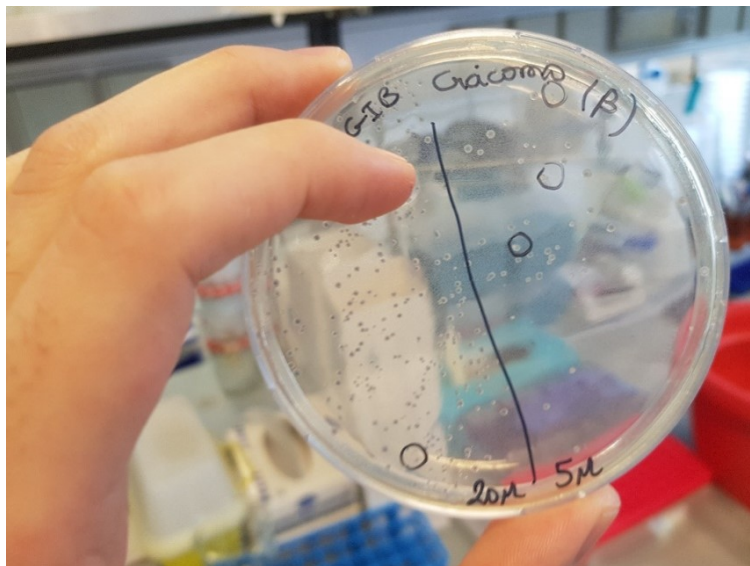


FIGURE 5.1: White/blue scan, carried out in order to select the *E. coli* cells with the recombinant bacmide of interest

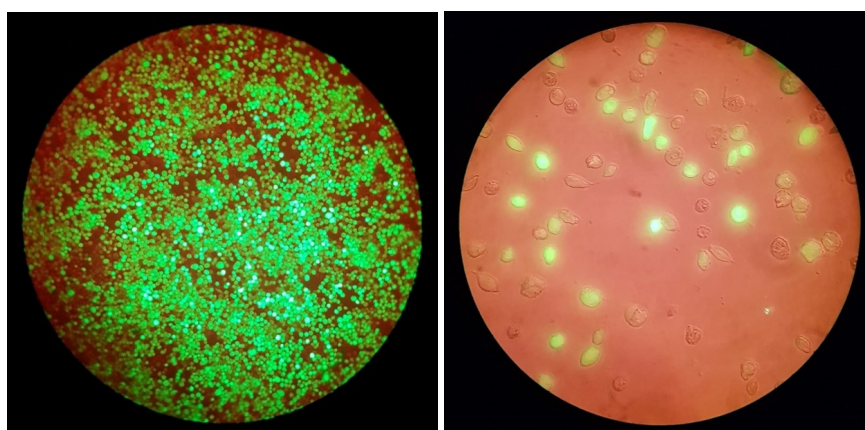


FIGURE 5.2: Fluorescent microscopy of the hi5 expressing the protein of interest

protein near the site where the recombinant gene is collocated. Basically, when the cells become fluorescent, with high probability the protein of interest is expressed. Finally, figure 5.3 shows the expression test through SDS-PAGE gels, where it is noticeable the high expression level of the protein of interest. The protocol for the purification was already established by

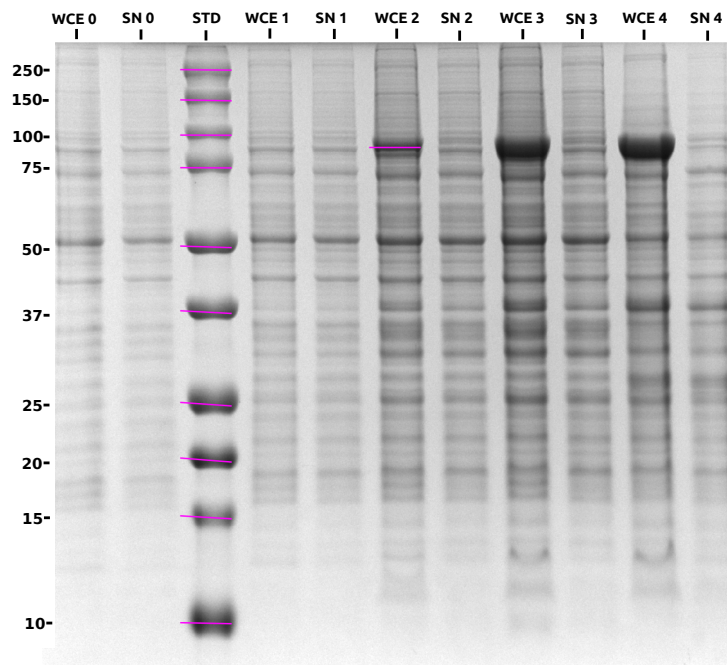


FIGURE 5.3: Expression test with an SDS-PAGE gel, where "WCE" is the whole cell extract and "SN" is the supernatant. The different numbers meant the days after the cells infection. Already a good expression level is achieved after 3 days. The expressed protein appears in the WCE, since the protocol for the extraction is not optimised for this kind of protein, since it is a general one.

[233], pellet are stored at -80° , ready for the purification and for the future analysis.

Chapter 6

CoruxFit



FIGURE 6.1: CoruxFit official logo

6.1 Introduction on the program

An in-house developed software was used for the NR data analysis. The software named "CoruxFit" enabled the design of customised models, which would have been difficult to implement in the already existing software for NR analysis. The project started at the beginning of my PhD, when the will and curiosity to deeply understand the physics and mathematics behind the reflectivity, inspired me to write in python an initial sketch. This initial core was then expanded over time, until it was able to perform some basic analysis. Thanks to the use of the already existing NR software such as Aurore [288] and MotoFit [289], we were able to check the correct results and mathematics behind the program. Some features were inspired also by Genfit [257], a program for small angle scattering analysis. Several subroutines in the program were born from useful discussion with friends and colleagues, that helped me to add more features to CoruxFit (such as the simulated annealing, evaluation of the errors, q resolution, and more). Therefore, CoruxFit is a python based program for neutron and X-ray reflectivity data analysis and simulation. The program runs on the principal operative systems, Windows and Unix systems (MacOS, Ubuntu and derivatives). For the moment CoruxFit does not have any graphic interface, and it can be controlled through a proper environment working directly into the command prompt. The commands for the software usage are listed and explained in detail in the paragraph 6.6.1. CoruxFit uses Gnuplot as a principal platform for the data plotting, and in addition it uses several python libraries that need to be installed to use the program (see paragraph 6.6.1).

The program starts creating the model of the sample under analysis, using the starting parameters given in the parameter file. Next, SLD profiles are calculated from the model and processed by the (3) Parratt algorithm, in order to calculate the theoretical reflectivity profiles.

Subsequently, if the user wants to fit the data, the minimisation subroutine compare the theoretical and the experimental curves, in order to obtain the χ^2 value, and the minimisation is based on minimise this value. The cycle during a fit is repeated until a good fit is obtained (goodness of the fit is decided by the user). In the following sections, all these processes are detailed described and discussed.

6.2 Model

Specular neutron reflectivity (NR) measures the in-plane reflection of the incoming neutron beam from an interface (see details in section 6.4.2). Therefore the technique is sensitive only to the features along the direction normal to the surface (z-axis), averaging the x and y properties. A common approach is to describe the sample as a stack of layers along z-axis. Each layer is characterised by a different SLD. Therefore an SLD profile (SLD(z)) can be built and optimised to the experimental data. Layers are described in CoruxFit with error functions, using the component group volume fraction distribution approach [290, 291], where thickness, sigma (roughness) and volume fraction (max level of the error function) are the layer (from now on component group) parameters. From the described model, the SLD profiles can be calculated, which is the starting point for the Parratt algorithm [292] to calculate the theoretical reflectivity curves.

6.2.1 Lipid bilayer modeling in CoruxFit

In CoruxFit the model is created as mentioned using the component group volume fraction distribution approach. The method consists of error functions (ERFs) describing the volume fraction probability of each component group of the sample, that corresponds to each chemical group of the lipid membrane (i.e. polar head, acyl chain region, etc) in the sample along the z-axis. The component groups used to model the lipid bilayer samples are listed as follows: (1) silicon crystal, (2) silicon oxide, (3) inner polar head region, (4) hydrophobic chains region, (5) outer polar head region. Figure 6.2 displays a scheme of a model supported lipid bilayer (SLB) with all the components described. The volume fraction distribution $\psi(\vec{z})$,

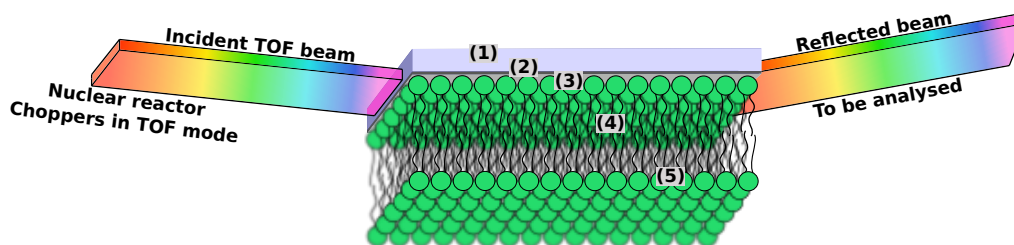


FIGURE 6.2: Sketch of the sample measured with NR. The numbers displayed corresponds to each part (layer) described in the main text, which constitutes the sample under analysis.

utilised for the description of each component group of the sample, is shown in equation 6.1. The approach was used by [290] to model lipid bilayers for small angle scattering, and

it can be also used for reflectivity technique, since the bilayer structure is analogous as also explained and discussed by [291].

$$\psi(\vec{z}) = \frac{1}{2} \cdot \left(\operatorname{erf} \frac{\vec{z} - z_{\mu} + \frac{d}{2}}{\sqrt{2}\sigma} - \operatorname{erf} \frac{\vec{z} - z_{\mu} - \frac{d}{2}}{\sqrt{2}\sigma} \right) \cdot (1 - \phi_{solv}) \quad (6.1)$$

where erf is defined as following:

$$\operatorname{erf}(x) = \frac{2}{\sqrt{\pi}} \int_0^x e^{-t^2} dt \quad (6.2)$$

z_{μ} describes where the component group is located along \vec{z} ; d is the thickness of the group; σ is the roughness of the interface between two component groups and ϕ_{solv} is the water content in that component. $\psi(\vec{z})$ is a function defined between 0 and 1, that corresponds to 0% and 100% of probability of finding the component group in a specific z position. Each volume fraction distribution is scaled with respect to the amount of water in that component group (ϕ_{solv}), resulting in a shift of the maximum of the $\psi(\vec{z})$ for the component groups that contain water. The final model is then created by placing all the $\psi(\vec{z})$ calculated for each component group together. Next, the water function is calculated by adding up to 1 every $\psi(\vec{z})$ where the sum of the $\psi(\vec{z})$ in the final model is lower than that (as explained in equation 6.3),

$$\Psi_{solv}(\vec{z}) = 1 - \sum_{i=1}^{n_{layer}} \psi_i(\vec{z}) \quad (6.3)$$

where $\Psi_{solv}(\vec{z})$ is the function describing the water volume fraction distribution along the z -axis of the sample.

In order to calculate the thicknesses of the component groups within the membrane, the lipids are considered as embedded inside a cylindrical shape as shown in figure 6.3, where the topological section of this cylinder corresponds to the area per lipid. This parameter is

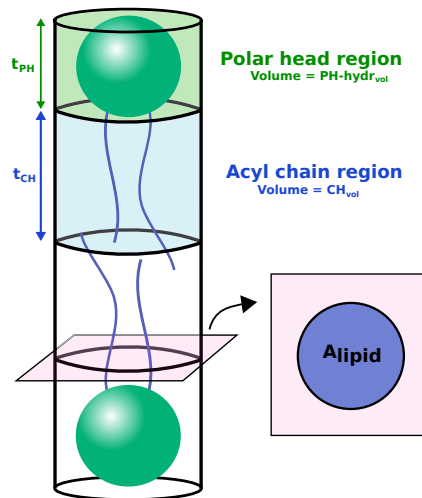


FIGURE 6.3: Cylinder describing the two phospholipid molecules placed along the vertical axis (z -axis) with respect to the bilayer surface.

assumed to be equal between the inner and outer leaflet for flat membranes. As displayed in the figure, the cylinder is divided in different sections, each one for every component group, whose volume fraction probabilities are described using $\psi(\vec{z})$, as explained before, along the cylinder (z -axis). The membrane is then considered as a set of cylinders placed near one another, in order to form a flat model membrane. A symmetrical and flat lipid membrane, can be described using only two thicknesses, since the t_{PH} and the t_{CH} are the same for the two leaflets. These two thicknesses can be constrained with the area per lipid (A_{lipid}) and molecular volumes of the phospholipid as shown in the equation 6.4,

$$t_{PH} = \frac{PH_{vol}}{A_{lipid} \cdot (1 - \phi_{PH_{hydr}})} \quad \text{and} \quad t_{CH} = \frac{CH_{vol}}{A_{lipid}} \quad (6.4)$$

where t_{PH} and t_{CH} are the thicknesses of the polar head and chains respectively; PH_{vol} is the dry polar head volume; A_{lipid} is the topological area per lipid; and $\phi_{PH_{hydr}}$ is the hydration water of the polar head. The volumes are calculated by employing the following volumes for lipids in the fluid phase: $V_{CH_2} = 27.5 \text{ \AA}^3$, $V_{CH_3} = 55.1 \text{ \AA}^3$, $V_{CH} = 22.2 \text{ \AA}^3$; and for lipid in gel phase: $V_{CH_2} = 25.3 \text{ \AA}^3$, $V_{CH_3} = 52.6 \text{ \AA}^3$ [259]. The polar head volumes are calculated by employing their mass density ($PC - PH_{vol} = 318 \text{ \AA}^3$, $PS - PH_{vol} = 263 \text{ \AA}^3$, $PG - PH_{vol} = 288 \text{ \AA}^3$). The $PH_{hydr_{vol}}$ displayed in figure 6.3, corresponds to the volume of the hydrated polar head, where PH_{vol} is corrected with the hydration water expressed as $\phi_{PH_{hydr}}$ according to equation 6.5.

$$PH_{hydr_{vol}} = \frac{PH_{vol}}{1 - \phi_{PH_{hydr}}} \quad (6.5)$$

The total amount of water in the polar head region, as is displayed in the tables in the Results sections, is calculated as follows: $\phi_{PH} = \phi_{PH_{hydr}} + \phi_{CH}$. Another parameter that has to be included in the model is the coverage of the bilayer. It consists on the evaluation of the amount of water along the lipid membrane. This value is expressed in fraction volume (ϕ_{CH}), which corresponds to the amount of water respect to lipids in the lipid bilayer. This water is also called "defect water", since in the model it creates pores within the membrane. Consequently, the parameters used to fit the data emanating from a SLB with the model described, are listed as follows: (1) A_{lipid} ; (2) ϕ_{CH} ; (3) $\phi_{PH_{hydr}}$; and (4) σ . The parameter (1) is the area per lipid; (2) corresponds to the amount of water through the bilayer (defects water) and the complement to 1 of ϕ_{CH} ($1 - \phi_{CH}$) is the coverage of the bilayer on the surface of the silicon crystal; (3) is the amount of hydration water ($\phi_{PH_{hydr}}$) in the polar head region, and (4) the interface roughness. For the bilayer measurements, the parameters describing the silicon crystal were fitted using the data collected on the surfaces in contact with water before lipid injection (usually in two contrasts), and kept them constant during the fitting of the bilayer, in order to reduce the number of variables during the bilayer analysis, increasing the accuracy.

At the end of the whole described process, the model displayed in figure 6.4 can be obtained. The model, as described previously, is a set of component groups volume fractions

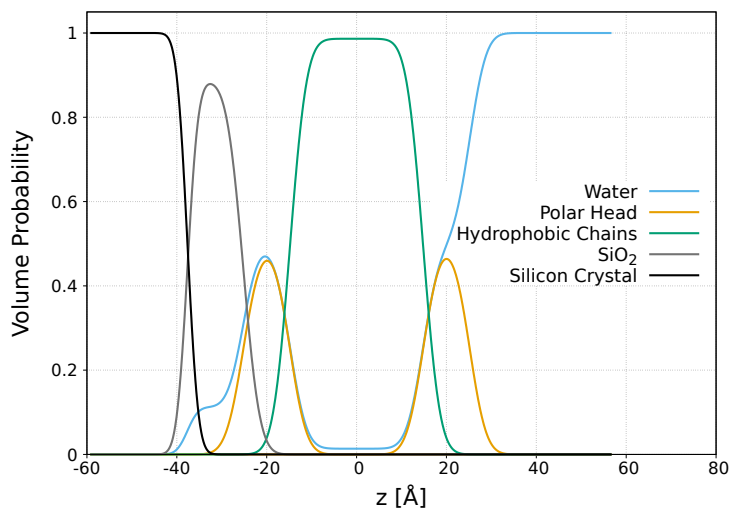


FIGURE 6.4: Example of component group volume fraction distribution model

characterising the position of the components group along the z -axis. The probability as mentioned is between 0 and 1 values. The total SLD profile is calculated then by multiplying each error function of the final model for the SLD value of the corresponding sample component, and summed them together to have the final profile. This SLD profile is then treated by the Parratt algorithm in order to obtain the theoretical reflectivity curve.

Usually, in a lipid bilayer model, a thin layer of water is inserted between the silicon support and the lipid bilayer. We had noticed a strong positive correlation (using the correlation matrix as described in the paragraph 6.5.2) between the thickness of this layer and ϕ_{CH} , where increasing its thickness, an increase of the ϕ_{CH} occurs. Since the relative error calculated for this water layer is large, it was completely removed, substituting it with hydration water of the polar head and of the silicon oxide of the support, thus improving the experimental data analysis and the error estimation.

6.2.2 Membrane proteins and protein/organic molecule-membrane interaction

CoruxFit modeling subroutine, allows the interpretation of molecules/peptides/proteins (from now "interacting object") in interaction with SLBs. CoruxFit interprets these interacting objects as simple geometrical objects, such as cylinder shapes, but several other shapes can be written and use as model. The following description concerns the cylindrical shape, since it was the ones employed in the thesis. As geometrical parameters for the cylinder, CoruxFit takes the molecular volume of the object under examination, as well as its theoretical topological area. From those two parameters, that can also be fitted, the thickness is calculated. In CoruxFit, the distribution of the interacting objects on the surface of the SLB, follows a hexagonal distribution as shown in figure 6.5. The hexagonal configuration is the one that gives the best distribution in the space and it allows the calculation of the average " $d_{lattice}$ ", which is the average distance between interacting objects on the membrane. This configuration has no influence on the final signal, since specular reflectivity is not sensitive to the lateral

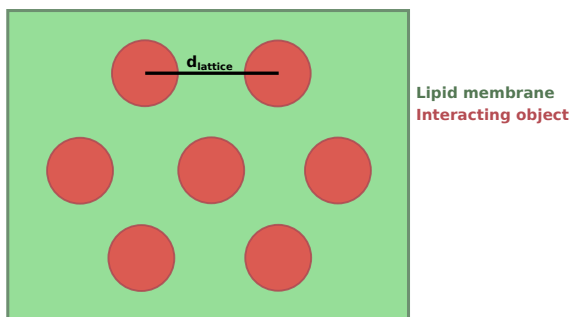


FIGURE 6.5: Top view representation of the hexagonal model configuration used in CoruxFit to model the dispersion of the interacting objects in/on the SLBs

distribution of objects onto the membrane. Nevertheless, from this hexagonal distribution, the space that the object occupies inside the membrane can be calculated. The sketch in figure 6.6, considers an example of interacting object that is for a part inside the SLB and for the rest outside the membrane. Taking into consideration the case explained in the sketch, in order to

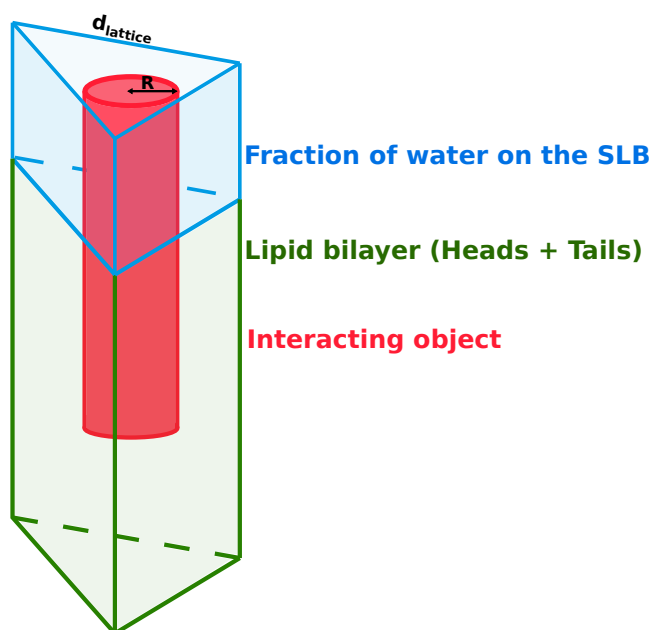


FIGURE 6.6: Sketch of an interacting object in interaction with a portion of an SLB. The blue part of the sketch is the bulk water, whereas the green part is the lipid membrane.

obtain a model with the component group volume fraction distribution approach, the volume fraction of the interacting object has to be calculated (ϕ_{obj}). The equation that CoruxFit uses is described in equation 6.6,

$$\phi_{obj} = \frac{A_{obj}}{\frac{mol_{lip}}{mol_{obj}} \cdot A_{lipid} + A_{obj}} \quad (6.6)$$

where mol_{lip} is the mol number of the lipids that can be calculated from the experimental coverage of the SLB; mol_{obj} is the mol number of interacting objects; A_{obj} is the topological area of the object. In CoruxFit, the ratio between mol_{lip} and mol_{obj} is a unique parameter that can be fitted during the analysis. The component group volume fraction distribution describing this interacting object can now be calculated as described in the previous paragraph, since all the necessary parameters are defined ([a] thickness, [b] fraction volume and [c] roughness that can be fitted). The $d_{lattice}$ can also be calculated using the equation 6.7.

$$d_{lattice} = \sqrt{\frac{A_{obj}}{\phi_{obj}} \cdot \frac{4}{\sqrt{3}}} \quad (6.7)$$

It can be noticed that $d_{lattice}$ is dependent on the A_{obj} , since considering the same fraction volume ϕ_{obj} and varying the area, the $d_{lattice}$ will vary. The position of the component group of the interacting object can be fitted during the analysis (z_{obj}), allowing the understanding of the interacting object position along the SLB (the position that gives the best chi square during the analysis).

In CoruxFit, membrane protein can be also modelled. An example of membrane protein that will be discussed is shown in figure 6.7. The model displayed has a part inside the membrane which is hydrophobic, and a small or large part outside the membrane. Also in this case the geometrical shapes can be changed and re-written in order to create a model that as near as possible to the protein under examination. In this case the equations behind the model were written following the model shown in figure 6.7. In order to calculate the

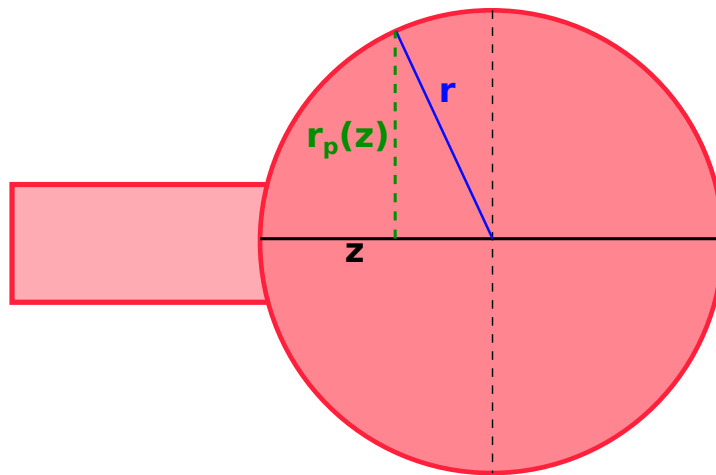


FIGURE 6.7: Sketch representing a membrane protein, where the cylindrical part corresponds to the hydrophobic part inserted into the membrane and the spherical portion the hydrophilic part, facing the bulk solution.

fraction volume distribution of this object, the topological area along the \vec{z} array of the sphere, needs to be acquired. From the geometrical parameters of the object displayed in

figure, the equation for the topological area can be extrapolated as shown in equation 6.8.

$$A_{TopSph}(\vec{z}) = (r^2 - (\vec{z} - z_\mu)^2)\pi \quad (6.8)$$

The A_{TopSph} is the topological area as a function of \vec{z} ; r as displayed in figure 6.7 is the radius of the sphere; \vec{z} the array of z-axis values; and z_μ is the position of the object along \vec{z} . It follows that the fraction volume distribution can be calculated as displayed in equation 6.9,

$$\phi_{ObjSph} = \frac{A_{TopSph}(\vec{z})}{\frac{mol_{lip}}{mol_{ObjSph}} \cdot A_{lipid} + A_{TopSph}(\vec{z})} \quad (6.9)$$

where the mol_{ObjSph} corresponds to the mol number of the sphere object. The fraction volume just calculated, it is then placed near to the fraction volume of the cylinder, that was calculated as mentioned before. The z-position of the cylinder is constrained to the one of the sphere considering a distance between the two objects of $r + t_{cyl}/2$, where t_{cyl} is the thickness of the cylinder. Figure 6.8 shows the final calculated fraction volume of the object sketched in figure 6.7. The two objects are then considered by the program as one single object, and

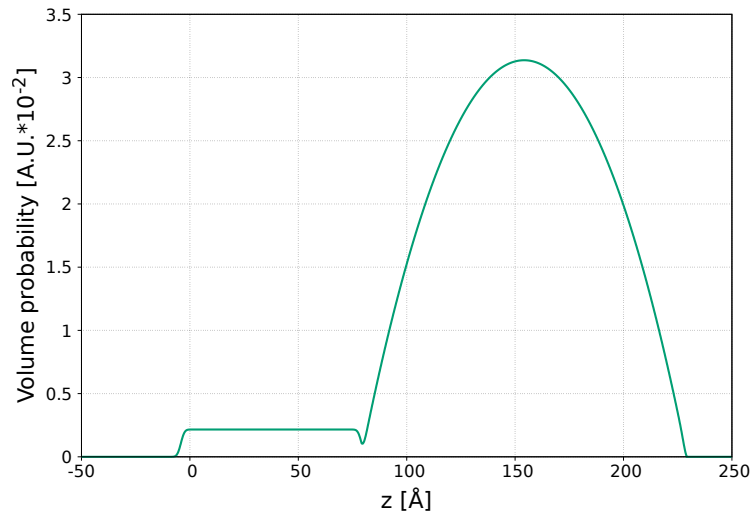


FIGURE 6.8: Volume fraction distribution of the trans-membrane protein sketched in figure 6.7

its z-position can be fitted during the analysis, obtaining the best z_{obj} of the protein along the lipid bilayer. This model has a lot of limitations, and a more advanced model can be used as suggested by [293, 294, 295].

After calculation of the interacting object volume fraction distribution, its SLD profile can be computed. CoruxFit has two different alternatives to proceed through this process. The first alternative is the automatic mode, where the program calculates directly the SLD of the protein taking into account the atomic composition; and in the second case the SLD can be manually added in the parameter file. Also the deuterium exchange is taken into account, since varying the contrast in the bulk solution, the acidic "H" in the protein can be exchanged with "D" atoms, varying its SLD slightly. For a better and more reliable

parameters, it is suggested to use the ISIS website for a proper protein SLD calculation (<http://psldc.isis.rl.ac.uk/Psldc/>).

6.2.3 Kinetic plug-in for phospholipase system

The kinetics plug-in for CoruxFit, consists of an algorithm working inside the main program, that was developed specifically for the phospholipases-bilayer interaction. After uploading the data in the program, where the first dataset must be the bilayer reflectivity curve measured in the same contrast as the kinetics performed, and after the activation of the plug-in directly from the parameters file (see details in the paragraph 6.6.1), the fit/simulation can be started.

The introduction of the PLA1-1 in the cell, where the bilayer has been previously deposited and characterised, causes the degradation of the bilayer over time, with a speed of the reaction that depends on the lipid contained in the bilayer. Therefore, the kinetic was measured right after the PLA1-1 injection, and followed until the reflectivity curve did not change much over time. Next, the cell was washed and the last measurements in 3 or 4 contrasts were performed. This Kinetic plug-in is a specific algorithm to analyse the kinetic data, from the injection to the final wash. The main parameters that control the model are listed as follows: (1) Area per lipid variation; (2) SLD variation; (3) Defects formation and finally (4) Flip-flop and bilayer asymmetry. Since the PLA1-1, during the hydrolysis reaction, removes acyl chains from the PC molecules releasing them in the bulk solution, the average area per lipid (1) varies during the course of the kinetics, along with the SLD of the bilayer (2), since partially deuterated PC molecules were utilised in this context. A consequence of the material removal is the defect formation (3), where the bulk solvent enters into the lipid bilayer due to pore formation. The lipid bilayers utilised were SLBs, where one leaflet of the lipid bilayer interacts with the silicon support and the other leaflet faces the bulk solution. Consequently, only one of the two leaflets is available for the PLA1-1 interaction, since the space between the inner leaflet and the silicon crystal is not large enough to host a protein. Nevertheless, the degradation of the lipids from this leaflet was also observed, raising the hypothesis of the flip-flop (4). The flip-flop of the PC molecules from the inner leaflet to the outer leaflet is probably a fundamental process in order to compensate the defect formation in the outer leaflet, making the lipid bilayer more stable. In order to avoid over-parameterisation of the model, the area per lipid, SLD variation and the defects formation are constrained between them as discussed below, in order to obtain those information analysing only few parameters. The degradation parameters (f_{kin1} and f_{kin2}) are the key variables of the model, since the SLD variation, as well as the defect formation depends on the amount of degradation of the lipid membrane. The parameter f_{kin1} contains information on the amount of degradation of the acyl chain placed in the sn1 position of the PC molecules in the bilayer. The multiplication of $nCHsn1$ (that contains the number of CH₂ or CH of the sn1 position acyl chain) by f_{kin1} , allows to obtain the amount of sn1 chains that remain in the lipid membrane. Every dataset (collected at a different time along the reaction) has a different value of f_{kin1} . The second parameter f_{kin2} describes the total hydrolysis of the PC molecules, since, as described, during the hydrolysis

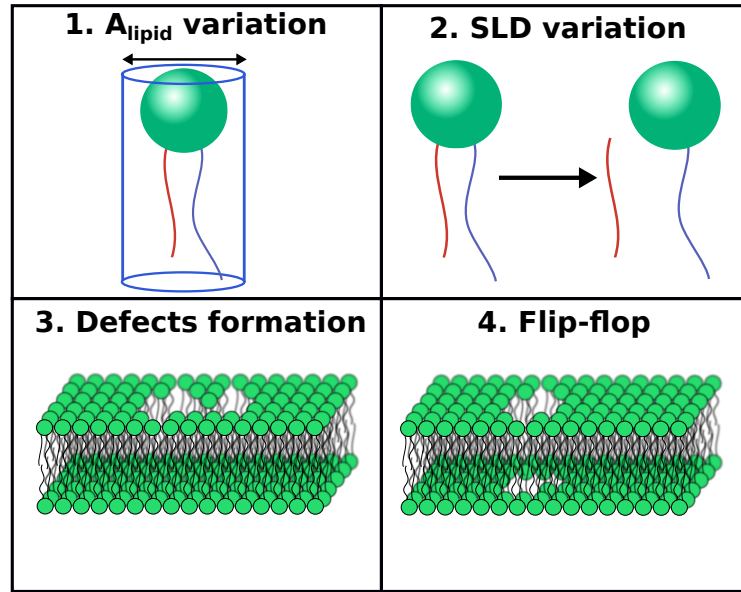


FIGURE 6.9: Sketch representing the 4 principal parameters for the kinetic model developed for the membrane - PLA1-1 interaction studies

reaction, the second chain $sn2$ is also hydrolysed after a certain period of time. Equation 6.10 and equation 6.11 display how the amount of acyl chain left during the kinetics is calculated. $nCHsn1$ is the average number of CH_2 and CH chemical groups in the first position acyl chain, whereas $nCHsn2$ in the second position.

$$nCHsn1 = nCHsn1_{tp0} \cdot f_{kin1} \quad (6.10)$$

$$nCHsn2 = nCHsn2_{tp0} \cdot f_{kin2} \quad (6.11)$$

$$A_{lipid} = A_{lipid\ tp0} \cdot (f_{kin1})^{A_{lipid\ factor}} \quad (6.12)$$

$$\phi_{CH} = \phi_{CH\ tp0} + \left(1 - \frac{nCHsn1 + nCHsn2}{nCHsn1_{tp0} + nCHsn2_{tp0}}\right) \quad (6.13)$$

$$\phi_{PH_{hydr}} = \phi_{PH_{hydr\ tp0}} \cdot f_{kin2} + 1 \cdot (1 - f_{kin2}) \quad (6.14)$$

The area per lipid A_{lipid} is calculated starting from the initial A_{lipid} ($A_{lipid\ tp0}$), that it is obtained from the characterisation of the bilayer before the injection of the protein ("tp0" = "time point 0"), and by using the kinetic factor f_{kin1} , since this parameter describes the removal of the $sn1$ positioned acyl chain from the phospholipid in the membrane. The A_{lipid} calculation is done using also the fitted parameter $A_{lipid\ factor}$, as displayed in equation 6.12, which is a global parameter, that is common for all the datasets of the kinetics. This parameter can assume positive or negative values, where with negative values the A_{lipid} decreases over kinetics time and with positive values it increases. The equation was designed empirically, since no other method was found to constrain the two parameters. This method allows to reduce drastically the number of fitted parameter, avoiding the overparametrisation of the model. The thickness of the bilayer and all the other parameters are then obtained considering

the new calculated A_{lipid} . Next, the amount of water through the bilayer is calculated as displayed in equation 6.13, where the amount of water is constrained with the degradation through the calculated $nCHsn1$ and $nCHsn2$ parameters, where $\phi_{CH\ tp0}$ and $\phi_{PH_{hydr\ tp0}}$ are the ϕ_{CH} $\phi_{PH_{hydr}}$ of the SLB before the protein injection (time point 0). An issue in equation 6.13, emerges in the extreme case, when the value of the fraction is 0 (when the bilayer is totally removed from the support). At this point the fraction of water calculated could be slightly more than one (is the case only if $\phi_{CH\ tp0}$ is more than 0), causing problems in the final model. This issue was resolved by inserting a limit in the fraction volumes, thus not allowing the ϕ_{CH} to reach values higher than 1. Consequently, also the water in the polar head region is calculated as the equation 6.14 shows. In this case, only the f_{kin2} parameter is utilised, since it is the one describing the complete hydrolysis of the PC molecules, that causes the leaving from the membrane of the polar head. The equation is a balance between the hydration water of the polar head at time point 0, and 1, that is 100% of water in the polar head region. Consequently, if also the second acyl chain is hydrolysed in the PC molecules, the polar head will also leave the lipid membrane. The $PH_{hydr\ vol}$ is not calculated every time, but is taken into consideration the one from the "tp0" as global parameter, otherwise problems regards the calculation of the t_{PH} would arise in kinetics datasets. The flip-flop is considered in model with one parameter per each dataset, describing the distribution within the two leaflets of the amount of degradation.

A last observation concerns the degradation products formed during the hydrolysis activity of the enzyme. It was noticed for some of the SLBs used, a rearrangement of those product of the reaction released from the membrane, in structures that were considered as micelles, that after a certain level of degradation, they attach back onto the membrane, forming a diluted layer on the top of it. This layer is described by the model using an fraction volume distribution, whose area is constrained to the amount of degradation. The model utilised is the interacting object described earlier in the section.

6.3 SLD profile calculation

Once the model is created, the SLD profiles need to be obtained as for the Parratt algorithm to calculate the theoretical reflectivity curve. Each of the ERF in the final model and the $\Psi_{solw}(\vec{z})$ (function describing the water distribution into the lipid bilayer), are then multiplied by the proper SLD value, and the final SLD profile can be obtained. The scattering length density (SLD), is defined as the sum of the scattering lengths of each atom constituting the chemical group under examination, divided by its molecular volume.

$$SLD = \frac{1}{V_m} \cdot \sum_{i=1}^N b_i \quad (6.15)$$

In equation 6.15, N corresponds to the total amount of atoms in that particular chemical group, b_i is the scattering length of the atom i and V_m is the corresponding molecular volume

of the chemical group. The scattering length in quantum mechanism, is a description of low energy scattering, and the interaction probe-atom (where probe is for instance the neutron particle), that can be described by the Fermi pseudopotential $V(\vec{r})$, that is displayed in equation 6.16,

$$V(\vec{r}) = \frac{2\pi\hbar^2}{m} \cdot b\delta(\vec{r}) \quad (6.16)$$

where \hbar is the Planck constant divided by 2π , m is the mass of the neutron, $\delta(\vec{r})$ is the Dirac delta function, b is the scattering length and \vec{r} is the distance from the center of the nucleus. It is seen that the neutron b can be very different between atoms, and within the isotopes of the same atom (for instance H and D atoms), that leads to a large difference in the $V(\vec{r})$. Consequently, deuterium labeling is largely used in neutron scattering, in order to perform contrast variation, hiding or highlighting some part of the sample under examination. The neutron scattering lengths across the period table, vary without any strict role, whereas the X-ray scattering lengths vary proportionally with the amount of electrons.

Figure 6.10 shows a typical SLD profile from the model shown in figure 6.4. In this

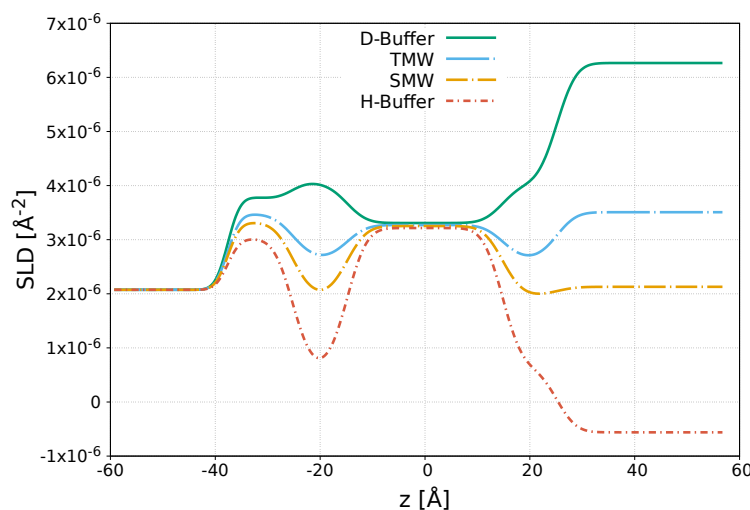


FIGURE 6.10: SLD profile of the 16:0|18:2 lipid bilayer taken as example.

case the measurement was carried out in 4 different contrasts (utilising different amount of deuterium labeled water), that lead to 4 different SLD profiles, caused by the different SLD values for the function $\Psi_{solv}(\vec{z})$. The ratio between H₂O and D₂O used are listed following: 100%, 59%, 39% and finally 0% in order to obtain the following contrasts: D-Buffer, TMW, SMW and H-Buffer (see next paragraph for more details).

6.3.1 Contrast variation method in neutron scattering

The change in the contrast between the sample and the bulk and hydration water by varying the D₂O content in the bulk, is one of the most important advantages of using neutrons as a probe to study the structure of the matter. Tuning with the contrast in a neutron experiment, can be comparable to the contrast or luminosity variation of a images. Figure 6.11 shows an example of contrast variation of two pictures, where the variable parameter is the exposition.

As can be noticed, in the first image of the first example, the shape of the sun and its position in the photo can be obtained, whereas the other signals are hidden or hardly visible. In the first image of the second example, the details of the clouds can be obtained, and also in this example all the other details are hardly visible. With the second images, the information of the sun are less visible, since the signal is too strong, but peoples shapes can be seen as well as in the second example, the signals from the trees and the water. Increasing more the exposition, different details appear, while others details become hard to see. Every part



FIGURE 6.11: Contrast variation of a picture. The figure represent how the contrast plays a key role in the understanding of the structure and details of a photo/sample, where utilising different contrasts, different part of the photo can be seen.

of the photo has a different best contrast to be visualised, like different chemical groups in the sample under examination. Similarly, changing the contrast between the solvent and the sample, provides more precise information about the sample structure and composition. In addition, the contrast variation experiment can be also designed so that the signal of a specific part of the sample is switched off, visualising only the parts of interest. Such matching out is when the contrast between the bulk solution and that chemical group of the sample is equal to zero, thus the object is not seen by the probe. The principle behind the contrast variation in neutron science is related to the variation of the refractive index, which is directly connected to the SLD. Consequently, in order to have the same contrast, the SLD between the bulk solution and the portion to be hidden, needs to be equal.

In order to change the contrast in a neutron experiment, different ratios of $\text{H}_2\text{O}/\text{D}_2\text{O}$ can be used, since, as mentioned earlier, heavy water and normal water have a large difference in their SLDs. For instance, in a NR experiment, usually 3 or 4 different contrasts are utilised. An example is given in figure 6.10, where for instance, the contrast "TMW" is the tail match water, which has the same SLD as the hydrophobic region of the lipid membrane. In fact, this region with this contrast is not visible, highlighting, for instance, a possible insertion with a protein. Another matched out contrast was utilised, SMW, where the silicon crystal support

was matched out, allowing for the visualisation of only the structure of the lipid bilayer and the layer of oxide (silicon oxide normally present on the substrate surface).

The different contrasts measured from the same sample are usually analysed together (global fit), since the structure of the sample is the same, increasing considerably the accuracy and precision of the fitted parameters.

6.4 Theory behind reflectivity and Parratt algorithm

Once the SLD profiles were calculated from the initial model, those profiles need to be treated by the Parratt algorithm [292] in order to obtain the theoretical reflectivity curve profiles.

6.4.1 Brief introduction to the reflectivity theory

Neutron and Xray are the most employed radiations to analyse the structure of matter under examination. These two particles/photons have different properties, and they interact differently with matter. Neutrons interact with nuclei of the atoms in the sample, and for possessing such a property are also called "gentle probe", since it does not destroy the sample during the measurement. X-rays are electromagnetic radiation, and are largely used to analyse bio-matter. The large disadvantage of using Xray radiation is the so called "radiation damage", that consists in the oxidation and chemical changing of the samples during the analysis. For that, when long exposition measurements in X-rays are required, for instance during an Xray reflectometry experiment (XRR), the energy, attenuators and the time of exposition per q point need to be carefully optimised. Due to the difference in the particle/photon-matter interaction, the two probes can be used as complementary techniques.

6.4.2 The Parratt algorithm

The theoretical description of the NR and XRR is analogous to that of reflection in visible light. Therefore, a refractive index n can be also defined for the description of the principle laws of neutrons and X-rays. n is the relevant parameter for the explanation of the laws behind the scattering of photons and particles, and it can be calculated as displayed in equation 6.17,

$$n = 1 - \delta + i\beta \quad (6.17)$$

$$\delta = \underbrace{\frac{\lambda^2}{2\pi} \cdot r_e \rho_e}_{Xray} \quad \text{or} \quad \underbrace{\frac{\lambda^2}{2\pi} \cdot nSLD}_{Neutrons} \quad (6.18)$$

where r_e is the radius of the electron (for X-rays), which corresponds to $2.8 \cdot 10^{-15}$ m; ρ_e is the electron density of the material taken into consideration; and $nSLD$ is the neutron SLD, previously defined. δ describe the dispersive and β the absorptive aspect of the photon/particle-matter interaction. Considering a flat and layered surface as an example (for instance see figure 6.12), the total external reflection phenomenon occurs from the layer where the incident beam illuminates, for incident angles below the critical one, which can be found as $\alpha_c = \sqrt{2\delta}$, where

α_c is the critical angle. All the incident angles below α_c , lead to the total external reflection. For organic matter, β is normally very small for X-rays and neutrons, and it is therefore usually neglected. Consequently n is dependent only on λ and ρ , which corresponds to the wavelength of the probe used and on electron or scattering length density of the material. Higher angles of the incident beam, different n values or different λ used, lead to the penetration of the incident beam into the sample (as shown in figure 6.12), where reflection and refraction occur at the same time between the different layers of the sample. A practical example explaining the total reflection, is present in optical cables, where the light remaining in the cable reaching very long distances. In this case, the angle of incidence is very low, and the refractive index does not permit the light to be refracted.

The law that can be used for the description of the refraction, is Snell's law. The refractive index can be also calculated as shown in equation 6.19,

$$n = \frac{\cos(\theta_{inc})}{\cos(\theta_{refrac})} \quad (6.19)$$

where θ_{refrac} is the angle of the refracted beam and θ_{inc} is angle of the incident beam. The condition for the total reflection is satisfied when $\theta_{refrac} = 0$ and $\theta_{inc} \leq \alpha_c$.

$$\sin(\alpha_c) \approx \alpha_c = \sqrt{\frac{\rho}{\pi}} \lambda \quad (6.20)$$

$$q_c = \frac{4\pi}{\lambda} \sin(\alpha_c) = 4\sqrt{\pi\Delta\rho} \quad (6.21)$$

Equation 6.21 shows the arrangement of the equation for the q_c calculation, where all the q points below that value are in the total reflection condition (where the reflection is equal to 1). The scattering vector q is usually utilised since inside this value the angle of incidence and the wavelength are taken into consideration, allowing the comparison of datasets taken from different instruments and with different wavelengths. It is usually expressed in \AA^{-1} in reflectivity experiments. Analogous equations can be formulated for the neutron refractive index description.

From the equations shown above, the Fresnel law can be formulated, as displayed in equation 6.22,

$$r = \left| \frac{\vec{k}_{iz} - \vec{k}_{tz}}{\vec{k}_{iz} + \vec{k}_{tz}} \right|^2 \quad (6.22)$$

where \vec{k}_{iz} is the vertical component of the vector describing the incident wave; \vec{k}_{tz} is the vertical component of the transmitted wave. Under the kinematic Born approximation, when the multiple scattering events are ignored, the Fresnel law can be rewritten as displayed in equation 6.23.

$$R_f(\vec{q}) \approx \frac{16\pi^2}{\vec{q}^4} \rho^2 \quad (6.23)$$

This equation is a good estimation of the reflectivity profile when the q range is greater than the q_c . This method can be used to fit a reflectivity profile from a single interface. When

the system is much more complex than a single interface system, the equation 6.24 can be utilised,

$$R(\vec{q}) \approx \frac{16\pi^2}{\vec{q}^4} \left| \int \frac{\delta\rho(\vec{z})}{\delta\vec{z}} e^{iq\vec{z}} dz \right|^2 \quad (6.24)$$

where $\delta\rho(\vec{z})$ is the variation of the electron density along \vec{z} . Also in this case, the equation is valid if the q values are higher than q_c .

Another more accurate way to compute reflectivity profiles from a stack layer system, which is currently used by CoruxFit, is the so-called Parratt formalism [292]. This algorithm accounts for all the reflection and refraction from each internal interface, including their coherent interference, in order to obtain the final reflection intensity from the sample.

$$X_j = \frac{R_j}{T_j} = \frac{r_{j,j+1} + X_{j+1}e^{2ik_{z,j}z_j}}{1 + r_{j,j+1}X_{j+1}e^{2ik_{z,j}z_j}} \quad (6.25)$$

In equation 6.25, the Parratt formalism is shown, where $r_{j,j+1}$ is expressed as shown in equation 6.26; z_j is the thickness of the layer j ; R_j is the reflected beam; T_j is the refracted/transmitted beam; and X_j is the final reflection amplitude.

$$r_{j,j+1} = \frac{k_{z,j} - k_{z,j+1}}{k_{z,j} + k_{z,j+1}} \quad (6.26)$$

For instance, if the q range under consideration is below the critical one, the transmitted beam equals 0, giving T_j a value of 1, and $X_j = R_j$, where all the incoming beam is reflected. When the q under examination moves away from the critical one, the transmission is higher than 0, resulting in a refraction of some of the incoming beam, interacting in turn with the "next" interface of the sample, as shown in figure 6.12. Therefore, the transmitted beam from one layer, is the new incident beam for the next layer, where again a reflection and refraction occur. This algorithm is consequently a recursive method, where the result X_{j+1} of the $j + 1$

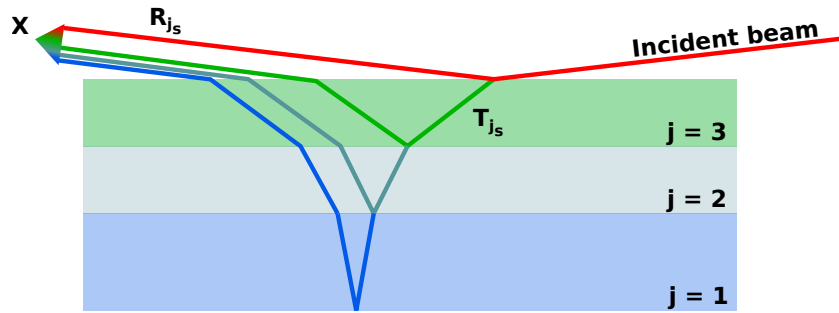


FIGURE 6.12: Sketch representing the reflection and refraction phenomena in a stacked layer sample

layer, is used to calculate the intensity X_j of the j layer. The resulting X tells us how much of the incoming beam is reflected from the sample. The final theoretical reflectivity curve, is then calculated in CoruxFit as displayed in equation 6.27,

$$R(\vec{q}) = |X|^2 \cdot s + bkg \quad (6.27)$$

where $R(\vec{q})$ is the final reflectivity profile of the sample under analysis; s is the scaling factor; and bkg is the background of the measurement.

In CoruxFit, as mentioned in section 6.2, the model used is a component group fraction volume distribution, using error functions to describe each component group of the sample under examination. The SLD profiles obtained from this model, are then directly treated with the Parratt formalism. The principle behind this treatment consists in the division of the SLD profiles, into a finite number N of layers, where N depends on the necessary resolution that a user needs to achieve. Basically, in CoruxFit, the SLD profiles coming from the modeling subroutine, are usually divided in slices of 1 \AA of thickness (defined as d_z), resulting at the end of this process, in a model with N number of total layers defined as SLABs. The thickness as mentioned, can be changed, depending on how complex and how detailed the SLD profile is. For instance, if the SLD profile of the model is simple, without many peaks or many details, the d_z can be increased. Consequently, the equation 6.25 can be rewritten substituting the parameter z_j with d_z , which by definition is constant per each SLAB (see equation 6.28).

$$X_j = \frac{R_j}{T_j} = \frac{r_{j,j+1} + X_{j+1}e^{2ik_{z,j}d_z}}{1 + r_{j,j+1}X_{j+1}e^{2ik_{z,j}d_z}} \quad (6.28)$$

This process results in the treatment of the SLD profile as it was constituted by an N SLAB layers model, where each layer has a slightly different refraction index or SLD that it is obtained directly by the SLD profile.

Unfortunately, because of the SLAB method, the Parratt algorithm in CoruxFit makes high demand on the processor, resulting in the largest bottleneck of the program (in term of speed). As will be explained during this section, the program for now uses only one core of the processor, since it is not yet optimised to work in a multiprocessing mode. This problem slows down the entire process, because the processor is not utilised to 100%. The parameter d_z is obviously a key parameter of the speed of the process, since this parameter contains information on how many SLABs the SLD profiles need to be divided into. A higher value of d_z leads to a higher speed in the calculation, since lower SLABs are needed to describe the SLD profiles, that leads to less demand on the processor per SLD profile treated. In summary, the d_z needs to be optimised, and a balance between resolution of the SLD profile and speed of the process need to be found considering the SLD profile model and the computer processor under use.

6.4.3 Q resolution algorithm

Data emanating from a neutron experiment, are affected by the so-called "q-resolution". Taking as an example a neutron or Xray experimental curve, the error in intensity is usually taken into consideration. This error derives from the detector, and it is the technical error from the instrument itself. In neutron scattering, the error in the q-axis is also present, and this is due to the mechanical parts that are usually used to obtain a monochromatic or a Time Of Flight (TOF) beam. In fact, mechanical selectors are used in neutron science, to improve

the already low flux that a neutron facility provide (compared to X-rays). Those selectors are constituted in case of NR, by choppers, as shown in Chapter 2, which can be used to obtain a monochromatic or TOF beam (in the case of Figaro, a TOF beam is utilised). The aperture, velocity and distance of the choppers between them, can be tuned in order to adjust the neutron intensity and resolution of an experiment. For instance, higher apertures lead to a higher flux with less resolution in q , since this configuration leads to the passage of different neutrons within a $\pm\Delta\lambda$ range, giving the low q -resolution. In the other hand, lower apertures lead to a less flux, while an improvement of the q -resolution occurs. The usual formula describing the q -resolution is displayed in equation 6.29,

$$\frac{\Delta q}{q} = \frac{\Delta\Theta}{\Theta} + \frac{\Delta\lambda}{\lambda} \quad (6.29)$$

where Δq is the absolute error in q ; $\Delta\Theta$ is the absolute error of the incident angle which depends on the collimation system; and finally $\Delta\lambda$ is the absolute error for the wavelength.

The Δq is, in the case of ILL instruments, a measure of the Full Wave Half Maximum (FWHM) of the gaussian curve representing the q distribution of a given q point. CoruxFit uses this value to calculate σ_{res} , which is the standard deviation of the gaussian function, equation 6.30.

$$\sigma_{res} = \frac{q_{res}}{2\sqrt{2\log(2)}} \quad (6.30)$$

The principle behind this algorithm [296] consists in the split of each q point (q_i) in different other point ($q_{i\ th\ res}$) distributed in the gaussian function ($G(q_{i\ th\ res})$) described and shown in equation 6.31, where i is the i -th point in q . In order to obtain the number of $q_{i\ th\ res}$ points to be added per each q point, the σ_{res} was multiplied by a factor 3.0. This process is performed for all the q points (q_i), and at the end the resulting maximum number of $q_{i\ th\ res}$ along the dataset is taken. Next, each q point (q_i) is splitted in $q_{i\ th\ res}$ points, and the theoretical reflectivity is calculated in these $N\ q_{i\ th\ res}$ and then integrated as displayed in equation 6.34 using the gaussian G described in equation 6.31.

$$G(q_{i\ th\ res}) = exp\left[-\frac{1}{2}\left(\frac{q_{i\ th\ res} - q_i}{2\sigma_{res}}\right)^2\right] \quad (6.31)$$

The gaussian G needs to be normalised in order to be utilised for the integration, and this process is performed using the equation 6.32 and equation 6.33

$$A_{G(q_i)} = \sum_{q_{i\ th\ res}} G(q_{i\ th\ res}) \quad (6.32)$$

$$G(q_{i\ th\ res})_{norm} = \frac{G(q_{i\ th\ res})}{A_{G(q_i)}} \quad (6.33)$$

After the normalisation, the area under the gaussian $G(q_{i\ th\ res})$ curve equals to 1, and can be used for the integration of the reflectivity as displayed in equation 6.34.

$$R(q_i)_{res} = \sum_{q_{i\ th\ res}} R(q_{i\ th\ res}) \cdot G(q_{i\ th\ res})_{norm} \quad (6.34)$$

From the calculated $R(q_i)_{res}$, the total reflectivity profile $R(q)$ with the resolution included can be obtained. Practically, the sharp minima in the reflectivity profile are smeared out, since the reflectivity signal from a given q_i point, is spread along a gaussian function built in each q point. Two gaussian in two close points can be overlapped, and consequently a part of the result $R(q_i)$ intensity of one point is considered as belonging to the second point.

The q resolution in the reflectivity instrument can be tuned with respect to the sample under examination, by adjusting the instrument configuration. For instance, if the reflectivity profile of the sample has several oscillations, a high q resolution is extremely important in order to not lose structural information. In the case of the present study, the resolution was set to 7%, since the samples were expected to produce smooth reflectivity profiles. This choice has the advantage of a high flux and shorter measurements time compare to a high resolution set-up. In figure 6.13 an example of the same model where the reflectivity was calculated with and without the q resolution algorithm. The q resolution values were taken from an experimental dataset measured on Figaro. By including the effect on the q resolution,

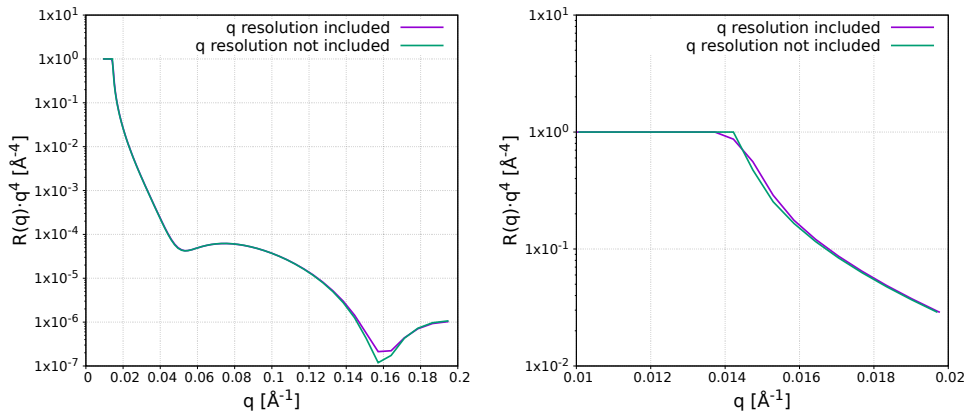


FIGURE 6.13: Different q resolution reflectivity curve calculation of a POPC lipid bilayer

as mentioned above, the reflectivity intensity of the sharp peaks is smeared out within the q points. The reflectivity profile shown in the figure is related to a POPC bilayer, and the major differences are near to the critical q range, and at the minimums of the curves. These differences are mainly related to the calculation of the bulk SLD, and it increases the accuracy of the fit as well as it decreases the value of the final chi square (χ^2).

6.5 Minimisation routine

In mathematics, the minimisation of a theoretical function into an experimental dataset, is a process on which the first one is adapted onto the second one, varying the parameters, with a proper algorithm, that defined the theoretical function. In CoruxFit, the minimisation is used to minimise the difference between the theoretical reflectivity function and the experimental data by varying the theoretical function parameters, in order to adapt the theoretical reflectivity profiles onto the experimental data. The key function that is used in CoruxFit for the minimisation is the chi square χ^2 that is calculated as shown in equation 6.35,

$$\chi^2 = \frac{1}{N \cdot nq_N} \cdot \sum_{i=1}^N \frac{(R_{i \text{ exp}} - R_{i \text{ th}})^2}{err_i^2} \quad (6.35)$$

where N is the number of dataset loaded into the program; nq_N is the number of q points in each dataset loaded; $R_{i \text{ exp}}$ is the experimental reflectivity; $R_{i \text{ th}}$ is the theoretical reflectivity calculated; and err_i is the experimental error from the instrument. In order to find the absolute minima of the χ^2 function during the minimisation, two algorithms are utilised in CoruxFit. The first one is the Simulated annealing algorithm [297, 298], randomizes all the parameters inside their own range; once the absolute minima is found, the steepest descent algorithm (from Scipy library, `least_squares`) is used in order to cool down the system even more, finding within the absolute minima, the minimised parameters.

CoruxFit can simultaneously analyse different datasets from different contrasts of the same sample, with the same simulated model, helping to achieve more precise and accurate parameters.

6.5.1 Simulated Annealing algorithm

The name "simulated annealing" refers to the physical process in which a solid is heated up until a maximum value, at which all the atoms of the solid randomly arrange themselves in a liquid phase, followed by the cooling step, where the atoms decrease their kinetic energy until they stop moving. In this way, all the atoms in the solid arrange themselves in the lowest possible energy called "ground state". The probability of finding a given energy of the system along different temperatures, is calculated through the Boltzmann distribution [299], displayed in equation 6.36.

$$p_E = \frac{1}{Z(T)} \cdot \underbrace{\exp\left(-\frac{E}{k_B T}\right)}_{B_f} \quad (6.36)$$

The equation shows the probability p_E of finding the system under examination at E energy state, where $Z(T)$ is a normalisation factor; k_B is the Boltzmann constant; and T is the temperature expressed in K. B_f is the Boltzmann factor, that contains already the description of the probability, consequently from now on, this factor is used instead of the P_E . Figure

6.14 displays how the probability of finding the same system at ΔE energy changes over temperature. In nature, a system has the tendency of assuming the lowest possible energy. It

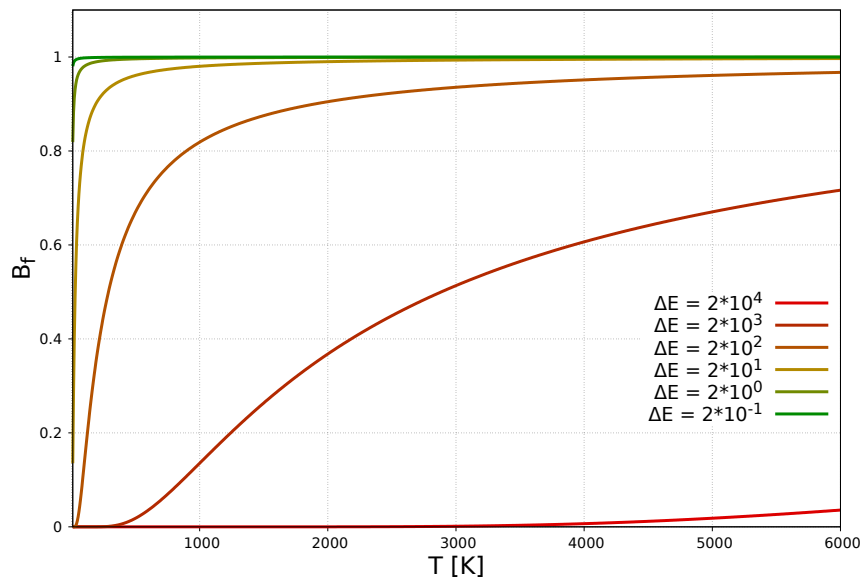


FIGURE 6.14: Profiles of the probability of finding the same system at ΔE energy vs temperature of the system

can be noticed from the graph that the probability of finding the system at higher energies in a low temperature range, is low compared to the probability of low energy system, where the probability is almost 1 at all the temperatures. Very high energy in the system have a very low probability to exist, even at high temperatures such as 6000 K (for instance the $\Delta E 2 \cdot 10^4$).

This method can be used for the optimisation of theoretical functions onto experimental data, since the vibrational energy of the atoms in the system (related to the temperature of the system) can be translated into the accept/refuse process step. In every minimisation cycle, the input parameters are randomised along the minimum and maximum range, and the selected value per parameter is sent for the theoretical curve calculation. The ΔE of the Boltzmann factor, is calculated using the $\Delta\chi^2$ values, where the first value is related to the previous minimisation cycle and the second one related to the current cycle. This difference corresponds to how far in energy the previous system was with respect to the current one. The ΔE so calculated, is then utilised for the calculation of the B_f , taking as temperature a smaller value during each minimisation cycles. The temperature during these cycles, is kept constantly decreasing by a factor α , which is defined by the user, and in each cycle the B_f is calculated considering the new values of T and ΔE . Moving to the selection part, the series of randomised parameters are taken into consideration if the related χ^2 is smaller than the χ^2 of the previous function. If this is the case, the selected parameters describe the experimental system better than the parameters in the previous cycle, and consequently the step is accepted. But if the current cycle results non-accepted, the Boltzmann factor B_f is taken into consideration. If a random number called as r is smaller than the calculated B_f of the current cycle, the step becomes an accepted step, whereas if r is greater than B_f , is

definitely not accepted. This last part of the algorithm permits the skipping of the relative minima of the χ^2 function during the fitting process.

An example of two-parameters simulated annealing analysis is displayed in figure 6.15. The χ^2 is placed on the z-axis and in x and y-axis are the two parameters under examination.

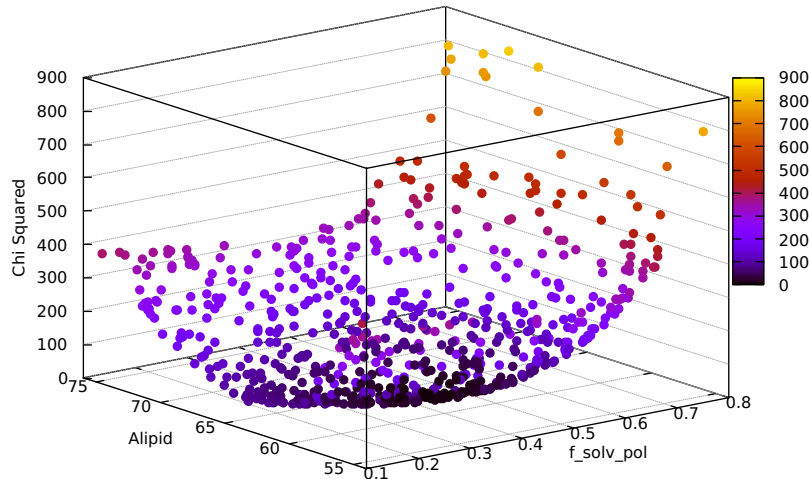


FIGURE 6.15: χ^2 function of a two parameters simulated annealing analysis, where the best values of the two parameters are placed on the minima of this function. Simulated annealing

A good correlation between the two parameters was found, where the minima of the resulted 2D χ^2 function is placed where the parameters assume the values ≈ 65 and ≈ 0.45 for the A_{lipid} and $\phi_{solv\ pol}$. It was seen that at least a number of $1 \cdot 10^3$ iterations are needed in order to obtain a great result. The same plot can be also performed for n number of parameters, resulting in a plot with more than 3 dimensions. A precise way to show this kind of plot is performing a principal component statistics, which was not included in the program.

Once the simulated annealing is performed and the absolute minima of the χ^2 function is found, the second algorithm, based on the steepest descent algorithm (from Scipy python library, `least_squares`), cools down the system, minimising the parameters inside the already found absolute minima.

6.5.2 Error calculation of the fitted parameters

After the minimisation, the errors of the fitted parameters need to be obtained. It is relevant to have this estimation, in order to assess the strength of the model used for the experimental datasets under examination. The principle of this algorithm consists on a slight variation of each fitted parameter by a factor ϵ that in CoruxFit is set by default to $1 \cdot 10^{-4} \cdot P_i$, where P_i is the value of each parameter i . This factor is then summed and subtracted to the same parameter in order to obtain a Min_{P_i} and a Max_{P_i} per fitted parameter. Next, the

theoretical curve calculation is performed using Min_{P_i} and Max_{P_i} , in order to obtain the two theoretical reflectivity profiles per parameter i ($R(q)_{Min_i}$ and $R(q)_{Max_i}$). Next, these profiles per i parameter are used as shown in equation 6.37,

$$\sigma_{P_i q_j} = \frac{R(q_j)_{Max_{P_i}} - R(q_j)_{Min_{P_i}}}{\epsilon_{P_i}} \quad (6.37)$$

where the $\sigma_{P_i q_j}$ is a measure of the deviation per parameter P_i calculated for the point q_j . Next, the Hessian matrix can be calculated as shown in equation 6.38,

$$H(q_j) = \begin{bmatrix} \frac{\sigma_{P_1 q_j}^2}{e_{q_j}^2} & \frac{\sigma_{P_1 q_j} \cdot \sigma_{P_2 q_j}}{e_{q_j}^2} & \dots & \frac{\sigma_{P_1 q_j} \cdot \sigma_{P_n q_j}}{e_{q_j}^2} \\ \frac{\sigma_{P_2 q_j} \cdot \sigma_{P_1 q_j}}{e_{q_j}^2} & \frac{\sigma_{P_2 q_j}^2}{e_{q_j}^2} & \dots & \frac{\sigma_{P_2 q_j} \cdot \sigma_{P_n q_j}}{e_{q_j}^2} \\ \vdots & \vdots & \ddots & \vdots \\ \frac{\sigma_{P_n q_j} \cdot \sigma_{P_1 q_j}}{e_{q_j}^2} & \frac{\sigma_{P_n q_j} \cdot \sigma_{P_2 q_j}}{e_{q_j}^2} & \dots & \frac{\sigma_{P_n q_j}^2}{e_{q_j}^2} \end{bmatrix} \quad (6.38)$$

where e is the experimental error from the reflectivity experimental data and n is the maximum number of parameters. The Hessian matrix is calculated per each point in q (q_j), and the sum of the matrix is performed (equation 6.39, where Nq is the total amount of q points).

$$H = \sum_{q_j}^{Nq} H(q_j) \quad (6.39)$$

Next, the inversion of the matrix is carried out, with the following normalisation as displayed in equation 6.40,

$$H_{norm\ r,t} = \frac{H_{r,t}}{\sqrt{H_{r,r} \cdot H_{t,t}}} \quad (6.40)$$

where the indices r and t describe the position of the element considered. As can be noticed in the matrix (equation 6.38, the diagonal of the matrix is the σ^2 , that corresponds to the variance of each parameter under analysis. This value measures how much the reflectivity profile changes, changing a parameter, in other words, how sensitive the parameter is on the theoretical reflectivity curve variation. From the diagonal of the inverted and not-normalised Hessian matrix, the absolute errors of the fitted parameters can be obtained. From the inverted and normalised Hessian matrix, the covariance between each pair of parameters can be obtained. The covariance is a measure of the correlation between two parameters, and this value is also important to asses the strength of the built model for the experimental data under analysis. In CoruxFit the inverted and normalised Hessian matrix can also be extrapolated, and an example is given in figure 6.16. The figure shows all the parameters that a user can fit for a lipid bilayer. The value 1 corresponds to the positive correlation, where if one parameter increases, the positively correlated one also increases, vice versa for negative values. It can be noticed as the diagonal (from the left-bottom to the top-right corner) the correlation is 1, since the correlation of one parameter with itself is always one. The correlation of other parameters vary along the matrix, and the result of this matrix is often important to improve

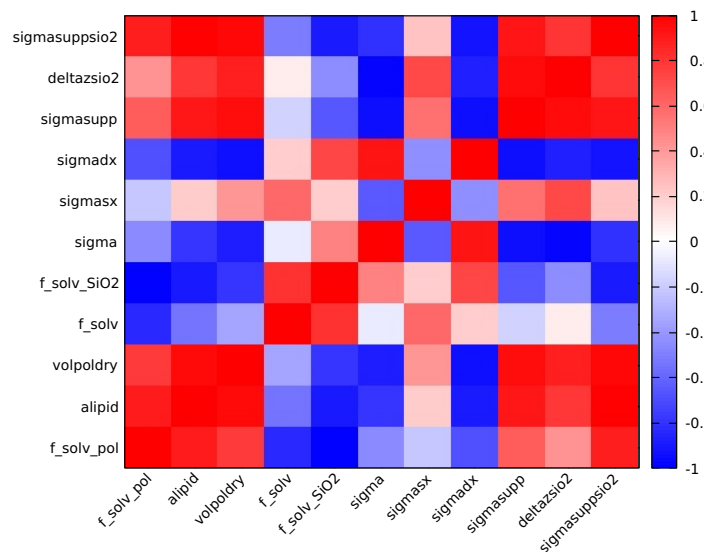


FIGURE 6.16: Example of a Hessian matrix from a CoruxFit analysis

the model and the analysis. For instance, in this example, the amount of water in the silicon oxide of the support is strongly negative correlated with the hydration water of the polar head region. In fact, since the two region are close, in one of the two leaflets, the hydration of one component can be affected by the other one. And many other of these correlations can be obtained. In order to asses the real correlations between parameters, it is important to fix some of these parameters, repeating the analysis, comparing the previous result with the current one, to keep improving the model for the experimental datasets under examination.

6.6 Software description

6.6.1 Installation of CoruxFit

In order to use the program, python3 needs to be installed, along with Gnuplot and Emacs (text editor, not mandatory but recommended). If you are a Windows user, all the three need to be added in your computer "environmental variables". Once the first step is done, CoruxFit can be downloaded. The program needs to be placed in a directory with all the other ".py" scripts that the main program uses. The program after the first run, will write several other scripts and files in the same directory, so it is recommended to place everything in a dedicated folder. The file "parameters.py" can also be moved out from this path, since it will be called back from the "global_par.py". For instance, the user can create three different directories, the first one is where the main program is, the second is where the file "parameter.py" is placed where also other files will be written (as explained later) and finally a directory for the experimental data. The libraries that need to be installed for the program are following listed:

- Numpy - This library is used by the program for the import of the experimental data as python arrays, and to make and handle 2D arrays;

- Scipy - This library is used for the data minimisation, one of the two algorithms that the program uses for the data minimisation (steepest descent algorithm, least squares);
- PyGnuplot - It is used for the data plotting after simulation or fit;
- Rich - To improve the graphics in the terminal;
- Colored - For colored text in the terminal.

All those libraries can be installed using from the terminal the command "pip install X" where "X" is the name of the library.

6.6.2 Data analysis with CoruxFit

The command prompt (terminal) of your OS needs to be opened where "*CoruxFit.py*" is collocated. At this point, to open the global parameter file, the string "*runemacs global_par.py*" for Windows system or "*emacs global_par.py &*" for Unix systems can be used. Inside this file a list of global parameters can be found:

- The path where the "parameters.py" file for the experiment is placed;
- the Gnuplot terminal ("qt" or "win" if your system is Unix or Windows respectively);
- the minimum variation of the chi-square to get the result of the fit (for the steepest descent algorithm minimisation);
- all the parameters for the simulated annealing optimisation algorithm;
- switcher for the q resolution (1/0);
- z resolution for the SLD profile treatment (dz);
- the q limit (Max_q);
- monolayer model switcher;
- list of parameters to be fitted;
- some graphical parameters, such as: dark mode, log(x) switcher,...

In the parameter file "*parameters.py*" the following listed parameters can be defined:

- list of experimental curves with the respective % amount of deuterated water in the bulk solution;
- the path where the experimental data are;
- job title and names of the exported files;
- all the parameters for the modeling of the sample.

Once all those parameters are defined, the simulation or the fit can be started. The principal command to control the program is the following: "*python CoruxFit.py X Y*", where the "*X*" is a switcher (0 or 1), where 0 is simulation of the system and 1 is the fit; "*Y*" parameter is a second switcher to disable (0) or enable (1) the plot windows at the end of the process of simulation or fit. For example the string "*python CoruxFit.py 0 1*" is going to simulate the system using the parameters inserted in the parameter file, with the final plot. The simulation takes anyway the experimental data to get the *q*-range, and it uses the parameters given as input in the "parameters.py" file. The final plot at the end of the process is a multiplot window from the Gnuplot program, and it is divided into 4 windows as displayed in figure 6.17. The

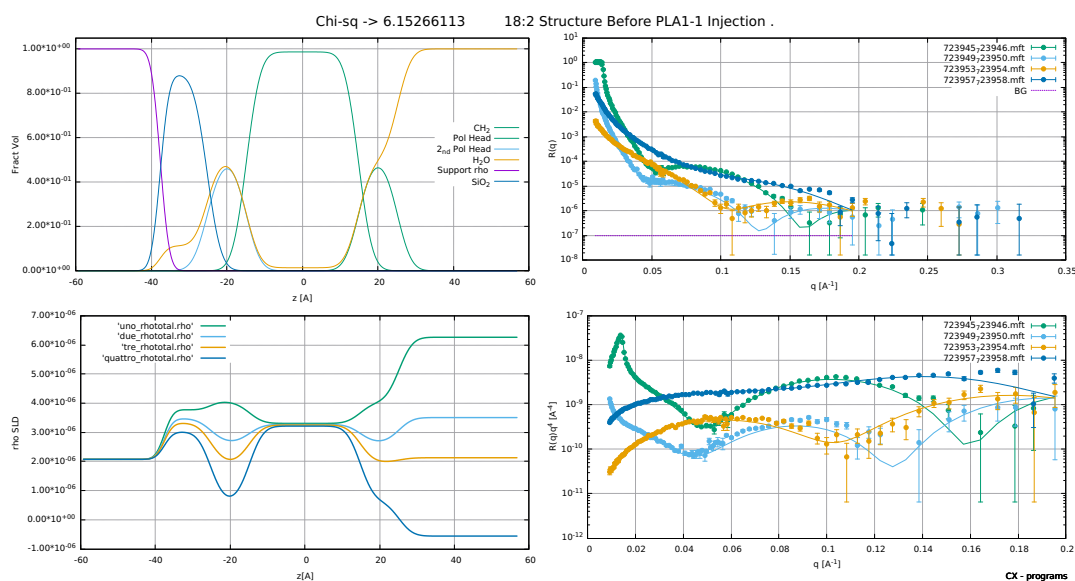


FIGURE 6.17: Raw plot from CoruxFit

first one is the fraction volume model, the second one the reflectivity curves (theoretical and experimental) in $R(q)$ scale, the third window is the calculated SLD profile of the sample and in the last window is displayed the reflectivity curves in $R(q) \cdot q^4$ scale. All the parameters and theoretical calculations are written in ASCII files, and they can also be plotted with external programs. On the top of the window, the χ^2 of the simulation or fit is displayed as well as the title of the job taken from the "parameter.py" file. The residuals plot window is also displayed at the end of the process, which is fundamental to assess how much the theoretical deviates from the experimental curve. With the command "*python CoruxFit.py 1 1*", the fit starts, using as minimisation algorithms the ones specified on the "global_par.py" file. The time of the process depends on the power of the processor, its number of cores and on the number of datasets under analysis. During the minimisation process the data are not written on the disk, in order to avoid any bottleneck during this process, since the Parratt and the *q* Resolution algorithm are already taking together almost 100% of the power of one core processor. If the kinetics plug-in for phospholipases is used, a third plot windows appears, showing the degradation plots obtained from the model. The Hessian matrix can also be plotted using gnuplot, for this purpose a gnuplot script is written at the end of the process by

the main program, and it can be loaded directly in the terminal window as follows: "gnuplot plot_Hess2.crx". All the files from the model, the SLD profiles, the theoretical curves and all the scripts are written at the end of the process into the directory where the main program is placed. Also the "final_parameters*" files are saved, where all the final parameters with the resulted absolute errors are written. One of these two files is a latex file, and it can be loaded directly inside a ".tex" file to have directly the table of parameters. At the end of a simulation, in the terminal some parameters can be already seen, as displays the figure 6.18. The program also gives an error panel in case any errors had occurred during the process, and

```

coruccilocal@coruccilnx: ~/Desktop/PLA1-1_Neutron_data
File Edit View Terminal Tabs Help

Chisquare cum uno : 2.347911737999257
Chisquare cum due : 4.2907555075978525
Chisquare cum tre : 5.2302752529704115
Chisquare cum quattro : 6.152661128944688

##### Parameters #####



| Parameter name            | Parameter value        |
|---------------------------|------------------------|
| Model weight =            | 5.574102647474644e-09  |
| dp =                      | 10.353917653036653     |
| d2 =                      | 13.194345218442418     |
| d3 =                      | 3.2597305967436045     |
| volpol =                  | 648.8567798440956      |
| volpar =                  | 929.8080808080801      |
| alipid =                  | 62.66775549            |
| rhoBuno =                 | 6.2661438e-06          |
| rhoBdue =                 | 3.5078957999999995e-06 |
| rhoBtre =                 | 2.1287718e-06          |
| rhoBquattro =             | -5.6052e-07            |
| f solv =                  | 0.01362977             |
| f solv SiO2 =             | 0.11241084             |
| ech2 =                    | 3.267642626480865e-06  |
| ep =                      | 1.8155948819951426e-06 |
| bcpolar =                 | 0.000600720000000001   |
| Total thickness bilayer = | 50.356256339701744     |
| conclip =                 | 3.298043               |
| vlip =                    | 1577.8567798440956     |
| pm =                      | 822.075                |



#####

##### STRUCTURE FACTOR #####
Number of stacking multilamellar: 1
#####

#### SURFACE EXCESS CALCULATION ####
4.298106656385855 mg/(m^2) +/- 0.0
#####

*****For sas*****
Tap "g1" or "gnuplot script.crx" to visualize the F(q) graf
Tap "g2" or "gnuplot script advanced.crx" to visualize the I(q) and others graf
Tap "g3" or "gnuplot script model.crx" to visualize the electron density/SLD of the model
Tap "g4" or "gnuplot script Iq experimental.crx" to visualize the fit

*****For reflectivity*****
Tap "g5" or "gnuplot script Rq experimental.crx" to visualize the fit
Tap "g6" or "gnuplot script Rq_q4" to visualize the fit in R(q)*q^4

cp fit_param.crx /users/coruccilocal/Desktop/PLA1-1_Neutron_data/Figaro_Feb/processed/18-2/fit_param_6_auto.crx
#####
Started ==> Fri Dec 2 17:29:46 2022
Finished ==> Fri Dec 2 17:29:46 2022
Time of calculation ==> 0 h 0 m 0.56 s
#####

Feedbacks simulation/fit:
Simulation went ok, enjoy the result!

*****
CORUX PROD
# Programs #
*****
>> END PROCESS
coruccilocal@coruccilnx:~/Desktop/PLA1-1_Neutron_data$

```

FIGURE 6.18: CoruXFit terminal at the end of the simulation

also suggestions on the commands for the visualisation of the data are given. A similar table of the parameters is also printed during the fitting, where the user can follow directly how the parameters changes over the minimisation as well as the χ^2 and other factors of the fit.


```
    return

def cal(i):
    #the result of the calculation is returned and printed
    import numpy as np
    print(i)
    return i

def global_par():
    #the command opens the global parameters
    import os
    command = "emacs global_par.py &"
    os.system(command)
    return

def save():
    #the command save all the output parameters in the proper folder
    import os
    from global_par import par_path
    command = "cp *final_parameters* " + par_path
    os.system(command)
    return
```

There are already some functions defined, and more functions can be defined in order to speed up the analysis with CoruxFit. For instance, in order to save everything after the analysis in a wanted directory, the command "save()" can also be used. Every time that a modification in this file is carried out, the command "reboot()" needs to be called in order to load the changes made. Calculations and definition of equations and functions can be also done directly into the CoruxFit terminal windows, with the python syntax (for instance $\sin(x)$ is defined using `numpy as np.sin(x)`).

6.7 Summary of the program

CoruxFit is a python program developed for reflectivity data simulation and analysis. CoruxFit is an open-source program, that can be modified by the user in order to create new models, or add new features. For the moment, the program works only in the terminal window, giving directly in the terminal, information on the simulation and fit with a quite clear graphics. The models available in CoruxFit for the moment are following listed: (1) lipid bilayers, (2) lipid monolayers, (3) membrane - protein/molecule interaction, (4) membrane - transmembrane protein interaction and finally (5) kinetics plug-in for membrane-phospholipase interaction. Once the modeling is carried out, the SLD profile is calculated and treated by the Parratt algorithm in order to obtain the theoretical reflectivity profiles. To fit the data, two minimisation algorithms are used; (1) the simulated annealing, as a first step, probes the χ^2 function along all the fit parameters, in order to find the absolute minima of the function; (2) steepest descent based algorithm from the Scipy library, where within the absolute minima it finds the

best series of parameters. At the end of the process of simulation or fit, the program plots every result using gnuplot. CoruxFit also writes at the end scripts and other files in order to plot the data using different software and to achieve the minimised parameters.

6.7.1 Future developments of CoruxFit

There are several points where the program needs to be improved and modified, in order to be easily used by the user. Firstly, changes need to be done to the CoruxFit environment. This point is really important as interface between the program and the user, since and it will simplify the use of it. I had just started working on this part, and since it is very young, still a certain amount of work needs to be done. At the moment this environment works only on Unix systems, but it will be soon translated also for Windows systems.

A second and important point is related to the speed of the program. Unfortunately, the way the program treats the SLD profiles and because of the Parratt and the q resolution algorithm, with a normal processor such as the Intel i5, a simulation a time of 0.25 second is needed per each dataset to calculate the theoretical reflectivity profile. During a fit with the simulated annealing method of a system with 4 different SLD profiles, the required time for the algorithm to reach a result can sometimes be very large. For that, a multiprocessing/multithreading method would be a reasonable way to improve the speed of the program. A computer processor is constituted by different cores, and each core can process one thread. CoruxFit 2.0 can unfortunately, for now, be processed only with one core, without utilising the full power of the processor. For instance taking an i5 8-cores and an i9 18-cores, the speed of the program is not significantly different, since the full power of the processor is not utilised in its 100%, but only in a fraction N of it, where N is the number of cores. The idea of the multiprocessing/multithreading is based on sending each calculation of the theoretical reflectivity from each SLD profile, to each of the cores available in the processor. In this configuration, the simulation process takes as long as it would take processing only one SLD profile, compressing the time of minimisation by a factor X , where X is the number of datasets loaded. This part is ongoing, and since the multiprocessing mode is not easily integrable in the program, it will take some time to be ready for use.

A third important point that is now ongoing, is related to the installation of the program. Since for now, the main program works much faster on Unix systems, and the CoruxFit environment only works for now in Unix, the idea of building a server would be a good compromise. Consequently, a server based on Raspberry was built as a first server, in order to assess the feasibility of the project. The server shown in Appendix A.7, is accessible through the *ssh* protocol, also from devices outside the local network (using an external IP address). The Raspberry in use has a 4-core processor with 8-Gb of RAM, where raspbian OS is installed. Every operative system can be connected to the server through this protocol, even Android smartphones using a proper android SSH client app. Since the server connection is an *ssh* protocol, no graphical interface is available, and the user, in order to plot and see the fitted data, has to download them and plot them directly in its own computer.

Chapter 7

Other open access programs

During the PhD, other python programs were designed and optimised in order to facilitate the extrapolation of the data from the different instruments utilised.

7.1 Mass spectrometry program - for MS hydrolysis kinetics

Mass spectrometry analyses were performed in order to obtain information on the substrate preferences of the PLA1-1 under analysis. Python programs were designed in order to treat the data. Data emanating from the mass spectrometry were initially treated using MassHunter software, where the TIC integration was performed to achieve the related spectra. Next, the spectra background subtraction were performed using the same program. Next, spectra were exported and a step 0 python program was written and employed in order to convert the exported data into different ASCII files ".txt", readable from the step 1 program. The converted spectra are subsequently treated by the step 1 program, that consists on the average of the replicates taken during the MS measurements (technical replicates). Each m/z point in the spectra is averaged between replicates (2 or 3) taken from the same samples. The error is then calculated as standard deviation using the formula displayed in equation 7.1,

$$I_{err} = \sqrt{\sum_{n=1}^N (I_n - I_{ave})^2} \quad (7.1)$$

where I_{err} is the error of the averaged signals; N is the total number of spectra averaged, I_n is the spectra n ; and I_{ave} is the averaged spectra. After this process, an averaged spectra is obtained where each point has an error which corresponds to its standard deviation. Next, the second step python program was utilised, consisting on the (1) normalization and the (2) integration of the peaks. The normalization (1) is performed taking into account the signal of the SM 24:0, that was added into the lipid mixtures as an internal standard, since the phospholipase under examination is not able to hydrolyse SM molecules. Firstly, the area under the SM peak is taken from the first sample as displayed in equation 7.2,

$$A = \sum_{n=l}^L I_n \quad A_{err} = \sqrt{\sum_{n=l}^L I_{err_n}^2} \quad (7.2)$$

where A is the area under the peak (integrated value of the peak); l and L is the lower and upper limit of the integration range; n is the m/z value, where I_n is the intensity of the spectra at a particular n value; A_{err} is the error calculated for the area under the peak; and finally I_{err_n} is the error previously calculated from equation 7.1 for a specific n value. The minimum and maximum of the integration range (l and L) is given directly into the parameter file that the program utilised to obtain information on the ongoing analysis. Next, the program integrates the area of the SM for all the other samples (time points), calculating the ratio factor by dividing the first sample SM area by the area of each sample. Once the ratio factors are calculated for each time point, the program multiplied each spectra with its calculated ratio factor. The spectra so normalised, are then saved as ".txt" files. The second part of the same program consists on the (2) peak integration. In the parameter file, a list of the expected lipids in the sample under examination is built, where their name, limits of integration and the related lysos are described. The program takes this information, for the peak integration. Every peak of each spectra per sample is integrated, and the values saved. In order to find the degradation profile of the kinetics, the first area values are used as dividing factors for the same peaks in the other samples. Consequently, a degradation profile can be obtained, where values near to 1 corresponds to no degradation occurring. The values at the end of the calculation are saved into a ".dat" file. A third step python program was designed in order to fit the data emanating from the second step just described. This third step is a fitting program, where two models can be used for the analysis. The first model built is the sigmoidal model, and the second the exponential decay model. The sigmoidal model was designed first, since a lag phase was expected. The model is shown in equation 7.3,

$$f(t) = -\frac{\exp(t \cdot \sigma + \epsilon)}{1 + \exp(t \cdot \sigma + \epsilon)} \cdot e_r + 1 \quad (7.3)$$

where t is time; σ is the slope of the function; ϵ is the x-translation of the flex of the sigmoidal function (along the time axis); and finally e_r is the degradation at the end of the reaction. The exponential decay model was then designed, since no lag phase was observed in the data under examination. The model is shown in equation 7.4,

$$f(t) = (1 - e_r) \cdot \exp(-\sigma \cdot t) + e_r \quad (7.4)$$

where e_r corresponds to the amount of degradation at the end of the reaction; σ is the rate constant of the exponential; and t is the reaction time measured in minutes. From the equation 7.4, the speed of the reaction (rate constant) as well as the amount of lipids at the end of the reaction (when the reaction plateau) can be obtained. The starting parameters, if the analysis is performed for the first time, are taken directly from the same parameter file taken for the normalization and integration of the spectra (from the previous python step program). The fitted parameters are then saved into a ".dat" file, in the same directory where the raw data are placed. Simulations can also be run using this program, where the fitted parameters can be changed by hand. The minimization algorithms used for the fitting of the experimental point

with the theoretical model, are the simulated annealing and the steepest descent. Those two algorithms are extensively described in the Chapter 6. The first algorithm is used to avoid relative minima, whereas with the second one the system is cooled down even more, leading to the obtainment of the minimised parameters. All the analysis displayed in the Results section, were analysed by using the exponential decay model.

7.2 GCMS and MS peak integration program

The GCMS and MS peak integration program, is similar to the second step python program described in the previous section. In this case, only the limits of the integration are set in a parameter file, and the areas under the peaks are calculated. This python program has been utilised for the integration of the GCMS peaks, in order to obtain the relative abundance of each of the FAMES in the sample under examination. The calculation of the relative abundance was carried out dividing each peak area for the total peak areas, obtaining the data shown in the results section.

7.3 BAM image recognition

A python program based on the image recognition (using openCV library) was written in order to analyse the Brewster Angle Microscopy images. As parameters the program needs the directory where the ".png" files are, a description of the experiment used then to save the calculated parameter of the entire experiment in a ".csv" file and a threshold for the detection of the spots. This last point is quite sensitive and needs to be optimized in order to get the right balance between noise and data. The program treated all the images in one shot, taking around 1 second per image. For each picture the program generates another picture in multiplot configuration, where the raw image and the processed one are placed near to the other, to facilitate the comparison (for the threshold adjustment for instance) figure 7.1.

The ".csv" file created at the end of the process, contains the spot parameters found by the program for all the images treated. The spot parameters are listed following:

- File name;
- Number of spots;
- Total spots area;
- Total image area;
- Ratio areas;
- Average area per spot.

From those parameters the graphs in figure 7.2 can be plotted.

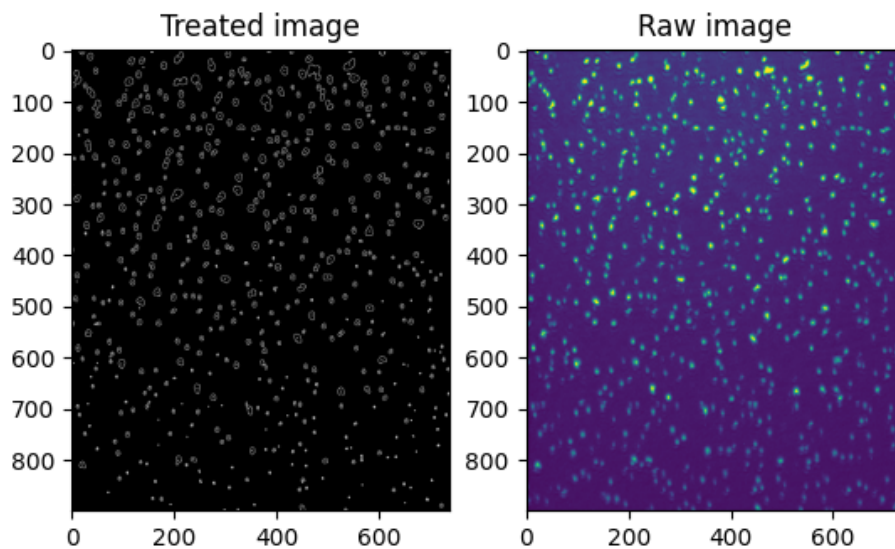


FIGURE 7.1: Output image from the program, where it is possible to compare the raw image with the treated one.

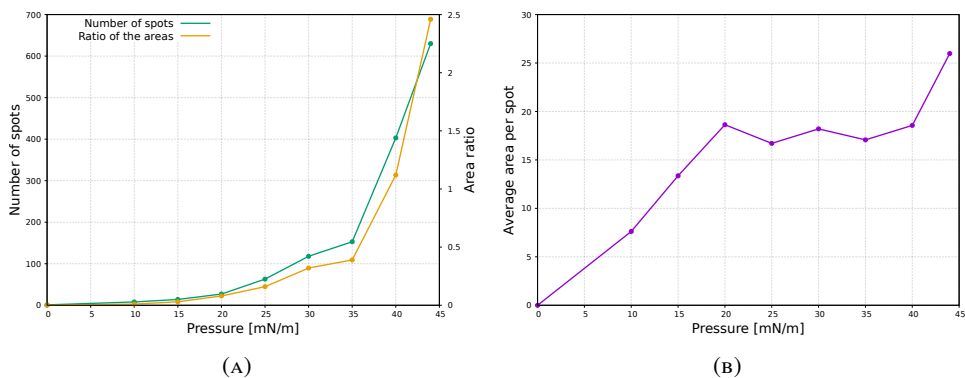


FIGURE 7.2: Examples of graphs from the parameters found by the program on BAM pictures. In figure A is plotted the number of spots and the ratio total area of the spots/ area of the BAM picture vs pressure; in figure B the averaged area per spot vs pressure

Appendix A

Appendix

A.1 Stock solution concentration

Chemical	Symbol	Storage	Usage
Ampicillin	AMP	100 mg · ml ⁻¹	0.1 mg · ml ⁻¹
Chloramphenicol	CLO	54 mg · ml ⁻¹	0.054 mg · ml ⁻¹
Isopropyl- β -D-1-galactopyranoside	IPTG	1 M	1 mM

TABLE A.1: Storage and usage concentrations of the chemicals for the protein expression

A.2 Nucleotide and amino acid sequences for MBP - PLA1-1

A.2.1 Nucleotide sequences

The capital letters correspond to the PLA1-1 sequence, and the capital ATG is the main starting codon.

MBP-PLA1-1

ATGaaatcgaagaaggtaaactggaatctggattaacggcgataaaggctataacggctcgcgtaagtcggaagaattcg
 agaaagataccggaattaaagtcaccgttgagcatccggataaactggaagagaaattcccacaggttgcggcaactggcgatgg
 ccctgacattatcttctgggcacacgaccgcttgggtggctacgctcaatctggcctgttgctgaaatcaccgccgacaaagcgttc
 caggacaagctgatccgtttacctgggatgccgtacgttacaacggcaagctgattgcttaccgatcgtgtgaagcgttatcgc
 tgattataacaaagatctgctgccgaaccgccaaaaaacctgggaagagatccggcgctggataaagaactgaaagcgaag
 gtaagagcgcgctgatgtcaacctgcaagaaccgtacttcacctggccgctgattgctgctgacgggggttatgcttcaagtatg
 aaaacggcaagtacgacattaaagacgtggcgctggataacgctggcgcaagcgggtctgaccttctggtgacctgattaa
 aaacaacacatgaatgcagacaccgattactccatcgagaagctgccttaataaaggcgaacagcgtgacctcaacggc
 ccgtgggcatggtccaacatcgacaccagcaagtgaaattatggtgtaacggctactgccgacctcaagggtcaacctcaaac
 gttcgttggcgtgctgagcgcaggtattaacgccccagctccgaacaaagagctggcaaaagagtctcctcgaaaactatctgctga
 ctgatgaagctggaagcgggtaataaagacaaaccgctgggtgccgtagcgtgaaagtcttacgaggaagagttggcgaaga
 tccacgtattgccccactatgaaaacgccagaaaggtgaaatcatgccgaacatcccgcagatgtccgcttctggtatgccgt
 gcgtactcgggtgatcaacgccgccagcggctcgtcagactgtcgtgatgaagccctgaaagacgcgcagactaattcgagctcgaac

aacaacaacaataacaataacaacaacctcgggatcgaggaaggatttcagaattcGGATCCGCCCGGCTTCA
CTGCGCAGAGATGTCAGCTCTTCCCTTCTCAATAACCTGGATCTCTTTGCACAGT
ACAGCGCCGCCGCATACTGTGATGAGAACCTGAACTCTACGGGGACCAAGTTG
ACATGCTCTGTTGGCAACTGTCCTTTGGTAGAAGCGGCCTCTACCCAATCATTG
GATGAATTCAACGAATCGTCATCCTACGGCAACCCCGCCGGGTACCTCGCCGCT
GATGAGACTAACAAGCTCCTAGTCCTGTCCTTCCGGGGTAGCGCTGACTTGCC
AATTGGGTCGCCAACCTGAATTTTGGTCTCGAGGATGCCAGCGATCTGTGTTCT
GGGTGCGAAGTGCACAGCGGCTTCTGGAAGGCATGGAGTGAAATCGCCGACAC
CATCACTTCCAAAGTGGAATCAGCTTTGTCTGGATCATTCCGATTATTCTTGGTC
TTGACCGGACATAGTTACGGCGCTGCGCTGGCAGCCCTCGCAGCGACTGCTCTG
CGGAACTCCGGCCATAGTGTGAGCTGTACAACCTACGGTCAACCTCGACTTGGA
AACGAGGCATTGGCAACATATATCACGGACCAAACAAGGGTGGCAACTATCG
CGTTACGCACACTAATGATATTGTGCCTAACTGCCACCCACGCTGCTCGGGTA
TCACCACTTCAGCCCAGAGTACTATATCAGCAGCGCCGACGAGGCAACGGTGA
CCACCACTGATGTGACTGAGGTTACGGGAATCGATGCTACGGGCGGTAATGAT
GGAACCGACGGAAGTACATCGATGCTCATCGGTGGTACTTTATTTATATTAGC
GAATGTTCATAG

PLA1-1

GCCCGGCTTCACTGCGCAGAGATGTCAGCTCTTCCCTTCTCAATAACCTGGAT
CTCTTTGCACAGTACAGCGCCGCCGCATACTGTGATGAGAACCTGAACTCTACG
GGGACCAAGTTGACATGCTCTGTTGGCAACTGTCCTTTGGTAGAAGCGGCCTCT
ACCCAATCATTGGATGAATTCAACGAATCGTCATCCTACGGCAACCCCGCCGGG
TACCTCGCCGCTGATGAGACTAACAAGCTCCTAGTCCTGTCCTTCCGGGGTAGC
GCTGACTTGCCAATTGGGTCGCCAACCTGAATTTTGGTCTCGAGGATGCCAGC
GATCTGTGTTCTGGGTGCGAAGTGCACAGCGGCTTCTGGAAGGCATGGAGTGA
AATCGCCGACACCATCACTTCCAAAGTGGAATCAGCTTTGTCTGGATCATTCCGA
TTATTCTTGGTCTTGACCGGACATAGTTACGGCGCTGCGCTGGCAGCCCTCGC
AGCGACTGCTCTGCGGAACTCCGGCCATAGTGTGAGCTGTACAACCTACGGTCA
ACCTCGACTTGAAAACGAGGCATTGGCAACATATATCACGGACCAAACAAGG
GTGGCAACTATCGCGTTACGCACACTAATGATATTGTGCCTAACTGCCACCCA
CGCTGCTCGGGTATCACCACTTCAGCCCAGAGTACTATATCAGCAGCGCCGACG
AGGCAACGGTGACCACCACTGATGTGACTGAGGTTACGGGAATCGATGCTACG
GGCGGTAATGATGGAACCGACGGAAGTACATCGATGCTCATCGGTGGTACTT
TATTATATTAGCGAATGTTCATAG

A.2.2 Amino acid sequences

MBP-PLA1-1

MKIEEGKLVWINGDKGYNGLAEVGGKFEKDTGIKVTVEHPDKLEEKFPQVAATG
DGPDIIFWAHDRFGGYAQSGLLAEITPDKAFQDKLYPFTWDAVRYNGKLIAYPIAV
EALSLIYNKDLLPNPPKTWEEIPALDKELKAKGKSALMFNLQEPYFTWPLIAADGG
YAFKYENGKYDIKDVGVNDAGAKAGLTFLVDLIKHKHMNADTDYSIAEAAFNKG
ETAMTINGPWAWSNIDTSKVNYGVTVLPTFKGQPSKPFVGVLSAGINAASPNKELA
KEFLENYLLTDEGLEAVNKDKPLGAVALKSYEEELAKDPRIAATMENAQKGEIMP
NIPQMSAFWYAVRTAVINAASGRQTVDEALKDAQTNSSSSNNNNNNNNNNNLGIEGR
ISEFGSAPASLRRDVSSSLLNLDLFAQYSAAAYCDENLNSTGKLTCSVGNCPLE
AASTQSLDEFNESSYGNPAGYLAADETNKLLVLSFRGSADLANWVANLNFGLED
ASDLCSGCEVHSGFWKAWSEIADTITSKVESALSDHSDYSLVLTGHSYGAALAALA
ATALRNSGHSVELYNYGQPRLGNEALATYITDQNKGGNYRVTHHTNDIVPKLPPTLL
GYHHFSPEYYISSADEATVTTTDTVTEVTGIDATGGNDGTDGTSIDHRWYFIYISEC
S

PLA1-1

ISEFGSAPASLRRDVSSSLLNLDLFAQYSAAAYCDENLNSTGKLTCSVGNCPLE
AASTQSLDEFNESSYGNPAGYLAADETNKLLVLSFRGSADLANWVANLNFGLED
ASDLCSGCEVHSGFWKAWSEIADTITSKVESALSDHSDYSLVLTGHSYGAALAALA
ATALRNSGHSVELYNYGQPRLGNEALATYITDQNKGGNYRVTHHTNDIVPKLPPTLL
GYHHFSPEYYISSADEATVTTTDTVTEVTGIDATGGNDGTDGTSIDHRWYFIYISEC
S

A.2.3 Deconvolution of the gel filtration chromatogram

The gel filtration chromatogram displayed in the result section in figure 3.4, was deconvoluted using 5 gaussian function. The UV intensity of the peak that corresponds to the MBP - PLA1-1 (from 71 ml to 79 ml) was integrated as well as the theoretical gaussian curve found for the same peak. The ratio of the two area was performed, obtaining a value of 96.3% of purity, were the 3.7% is the contamination from the two gaussian curves before and after. In figure A.1 is shown the deconvolution of the gel filtration.

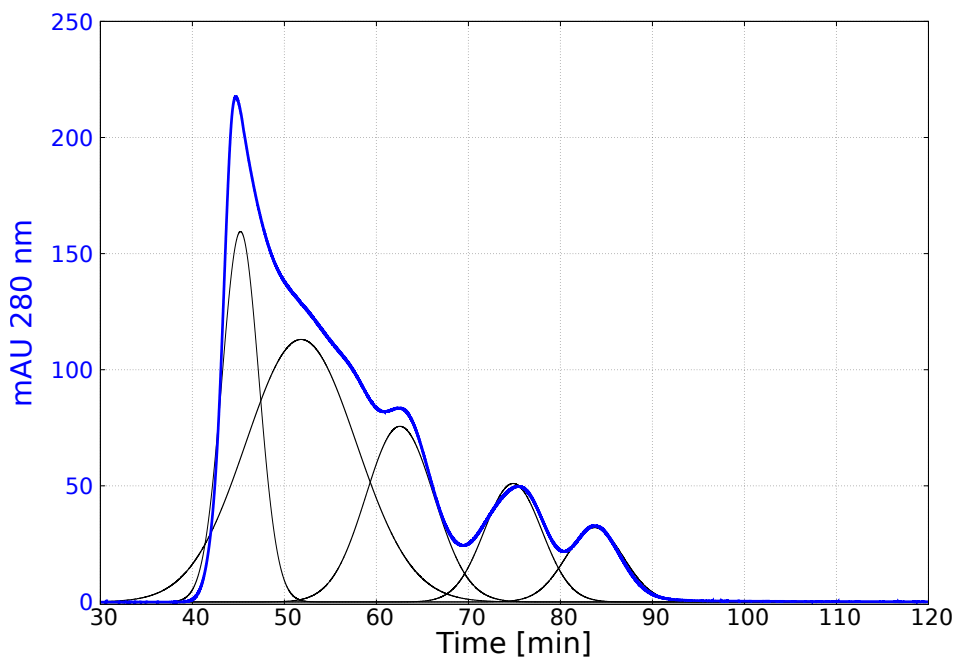


FIGURE A.1: Gaussian deconvolution of the gel filtration chromatogram displayed in figure 3.4 in Chapter Results.

A.3 GC-MS peaks identification table

RT (min)	FAME	m/z
14.34	16:1	268.3
14.74	16:0	270.4
16.05	17:1	282.2
16.46	17:0	284.2
17.74	18:2	294.3
17.89	18:1	296.3
18.27	18:0	298.3
23.18	21:0	340.4
30.74	25:0	396.4

TABLE A.2: GC-MS retention time of the found FAMEs

A.4 Pictures of used equipment

A.4.1 NR cells - Pictures and description

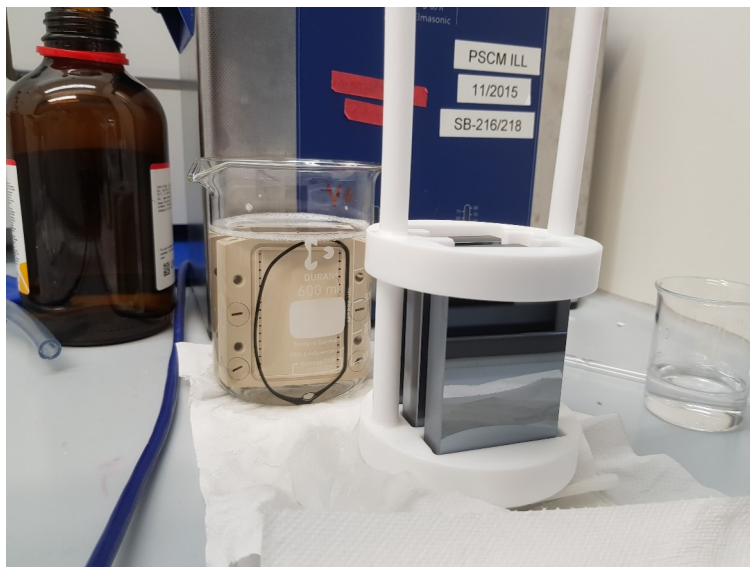


FIGURE A.2: Picture representing the PEEK cells and the silicon crystals used in NR experiments

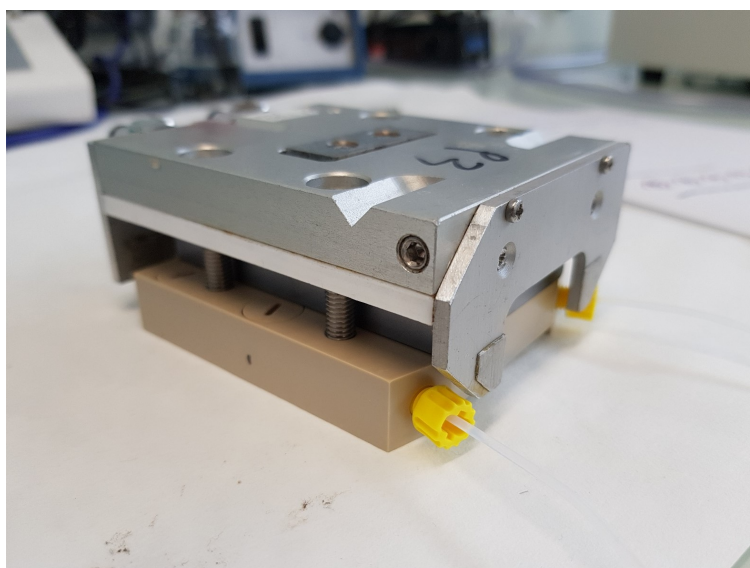


FIGURE A.3: NR cell

A.4.2 Langmuir troughs

Langmuir troughs for the preparation of bilayers from synthesised saturated partially deuterated PC molecules.

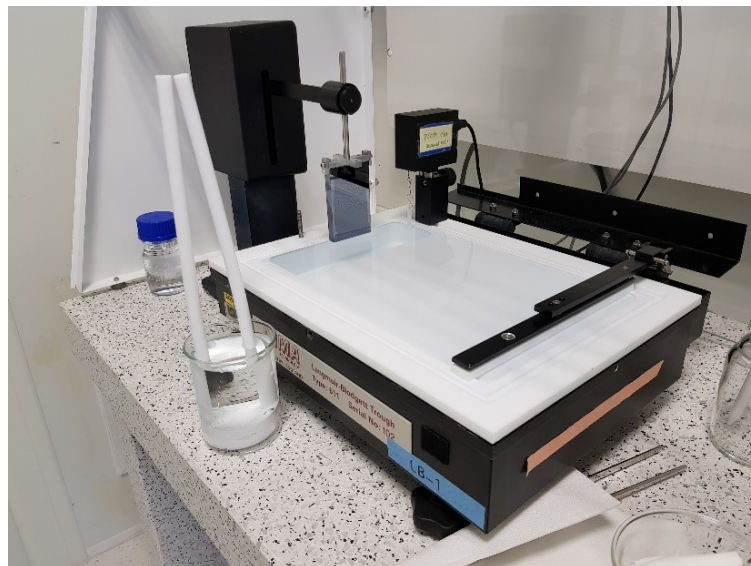


FIGURE A.4: Trough Nima, used for the first leaflet deposition

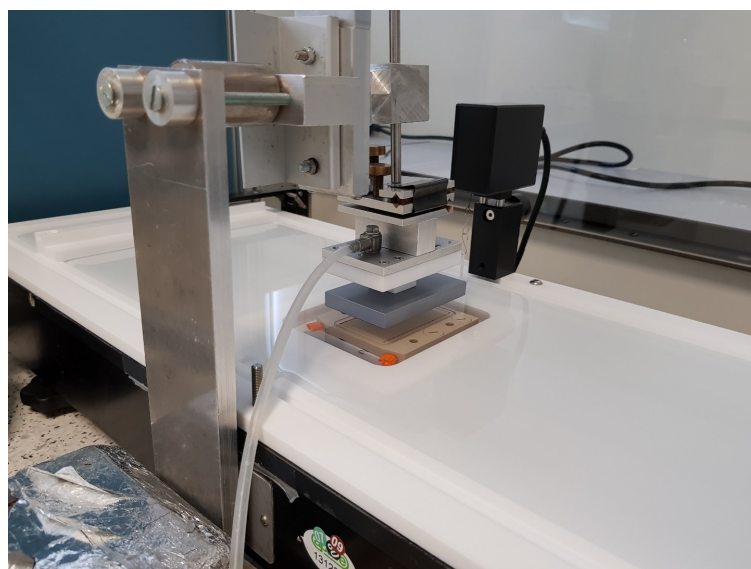


FIGURE A.5: Trough Nima, used for the second leaflet deposition

A.4.3 Ellipsometry cell

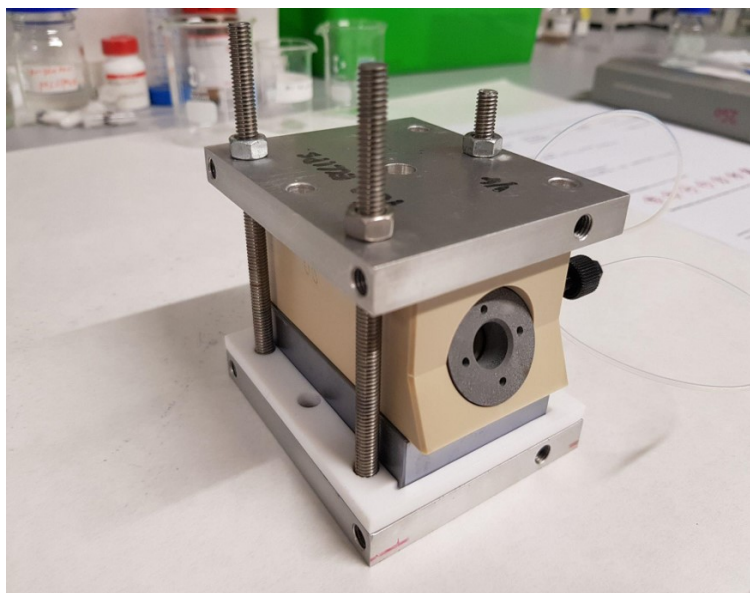


FIGURE A.6: Ellipsometry cell, used to assess the amount of protein needed for NR experiments

A.5 NR fitted parameters

A.5.1 Natural lipids

Parameters	PC		PC/PS		PC/PG	
	Hydrogenous	Deuterated	Hydrogenous	Deuterated	Hydrogenous	Deuterated
Thickness polar head [\AA]	9 ± 1	10 ± 1	10 ± 1	9 ± 1	9 ± 1	10 ± 1
Thickness par layer [\AA]	15 ± 1	14 ± 1	15 ± 1	15 ± 1	15 ± 1	15 ± 1
Total thickness bilayer [\AA]	46 ± 1	48 ± 1	49 ± 1	49 ± 1	48 ± 1	51 ± 1
Polar head vol dry [\AA^3]	319 ± 15	319 ± 14	307 ± 10	307 ± 13	312 ± 17	312 ± 17
Par volume [\AA^3]	941	951	940	948	941	959
Alipid [\AA^2]	64 ± 1	66 ± 1	64 ± 1	62 ± 1	62 ± 1	62 ± 1
ϕ_{Heads}	$46\% \pm 2\%$	$57\% \pm 2\%$	$53\% \pm 2\%$	$46\% \pm 2\%$	$49\% \pm 2\%$	$51\% \pm 3\%$
ϕ_{Tails}	$4.4\% \pm 0.6\%$	$6\% \pm 1\%$	$0.8\% \pm 0.6\%$	$0.7\% \pm 0.7\%$	$6.3\% \pm 0.7\%$	$1\% \pm 1\%$
SLD par [\AA^{-2}]	-0.16	6.60 ± 0.03	-0.17	6.53 ± 0.03	-0.15	6.80 ± 0.03
SLD polar head [\AA^{-2}]	1.88	7.40 ± 0.05	2.12	7.24 ± 0.03	2.06	7.39 ± 0.03
Γ [$mg \cdot m^{-2}$]	4.15 ± 0.04	3.99 ± 0.05	4.30 ± 0.03	4.48 ± 0.04	4.21 ± 0.05	4.45 ± 0.06

TABLE A.3: Fitted parameters of the SLBs containing different mixtures of natural lipids.

A.6 CoruxFit raspberry server



FIGURE A.7: Raspberry server

And... as figure A.8 shows, this is the end of the thesis. Thank you for coming this far and I hope you enjoyed it in all its facets and found it interesting and exciting at the same time!

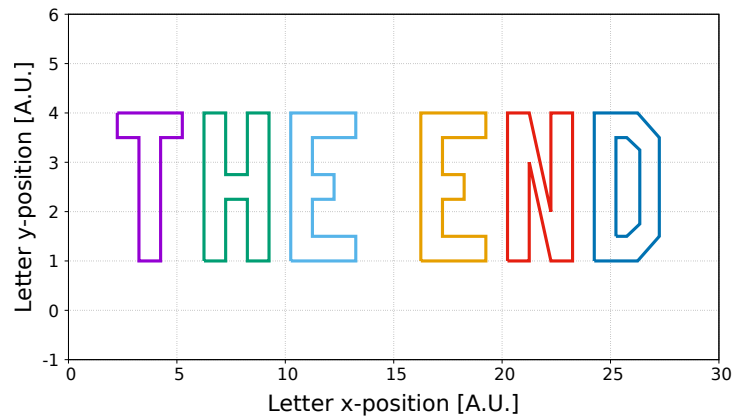


FIGURE A.8: "The end" graph

Bibliography

- [1] MA De Matteis and A Godi. “Protein–lipid interactions in membrane trafficking at the Golgi complex”. In: *Biochimica et Biophysica Acta (BBA)-Biomembranes* 1666.1-2 (2004), pp. 264–274.
- [2] Kathleen M Eyster. “New paradigms in signal transduction”. In: *Biochemical pharmacology* 73.10 (2007), pp. 1511–1519.
- [3] Steven H Zeisel. “Choline phospholipids: signal transduction and carcinogenesis.” In: *FASEB journal: official publication of the Federation of American Societies for Experimental Biology* 7.6 (1993), pp. 551–557.
- [4] Richard PH Huijbregts, Lora Topalof, and Vytas A Bankaitis. “Lipid metabolism and regulation of membrane trafficking”. In: *Traffic* 1.3 (2000), pp. 195–202.
- [5] Takeshi Harayama and Howard Riezman. “Understanding the diversity of membrane lipid composition”. In: *Nature reviews Molecular cell biology* 19.5 (2018), pp. 281–296.
- [6] Gerrit van Meer and Anton IPM de Kroon. “Lipid map of the mammalian cell”. In: *Journal of cell science* 124.1 (2011), pp. 5–8.
- [7] Andrej Shevchenko and Kai Simons. “Lipidomics: coming to grips with lipid diversity”. In: *Nature reviews Molecular cell biology* 11.8 (2010), pp. 593–598.
- [8] Gerrit Van Meer, Dennis R Voelker, and Gerald W Feigenson. “Membrane lipids: where they are and how they behave”. In: *Nature reviews Molecular cell biology* 9.2 (2008), pp. 112–124.
- [9] Jean E Vance and Dennis E Vance. “Phospholipid biosynthesis in mammalian cells”. In: *Biochemistry and cell biology* 82.1 (2004), pp. 113–128.
- [10] Rineke Steenbergen et al. “Disruption of the phosphatidylserine decarboxylase gene in mice causes embryonic lethality and mitochondrial defects”. In: *Journal of Biological Chemistry* 280.48 (2005), pp. 40032–40040.
- [11] Limin Wang et al. “Early embryonic lethality in mice with targeted deletion of the CTP: phosphocholine cytidyltransferase α gene (*Pcyt1a*)”. In: *Molecular and cellular biology* 25.8 (2005), pp. 3357–3363.
- [12] Jinjin Cai et al. “Diacylglycerol kinases as sources of phosphatidic acid”. In: *Biochimica et Biophysica Acta (BBA)-Molecular and Cell Biology of Lipids* 1791.9 (2009), pp. 942–948.

- [13] Karin Athenstaedt and Günther Daum. "Phosphatidic acid, a key intermediate in lipid metabolism". In: *European Journal of Biochemistry* 266.1 (1999), pp. 1–16.
- [14] JM Ordovas and ES Taib. "Current Opinion in Lipidology". In: (2008).
- [15] Paul A Davis and Amiya K Hajra. "The enzymatic exchange of the acyl group of acyl dihydroxyacetone phosphate with free fatty acids". In: (1977).
- [16] Edward F LaBelle and Amiya K Hajra. "Purification and kinetic properties of acyl and alkyl dihydroxyacetone phosphate oxidoreductase". In: *Journal of Biological Chemistry* 249.21 (1974), pp. 6936–6944.
- [17] W Dowhan. "Molecular basis for membrane phospholipid diversity: why are there so many lipids?" In: *Annual review of biochemistry* 66.1 (1997), pp. 199–232.
- [18] David N Brindley. "Lipid phosphate phosphatases and related proteins: signaling functions in development, cell division, and cancer". In: *Journal of cellular biochemistry* 92.5 (2004), pp. 900–912.
- [19] Lauren S Csaki and Karen Reue. "Lipins: multifunctional lipid metabolism proteins". In: *Annual review of nutrition* 30 (2010), pp. 257–272.
- [20] David N Brindley and Carlos Pilquill. "Lipid phosphate phosphatases and signaling". In: *Journal of lipid research* 50 (2009), S225–S230.
- [21] Mark A Miller and Claudia Kent. "Characterization of the pathways for phosphatidylethanolamine biosynthesis in Chinese hamster ovary mutant and parental cell lines." In: *Journal of Biological Chemistry* 261.21 (1986), pp. 9753–9761.
- [22] Dennis R Voelker. "Phosphatidylserine functions as the major precursor of phosphatidylethanolamine in cultured BHK-21 cells." In: *Proceedings of the National Academy of Sciences* 81.9 (1984), pp. 2669–2673.
- [23] Osamu Kuge and Masahiro Nishijima. "Phosphatidylserine synthase I and II of mammalian cells". In: *Biochimica et Biophysica Acta (BBA)-Lipids and Lipid Metabolism* 1348.1-2 (1997), pp. 151–156.
- [24] Osamu Kuge et al. "Control of phosphatidylserine biosynthesis through phosphatidylserine-mediated inhibition of phosphatidylserine synthase I in Chinese hamster ovary cells". In: *Proceedings of the National Academy of Sciences* 95.8 (1998), pp. 4199–4203.
- [25] Denis Rontein et al. "Plants synthesize ethanolamine by direct decarboxylation of serine using a pyridoxal phosphate enzyme". In: *Journal of Biological Chemistry* 276.38 (2001), pp. 35523–35529.
- [26] Federica Gibellini and Terry K Smith. "The Kennedy pathway—de novo synthesis of phosphatidylethanolamine and phosphatidylcholine". In: *IUBMB life* 62.6 (2010), pp. 414–428.
- [27] Dennis E Vance, Zhaoyu Li, and René L Jacobs. "Hepatic phosphatidylethanolamine N-methyltransferase, unexpected roles in animal biochemistry and physiology". In: *Journal of Biological Chemistry* 282.46 (2007), pp. 33237–33241.

- [28] Dennis E Vance. "Physiological roles of phosphatidylethanolamine N-methyltransferase". In: *Biochimica et Biophysica Acta (BBA)-Molecular and Cell Biology of Lipids* 1831.3 (2013), pp. 626–632.
- [29] Chieko Aoyama, Huanan Liao, and Kozo Ishidate. "Structure and function of choline kinase isoforms in mammalian cells". In: *Progress in lipid research* 43.3 (2004), pp. 266–281.
- [30] Shih Kwang Wu and Wonhwa Cho. "Use of polymerized mixed liposomes to study interactions of phospholipase A2 with membranes". In: *Biochemistry* 32.50 (1993), pp. 13902–13908.
- [31] JUAN P Infante. "Rate-limiting steps in the cytidine pathway for the synthesis of phosphatidylcholine and phosphatidylethanolamine." In: *Biochemical Journal* 167.3 (1977), p. 847.
- [32] JUAN P Infante and JOHN E Kinsella. "Control of phosphatidylcholine synthesis and the regulatory role of choline kinase in rat liver. Evidence from essential-fatty acid-deficient rats". In: *Biochemical Journal* 176.2 (1978), pp. 631–633.
- [33] M Nishijima et al. "Regulation of phosphatidylcholine metabolism in mammalian cells. Isolation and characterization of a Chinese hamster ovary cell pleiotropic mutant defective in both choline kinase and choline-exchange reaction activities." In: *Journal of Biological Chemistry* 259.11 (1984), pp. 7101–7108.
- [34] Roger Sundler. "Ethanolaminephosphate cytidyltransferase. Purification and characterization of the enzyme from rat liver." In: *Journal of Biological Chemistry* 250.22 (1975), pp. 8585–8590.
- [35] T_A Zelinski et al. "Phosphatidylcholine biosynthesis in isolated hamster heart". In: *Journal of Biological Chemistry* (1980).
- [36] Wei Tang, George A Keesler, and Ira Tabas. "The structure of the gene for murine CTP: phosphocholine cytidyltransferase, Ctpct: relationship of exon structure to functional domains and identification of transcriptional start sites and potential upstream regulatory elements". In: *Journal of Biological Chemistry* 272.20 (1997), pp. 13146–13151.
- [37] Mohammad Karim, Pam Jackson, and Suzanne Jackowski. "Gene structure, expression and identification of a new CTP: phosphocholine cytidyltransferase β isoform". In: *Biochimica et Biophysica Acta (BBA)-Molecular and Cell Biology of Lipids* 1633.1 (2003), pp. 1–12.
- [38] Rosemary B Cornell and Ingrid C Northwood. "Regulation of CTP: phosphocholine cytidyltransferase by amphitropism and relocalization". In: *Trends in biochemical sciences* 25.9 (2000), pp. 441–447.

- [39] M Houweling et al. "CTP: phosphocholine cytidyltransferase is both a nuclear and cytoplasmic protein in primary hepatocytes." In: *European journal of cell biology* 69.1 (1996), pp. 55–63.
- [40] Claudia Kent. "Regulatory enzymes of phosphatidylcholine biosynthesis: a personal perspective". In: *Biochimica et Biophysica Acta (BBA)-Molecular and Cell Biology of Lipids* 1733.1 (2005), pp. 53–66.
- [41] Athanasios Lykidis, Irina Baburina, and Suzanne Jackowski. "Distribution of CTP: phosphocholine cytidyltransferase (CCT) isoforms: identification of a new CCT β splice variant". In: *Journal of Biological Chemistry* 274.38 (1999), pp. 26992–27001.
- [42] Claudia Kent. "Eukaryotic phospholipid biosynthesis". In: *Annual review of biochemistry* 64.1 (1995), pp. 315–343.
- [43] YULI Wang et al. "Nuclear localization of soluble CTP: phosphocholine cytidyltransferase." In: *Journal of Biological Chemistry* 268.8 (1993), pp. 5899–5904.
- [44] Yong Tian et al. "Role of phosphocholine cytidyltransferase α in lung development". In: *Molecular and Cellular Biology* 27.3 (2007), pp. 975–982.
- [45] René L Jacobs et al. "Targeted deletion of hepatic CTP: phosphocholine cytidyltransferase α in mice decreases plasma high density and very low density lipoproteins". In: *Journal of Biological Chemistry* 279.45 (2004), pp. 47402–47410.
- [46] Paolo Fagone et al. "CTP: phosphocholine cytidyltransferase α is required for B-cell proliferation and class switch recombination". In: *Journal of Biological Chemistry* 284.11 (2009), pp. 6847–6854.
- [47] Dajun Zhang et al. "Macrophages Deficient in CTP: Phosphocholine Cytidyltransferase- α Are Viable under Normal Culture Conditions but Are Highly Susceptible to Free Cholesterol-induced Death: Molecular Genetic Evidence that the Induction of Phosphatidylcholine Biosynthesis in Free Cholesterol-Loaded Macrophages is an Adaptive Response". In: *Journal of Biological Chemistry* 275.45 (2000), pp. 35368–35376.
- [48] Suzanne Jackowski et al. "Disruption of CCT β 2 expression leads to gonadal dysfunction". In: *Molecular and cellular biology* 24.11 (2004), pp. 4720–4733.
- [49] Dennis E Vance and Jean E Vance. "Physiological consequences of disruption of mammalian phospholipid biosynthetic genes". In: *Journal of lipid research* 50 (2009), S132–S137.
- [50] Christopher R McMaster and Robert M Bell. "CDP-ethanolamine: 1, 2-diacylglycerol ethanolaminephosphotransferase". In: *Biochimica et Biophysica Acta (BBA)-Lipids and Lipid Metabolism* 1348.1-2 (1997), pp. 117–123.
- [51] Annette L HENNEBERRY and Christopher R McMASTER. "Cloning and expression of a human choline/ethanolaminephosphotransferase: synthesis of phosphatidylcholine and phosphatidylethanolamine". In: *Biochemical Journal* 339.2 (1999), pp. 291–298.

- [52] Annette L Henneberry, Graeme Wistow, and Christopher R McMaster. "Cloning, genomic organization, and characterization of a human cholinephosphotransferase". In: *Journal of Biological Chemistry* 275.38 (2000), pp. 29808–29815.
- [53] Dennis E Vance, Christopher J Walkey, and Zheng Cui. "Phosphatidylethanolamine N-methyltransferase from liver". In: *Biochimica et Biophysica Acta (BBA)-Lipids and Lipid Metabolism* 1348.1-2 (1997), pp. 142–150.
- [54] Cynthia J DeLong et al. "Molecular distinction of phosphatidylcholine synthesis between the CDP-choline pathway and phosphatidylethanolamine methylation pathway". In: *Journal of Biological Chemistry* 274.42 (1999), pp. 29683–29688.
- [55] Anna A Noga, Yang Zhao, and Dennis E Vance. "An unexpected requirement for phosphatidylethanolamine N-methyltransferase in the secretion of very low density lipoproteins". In: *Journal of Biological Chemistry* 277.44 (2002), pp. 42358–42365.
- [56] Anna A Noga and Dennis E Vance. "A gender-specific role for phosphatidylethanolamine N-methyltransferase-derived phosphatidylcholine in the regulation of plasma high density and very low density lipoproteins in mice". In: *Journal of Biological Chemistry* 278.24 (2003), pp. 21851–21859.
- [57] Anna A Noga and Dennis E Vance. "Insights into the requirement of phosphatidylcholine synthesis for liver function in mice". In: *Journal of lipid research* 44.10 (2003), pp. 1998–2005.
- [58] Zhaoyu Li, Luis B Agellon, and Dennis E Vance. "Phosphatidylcholine homeostasis and liver failure". In: *Journal of Biological Chemistry* 280.45 (2005), pp. 37798–37802.
- [59] Athanasios Lykidis et al. "Overexpression of a mammalian ethanolamine-specific kinase accelerates the CDP-ethanolamine pathway". In: *Journal of Biological Chemistry* 276.3 (2001), pp. 2174–2179.
- [60] Marica Bakovic, Morgan D Fullerton, and Vera Michel. "Metabolic and molecular aspects of ethanolamine phospholipid biosynthesis: the role of CTP: phosphoethanolamine cytidyltransferase (Pcyt2)". In: *Biochemistry and Cell Biology* 85.3 (2007), pp. 283–300.
- [61] Morgan D Fullerton, Fatima Hakimuddin, and Marica Bakovic. "Developmental and metabolic effects of disruption of the mouse CTP: phosphoethanolamine cytidyltransferase gene (Pcyt2)". In: *Molecular and cellular biology* 27.9 (2007), pp. 3327–3336.
- [62] Roberta Leonardi et al. "Elimination of the CDP-ethanolamine pathway disrupts hepatic lipid homeostasis". In: *Journal of Biological Chemistry* 284.40 (2009), pp. 27077–27089.

- [63] Onno B Bleijerveld et al. "The CDP-ethanolamine pathway and phosphatidylserine decarboxylation generate different phosphatidylethanolamine molecular species". In: *Journal of Biological Chemistry* 282.39 (2007), pp. 28362–28372.
- [64] Jean E Vance. "Phosphatidylserine and phosphatidylethanolamine in mammalian cells: two metabolically related aminophospholipids". In: *J Lipid Res* 49.7 (2008), pp. 1377–1387.
- [65] Liisa Heikinheimo and Pentti Somerharju. "Translocation of pyrene-labeled phosphatidylserine from the plasma membrane to mitochondria diminishes systematically with molecular hydrophobicity: implications on the maintenance of high phosphatidylserine content in the inner leaflet of the plasma membrane". In: *Biochimica et Biophysica Acta (BBA)-Molecular Cell Research* 1591.1-3 (2002), pp. 75–85.
- [66] Dennis R Voelker. "Disruption of phosphatidylserine translocation to the mitochondria in baby hamster kidney cells." In: *Journal of Biological Chemistry* 260.27 (1985), pp. 14671–14676.
- [67] Scot J Stone and Jean E Vance. "Phosphatidylserine synthase-1 and-2 are localized to mitochondria-associated membranes". In: *Journal of Biological Chemistry* 275.44 (2000), pp. 34534–34540.
- [68] Devi Ariketh, Randy Nelson, and Jean E Vance. "Defining the importance of phosphatidylserine synthase-1 (PSS1): unexpected viability of PSS1-deficient mice". In: *Journal of Biological Chemistry* 283.19 (2008), pp. 12888–12897.
- [69] Martin O Bergo et al. "Defining the importance of phosphatidylserine synthase 2 in mice". In: *Journal of Biological Chemistry* 277.49 (2002), pp. 47701–47708.
- [70] Anne M Heacock and Bernard W Agranoff. "CDP-diacylglycerol synthase from mammalian tissues". In: *Biochimica et Biophysica Acta (BBA)-Lipids and Lipid Metabolism* 1348.1-2 (1997), pp. 166–172.
- [71] Haifa Shen and William Dowhan. "Regulation of phospholipid biosynthetic enzymes by the level of CDP-diacylglycerol synthase activity". In: *Journal of Biological Chemistry* 272.17 (1997), pp. 11215–11220.
- [72] Bruno Antonsson. "Phosphatidylinositol synthase from mammalian tissues". In: *Biochimica et Biophysica Acta (BBA)-Lipids and Lipid Metabolism* 1348.1-2 (1997), pp. 179–186.
- [73] A Imai and MC Gershengorn. "Regulation by phosphatidylinositol of rat pituitary plasma membrane and endoplasmic reticulum phosphatidylinositol synthase activities. A mechanism for activation of phosphoinositide resynthesis during cell stimulation." In: *Journal of Biological Chemistry* 262.14 (1987), pp. 6457–6459.
- [74] T Ohtsuka et al. "Mitochondrial dysfunction of a cultured Chinese hamster ovary cell mutant deficient in cardiolipin." In: *Journal of Biological Chemistry* 268.30 (1993), pp. 22914–22919.

- [75] T Ohtsuka, M Nishijima, and Y Akamatsu. "A somatic cell mutant defective in phosphatidylglycerophosphate synthase, with impaired phosphatidylglycerol and cardiolipin biosynthesis." In: *Journal of Biological Chemistry* 268.30 (1993), pp. 22908–22913.
- [76] Kiyoshi Kawasaki et al. "Isolation of a Chinese hamster ovary (CHO) cDNA encoding phosphatidylglycerophosphate (PGP) synthase, expression of which corrects the mitochondrial abnormalities of a PGP synthase-defective mutant of CHO-K1 cells". In: *Journal of Biological Chemistry* 274.3 (1999), pp. 1828–1834.
- [77] LMG Van Golde, GL Scherphof, and LLM Van Deenen. "Biosynthetic pathways in the formation of individual molecular species of rat liver phospholipids". In: *Biochimica et Biophysica Acta (BBA)-Lipids and Lipid Metabolism* 176.3 (1969), pp. 635–637.
- [78] Daisuke Hishikawa et al. "Diversity and function of membrane glycerophospholipids generated by the remodeling pathway in mammalian cells". In: *Journal of lipid research* 55.5 (2014), pp. 799–807.
- [79] WE Lands. "Stories about acyl chains". In: *Biochimica et biophysica acta* 1483.1 (2000), pp. 1–14.
- [80] Patricia C Schmid, Ilona Spimrova, and Harald HO Schmid. "Generation and remodeling of highly polyunsaturated molecular species of rat hepatocyte phospholipids". In: *Lipids* 32.11 (1997), pp. 1181–1187.
- [81] Maria A Balboa and Jesus Balsinde. "Involvement of Calcium-independent Phospholipase A2 in Hydrogen Peroxide-induced Accumulation of Free Fatty Acids in Human U937 Cells". In: *Journal of Biological Chemistry* 277.43 (2002), pp. 40384–40389.
- [82] Jesus Balsinde, Maria A Balboa, and Edward A Dennis. "Antisense inhibition of group VI Ca²⁺-independent phospholipase A2 blocks phospholipid fatty acid remodeling in murine P388D1 macrophages". In: *Journal of biological chemistry* 272.46 (1997), pp. 29317–29321.
- [83] Phillip L Butler and Rama K Mallampalli. "Cross-talk between remodeling and de novo pathways maintains phospholipid balance through ubiquitination". In: *Journal of Biological Chemistry* 285.9 (2010), pp. 6246–6258.
- [84] WP Wilkins Iii, SE Barbour, et al. "Group VI phospholipases A2: homeostatic phospholipases with significant potential as targets for novel therapeutics". In: *Current drug targets* 9.8 (2008), pp. 683–697.
- [85] Makoto Murakami et al. "Group VIB Ca²⁺-independent phospholipase A2 γ promotes cellular membrane hydrolysis and prostaglandin production in a manner distinct from other intracellular phospholipases A2". In: *Journal of Biological Chemistry* 280.14 (2005), pp. 14028–14041.

- [86] Kenji Asai et al. "Human group IVC phospholipase A2 (cPLA2 γ): roles in the membrane remodeling and activation induced by oxidative stress". In: *Journal of Biological Chemistry* 278.10 (2003), pp. 8809–8814.
- [87] Ichiro Kudo and Makoto Murakami. "Phospholipase A2 enzymes". In: *Prostaglandins & other lipid mediators* 68 (2002), pp. 3–58.
- [88] Allison Stewart et al. "Enzymatic properties of human cytosolic phospholipase A2 γ ". In: *Journal of Biological Chemistry* 277.33 (2002), pp. 29526–29536.
- [89] BJ Holub and A Kuksis. "Metabolism of molecular species of diacylglycerophospholipids". In: *Advances in lipid research* 16 (1978), pp. 1–125.
- [90] Hideo Shindou et al. "A single enzyme catalyzes both platelet-activating factor production and membrane biogenesis of inflammatory cells: cloning and characterization of acetyl-CoA: LYSO-PAF acetyltransferase". In: *Journal of Biological Chemistry* 282.9 (2007), pp. 6532–6539.
- [91] B Åkesson, J Elovson, and G Arvidson. "Initial incorporation into rat liver glycerolipids of intraportally injected [9, 10-³H₂] palmitic acid". In: *Biochimica et Biophysica Acta (BBA)-Lipids and Lipid Metabolism* 218.1 (1970), pp. 44–56.
- [92] GAE Arvidson. "Structural and metabolic heterogeneity of rat liver glycerophosphatides". In: *European Journal of Biochemistry* 4.4 (1968), pp. 478–486.
- [93] Edward E Hill and William EM Lands. "Incorporation of long-chain and polyunsaturated acids into phosphatidate and phosphatidylcholine". In: (1968).
- [94] Kanoh Hideo. "Biosynthesis of molecular species of phosphatidyl choline and phosphatidyl ethanolamine from radioactive precursors in rat liver slices". In: *Biochimica et Biophysica Acta (BBA)-Lipids and Lipid Metabolism* 176.4 (1969), pp. 756–763.
- [95] Xueni Chen et al. "Identification and characterization of a lysophosphatidylcholine acyltransferase in alveolar type II cells". In: *Proceedings of the National Academy of Sciences* 103.31 (2006), pp. 11724–11729.
- [96] Hiroki Nakanishi et al. "Cloning and characterization of mouse lung-type acyl-CoA: lysophosphatidylcholine acyltransferase 1 (LPCAT1): expression in alveolar type II cells and possible involvement in surfactant production". In: *Journal of Biological Chemistry* 281.29 (2006), pp. 20140–20147.
- [97] Daisuke Hishikawa et al. "Discovery of a lysophospholipid acyltransferase family essential for membrane asymmetry and diversity". In: *Proceedings of the National Academy of Sciences* 105.8 (2008), pp. 2830–2835.
- [98] Hideo Shindou et al. "Recent progress on acyl CoA: lysophospholipid acyltransferase research". In: *Journal of lipid research* 50 (2009), S46–S51.
- [99] Shinji Matsuda et al. "Member of the membrane-bound O-acyltransferase (MBOAT) family encodes a lysophospholipid acyltransferase with broad substrate specificity". In: *Genes to Cells* 13.8 (2008), pp. 879–888.

- [100] Koichi Yuki et al. "Characterization of mouse lysophosphatidic acid acyltransferase 3: an enzyme with dual functions in the testis1 [S]". In: *Journal of lipid research* 50.5 (2009), pp. 860–869.
- [101] Yang Zhao et al. "Identification and characterization of a major liver lysophosphatidylcholine acyltransferase". In: *Journal of Biological chemistry* 283.13 (2008), pp. 8258–8265.
- [102] Kay Hofmann. "A superfamily of membrane-bound O-acyltransferases with implications for wnt signaling." In: *Trends in biochemical sciences* 25.3 (2000), pp. 111–112.
- [103] Anton IPM de Kroon. "Metabolism of phosphatidylcholine and its implications for lipid acyl chain composition in *Saccharomyces cerevisiae*". In: *Biochimica et Biophysica Acta (BBA)-Molecular and Cell Biology of Lipids* 1771.3 (2007), pp. 343–352.
- [104] Atsushi Yamashita, Takayuki Sugiura, and Keizo Waku. "Acyltransferases and transacylases involved in fatty acid remodeling of phospholipids and metabolism of bioactive lipids in mammalian cells". In: *The journal of biochemistry* 122.1 (1997), pp. 1–16.
- [105] Merle L Blank et al. "Metabolism of unique diarachidonoyl and linoleoylarachidonoyl species of ethanolamine and choline phosphoglycerides in rat testes". In: *Biochimica et Biophysica Acta (BBA)-Lipids and Lipid Metabolism* 833.3 (1985), pp. 366–371.
- [106] Odile Colard, Michelyne Breton, and Gilbert Bereziat. "Arachidonyl transfer from diacyl phosphatidylcholine to ether phospholipids in rat platelets". In: *Biochemical Journal* 222.3 (1984), pp. 657–662.
- [107] Odile Colard, Michelyne Breton, and Gilbert Bereziat. "Induction by lysophospholipids of CoA-dependent arachidonyl transfer between phospholipids in rat platelet homogenates". In: *Biochimica et Biophysica Acta (BBA)-Lipids and Lipid Metabolism* 793.1 (1984), pp. 42–48.
- [108] Deny Hartono et al. "An air-supported liquid crystal system for real-time and label-free characterization of phospholipases and their inhibitors". In: *Advanced Functional Materials* 18.19 (2008), pp. 2938–2945.
- [109] Robert V Stahelin. "Phospholipid Catabolism". In: *Biochemistry of Lipids, Lipoproteins and Membranes, 6th ed.; Ridgway, ND, McLeod, RS, Eds* (2015), pp. 237–257.
- [110] Yugo Iwasaki and Tsuneo Yamane. "Enzymatic synthesis of structured lipids". In: *Recent Progress of Biochemical and Biomedical Engineering in Japan I: -/-* (2004), pp. 151–171.
- [111] Krishna Chaithanya Batchu et al. "Factors regulating the substrate specificity of cytosolic phospholipase A2-alpha in vitro". In: *Biochimica et Biophysica Acta (BBA)-Molecular and Cell Biology of Lipids* 1861.11 (2016), pp. 1597–1604.

- [112] Geoffrey D Robson. "Phospholipases of *Aspergillus fumigatus*". In: *Aspergillus fumigatus and Aspergillosis* (2008), pp. 75–86.
- [113] Shivendra D Shukla and Stephen P Halenda. "Phospholipase D in cell signalling and its relationship to phospholipase C". In: *Life Sciences* 48.9 (1991), pp. 851–866.
- [114] Kanchan Sonkar et al. "Focus on the glycerophosphocholine pathway in choline phospholipid metabolism of cancer". In: *NMR in Biomedicine* 32.10 (2019), e4112.
- [115] Gary B Quistad et al. "Evidence that mouse brain neuropathy target esterase is a lysophospholipase". In: *Proceedings of the National Academy of Sciences* 100.13 (2003), pp. 7983–7987.
- [116] Vittorio Luzzati and A Tardieu. "Lipid phases: structure and structural transitions". In: *Annual Review of Physical Chemistry* 25.1 (1974), pp. 79–94.
- [117] David Chandler. "Hydrophobicity: Two faces of water". In: *Nature* 417.6888 (2002), pp. 491–491.
- [118] PR t Cullis and B De Kruijff. "Lipid polymorphism and the functional roles of lipids in biological membranes". In: *Biochimica et Biophysica Acta (BBA)-Reviews on Biomembranes* 559.4 (1979), pp. 399–420.
- [119] PR Cullis and B De Kruijff. "Polymorphic phase behaviour of lipid mixtures as detected by ³¹P NMR. Evidence that cholesterol may destabilize bilayer structure in membrane systems containing phosphatidylethanolamine". In: *Biochimica et Biophysica Acta (BBA)-Biomembranes* 507.2 (1978), pp. 207–218.
- [120] AC McLaughlin et al. "³¹P NMR of Phospholipid membranes: Effects of chemical and anisotropy at high magnetic field strengths". In: *Journal of Magnetic Resonance (1969)* 20.1 (1975), pp. 146–165.
- [121] Hans U Gally, Werner Niederberger, and Joachim Seelig. "Conformation and motion of the choline head group in bilayers of dipalmitoyl-3-sn-phosphatidylcholine". In: *Biochemistry* 14.16 (1975), pp. 3647–3652.
- [122] Joachim Seelig. "³¹P nuclear magnetic resonance and the head group structure of phospholipids in membranes". In: *Biochimica et Biophysica Acta (BBA)-Reviews on Biomembranes* 515.2 (1978), pp. 105–140.
- [123] PR Cullis and B De Kruijff. "The polymorphic phase behaviour of phosphatidylethanolamines of natural and synthetic origin. A ³¹P NMR study". In: *Biochimica et Biophysica Acta (BBA)-Biomembranes* 513.1 (1978), pp. 31–42.
- [124] RP Rand and S Sengupta. "Cardiolipin forms hexagonal structures with divalent cations". In: *Biochimica et Biophysica Acta (BBA)-Biomembranes* 255.2 (1972), pp. 484–492.
- [125] PR t Cullis and B De Kruijff. "Lipid polymorphism and the functional roles of lipids in biological membranes". In: *Biochimica et Biophysica Acta (BBA)-Reviews on Biomembranes* 559.4 (1979), pp. 399–420.

- [126] Philip L Yèagle. “Lipid regulation of cell membrane structure and function”. In: *The FASEB journal* 3.7 (1989), pp. 1833–1842.
- [127] TK Bills, JB Smith, MJ Silver, et al. “Selective release of archidonic acid from the phospholipids of human platelets in response to thrombin.” In: *The Journal of clinical investigation* 60.1 (1977), pp. 1–6.
- [128] Ruth M Kramer and Daniel Deykin. “Arachidonoyl transacylase in human platelets. Coenzyme A-independent transfer of arachidonate from phosphatidylcholine to lysoplasmenylethanolamine.” In: *Journal of Biological Chemistry* 258.22 (1983), pp. 13806–13811.
- [129] Baran A Ersoy et al. “Phosphatidylcholine transfer protein interacts with thioesterase superfamily member 2 to attenuate insulin signaling”. In: *Science Signaling* 6.286 (2013), ra64–ra64.
- [130] Takeru Sakai et al. “Leptin restores the insulinotropic effect of exenatide in a mouse model of type 2 diabetes with increased adiposity induced by streptozotocin and high-fat diet”. In: *American Journal of Physiology-Endocrinology and Metabolism* 307.8 (2014), E712–E719.
- [131] Peter A Leventis and Sergio Grinstein. “The distribution and function of phosphatidylserine in cellular membranes”. In: *Annual review of biophysics* 39 (2010), pp. 407–427.
- [132] Jason G Kay and Gregory D Fairn. “Distribution, dynamics and functional roles of phosphatidylserine within the cell”. In: *Cell Communication and Signaling* 17.1 (2019), pp. 1–8.
- [133] Tony Yeung et al. “Membrane phosphatidylserine regulates surface charge and protein localization”. In: *Science* 319.5860 (2008), pp. 210–213.
- [134] Yeun Ju Kim, Maria Luisa Guzman-Hernandez, and Tamas Balla. “A highly dynamic ER-derived phosphatidylinositol-synthesizing organelle supplies phosphoinositides to cellular membranes”. In: *Developmental cell* 21.5 (2011), pp. 813–824.
- [135] Chi-Lun Chang et al. “Feedback regulation of receptor-induced Ca²⁺ signaling mediated by E-Syt1 and Nir2 at endoplasmic reticulum-plasma membrane junctions”. In: *Cell reports* 5.3 (2013), pp. 813–825.
- [136] Yeun Ju Kim, Maria-Luisa Guzman Hernandez, and Tamas Balla. “Inositol lipid regulation of lipid transfer in specialized membrane domains”. In: *Trends in cell biology* 23.6 (2013), pp. 270–278.
- [137] Bandana Chakravarti, Naibedya Chattopadhyay, and Edward M Brown. “Signaling through the extracellular calcium-sensing receptor (CaSR)”. In: *Calcium signaling* (2012), pp. 103–142.

- [138] Samuel Furse and Gemma C Shearman. "Do lipids shape the eukaryotic cell cycle?" In: *Biochimica et Biophysica Acta (BBA)-Molecular and Cell Biology of Lipids* 1863.1 (2018), pp. 9–19.
- [139] Vanessa Zhendre et al. "Key role of polyphosphoinositides in dynamics of fusogenic nuclear membrane vesicles". In: *PloS one* 6.9 (2011), e23859.
- [140] Irina Baburina and Suzanne Jackowski. "Cellular responses to excess phospholipid". In: *Journal of Biological Chemistry* 274.14 (1999), pp. 9400–9408.
- [141] Christopher J Walkey, Gabriel B Kalmar, and Rosemary B Cornell. "Overexpression of rat liver CTP: phosphocholine cytidyltransferase accelerates phosphatidylcholine synthesis and degradation." In: *Journal of Biological Chemistry* 269.8 (1994), pp. 5742–5749.
- [142] Athanasios Lykidis and Suzanne Jackowski. "Regulation of mammalian cell membrane biosynthesis". In: (2000).
- [143] Scot J Stone, Zheng Cui, and Jean E Vance. "Cloning and expression of mouse liver phosphatidylserine synthase-1 cDNA: overexpression in rat hepatoma cells inhibits the CDP-ethanolamine pathway for phosphatidylethanolamine biosynthesis". In: *Journal of Biological Chemistry* 273.13 (1998), pp. 7293–7302.
- [144] MA Polokoff, DC Wing, and CR Raetz. "Isolation of somatic cell mutants defective in the biosynthesis of phosphatidylethanolamine." In: *Journal of Biological Chemistry* 256.15 (1981), pp. 7687–7690.
- [145] Jesús Balsinde and María A Balboa. "Cellular regulation and proposed biological functions of group VIA calcium-independent phospholipase A2 in activated cells". In: *Cellular signalling* 17.9 (2005), pp. 1052–1062.
- [146] Chun-Hung Chiu and Suzanne Jackowski. "Role of calcium-independent phospholipases (iPLA2) in phosphatidylcholine metabolism". In: *Biochemical and Biophysical Research Communications* 287.3 (2001), pp. 600–606.
- [147] Paul Glynn. "Neuropathy target esterase and phospholipid deacylation". In: *Biochimica et Biophysica Acta (BBA)-Molecular and Cell Biology of Lipids* 1736.2 (2005), pp. 87–93.
- [148] Alex D Manguikian and Suzanne E Barbour. "Cell cycle dependence of group VIA calcium-independent phospholipase A2 activity". In: *Journal of Biological Chemistry* 279.51 (2004), pp. 52881–52892.
- [149] Jerold Chun et al. "International union of basic and clinical pharmacology. LXXVIII. Lysophospholipid receptor nomenclature". In: *Pharmacological reviews* 62.4 (2010), pp. 579–587.

- [150] Henry N Higgs and John A Glomset. "Purification and Properties of a Phosphatidic Acid-preferring Phospholipase A1 from Bovine Testis: EXAMINATION OF THE MOLECULAR BASIS OF ITS ACTIVATION". In: *Journal of Biological Chemistry* 271.18 (1996), pp. 10874–10883.
- [151] María Laura Belaunzarán et al. "Phospholipase A1: a novel virulence factor in *Trypanosoma cruzi*". In: *Molecular and biochemical parasitology* 187.2 (2013), pp. 77–86.
- [152] Susana Merino et al. "Cloning, sequencing, and role in virulence of two phospholipases (A1 and C) from mesophilic *Aeromonas* sp. serogroup O: 34". In: *Infection and Immunity* 67.8 (1999), pp. 4008–4013.
- [153] Junken Aoki et al. "Structure and function of phosphatidylserine-specific phospholipase A1". In: *Biochimica et Biophysica Acta (BBA)-Molecular and Cell Biology of Lipids* 1582.1-3 (2002), pp. 26–32.
- [154] Yang Zhao, Stephan Hasse, and Sylvain G Bourgoin. "Phosphatidylserine-specific phospholipase A1: A friend or the devil in disguise". In: *Progress in Lipid Research* 83 (2021), p. 101112.
- [155] Kumiko Makide and Junken Aoki. "GPR34 as a lysophosphatidylserine receptor". In: *The Journal of Biochemistry* 153.4 (2013), pp. 327–329.
- [156] David A Six and Edward A Dennis. "The expanding superfamily of phospholipase A2 enzymes: classification and characterization". In: *Biochimica et Biophysica Acta (BBA)-Molecular and Cell Biology of Lipids* 1488.1-2 (2000), pp. 1–19.
- [157] Gérard Lambeau and Michael H Gelb. "Biochemistry and physiology of mammalian secreted phospholipases A2". In: *Annual review of biochemistry* 77.1 (2008), pp. 495–520.
- [158] Edward A Dennis. "Diversity of group types, regulation, and function of phospholipase A2." In: *The Journal of biological chemistry* 269.18 (1994), pp. 13057–13060.
- [159] ROBERT L Heinrikson, ELAINE T Krueger, and PAMELA S Keim. "Amino acid sequence of phospholipase A2-alpha from the venom of *Crotalus adamanteus*. A new classification of phospholipases A2 based upon structural determinants." In: *Journal of Biological Chemistry* 252.14 (1977), pp. 4913–4921.
- [160] R Manjunatha Kini. "Excitement ahead: structure, function and mechanism of snake venom phospholipase A2 enzymes". In: *Toxicon* 42.8 (2003), pp. 827–840.
- [161] Jesper J Madsen et al. "Secretory phospholipase A2 activity toward diverse substrates". In: *The Journal of Physical Chemistry B* 115.21 (2011), pp. 6853–6861.
- [162] Nhat D Quach, Robert D Arnold, and Brian S Cummings. "Secretory phospholipase A2 enzymes as pharmacological targets for treatment of disease". In: *Biochemical pharmacology* 90.4 (2014), pp. 338–348.

- [163] Alan G Singer et al. "Interfacial kinetic and binding properties of the complete set of human and mouse groups I, II, V, X, and XII secreted phospholipases A2". In: *Journal of Biological Chemistry* 277.50 (2002), pp. 48535–48549.
- [164] Lionel Cupillard et al. "Cloning, chromosomal mapping, and expression of a novel human secretory phospholipase A2". In: *Journal of Biological Chemistry* 272.25 (1997), pp. 15745–15752.
- [165] Kohji Hanasaki and Hitoshi Arita. "Biological and pathological functions of phospholipase A2 receptor". In: *Archives of Biochemistry and Biophysics* 372.2 (1999), pp. 215–223.
- [166] David L Scott et al. "The electrostatic basis for the interfacial binding of secretory phospholipases A2". In: *Biophysical journal* 67.2 (1994), pp. 493–504.
- [167] Michael H Gelb et al. "Interfacial enzymology of glycerolipid hydrolases: lessons from secreted phospholipases A2". In: *Annual review of biochemistry* 64.1 (1995), pp. 653–688.
- [168] Farideh Ghomashchi et al. "Interfacial catalysis by phospholipase A2: substrate specificity in vesicles". In: *Biochemistry* 30.29 (1991), pp. 7318–7329.
- [169] Mahendra Kumar Jain et al. "The affinity of phospholipase A2 for the interface of the substrate and analogs". In: *Biochimica et Biophysica Acta (BBA)-Biomembranes* 860.3 (1986), pp. 475–483.
- [170] Mahendra Kumar Jain et al. "Kinetics of interfacial catalysis by phospholipase A2 in intravesicle scooting mode, and heterofusion of anionic and zwitterionic vesicles". In: *Biochimica et Biophysica Acta (BBA)-Biomembranes* 860.3 (1986), pp. 435–447.
- [171] Mahendra Kumar Jain, Bao Zhu Yu, and Otto G Berg. "Relationship of interfacial equilibria to interfacial activation of phospholipase A2". In: *Biochemistry* 32.42 (1993), pp. 11319–11329.
- [172] Michael A Wells. "Mechanism of interfacial activation of phospholipase A2". In: *Biochemistry* 13.11 (1974), pp. 2248–2257.
- [173] David L Scott et al. "Structures of free and inhibited human secretory phospholipase A2 from inflammatory exudate". In: *Science* 254.5034 (1991), pp. 1007–1010.
- [174] Dominick Mobilio and Lisa A Marshall. "Recent advances in the design and evaluation of inhibitors of phospholipase A2". In: *Annual Reports in Medicinal Chemistry* 24 (1989), pp. 157–166.
- [175] Andreas Plückthun and Edward A Dennis. "Activation, aggregation, and product inhibition of cobra venom phospholipase A2 and comparison with other phospholipases." In: *Journal of Biological Chemistry* 260.20 (1985), pp. 11099–11106.
- [176] Shan-Shan Qin et al. "Interaction of human synovial phospholipase A2 with mixed lipid bilayers: a coarse-grain and all-atom molecular dynamics simulation study". In: *Biochemistry* 52.8 (2013), pp. 1477–1489.

- [177] Bauke W Dijkstra, Jan Drenth, and Kor H Kalk. "Active site and catalytic mechanism of phospholipase A2". In: *Nature* 289.5798 (1981), pp. 604–606.
- [178] Ying H Pan et al. "Crystal structure of phospholipase A2 complex with the hydrolysis products of platelet activating factor: equilibrium binding of fatty acid and lysophospholipid-ether at the active site may be mutually exclusive". In: *Biochemistry* 41.50 (2002), pp. 14790–14800.
- [179] Bonnie L Richmond et al. "Compensatory phospholipid digestion is required for cholesterol absorption in pancreatic phospholipase A2–Deficient mice". In: *Gastroenterology* 120.5 (2001), pp. 1193–1202.
- [180] Emmanuel Valentin et al. "On the diversity of secreted phospholipases A2: cloning, tissue distribution, and functional expression of two novel mouse group II enzymes". In: *Journal of Biological Chemistry* 274.44 (1999), pp. 31195–31202.
- [181] William R Henderson Jr et al. "Importance of group X–secreted phospholipase A2 in allergen-induced airway inflammation and remodeling in a mouse asthma model". In: *The Journal of experimental medicine* 204.4 (2007), pp. 865–877.
- [182] Yoshihiro Kita et al. "Biochemical properties and pathophysiological roles of cytosolic phospholipase A2s". In: *Biochimica et Biophysica Acta (BBA)-Molecular and Cell Biology of Lipids* 1761.11 (2006), pp. 1317–1322.
- [183] Takayo Ohto et al. "Identification of novel cytosolic phospholipase A2s, murine cPLA2 δ , ϵ , and ζ , which form a gene cluster with cPLA2 β ". In: *Journal of Biological Chemistry* 280.26 (2005), pp. 24576–24583.
- [184] R Todd Pickard et al. "Molecular cloning of two new human paralogs of 85-kDa cytosolic phospholipase A2". In: *Journal of Biological Chemistry* 274.13 (1999), pp. 8823–8831.
- [185] Günther H Peters et al. "Secretory phospholipase A2 hydrolysis of phospholipid analogues is dependent on water accessibility to the active site". In: *Journal of the American Chemical Society* 129.17 (2007), pp. 5451–5461.
- [186] John E Burke and Edward A Dennis. "Phospholipase A2 structure/function, mechanism, and signaling1". In: *Journal of lipid research* 50 (2009), S237–S242.
- [187] David H Adler et al. "Inherited human cPLA 2 α deficiency is associated with impaired eicosanoid biosynthesis, small intestinal ulceration, and platelet dysfunction". In: *The Journal of clinical investigation* 118.6 (2008), pp. 2121–2131.
- [188] Joseph V Bonventre et al. "Reduced fertility and postischemic brain injury in mice deficient in cytosolic phospholipase A2". In: *Nature* 390.6660 (1997), pp. 622–625.
- [189] Laure J Reynolds et al. "Metal ion and salt effects on the phospholipase A2, lysophospholipase, and transacylase activities of human cytosolic phospholipase A2". In: *Biochimica et Biophysica Acta (BBA)-Lipids and Lipid Metabolism* 1167.3 (1993), pp. 272–280.

- [190] James D Clark et al. "Cytosolic phospholipase A2". In: *Journal of lipid mediators and cell signalling* 12.2-3 (1995), pp. 83–117.
- [191] Ichiro Kudo et al. "Mammalian non-pancreatic phospholipases A2". In: *Biochimica et Biophysica Acta (BBA)-Lipids and Lipid Metabolism* 1170.3 (1993), pp. 217–231.
- [192] Elsa Regan-Klapisz et al. "Golgi-associated cPLA2 α regulates endothelial cell–cell junction integrity by controlling the trafficking of transmembrane junction proteins". In: *Molecular Biology of the Cell* 20.19 (2009), pp. 4225–4234.
- [193] Ruth M Kramer et al. "Solubilization and properties of Ca²⁺-dependent human platelet phospholipase A2". In: *Biochimica et Biophysica Acta (BBA)-Lipids and Lipid Metabolism* 878.3 (1986), pp. 394–403.
- [194] David A Six and Edward A Dennis. "Essential Ca²⁺-independent role of the group IVA cytosolic phospholipase A2 C2 domain for interfacial activity". In: *Journal of Biological Chemistry* 278.26 (2003), pp. 23842–23850.
- [195] Miguel A Gijón et al. "Role of phosphorylation sites and the C2 domain in regulation of cytosolic phospholipase A2". In: *The Journal of cell biology* 145.6 (1999), pp. 1219–1232.
- [196] John E Burke et al. "A phospholipid substrate molecule residing in the membrane surface mediates opening of the lid region in group IVA cytosolic phospholipase A2". In: *Journal of Biological Chemistry* 283.45 (2008), pp. 31227–31236.
- [197] Varnavas D Mouchlis et al. "Membranes serve as allosteric activators of phospholipase A2, enabling it to extract, bind, and hydrolyze phospholipid substrates". In: *Proceedings of the National Academy of Sciences* 112.6 (2015), E516–E525.
- [198] Zoran Pavicevic, Christina C Leslie, and Kafait U Malik. "cPLA2 phosphorylation at serine-515 and serine-505 is required for arachidonic acid release in vascular smooth muscle cells". In: *Journal of lipid research* 49.4 (2008), pp. 724–737.
- [199] Christina C Leslie. "Properties and regulation of cytosolic phospholipase A2". In: *Journal of Biological Chemistry* 272.27 (1997), pp. 16709–16712.
- [200] Tetsuya Hirabayashi, Toshihiko Murayama, and Takao Shimizu. "Regulatory mechanism and physiological role of cytosolic phospholipase A2". In: *Biological and Pharmaceutical Bulletin* 27.8 (2004), pp. 1168–1173.
- [201] Lih-Ling Lin, Alice Y Lin, and John L Knopf. "Cytosolic phospholipase A2 is coupled to hormonally regulated release of arachidonic acid." In: *Proceedings of the National Academy of Sciences* 89.13 (1992), pp. 6147–6151.
- [202] Zhi-Hua Qiu and Christina C Leslie. "Protein kinase C-dependent and-independent pathways of mitogen-activated protein kinase activation in macrophages by stimuli that activate phospholipase A2." In: *Journal of Biological Chemistry* 269.30 (1994), pp. 19480–19487.

- [203] Takahide Nagase et al. "A pivotal role of cytosolic phospholipase A2 in bleomycin-induced pulmonary fibrosis". In: *Nature medicine* 8.5 (2002), pp. 480–484.
- [204] Takahide Nagase et al. "Acute lung injury by sepsis and acid aspiration: a key role for cytosolic phospholipase A2". In: *Nature immunology* 1.1 (2000), pp. 42–46.
- [205] Chisato Miyaura et al. "An essential role of cytosolic phospholipase A2 α in prostaglandin E2-mediated bone resorption associated with inflammation". In: *The Journal of experimental medicine* 197.10 (2003), pp. 1303–1310.
- [206] Suzana Marusic et al. "Cytosolic phospholipase A2 α -deficient mice are resistant to experimental autoimmune encephalomyelitis". In: *The Journal of experimental medicine* 202.6 (2005), pp. 841–851.
- [207] Y Oikawa et al. "Protective role for cytosolic phospholipase A2 α in autoimmune diabetes of mice". In: *FEBS letters* 579.18 (2005), pp. 3975–3978.
- [208] Chuanzheng Song et al. "Molecular characterization of cytosolic phospholipase A2- β ". In: *Journal of Biological Chemistry* 274.24 (1999), pp. 17063–17067.
- [209] Moumita Ghosh et al. "Properties of the Group IV phospholipase A2 family". In: *Progress in lipid research* 45.6 (2006), pp. 487–510.
- [210] Petra C Kienesberger et al. "Mammalian patatin domain containing proteins: a family with diverse lipolytic activities involved in multiple biological functions". In: *Journal of lipid research* 50 (2009), S63–S68.
- [211] Makoto Murakami and Ichiro Kudo. "Phospholipase A2". In: *The journal of biochemistry* 131.3 (2002), pp. 285–292.
- [212] Makoto Murakami et al. "The functions of five distinct mammalian phospholipase A2s in regulating arachidonic acid release: type IIA and type V secretory phospholipase A2s are functionally redundant and act in concert with cytosolic phospholipase A2". In: *Journal of Biological Chemistry* 273.23 (1998), pp. 14411–14423.
- [213] Michelle V Winstead, Jesús Balsinde, and Edward A Dennis. "Calcium-independent phospholipase A2: structure and function". In: *Biochimica et Biophysica Acta (BBA)-Molecular and Cell Biology of Lipids* 1488.1-2 (2000), pp. 28–39.
- [214] Satoshi Akiba and Takashi Sato. "Cellular function of calcium-independent phospholipase A2". In: *Biological and Pharmaceutical Bulletin* 27.8 (2004), pp. 1174–1178.
- [215] Zhongmin Ma et al. "Human pancreatic islets express mRNA species encoding two distinct catalytically active isoforms of group VI phospholipase A2 (iPLA2) that arise from an exon-skipping mechanism of alternative splicing of the transcript from the iPLA2 gene on chromosome 22q13. 1". In: *Journal of Biological Chemistry* 274.14 (1999), pp. 9607–9616.

- [216] Yi-Ching Lio and Edward A Dennis. "Interfacial activation, lysophospholipase and transacylase activity of group VI Ca²⁺-independent phospholipase A₂". In: *Biochimica et Biophysica Acta (BBA)-Lipids and Lipid Metabolism* 1392.2-3 (1998), pp. 320–332.
- [217] Matthew J Wolf and Richard W Gross. "Expression, purification, and kinetic characterization of a recombinant 80-kDa intracellular calcium-independent phospholipase A₂". In: *Journal of Biological Chemistry* 271.48 (1996), pp. 30879–30885.
- [218] Haowei Song et al. "A bromoenol lactone suicide substrate inactivates group VIA phospholipase A₂ by generating a diffusible bromomethyl keto acid that alkylates cysteine thiols". In: *Biochemistry* 45.3 (2006), pp. 1061–1073.
- [219] Elizabeth J Ackermann, ES Kempner, and EA Dennis. "Ca (2+)-independent cytosolic phospholipase A₂ from macrophage-like P388D1 cells. Isolation and characterization." In: *Journal of Biological Chemistry* 269.12 (1994), pp. 9227–9233.
- [220] John E Burke and Edward A Dennis. "Phospholipase A₂ biochemistry". In: *Cardiovascular drugs and therapy* 23.1 (2009), pp. 49–59.
- [221] David A Ford et al. "The rapid and reversible activation of a calcium-independent plasmalogen-selective phospholipase A₂ during myocardial ischemia." In: *The Journal of clinical investigation* 88.1 (1991), pp. 331–335.
- [222] Stanley L Hazen and Richard W Gross. "Human myocardial cytosolic Ca²⁺-independent phospholipase A₂ is modulated by ATP. Concordant ATP-induced alterations in enzyme kinetics and mechanism-based inhibition". In: *Biochemical Journal* 280.3 (1991), pp. 581–587.
- [223] Christopher M Jenkins et al. "Identification of the calmodulin-binding domain of recombinant calcium-independent phospholipase A₂β: implications for structure and function". In: *Journal of Biological Chemistry* 276.10 (2001), pp. 7129–7135.
- [224] John Turk and Sasanka Ramanadham. "The expression and function of a group VIA calcium-independent phospholipase A₂ (iPLA₂β) in β-cells". In: *Canadian journal of physiology and pharmacology* 82.10 (2004), pp. 824–832.
- [225] David J Mancuso, Christopher M Jenkins, and Richard W Gross. "The genomic organization, complete mRNA sequence, cloning, and expression of a novel human intracellular membrane-associated calcium-independent phospholipase A₂". In: *Journal of Biological Chemistry* 275.14 (2000), pp. 9937–9945.
- [226] Martin Hermansson, Kati Hokynar, and Pentti Somerharju. "Mechanisms of glycerophospholipid homeostasis in mammalian cells". In: *Progress in lipid research* 50.3 (2011), pp. 240–257.

- [227] Shunzhong Bao et al. “Effects of stable suppression of Group VIA phospholipase A2 expression on phospholipid content and composition, insulin secretion, and proliferation of INS-1 insulinoma cells”. In: *Journal of biological chemistry* 281.1 (2006), pp. 187–198.
- [228] Bin Sun et al. “Inhibition of calcium-independent phospholipase A2 activates p38 MAPK signaling pathways during cytotaxis in prostate cancer cells”. In: *Biochemical pharmacology* 79.12 (2010), pp. 1727–1735.
- [229] Sasanka Ramanadham et al. “Age-related changes in bone morphology are accelerated in group VIA phospholipase A2 (iPLA2 β)-null mice”. In: *The American journal of pathology* 172.4 (2008), pp. 868–881.
- [230] Shunzhong Bao et al. “Male mice that do not express group VIA phospholipase A2 produce spermatozoa with impaired motility and have greatly reduced fertility”. In: *Journal of Biological Chemistry* 279.37 (2004), pp. 38194–38200.
- [231] Goichi Beck et al. “Neuroaxonal dystrophy in calcium-independent phospholipase A2 β deficiency results from insufficient remodeling and degeneration of mitochondrial and presynaptic membranes”. In: *Journal of Neuroscience* 31.31 (2011), pp. 11411–11420.
- [232] Julie Allyson et al. “Maintenance of synaptic stability requires calcium-independent phospholipase A2 activity”. In: *Neural plasticity* 2012 (2012).
- [233] Krishna Chaithanya Batchu et al. “Substrate efflux propensity is the key determinant of Ca²⁺-independent phospholipase A- β (iPLA β)-mediated glycerophospholipid hydrolysis”. In: *Journal of Biological Chemistry* 290.16 (2015), pp. 10093–10103.
- [234] Perttu Haimi et al. “Substrate efflux propensity plays a key role in the specificity of secretory A-type phospholipases”. In: *Journal of Biological Chemistry* 285.1 (2010), pp. 751–760.
- [235] Krishna Chaithanya Batchu. “ACADEMIC DISSERTATION”. In: ().
- [236] A Marek Brzozowski et al. “Structural origins of the interfacial activation in *Thermomyces* (*Humicola*) *lanuginosa* lipase”. In: *Biochemistry* 39.49 (2000), pp. 15071–15082.
- [237] Chrislaine Withers-Martinez et al. “A pancreatic lipase with a phospholipase A1 activity: crystal structure of a chimeric pancreatic lipase-related protein 2 from guinea pig”. In: *Structure* 4.11 (1996), pp. 1363–1374.
- [238] Eduardo Mateos-Diaz et al. “IR spectroscopy analysis of pancreatic lipase-related protein 2 interaction with phospholipids: 1. Discriminative recognition of mixed micelles versus liposomes”. In: *Chemistry and Physics of Lipids* 211 (2018), pp. 52–65.

- [239] Ivan Panaiotov, Margarita Ivanova, and Robert Verger. “Interfacial and temporal organization of enzymatic lipolysis”. In: *Current opinion in colloid & interface science* 2.5 (1997), pp. 517–525.
- [240] Morten Ø Jensen et al. “Orientation and conformation of a lipase at an interface studied by molecular dynamics simulations”. In: *Biophysical journal* 83.1 (2002), pp. 98–111.
- [241] Torben R Jensen et al. “Novel methods for studying lipids and lipases and their mutual interaction at interfaces. Part II. Surface sensitive synchrotron X-ray scattering”. In: *Biochimie* 83.5 (2001), pp. 399–408.
- [242] Ming-Hon Hou et al. “Crystal structure of vespid phospholipase A1 reveals insights into the mechanism for cause of membrane dysfunction”. In: *Insect biochemistry and molecular biology* 68 (2016), pp. 79–88.
- [243] Chisaki Nakagawara and Manabu Arioka. “Distinct enzymatic and cellular characteristics of two phospholipases A1 in *Aspergillus oryzae*”. In: *Biochemical and Biophysical Research Communications* 518.4 (2019), pp. 644–650.
- [244] Konstantin Balashev et al. “Atomic force microscope visualization of lipid bilayer degradation due to action of phospholipase A2 and *Humicola lanuginosa* lipase”. In: *Biochimica et Biophysica Acta (BBA)-Biomembranes* 1768.1 (2007), pp. 90–99.
- [245] Lei Wang et al. “Bract suppression regulated by the miR156/529-SPLs-NL1-PLA1 module is required for the transition from vegetative to reproductive branching in rice”. In: *Molecular Plant* 14.7 (2021), pp. 1168–1184.
- [246] JK Beckman, SM Borowitz, and IM Burr. “The role of phospholipase A activity in rat liver microsomal lipid peroxidation.” In: *Journal of Biological Chemistry* 262.4 (1987), pp. 1479–1484.
- [247] Hanna P Wacklin et al. “Distribution of reaction products in phospholipase A2 hydrolysis”. In: *Biochimica et Biophysica Acta (BBA)-Biomembranes* 1768.5 (2007), pp. 1036–1049.
- [248] Hanna P Wacklin. “Interfacial mechanism of phospholipase A2: pH-dependent inhibition and Me- β -cyclodextrin activation”. In: *Biochemistry* 48.25 (2009), pp. 5874–5881.
- [249] John Jumper et al. “Highly accurate protein structure prediction with AlphaFold”. In: *Nature* 596.7873 (2021), pp. 583–589.
- [250] Petra Pernot, Martha Brennich, and Mark Tully. “The rise of BioSAXS at the ESRF: BM29 beamline for SAXS on proteins in solution”. In: *Acta Crystallogr. Sect. A Found. Adv* 74 (2018), a7–a7.
- [251] Jordi Folch, Mark Lees, Gerald H Sloane Stanley, et al. “A simple method for the isolation and purification of total lipids from animal tissues”. In: *J Biol Chem* 226.1 (1957), pp. 497–509.

- [252] Kanu M Patel, Joel D Morrisett, and James T Sparrow. “A convenient synthesis of phosphatidylcholines: acylation of sn-glycero-3-phosphocholine with fatty acid anhydride and 4-pyrrolidinopyridine.” In: *Journal of Lipid Research* 20.5 (1979), pp. 674–677.
- [253] Alexis de Ghellinck et al. “Production and analysis of perdeuterated lipids from *Pichia pastoris* cells”. In: *PLoS One* 9.4 (2014), e92999.
- [254] F Höök et al. “Energy dissipation kinetics for protein and antibody- antigen adsorption under shear oscillation on a quartz crystal microbalance”. In: *Langmuir* 14.4 (1998), pp. 729–734.
- [255] RA Campbell et al. “FIGARO: The new horizontal neutron reflectometer at the ILL”. In: *The European Physical Journal Plus* 126.11 (2011), pp. 1–22.
- [256] Maria Grazia Ortore et al. “Combining structure and dynamics: non-denaturing high-pressure effect on lysozyme in solution”. In: *Journal of The Royal Society Interface* 6.suppl_5 (2009), S619–S634.
- [257] Francesco Spinozzi et al. “GENFIT: software for the analysis of small-angle X-ray and neutron scattering data of macromolecules in solution”. In: *Journal of applied crystallography* 47.3 (2014), pp. 1132–1139.
- [258] Alexis de Ghellinck et al. “Lipid polyunsaturation determines the extent of membrane structural changes induced by Amphotericin B in *Pichia pastoris* yeast”. In: *Biochimica et Biophysica Acta (BBA) - Biomembranes* 1848.10, Part A (2015), pp. 2317–2325. DOI: [10.1016/j.bbamem.2015.06.006](https://doi.org/10.1016/j.bbamem.2015.06.006).
- [259] John F Nagle et al. “Revisiting volumes of lipid components in bilayers”. In: *The Journal of Physical Chemistry B* 123.12 (2019), pp. 2697–2709.
- [260] T. Harayama and H. Riezman. “Understanding the diversity of membrane lipid composition”. In: *Nat Rev Mol Cell Biol* 19 (2018), pp. 281–296. DOI: [10.1038/nrm.2017.138](https://doi.org/10.1038/nrm.2017.138).
- [261] Noel M Rysavy et al. “Beyond apoptosis: the mechanism and function of phosphatidylserine asymmetry in the membrane of activating mast cells”. In: *Bioarchitecture* 4.4-5 (2014), pp. 127–137.
- [262] Manuel Ferrer et al. “Comparative surface activities of di-and trisaccharide fatty acid esters”. In: *Langmuir* 18.3 (2002), pp. 667–673.
- [263] Christopher D Stubbs and Anthony D Smith. “The modification of mammalian membrane polyunsaturated fatty acid composition in relation to membrane fluidity and function”. In: *Biochimica et Biophysica Acta (BBA)-Reviews on Biomembranes* 779.1 (1984), pp. 89–137.
- [264] Joshua A Jackman et al. “Interfacial binding dynamics of bee venom phospholipase A2 investigated by dynamic light scattering and quartz crystal microbalance”. In: *Langmuir* 26.6 (2010), pp. 4103–4112.

- [265] Ralph H Schaloske and Edward A Dennis. "The phospholipase A2 superfamily and its group numbering system". In: *Biochimica et Biophysica Acta (BBA)-Molecular and Cell Biology of Lipids* 1761.11 (2006), pp. 1246–1259.
- [266] Sajal Chakraborti. "Phospholipase A2 isoforms: a perspective". In: *Cellular signalling* 15.7 (2003), pp. 637–665.
- [267] Xiaoyong Lei, Suzanne E Barbour, and Sasanka Ramanadham. "Group VIA Ca²⁺-independent phospholipase A2 (iPLA2 β) and its role in β -cell programmed cell death". In: *Biochimie* 92.6 (2010), pp. 627–637.
- [268] Sherry C Morash, Harold W Cook, and Matthew W Spence. "Phosphatidylcholine metabolism in cultured cells: catabolism via glycerophosphocholine". In: *Biochimica Et Biophysica Acta (BBA)-Lipids and Lipid Metabolism* 961.2 (1988), pp. 194–202.
- [269] Lilian BM Tijburg, Tomoko Nishimaki-Mogami, and Dennis E Vance. "Evidence that the rate of phosphatidylcholine catabolism is regulated in cultured rat hepatocytes". In: *Biochimica et Biophysica Acta (BBA)-Lipids and Lipid Metabolism* 1085.2 (1991), pp. 167–177.
- [270] George S Attard et al. "Modulation of CTP: phosphocholine cytidyltransferase by membrane curvature elastic stress". In: *Proceedings of the National Academy of Sciences* 97.16 (2000), pp. 9032–9036.
- [271] JA Op den Kamp, M Th Kauerz, and LL Van Deenen. "Action of pancreatic phospholipase A2 on phosphatidylcholine bilayers in different physical states." In: *Biochimica et Biophysica Acta* 406.2 (1975), pp. 169–177.
- [272] R Cohen and Y Barenholz. "Correlation between the thermotropic behavior of sphingomyelin liposomes and sphingomyelin hydrolysis by sphingomyelinase of *Staphylococcus aureus*". In: *Biochimica et Biophysica Acta (BBA)-Biomembranes* 509.1 (1978), pp. 181–187.
- [273] Hsio-Wen Huang, Edward M Goldberg, and Raphael Zidovetzki. "Ceramide induces structural defects into phosphatidylcholine bilayers and activates phospholipase A2". In: *Biochemical and biophysical research communications* 220.3 (1996), pp. 834–838.
- [274] Alma M Astudillo et al. "Dynamics of arachidonic acid mobilization by inflammatory cells". In: *Biochimica et Biophysica Acta (BBA)-Molecular and Cell Biology of Lipids* 1821.2 (2012), pp. 249–256.
- [275] Nicholas S Kirkby et al. "Inherited human group IVA cytosolic phospholipase A2 deficiency abolishes platelet, endothelial, and leucocyte eicosanoid generation". In: *The FASEB Journal* 29.11 (2015), pp. 4568–4578.
- [276] Ruth J Mayer and Lisa A Marshall. "New insights on mammalian phospholipase A2 (s); comparison of arachidonoyl-selective and-nonselective enzymes". In: *The FASEB Journal* 7.2 (1993), pp. 339–348.

- [277] James D Clark et al. “A novel arachidonic acid-selective cytosolic PLA2 contains a Ca²⁺-dependent translocation domain with homology to PKC and GAP”. In: *Cell* 65.6 (1991), pp. 1043–1051.
- [278] Dörte Otten, Michael F Brown, and Klaus Beyer. “Softening of membrane bilayers by detergents elucidated by deuterium NMR spectroscopy”. In: *The Journal of Physical Chemistry B* 104.51 (2000), pp. 12119–12129.
- [279] Sandro Keller et al. “Thermodynamics of lipid membrane solubilization by sodium dodecyl sulfate”. In: *Biophysical journal* 90.12 (2006), pp. 4509–4521.
- [280] Oumaima Et-Thakafy et al. “Mechanical properties of membranes composed of gel-phase or fluid-phase phospholipids probed on liposomes by atomic force spectroscopy”. In: *Langmuir* 33.21 (2017), pp. 5117–5126.
- [281] Andreas Plueckthun and Edward A Dennis. “Acyl and phosphoryl migration in lysophospholipids: importance in phospholipid synthesis and phospholipase specificity”. In: *Biochemistry* 21.8 (1982), pp. 1743–1750.
- [282] Supriyo Ray, Jennifer L Scott, and Suren A Tatulian. “Effects of lipid phase transition and membrane surface charge on the interfacial activation of phospholipase A2”. In: *Biochemistry* 46.45 (2007), pp. 13089–13100.
- [283] W Richard Burack et al. “Changes in vesicle morphology induced by lateral phase separation modulate phospholipase A2 activity”. In: *Biochemistry* 36.34 (1997), pp. 10551–10557.
- [284] Leslie R Ballou and Wai Yiu Cheung. “Inhibition of human platelet phospholipase A2 activity by unsaturated fatty acids.” In: *Proceedings of the National Academy of Sciences* 82.2 (1985), pp. 371–375.
- [285] Mahendra K Jain and Rafael C Apitz-Castro. “Lag phase during the action of phospholipase A2 on phosphatidylcholine modified by alkanols.” In: *Journal of Biological Chemistry* 253.19 (1978), pp. 7005–7010.
- [286] Xin Gao et al. “Quantitative analysis of cold stress inducing lipidomic changes in *Shewanella putrefaciens* using UHPLC-ESI-MS/MS”. In: *Molecules* 24.24 (2019), p. 4609.
- [287] Maciej Turowski et al. “Deuterium isotope effects on hydrophobic interactions: the importance of dispersion interactions in the hydrophobic phase”. In: *Journal of the American Chemical Society* 125.45 (2003), pp. 13836–13849.
- [288] Yuri Gerelli. “Aurore: new software for neutron reflectivity data analysis”. In: *Journal of Applied Crystallography* 49.1 (2016), pp. 330–339.
- [289] Andrew Nelson. “Co-refinement of multiple-contrast neutron/X-ray reflectivity data using MOTOFIT”. In: *Journal of applied crystallography* 39.2 (2006), pp. 273–276.

- [290] Norbert Kučerka et al. “Lipid bilayer structure determined by the simultaneous analysis of neutron and X-ray scattering data”. In: *Biophysical journal* 95.5 (2008), pp. 2356–2367.
- [291] Michal Belička et al. “The component group structure of DPPC bilayers obtained by specular neutron reflectometry”. In: *Soft Matter* 11.31 (2015), pp. 6275–6283.
- [292] Lyman G Parratt. “Surface studies of solids by total reflection of X-rays”. In: *Physical review* 95.2 (1954), p. 359.
- [293] Hirsh Nanda et al. “Electrostatic interactions and binding orientation of HIV-1 matrix studied by neutron reflectivity”. In: *Biophysical Journal* 99.8 (2010), pp. 2516–2524.
- [294] Siddhartha AK Datta et al. “HIV-1 Gag extension: conformational changes require simultaneous interaction with membrane and nucleic acid”. In: *Journal of molecular biology* 406.2 (2011), pp. 205–214.
- [295] Frank Heinrich and Mathias Lösche. “Zooming in on disordered systems: Neutron reflection studies of proteins associated with fluid membranes”. In: *Biochimica et Biophysica Acta (BBA)-Biomembranes* 1838.9 (2014), pp. 2341–2349.
- [296] J Skov Pedersen, Dorthe Posselt, and Kell Mortensen. “Analytical treatment of the resolution function for small-angle scattering”. In: *Journal of Applied Crystallography* 23.4 (1990), pp. 321–333.
- [297] Peter JM Van Laarhoven et al. *Simulated annealing*. Springer, 1987.
- [298] Dimitris Bertsimas and John Tsitsiklis. “Simulated annealing”. In: *Statistical science* 8.1 (1993), pp. 10–15.
- [299] Scott Kirkpatrick, C Daniel Gelatt Jr, and Mario P Vecchi. “Optimization by simulated annealing”. In: *science* 220.4598 (1983), pp. 671–680.